NUCLEAR MAGNETIC RESONANCE AND MASS SPECTROSCOPY

STUDY OF SOME MACROCYCLIC COMPLEXES

By

Yang-Chih Lee

A DISSERTATION

Submitted to
Michigan State University
in partial fulfillment of the requirements
for the degree of

DOCTOR OF PHILOSOPHY

Department of Chemistry

1983

in va
resul
in di
Gutma
mixt
dimet
plexi
eral
comp
tratic
the

II

ABSTRACT

NUCLEAR MAGNETIC RESONANCE AND MASS SPECTROSCOPY
STUDY OF SOME MACROCYCLIC COMPLEXES

By

Yang-Chih Lee

The complexation of the Tl^+ ion by 18C6 and its analogs in various solvents has been studied by ^{205}Tl NMR. The results show that the stability constants of five complexes in different solvents generally decrease with increasing Gutmann donor number in the order: nitromethane > aceto-nitrile > acetone > sulfolane > dimethylformamide > water > dimethylsulfoxide > hexamethylphosphoramide. Also, the com-plexing strength of different ligands with the Tl^+ ion gen-erally decreases in the order DA18C6 > 18C6 > cis-syn-cis-DC18C6 > DB18C6 > DT18C6. Proton and carbon-13 NMR spectra indicate that the conformation changes occur during complexa-tion for DT18C6.

Thermodynamic parameters of the Tl^+ ion complexed by

1906,

reacti

entrop

in se

been s

iso-s

which

portar

its re

Co

was in

tively

ing an

respec

Ma

sively

mechar

interm

polyes

functi

propos

18C6, DB18C6 and DT18C6 indicate that these complexation reactions are generally enthalpy stabilized ($\Delta H_c^o < 0$) but entropy destabilized ($\Delta S_c^o < 0$). The solvation of the Tl^+ ion in several low and high solvating power mixed solvents has been studied. A good correletion was observed between the iso-solvation point and the donor number of the solvent which indicate that the donicity of a solvent is more important than its dielectric constant scale in determining its relative solvating ability.

Complex formation of the Tl^+ ion with DA18C6 or DT18C6 was investigated in DMF/H_2O or DMF/AN mixed solvents respectively. The formation constant, K_f, increases with increasing amounts of dimethylformamide and acetonitrile in the respective binary mixtures.

Mass spectra of 12C4, 15C5, 18C6 and 21C7 were intensively studied. According to the results, the fragmentation mechanisms of these macrocycles were developed and a linear intermediate was proposed. The mass spectra of two linear polyethers were taken at 70 eV and ion abundances as a function of electron energy for 18C6 were used to verify the proposed fragmentation pathways.

To My Wife and My Parents

Th

Profes

contin

rance

C. H.

their

Fi

State

Chemis

S

resea

discu

M

for t

are g

the N

obtai

A

wide

F

lore,

study

dedica

ACKNOWLEDGEMENTS

TABLE OF CONTENTS

LIST OF TABLES

ix

LIST OF FIGURES

Figure   Page

1. LIG

2. SCI

LIST OF ABBREVIATIONS

1. LIGANDS

3-EGDME	Trienthylene glycol dimethyl ether
4-EGDME	Tetraethylene glycol dimethyl ether
12C4	12-crown-4
15C5	15-crown-5
18C6	18-crown-6
21C7	21-crown-7
DA18C6	Diaza-18-crown-6
DT18C6	Dithia-18-crown-6
DC18C6	Dicyclohexyl-18-crown-6
DB18C6	Dibenzo-18-crown-7

2. SOLVENTS

AN	Acetonitrile
AC	Acetone
NM	Nitromethane
SF	Sulfolane
PY	Pyridine
PC	Propylene carbonate
DMF	Dimethylformamide
THF	Tetrahydrofuran
DMSO	Dimethylsulfoxide
HMPA	Hexamethylphosphoramide

PART I

NUCLEAR MAGNETIC RESONANCE STUDY

OF SOME MACROCYCLIC COMPLEXES

CHAPTER I

INTRODUCTION AND HISTORICAL

The b

generall

1967 (1)

and thei

ions. S

polyethe

studied

subject

For

tively

15-crown

selectiv

its cavi

benzo-15

tivities

ation

ligand

For

most ca

cavity

major fa

become i

cluded t

INTRODUCTION

The beginning of macrocyclic polyether chemistry
generally dates to Pedersen's first paper published in
1967 (1), where he reported the synthesis of 33 macrocycles
and their potential as complexing agents for the alkali
ions. Since then, the complexation reactions of macrocyclic
polyethers with alkali and alkaline earth ions have been
studied extensively and some comprehensive reviews on the
subject are available (2-9).

For macrocyclic crowns smaller than 18-crown-6, rela-
tively few studies have been reported. In the case of
15-crown-5 (10), results show almost no alkali cation
selectivity in aqueous solution, which is consistent with
its cavity being too small for most alkali cations. For
benzo-15-crown-5 and cyclohexo-15-crown-5 (11,12), selec-
tivities are difficult to distinguish because of the for-
mation of 2:1 complexes if the cation is larger than the
ligand cavity.

For crowns larger than 18-crown-6 which are too large for
most cations in the alkali or alkaline earth series (Table 1)
cavity size of the crown ether does not appear to be the
major factor in determining selectivity. Other factors
become increasingly important (11,13,14). It may be con-
cluded that, for macrocyclic polyethers, correlation of

selectivi

18-crown-

Thall

of potass

and the p

Complexe

analogs

separati

investig

across s

This

magneti

sented

tions a

DB18C6,

been st

I resp

thalli

system

In

metal

solven

tetras

18-cr

fragm

of th

selectivity with cavity size is restricted essentially to 18-crown-6 and its substituted analogs.

Thallium-205 NMR is a good probe for studies of the role of potassium ions in biological systems (15) since the size and the properties of the two ions are very similar. Complexes of the Tl^+ ion with 18-crown-6 and its substituted analogs (Figure 1) in various solvents can be used in separation chemistry and can also be used as a model for the investigation of the transport reaction of potassium ions across some biological membrane.

This dissertation is divided into two parts. Nuclear magnetic resonance and mass spectrometry studies are pre-sented in Parts I and II respectively. Complexation reac-tions and thermodynamic studies of the Tl^+ ion with 18C6, DB18C6, DC18C6, DA18C6 and DT18C6 in various solvents have been studied and are discussed in Chapters III and IV of Part I respectively. Also preferential solvation effects on the thallium(I) ion and thallium(I)-crown complex in mixed solvent systems are described in Chapter V of Part I.

In order to investigate ion-molecule reactions involving metal ions and macrocyclic polyethers in the absence of solvent, mass spectra of triethylene glycol dimethylether, tetraethylene glycol dimethylether, 12-crown-4, 15-crown-5, 18-crown-6 and 21-crown-7 were intensively studied. The fragmentation patterns for non-substituted macrocycles and of their linear analogs are proposed in Part II.

R¹=R²=R³=R⁴=CH₃   NONACTIN

R¹=R²=R³=CH₃   R⁴=C₂H₅   MONACTIN

R¹=R³=CH₃   R²=R⁴=C₂H₅   DINACTIN

R¹=CH₃   R²=R³=R⁴=C₂H₅   TRINACTIN

R¹=R²=R³=R⁴=C₂H₅   TETRANACTIN

VALINOMYCIN

18-CROWN-6
(18C6)

1,10-DITHIA-18C6
(DT 18C6)

1,10-DIAZA-18C6
(DA18C6)

DIBENZO-18-CROWN-6
(DB18C6)

DICYCLOHEXYL-18C6
(DC18C6)
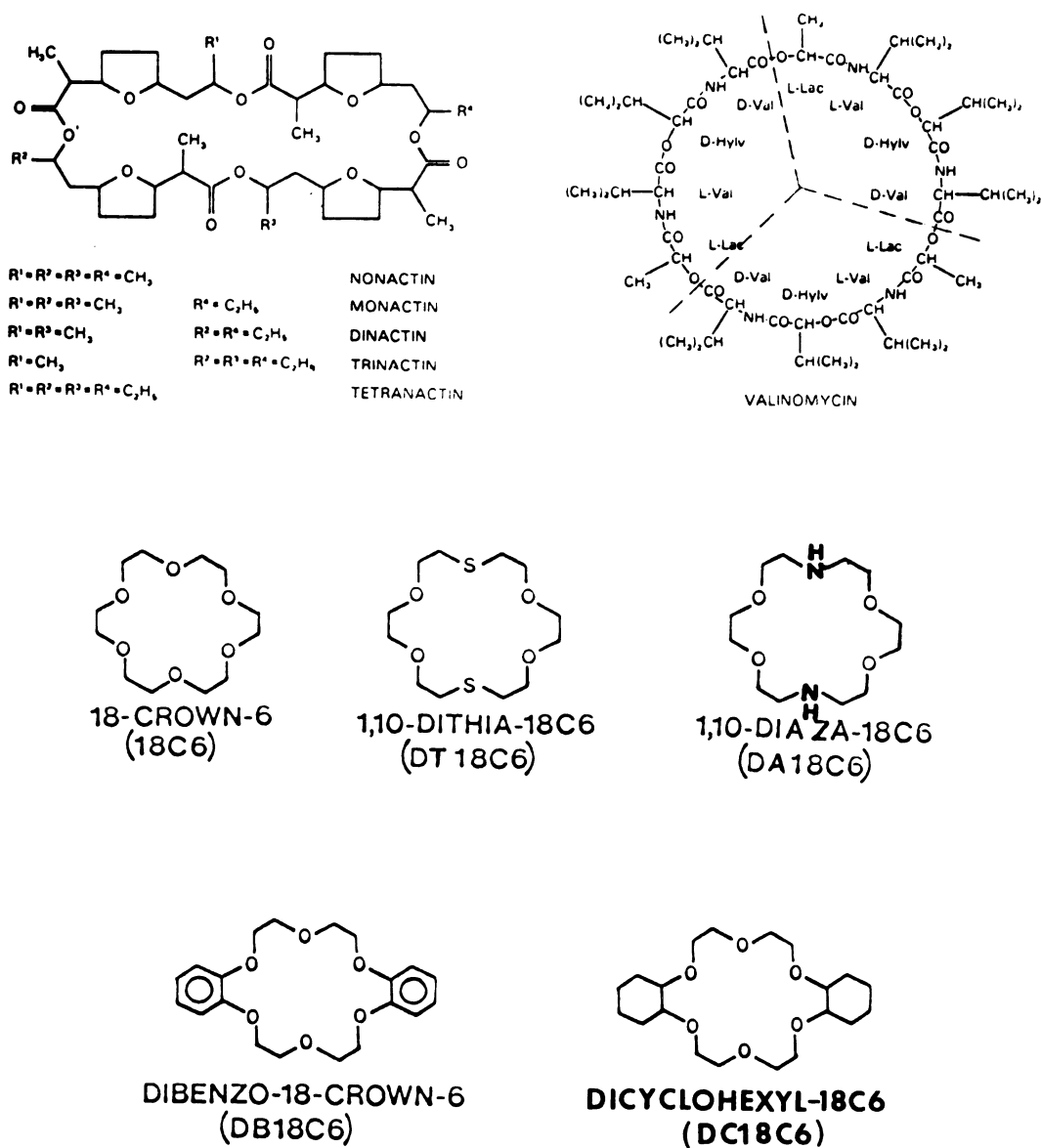
Figure 1.   Structures of some naturally occuring and of
some synthetic macrocyclic compounds.

HISTORICAL REVIEW

A. Neutral Macrocycles

Macrocyclic ligands are uncharged species and contain
a cavity in which a cation can be encapuslated. Some
naturally occuring macrocycles, which are antibiotics, have
been shown to be capable of actively transporting certain
metal ions across some biological membranes. Moore and
Pressman (16) reported in 1964 that antibiotic valinomycin
(Figure 1) is highly selective toward the K^+ ion as compared
to Na^+. The observation has stimulated studies of metal ions
complexed with various antibiotics and synthetic multidentate
macrocycles such as crown ethers and cryptands (7,17-20).
One goal of this work was to understand conditions which lead
to differences in the transportation of alike alkali ions by
the cell membrane in living systems (21,22). The antibiotic
ionophores can be cyclic or acyclic whereas the synthetic
ligands can be acyclic, monocyclic or polycyclic. Various
antibiotics were used as models for the transport carriers
(23) in the study of transport reactions of metal ions across
synthetic or natural membranes (19,24,25); during transport
the transport carrier separates the cation from its coun-
terion and solvating liquid. Transport reactions can also be
induced by synthetic carriers such as macrocyclic polyethers.
A liquid hydrocarbon phase (containing carrier) interposed
between two aqueous phase has frequently been utilized as
a model for studying ion transport through natural

membranes (26-28). The most well-know antibiotic ionophores are valinomycin and nactin (Figure 1); their selectivity toward metal ions depends on the coordinative characteristics of the cation as well as the reaction medium. The general selective sequence of alkali ions with these two antibiotics in aqueous solution is $K^+ > Rb^+ > Cs^+ > Na^+ > Li^+$ (29-31) which is the same as that with the 30-skeletal atom crown ether, DB30C10 (32). The sequence for the larger three cations varies oppositely with their hydration energy criterion (33) ($Cs^+ > Rb^+ > K^+ > Na^+ > Li^+$) which indicates that the cavity size has a strong influence on the stability of macrocyclic complexes.

B. Macrocyclic Polyethers and Their Complexes in the Solid State

Complexes of transition-metal cations with conventional ligands have been known for a long time, whereas 15 years ago only a few stable alkali cation complexes had been identified. Coordination chemistry of alkali and alkaline earth cations has started developing rapidly only in this decade. Macrocyclic polyethers, which are similar to the antibiotic ligands both in structure and in their ability to form stable complexes with alkali and alkaline earth cations, were first reported in 1967 by Pedersen (1,34).

On the Pauling scale, the electronegativity values of all alkali and alkaline earth metals very from 0.7 to 1.2.

Taking the electronegativity of oxygen as 3.5, the bonds between these metals and oxygen should be about 70-85% ionic in character. Furthermore, in view of the low ionization potential of such metals and their hard acidic character, a covalent bond between these ions and hard base like oxygen atoms is rather unlikely.

Macrocyclic polyethers are neutral compounds containing four to twenty oxygen atoms each separated from the next by two or more carbon atoms. The most effective complexing agents are those containing five to ten oxygen atom each separated from the next by two methylene groups ($-CH_2CH_2-$). These compounds form polyether-salt complexes in which the cation is encircled by the oxygen atoms of the polyether ring and held by ion-dipole attraction between the negatively charged oxygens of the C-O dipoles and the cation. The stability constants of macrocyclic polyethers are three to four orders of magnitude higher than those of open chain analogs (35). This effect has been referred to as the macrocyclic effect. One of the most striking characteristics of the macrocyclic polyethers is their ability to form complexes selectively with various cations. The factors affecting the formation and stability of these ion-macrocycle complexes include (a) the relative size of the ion and macrocyclic cavity (b) the electrical charge of the cation (c) the nature of the donor atom in the ring (d) the number of binding sites in the ring (e) steric hindrance in the ring (f) the solvent

and e

the n

T

cavity

widely

metal-

appear

(1,34),

with a

cation

The

cavity s

given in

plexes a

the soli

crown et

which rem

and/or so

(Figure 2

complex wi

that the m

As the cav

size of ca

ligand tend

ed as wrapa

has been ob

and extent of solvation of the ion and the binding sites (g) the nature of the counterion.

The relationship between the cationic diameter and the cavity size is the most important factor which has been used widely to explain the stability and the stoichiometry of metal-crown ether complexes (4,7,17-20). Ever since the appearance of the first comprehensive report by Pedersen (1,34), it has been believed that complexation of a cation with a crown ether is determined basically by the fit of the cation in the cavity of the ligand.

The ionic diameters of some cations and the estimated cavity size of the holes of selected cyclic polyethers are given in Table 1. For those having the best fit, 1:1 complexes are postulated to be formed in solution as well as in the solid state. In such a complex the ring oxygens of the crown ether are arranged equatorially around the cation, which remains exposed on the axial sides to the counteranion and/or solvent molecules as shown in the complex of KSCN·18C6 (Figure 2) (35). The fact that a metal ion forms a 1:1 complex with a cyclic polyethers does not always indicate that the metal ion is located in the cavity of the polyether. As the cavity size of the crown ether increases for a given size of cation, 1:1 complexes are still obtained, but the ligand tends to be folded around the cation (this is designated as wraparound encapsulate). Such folding of the ligand has been observed for dibenzo-30-crown-10 around potassium in

Table 1. Diameter in Å of Selected Macrocyclic Ethers and Cations (1, 34, 40).

Ligand

Table 1. Diameter in Å of Selected Macrocyclic Ethers and Cations (1,34,40).

Ligand	Cavity diameter (Å)[a]	Cation	Cation diameter (Å)
All 12-crown-4	1.2-1.5	Li^+	1.20
All 15-crown05	1.7-2.2	Na^+	1.90
All 18-crown-6	2.6-3.2	K^+	2.66
All 21-crown-7	3.4-4.3	Rb^+	2.96
		Cs^+	3.34
		Ag^+	2.52
		Tl^+	2.80
		Ba^{2+}	2.70
		NH_4^+	2.84
		Mg^{2+}	1.44
		Ca^{2+}	2.00
		Sr^{2+}	2.32
		Pb^{2+}	2.40
		La^{3+}	2.28

[a]cavity difference is due to the Corey-Pauling-Kolton(CPK) models and the Fisher-Hirschfelder-Taylor (FHT) models used.
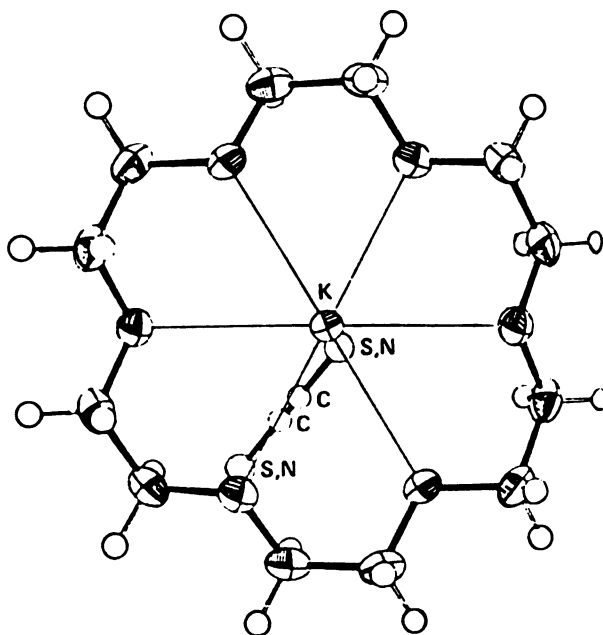
Figure 2. Crystalline structure of (KSCN·18C6).
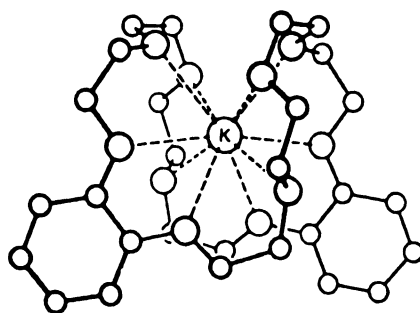
Figure 3. Three-dimensional crown complex of (KI·DB30C10).

the complex K(DB30C10)I (36) (Figure 3) and for dibenzo-24-crown-8 around sodium in the complex Na(DB24C8)X (37).
Alternatively, bimetallic complexes are produced in which two cations are complexed in the unfolded cavity of the ligand as found in the complexes $(KNCS)_2(DB24C8)$ (38) (Figure 4), $(Na-O-nitrophenolate)_2(DB24C8)$ (39) and as expected for the complex of Na with DB30C10 (41). Also, three kinds of sodium-DB30C10 $[Na \cdot DB30C10, Na_2 \cdot DB30C10$ and $Na_3 \cdot (DB30C10)_2]$ complexes are found in the complexation of DB30C10 with a sodium salt in nitromethane and acetonitrile by a ^{23}Na and ^{13}C NMR study (42).

When the size of the cation exceeds the cavity size of the crown ether, the metal ion is too large to fit exactly in the hole. In such cases ML_2 sandwich complexes are formed (L= crown ether). Sandwich complexes are formed by B15C5 with potassium, rubidium and cesium ions in solution (43,44) as well as in the solid state (Figure 5) (23,41). The formation of sandwich complexes of Cs^+ with 18-crown-6 and K^+ with 15-crown-5 in different solvents were also reported by Mei (11) and Shih (45).

In the sandwich and wraparound complexes, the crown ethers isolate the cation from the counterion and the solvent molecules. These encapsulates are comparable to those obtained from cyclic antibiotics (46,47) and information derived from the formation of the former is used to understand the latter.

When the relation between cation size and polyether cavity size is the only consideration, cation-crown ether interaction

Fig

Figure
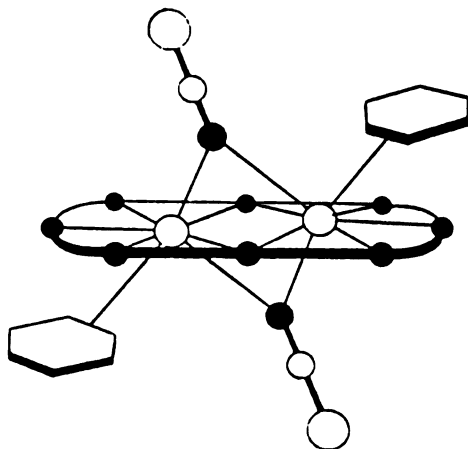
Figure 4. Crown complex of (2KSCN·DB24C8).
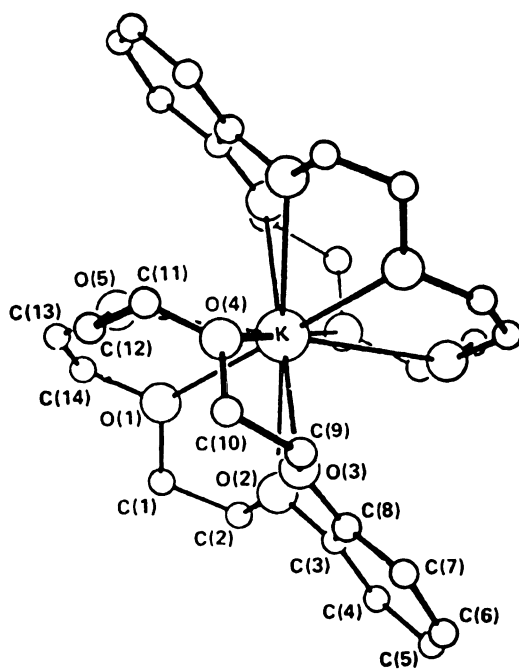
Figure 5. Sandwich structure of (K$^+$·2B15C5).

is most favored for a cation of the size nearest to that of
the cavity. For example, 12C4 is most selective for Li^+,
B15C5 is for Na^+, DC18C6 is for K^+, and DB24C8 is for Cs^+
(43,48-50). The next preference of a crown is for a cation
which is larger than its cavity. For example, B15C5 forms
a more stable complex with Rb^+ and Cs^+ than with K^+ (9).
The least favored ion of a crown ether is for a cation of a
size smaller than the cavity (51). The general cation selec-
tivity of several neutral ionophores was compiled and is
shown in Table 2 (52). Izatt et al. (52) has discussed in
detail the other factors affecting the formation and
stability of ion-macrocycle complexes.

C. <u>Complexation of 18-Crown-6 and Its Substituted
    Analogs in Solution</u>

Over the years, 18-crown-6 and its substituted analogs
have probably been more studied than any other crown ethers
since the cyclic ethers' coorelation of selectivity with
cavity size is restricted essentially to 18-crown-6.

The first synthesis of 18-crown-6 was reported by
Pedersen (1). The method used was potassium t-butoxide
catalyzed cyclization of hexaethylene glycol monochloride in
1,2-dimethoxyethane. Unfortunately, the yield by this method
was only 1.8%. Improved methods were developed by succeeding
workers (53-56).

The stability constants of 18C6 complexes with alkali and

Table 2. Cation Selectivities of Several Neutral Iono-
phores (56) in Solution.

Ionophore	Selectivity Sequence
Valinomycin	Rb > K > Cs > Ag > Tl >> NH$_4$ > Na > Li
	Ba > Ca >Sr > Mg
Enniatin A	K > Rb≈ Na > Cs >> Li
Enniatin B	Rb > K > Cs > Na >> Li
	Ca > Ba > Sr > Mg
Beauvericin	Rh > Cs > K >> Na > Li
Nonactin	NH$_4$ > K≈Rb > Cs > Na
Monactin	NH$_4$ > K > Rb > Cs > Na > Ba
Dinactin	NH$_4$ > K≈Rb > Cs > Na > Ba
Trinactin	NH$_4$ > Rb > Na > Cs
Antanamide	Na > Li > Tl > K > Rb > Cs
Cryptate 211	Li > Na > K≈Rb≈Cs
	Ca > Sr≈Ba
Cryptate 221	Ag > Tl > Na > K > Li≈Rb > Cs
	Sr > Ca > Ba > Mg
Cryptate 222	Ag > Tl > K > Rb > Na > Cs≈Li
	Ba > Sr > Ca > Mg
15-Crown-5	Tl > Ag > Cs≈K≈Na≈Rb
18-Crown-6	Tl > K > Rb≈Ag > Cs > Na > Li > Ca > Mg
18-Crown-6	Pb > Ba > Sr > K > Rb > Cs≈Na
Benzo-15-crown-5	Pb > Na≈Rb > K
Dibenzo-24-crown-8	Rb≈Cs≈K > Na
Dibenzo-27-crown-9	K > Na≈Cs

alkaline earth cations are compiled and shown in Table 3.
Complexation of 18C6 with alkali and alkaline earth cations
in water and 70% methanol/water solution was studied by
Izatt et al. (12). Using a calorimetric technique, they
found the maximum stability for complexes of 18C6 occurs at
a metal ion to cavity diameter ratio of unity. The increased
stability of the complexes is due to the enthalpy term.
Some trends of stability constants for complexes of 18C6 with
alkali metal ions were also found by Frensdorff (43) using
potentiometric techniques. Recent multinuclear NMR studies
on complexes of Na^+, Cs^+, and Tl^+ ion with 18C6 in several
organic solvents shows that the stability of 18C6 complex is
strongly influenced by solvent (57).

Two of the most widely used crown ethers have been
dibenzo-18-crown-6 (DB18C6) and dicyclohexano-18-crown-6
(DC18C6). A major reason for this is that Pedersen reported
complete details of the preparation of both compounds (58).

The stability constants of DB18C6 and four isomers of
DC18C6 with alkali and alkaline earth cations are compiled
in Table 4 and 5 respectively. Complexation of DB18C6, cis-
syn-cis-DC18C6, and cis-anti-cis-DC18C6 with alkali and alka-
line earth cations were studied by Shchori et al. (59) using
spectrophotometric technique. The representative structure
of the complex of DB18C6 with RbSCN is shown in Figure 6.
For all ligands, the strongest complexes are formed with K^+
and Ba^{2+} which are of exactly the correct size to fit into

Table 3. Stability Constants of M^{n+}-18C6 Complexes.

Cation	Medium	Log K_f	Method[a]	Reference
Na	H_2O	0.80	CAL	10
K		2.03		
Rb		1.56		
Cs		0.99		
Ag		1.50		
Tl		2.27		
Ca		< 0.5		
Sr		2.72		
Ba		3.87		
Na	70/30 wt% MeOH/H_2O	2.76	CAL	16
K		4.33		
Rb		3.46		
Cs		2.84		
Ca		2.51		
Sr		5.0		
Ba		6.0		
Na	H_2O	< 0.3	POT	43
K		2.05		
Cs		0.80		
NH_4	H_2O	1.1	POT	
Ag		1.6		

Table 3. Continued.

Cation	Medium	Log K_f	Method[a]	Reference
Na	MeOH	4.32	POT	43
K		6.10		
Cs		4.62		
		1.30(log K_2)		
Tl	crystal	1:1 complex	SPEC	125
Na	PC	> 4	^{23}Na,^{133}Cs ^{205}Tl NMR	57
Cs		4.14		
Na	AN	3.80		
Cs		> 5		
Tl		> 5		
Na	DMF	2.23		
Cs		3.93		
Tl		3.35		
Na	DMSO	1.41		
Cs		3.04		
Tl		1.92		
Na	H_2O	0.8		
Cs		0.99		
Tl		2.27		

[a]POT, potentiometry; CAL, calorimetry; SPEC, spectrophotometry.

Table 4. Stability Constants of M^{n+}-DB18C6 Complexes.

Cation	Medium	Log K_f	Method[a]	Reference
Li	H_2O	$\approx$ 0	SPEC	59
Na		1.16		
K		1.67		
Rb		1.08		
Cs		0.83		
Ag		1.41		
Tl		1.50		
NH_4		0.30		
Ca		$\approx$ 0		
Sr		1.0		
Ba		1.95		
Li	DMSO	$\approx$ 0	CON	51
Na		3.31		
K		3.39		
Rb		3.36		
Cs		3.07		
Li	DMF	2.99		
Na		3.35		
K		3.56		
Rb		3.52		

Table 4. Continued.

Cation	Medium	Log K_f	Method[a]	Reference
Cs	DMF	3.48	CON	51
Li	PC	3.22		
Na		3.86		
K		5.10		
Rb		3.74		
Cs		3.54		
Na	AN	5.00	POL	
K		4.70		
Rb		3.70		
Cs		3.50		
Tl		4.90		
K	MeOH	4.60		
Tl		4.00		
Cs	AN	1.54	^{133}Cs NMR	11
	AC	> 3		
	PC	≈ 3		
	PY	3.84		
		2.36(log K_2)		
	DMF	1.48		
	DMSO	1.34		

[a]CON, conductometry; POL, polarography; SPEC, spectrophotometry.

Table 5. Stability Constants of M^{n+} palace...

Table 5. Stability Constants of M^{n+}-DC18C6 Complexes.

Ligand	Cation	Medium	Method[a]	Log K_f	Reference
cis-syn-cis-DC18C6	Li	H_2O,25	SPEC	0.6	59
	Na			1.47-1.85	
	K			2.18	
	Rb			1.52	
	Cs			1.25	
	Ca			$\approx$ 0	
	Sr			3.24	
	Ba			3.57	
	Li	H_2O	POT	0.6	11
	Na	MeOH		4.08	
	K			6.01	
	Cs			4.61	
	Na	H_2O	CAL	1.21	10
	K			2.02	
	Rb			1.52	
	Cs			0.96	
	Ag			2.36	
	Tl			2.44	

Table 5. Continued.

Ligand	Cation	Medium	Method[a]	Log K_f	Reference
cis-syn-cis-DC18C6	Sr	H_2O	CAL	3.24	10
	Ba			3.57	
	Ag			1.59	
	Tl			1.83	
	Sr			2.64	
	Ba			3.27	
	Hg			2.60	
	Pb			4.43	
	NH_4			0.80	
	CH_3NH_3			0.66	
trans-syn-trans-DC18C6	Na	MeOH	POT	2.99	60,61
	K			4.14	
	Rb			3.42	
	Cs			3.00	
trans-anti-trans-DC18C6	Na	MeOH	POT	2.52	
	K			3.26	
	Rb			2.73	
	Cs			2.27	

Table 5. Continued.

Ligand	Cation	Medium	Method[a]	Log K_f	Reference
DC18C6(mixture)	K	AN	POL	6.60	48
	Rb			5.40	
	Cs			5.10	
	Tl			7.40	
	Tl	MeOH		5.20	
	Hg	H_2O	CAL	2.75	
	pb			4.95	
	NH_4			1.33	
	CH_3NH_3			0.82	
cis-anti-cis-DC18C6	Na	H_2O	SPEC	1.18-1.60	59
	K			1.78	
	Rb			0.88	
	Cs			0.90	
	Ca			≈ 0	
	Sr			2.63	
	Ba			3.28	
	Na	MeOH	POT	3.68	11
	K			5.38	

Table 5. Continued.

Ligand	Cation	Medium	Method[a]	Log K_f	Reference
cis-anti-cis-DC18C6	Cs	MeOH	POT	3.49	11
	Na	H_2O	CAL	0.69	10
	Na	DMSO		1.70	
	Na	EtOH		$\approx$ 4.50	
	K	H_2O		1.63	
	K	DMSO		2.70	
	Rb	H_2O		0.87	

[a]CAL, calorimetry; SPEC, spectrophotometry; POT, potentiometry; POL, polarography.
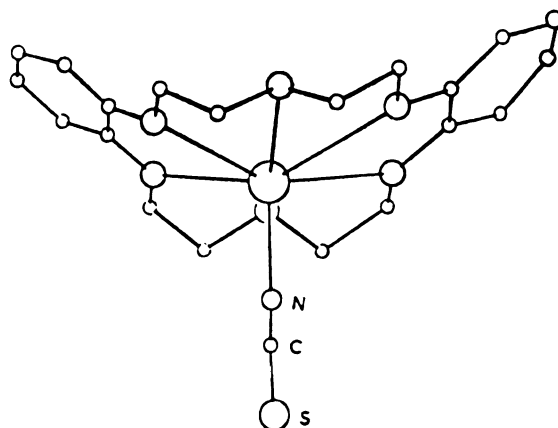
Figure 6. The structure of dibenzo-18-crown-6 complex with RbSCN.
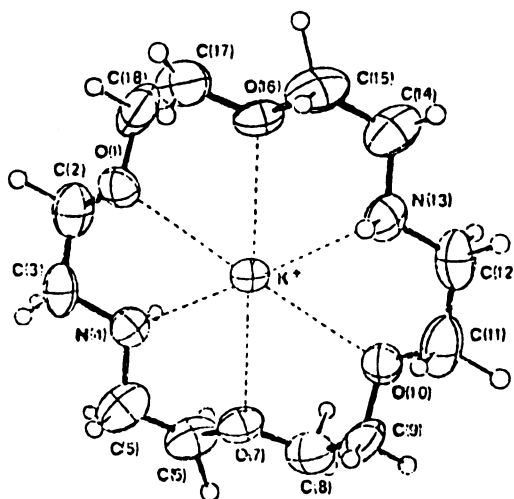
Figure 7. The structure of crown complex of $(K \cdot DA18C6)^+$.

the ring. The presence of two benzo groups in DB18C6 causes a rise in the stability of the Na^+ complex and a drop in the stabilities of the complexes with K^+ and Ba^{2+} cations as compared with the 18C6 complexes. In water, the formation constant of the Ba^{2+} complex of 18-crown-6 is larger than that of the K^+ complex by a factor of 10. However, the stability constants of Ba^{2+} and K^+ complexes with DB18C6 are nearly the same. These results indicate that the two benzo rings lend rigidity to the ligand and also decrease the cavity size. At the same time these groups withdraw electrons from the basic oxygen atoms, thus decreasing the metal-ligand interaction.

The presence of two cyclohexo substituent in DC18C6 causes a smaller effect on the stability of alkali and alkaline earth complexes compared with DB18C6 complexes. The ligand containing the aliphatic substituent is more flexible than the benzo substituted ligand and thus is more analogous to the binding properties of the unsubstituted ring. Potentiometric studies (11,60,61) on the complexation of alkali ions with four isomers of DC18C6 in methanol show that the general selectivity sequence for DC18C6 isomers with alkali ion is cis-syn-cis-DC18C6 > cis-anti-cis-DC18C6 > trans-syn-trans-DC18C6 > trans-anti-trans-DC18C6.

Several mixed donor macrocyclic polyethers have been reported (62) in which some or all of the ether oxygens were replaced by other atoms, such as S and NH. This replacement

affects not only the size of the cavity but also the type of coordination and the selectivity. By using potentiometric techniques, Frensdorff (43) first noted that when amine or sulfur is substituted for oxygen in a crown ether, the macrocyclic effect of 1,10-diaza-18-crown-6 (DA18C6) and aza-18-crown-6 disappears. Anderegg (63) studied the complexation of Ag^+, Cd^{2+} and Hg^{2+} with cryptand 222, DA18C6 and $H_2N(-CH_2-CH_2-O)_2-CH_2-CH_2NH_2$ in water. Nearly the same value of the stability constant for cryptand 222, DA18C6 and their linear analogs verify that for the above cation the macrocyclic effect does not exist for the above macrocycles. The representative results are shown in Table 6.

Metal complexes of macrocyclic ligands containing both nitrogen and oxygen donor groups have been found (43,64-66) to form 1:1 complexes with metal ions located in the center of the ligand cavity. The complexing of alkali or alkaline earth ions is diminished appreciably as nitrogen is substituted in the ring, and the stability constant falls in the order of decreasing electronegativity of the substituted group, O > NR >NH. The effects on the complexes of post-transition-metal ions of similar sizes, e.g., Ag^+, were exactly the opposite and the stability of the complexes increased with substitution. It was concluded that only electrostatic bonding exists in the potassium complexes whereas the Ag^+ complexes have both electrostatic and covalent bonding (43).

The structure of KSCN·DA18C6 (67) complex consists of

Table 6. Thermodynamics of M^{n+}-Aza-or-Thia-Substituted Polyethers in Aqueous Solution at 25°C.

Ligand[a]	Cation	Log K_1[b]	ΔH_1^o (Kcal/mol)	$T\Delta S_1^o$ (Kcal/mol)	Log K_2^c	ΔH_2^o (Kcal/mol)	$T\Delta S_2^o$ (Kcal/mol)	Ref.
D	Ag^+	7.7	-13.75	-3.25				63
	Hg^{2+}	18.55	-24.5	0.8				
	Cd^{2+}	5.68						
DA18C6	Ag^+	7.8	-9.15	1.49				
	Hg^{2+}	17.85	-17.15	7.24				
	Cd^{2+}	5.25	-0.7	6.44				
C222	Ag^+	9.6	-12.8	0.3				
	Hg^{2+}	18.2	-15.95	8.88				
	Cd^{2+}	6.8	0.5	9.83				
E	Ag^+	d	-14.13		3.06	-3.68	0.49	76
	Hg^{2+}	d	-14.02		3.22	-7.09	-2.70	
F	Ag^+	d	-16.57		2.70	-1.00	2.70	
	Hg^{2+}	d	-16.10		2.91	-5.00	-1.03	

[a]D, $H_2N-CH_2-CH_2-O-CH_2-CH_2-O-CH_2-CH_2-NH_2$; E, $H_3C-O-CH_2-CH_2-S-CH_2-CH_2-O-CH_2-CH_2-S-CH_2-CH_2-O-CH_3$; F, 1,7-dithia-15-crown-5.

[b]For reaction $M + L \rightleftharpoons ML$

[c]For reaction $ML + L \rightleftharpoons ML_2$

[d]Log K_1 is too large for measurement.

(0,

an

tw

(i

th

in

th

S

b

l

$(C_{12}H_{26}N_2O_4 \cdot K)^+$ ion (Figure 7) linked to the disordered SCN^- anion which reveals that the potassium ion is surrounded by two nitrogen atoms (K-N = 2.856 $\overset{o}{A}$) and four oxygen atoms (K-O = 2.83 $\overset{o}{A}$), and, unlike in the complex [K(18C6)NCS] (35) the SCN^- anion interacts weakly with K^+. Both these features indicate that the N atoms are weaker donors than O atoms and this K^+ complex is less stabilized than with 18C6. Structures of Pb^{2+} and Cu^{2+} complexes with DA18C6 also have been reported (68,69). The Pb^{2+} lies in the cavity of the DA18C6, interacts with all hetero atoms, and bonds to S of two SCN^- ligands. The Cu^{2+} complex shows the metal ion coordinates to both nitrogen atoms, to two of the four oxygen donor atoms and also to two chloro counterions. If the counterion is an anion (e.g. ClO_4^-) which does not form strong complexes with the metal ion, Cu^{2+} might have coordinated to all the hetero atoms.

The stability constants of DA18C6 or DT18C6 with metal ions are compiled in Table 7. Using a calometric technique, Anderegg (63) has determined the stability constants and the heat evolved by formation of the 1:1 complexes of Ag^+, Sr^{2+}, Ba^{2+} and Hg^{2+} with DA18C6 in aqueous solution. The results show that the selectivity for M^{n+} with DA18C6 follows the ordering: $Hg^{2+} > Ag^+ > Cd^{2+} > Ba^{2+} > Sr^{2+}$. Recent multinuclear NMR studies on the complexation of Li^+, Na^+, and Cs^+ ion with DA18C6 in several nonaqueous solvents show that the general selectivity sequence for M^+ with DA18C6 is $Li^+ > Na^+ > Cs^+$ (70).

Table 7. Stability Constants of M^{n+}-DA18C6 or -DT18C6 Complex.

Ligand	Cation	Medium	Method[a]	Log K_f	Reference
DA18C6	K	MeOH	POT	2.04	43
	Ag	H_2O	CAL	7.8	63
	Sr	H_2O		2.56	
	Ba			2.97	
	Cd			5.25	
	Hg			17.85	
	Li	NM	$^7Li, ^{23}Na, ^{133}Cs$ NMR	> 5	70
	Na			3.37	
	Cs			2.79	
	Li	AN		4.39	
	Cs			2.26	
	Li	PC		3.67	
	Cs			1.95	
	Li	AC		2.13	
	Na			1.96	
	Cs			1.89	

Table 7. Continued.

Ligand	Cation	Medium	Method[a]	$\log K_f$	Reference
DA18C6	Cs	DMF	^{7}Li, ^{23}Na, ^{133}Cs NMR	0.61	70
	Na	DMSO		1.19	
	Li	PY		0.43	
	Na			4.12	
	Cs			2.62	
DT18C6	K	MeOH	POT	1.15	7
	Ag	H$_2$O		4.34	
	Tl	H$_2$O	CAL	0.93	76
	Pb			3.13	
	Na	NM	Na^{23},Cs^{133}, Tl^{205}NMR	3.25	57
	Cs			1.16	
	Tl			> 5	
	Na	AC		2.42	
	Cs			0.61	
	Tl			2.98	

Table 7. Continued.

Ligand	Cation	Medium	Method[a]	Log K_f	Reference
DT18C6	Na	PC	$Na^{23}, Cs^{133}, Tl^{205}$ NMR	1.87	57
	Cs	PC		0.96	
	Na	AN		1.82	
	Cs	AN		0.97	
	Tl	AN		> 5	
	Na	DMF		1.52	
	Cs	DMF		0.56	
	Tl	DMF		1.24	
	Tl	H_2O		0.93	

[a]CAL, calorimetry; POT, potentiometry.

Don

oxygen

propert

the Kod

crown-6

1,2-bis

contain

(72-74)

substit

their s

(76) co

ethers

are sh

Hg^{2+} co

than t

contras

the th

The

shows

in coo

Pd^{2+} i

This c

1,4-di

effect

the fa

coordi

Donor atoms such as sulfur has been used to replace oxygen in macrocyclic ethers to vary the metal ion binding properties in the ring. In 1960, Dann, Chiesa and Gates of the Kodak Research Laboratories synthesized 1,10-dithia-18-crown-6 (DT18C6) by the reaction of sodium sulfide and 1,2-bis(2-chloroethoxy)ethane (71). The first study sulfur-containing crowns seems to have been conducted by Pedersen (72-74). Crystal structure studies show that the sulfur substituted 12-crown-4, 15-crown-5, and 18-crown-6 direct their sulfur atoms away from the cavity (75). Izatt et al. (76) compared the complexes of several thia-substituted poly-ethers to their linear analogs, and representative results are shown in Table 6. The formation constants of Ag^+ and Hg^{2+} complexes of the linear ligand are only sligtly larger than those of the cyclic ligand. The results show that, in contrast to the aza-crowns, no macrocyclic effect exists in the thia-substituted crowns.

The crystal structure of $PdCl_2$ complex of DT18C6 (77) shows that only outwardly turned sulfur atoms participate in coordination with the Pd^{2+} ion. As shown in Figure 8, the Pd^{2+} ion lies outside the ring which is bent like a bow. This coordination is also observed in the crystal of $HgCl_2$-1,4-dithia-18-crown-6 (78). The absence of a macrocyclic effect in these thia-substituted crowns is probably due to the fact that only sulfur atoms of crowns participate in the coordination with metal ion. In the series of studies of
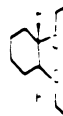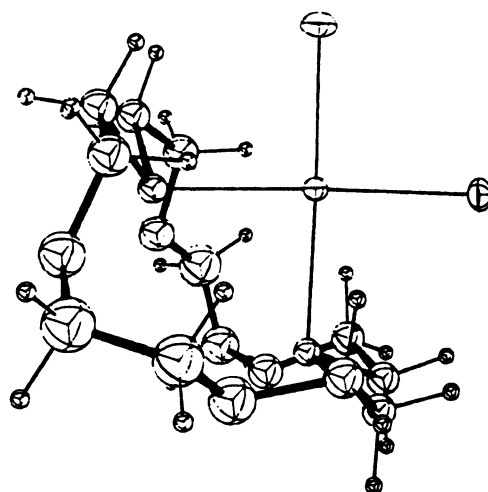
trans-a

Figure 8. The structure of the (PdCl$_2$·DT18C6) complex
(the Pd coordinate to two chloro ligand and
two sulfur atoms of thia ether).
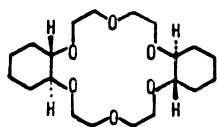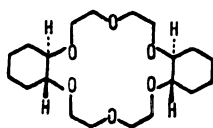
trans-anti-trans   trans-syn-trans   cis-anti-cis
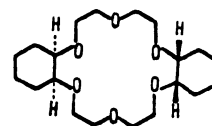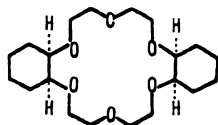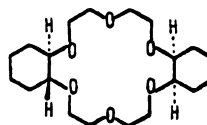
cis-syn-cis   trans-cis

Figure 9. The isomers of DC18C6.

th

(7

in

of

ar

th

th

cr

aq

ri

5 a

the

nit

met

Ag⁺

and

oxy

dec

1.1

4.3

sil

siu

(II

thia-substituted crown with Ag^+ and Hg^{2+} ions, Izatt et al. (75) have found that the complex stability is enhanced by increasing the number of sulfur atoms in the ring.

Alkali and alkaline earth metal ions give no evidence of complexation when all of the oxygen atoms in crown ethers are replaced by sulfur atoms (79,80). However, complexes of these ions are expected for the mixed crown ethers.

Izatt et al. (76) studied the complexation of several thia derivatives of 9-crown-3, 12-crown-4, 15-crown-5, 18-crown-6, and 24-crown-8 with Ag^+, Hg^{2+}, Tl^+, and Pb^{2+} ions in aqueous solutions and in 70% methanol by calorimetric technique.

A partial substitution of sulfur for oxygen in 15-crown-5 and 18-crown-6 ligands greatly increases the affinity of these ligands for Ag^+ and Hg^{2+} ions but decreases the affinity for Tl^+ and Pb^{2+} ions. Stoichiometries of 2:1 (ligand/metal ion) were found for many thia-substituted crowns with Ag^+ and Hg^{2+} ions but only 1:1 complexes were found for Tl^+ and Pb^{2+}. Frensdorff (43) showed that the substitution of two oxygen atoms by two sulfur atoms in 18-crown-6 drastically decreases the log K_f (formation constant) value from 6.10 to 1.15 for the potassium complex, but increases it from 1.60 to 4.34 for the silver complex. The results also show that the silver ion has a greater affinity for DT18C6 than the potassium ion. In this case, Frensdorff postulated that in (DT18C6·Ag^+) complex the silver ion can form ionic bonds with

oxygen atoms as well as covalent bonds with sulfur atoms. In a calorimetric study of monothia-18C6 complexes in methanol, Izatt et al. (81) showed that the substitution severely decreases the stability of the Na^+ and K^+ complexes but increases that of the Ag^+ complex. Recent multi-nuclear NMR studies (57) on complexes of Li^+, Na^+, Cs^+, Tl^+ and Ag^+ ion with DT18C6, 18-crown-6, trithia-12-crown-4 and 12-crown-4 in several nonaqueous solvents have showed that in all cases the substitution of the sulfur atoms for the oxygens results in a substantial decrease in the stability of complexes, while the stability of complexes varies inversely with the Gutmann's donor number of the studied solvent (57).

D. Effect of Solvent on The Stability of Macrocyclic Complexes

In the complexation process between crowns and metal ions in solution, macrocycles must compete with the solvent molecules and counterions for the cations in solution. In the case of no data available in literature about the ion pair formation constant of salt, the relative complexing abilities of the ligand without considering the ion pairs formation can be used to represent the lower limits of complex formation constant. The complexation process can be represented by following equation:

$$(M^{n+}) S_x + (Crown) S_y \rightleftharpoons (Crown)^{n+} S_z + (x + y - z)S \qquad (1.1)$$

in w

and

and

the

mat

met

cha

tio

tar

de

ob

ar

st

ma

NP

st

la

r

P

t

t

c

c

s
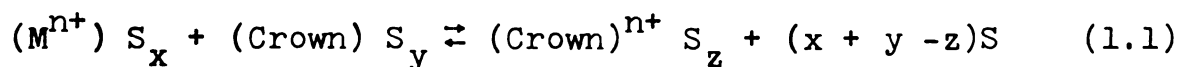
in which M^{n+} is metal ion, S is the solvent molecule, x,y and z are the solvation numbers of the metal ion, the ligand, and the complex respectively. In solution, the metal ion, the crown and the complex are solvated. Therefore, the formation of a complex is a result of competition among the metal ion, the macrocycle, and the solvent. As a result, changing the solvent can significantly affect the complexation process.

In 1971, Frensdorff (43) noted that the stability constant of 18C6 complexes with alkali cation were three to four decades high in methanol than in water. The same effect is observed in the complexation reactions of cis-syn-cis-DC18C6 and cis-anti-cis-DC18C6 (11,59). Popov and co-workers have studied extensively the complexation of alkali cations by macrocycles in various organic solvents using multinuclear NMR techniques (11,82-86). Their studies showed that the stability of macrocyclic complexes depends not only on relative cation size and macrocyclic cavity but also on the nature of the solvent in which complexation takes place.

Observations on DB18C6-cation complexes in DMSO, DMF and PC solutions (51) show a strong solvent effect on complexation. The results are listed in Table 4. In all of the three solvents, the stability constants of alkali ion complexes are enhanced as the donating ability of the medium decreases. When the solvent is changed from the most strongly solvating solvent, DMSO, to the weakest one, PC, the stability

co

3.

th

af

di

th

sn

In

ca

sn

ca

in

Sp

ri

In

t

i

K

r

H

p

i

p

constants (log K) of Li^+ and Cs^+ complexes shift from ≈ 0 to 3.22 and 3.07 to 3.54 respectively. The results indicate the stabilities of the complexes of larger cations are less affected by solvent than those of smaller ones. The large difference in ionic radii between Li^+ and Cs^+ ions derive that the more strongly solvated Li^+ ion has a significantly smaller relative stability constant than the Cs^+ ion in DMSO. In the weakest donor medium (PC), solvent competition toward cation-crown interaction is reduced mostly in the case of smaller cations, so that the interaction effects of the cation with the anionic species become pronounced.

The largely ignored crown-solvent interaction is also an important factor which affects the complexation reaction. Such an interaction appears to be important when the donor ring is small or flexible to form a protonated crown (2). In inclusive and sandwich complexes, the solvent is effectively excluded from the first coordination shell, as shown in Li^+C211, Na^+C222, K^+C222 (inclusive complex) (87,88), and $K^+ (B15C5)_2$ (sandwich complex) (11), the measured physical property becomes insensitive to the solvent and counterion. However, for the $(Cs^+ \cdot C222)$ complex (89) the cation is only partially encapsulated, the solvent or counterion can still interact with the complexed cation, the measured physical property remains depend on the nature of the solvent.

e

n

c

s

T

r

qi

pa

li

po

se

Th

to

po

pro

glo

se

nu

pot

(28

in v

E. Thallium-205 NMR Measurement

The determination of thermodynamics and kinetics of the macrocyclic complexes in solution has been achieved by electrochemical (90,91) spectroscopic (92,93), and calorimetric techniques (94,95). In recent years, NMR spectroscopy has become a powerful technique for studying ionic solvation and complexation reactions in solution (96,97). To a very large extent, this progress is due to the development of Fourier transform NMR spectroscopy. Resonance frequencies and linewidths of alkali ion NMR spectra have been particularly useful in the studies of the alkali complexes.

Nuclear properties of alkali and thallium nuclei are listed in Table 8. Three potassium nuclei, ^{39}K, ^{40}K and ^{41}K, possess a magnetic moment (98). Of these, ^{39}K is the most sensitive as well as the most abundant in nature (93.08%). The sensitivity of this nucleus (5.08 x 10^{-4}) is, however, too low to get good NMR spectra for dilute solutions of potassium salts. Thallium-205 has been proposed as a useful probe for studies of the role of the potassium ion in biological systems (18) because of its relatively large NMR sensitivity, which is 285 times higher than that of the ^{39}K nucleus. Also, its ionic diameter (2.80 Å) is similar to the potassium ion (2.66 Å). The large chemical shift difference (280 ppm) between ^{205}Tl$^+$ in the actins (Figure 1) and ^{205}Tl$^+$ in valinomycin indicates that Tl-205 NMR could be a very

Table 8. *Nuclear Properties of Alkali and Thallium Elements*

Table 8. Nuclear Properties of Alkali and Thallium Elements.

Nucleus	NMR frequency at 14.09 Kilogauss (MHz)	Natural Abundance (%)	Nuclear Spin	Sensitivity Relative to ^{1}H at Constant Field
^{6}Li	8.827	7.43	1	8.51×10^{-3}
^{7}Li	23.315	92.57	3/2	0.294
^{23}Na	15.868	100	3/2	9.27×10^{-2}
^{39}K	2.800	93.08	3/2	5.08×10^{-4}
^{40}K	3.480	1.19×10^{-2}	4	5.21×10^{-3}
^{41}K	1.539	6.91	3/2	8.39×10^{-6}
^{85}Rb	5.792	72.8	5/2	1.05×10^{-2}
^{87}Rb	19.630	27.2	3/2	0.177
^{133}Cs	7.864	100	7/2	4.74×10^{-2}
^{203}Tl	34.284	25.90	1/2	0.187
^{205}Tl	34.619	70.48	1/2	0.192

sensitive probe for the studies of ionic transport across membranes. Thallium-205 NMR could well be used to elucidate details about the type and arrangement of ligand atoms, and the dynamics of the binding and transport processes in naturally occuring membrane channels and pores (99). Bystrov et al. (100) presented the fact that the K^+ and Tl^+ complexes with valinomycin have nearly identical solution structures. The chemical properties of the two ions are sufficiently alike that the Tl^+ ion can replace the K^+ ion in several enzymes.

The solvent dependence of the chemical shift for ^{205}Tl is over 2600 ppm (101) in contrast to a shift range of ≈ 8 ppm for ^7Li (102,82), ≈ 30 ppm for ^{23}Na (103,104), and ≈ 120 ppm for ^{133}Cs (105). The greater sensitivity of the thallium-205 chemical shift to the environment of the Tl^+ ion makes it a better probe than alkali metal ions in ion solvation studies. The chemical shift of thallium-205 has been measured in aqueous solutions of thallium(I) hydroxide, fluoride, acetate formate, nitrate, and perchlorate of varying concentrations (106). In these salts, the ion pair formation is greatest for the hydroxide ion and least for the perchlorate ion.

Thallium-205 NMR has been used for studying preferential solvation (101,107) and the relative solvating ability of the solvent in binary solvent mixtures (108). The order of preferential solvation toward the dimethylthallium ion is HMPA > DMA > DMF > pyridine.

The studies of Tl^+ ion solvation in aqueous amide, mixed amide, water/pyridine, water/DMSO, and pyridine/DMSO mixed solvents were carried out by Hinton et al. (109,110). The results indicate that the structural effects of the solution are important in determining preferential solution. Convington's nonstatistical distribution theory has been used to study preferential solvation of thallium(I) ion in nine binary solvent systems. Using this theory, the equilibrium constants and free energies of preferential solvation were obtained by Hinton et al. (111). Ion pair formation constants of thallium (I) salt in several solvents have been obtained by Hinton et al. (112,113).

CHAPTER II

EXPERIMENTAL

1. Salt and Ligands Purification

Thallium salts were of reagent grade quality.
Thallium(I) nitrate (Alfa) and perchlorate (K & K) were
purified by recrystallization from deionized distilled water
and then dried at 120°C for two days. Ultrapure lithium
chloride and perchlorate (both Alfa) were dried at 190°C for
two days. Anhydrous silver nitrate (Baker, AR) was dried
over P_2O_5 in a vaccum at 65°C for two days. Potassium
hexafluorophosphate (Pfaltz and Bauer) was recrystallized
from deionized distilled water and then dried under vaccum
at 110°C for three days. Potassium tetraphenoborate was
precipitated by reacting potassium nitrite and sodium tetra-
phenoborate in water. The precipitate was washed with
deionized distilled water, recrystallized from acetone and
then dried under vaccum at 60°C for three days.

The ligand, 18-crown-6 (18C6) obtained from the Parish
Chemical Company, was recrystallized by complexing with ace-
tonitrile (114) and then dried under vaccum at 25°C for 2
days. The purified 18C6 melts at 36-37°C [lit. m.p. 36.5-
38.0°C (126), 39-40°C (1)]. Dibenzo-18-crown-6 (DB18C6,
Parish) was recrystallized twice from benzene and dried under
vaccum at room temperature for three days. The purified
DB18C6 melts at 165-166°C [lit. m.p. 164°C (1)]. Substituted
crown, 1,7,10 16-tetraoxa-4,13-diaza-cyclooctadecane (Diaza-

C
T
i
d
6
oj
co
us
Hov
sur

18-crown-6, DA18C6, Merck) was recrystallized from heptane and dried under vaccum at $25^{\circ}C$ for 3 days, while 1,10-dithia-18-crown-6 (DT18C6), obtained from the Parish Chemical company, was dried in vaccum at $50^{\circ}C$ for one day.

The mixture dicyclohexyl-18-crown-6 (DC18C6) diastereomers was separated into two principal components by Izatt and co-workers (115) who had previously identified the two major isomers as the cis-syn-cis (DC18C6-A, m.p. $61-62^{\circ}C$) and cis-anti-cis (DC18C6-B, m.p. $83-84^{\circ}C$) isomers. The structure of these five diastereomers is shown in Figure 9. It should be noted that DC18C6-B also exists in a second crystalline from with m.p. $69-70^{\circ}C$ (49). The two isomers were separated by following the procedure developed by Izatt et al. (115) except that the hydrogen sulfide gas was obtained by the decomposition of a sodium sulfide in a concentrated aqueous solution with 20-30% phosphoric acid. The acid was allowed to drip slowly from a separatory funnel into the sodium sulfide folution, and the evolving H_2S gas dried over $CaCl_2$. Using this method, 31% of isomer B (m.p. $69.0-69.6^{\circ}C$) and 26% of isomers A (m.p. $60.5-61.2^{\circ}C$) were obtained. The two isomers also have been separated by column chromatography on Woelm alumina (activity grade 1) using n-hexane-diethyl ether solvent mixture as eluents (49). However, this separation method is costly and very time consuming with low yields of each isomer (115).

2. Solvent Purification

Propylene carbonate (PC, Aldrich), nitromethane (NM, Aldrich), dimethylformamide (DMF, Mallinckrodt), dimethylsulfoxide (DMSO, Fisher), and tetramethylguanidine (TMG, Eastman) were refluxed over calcium hydride (Aldrich) under reduced pressure for one to three days, then fractionally distilled. Hexamethylphosphoramide (HMPA, Aldrich) was refluxed over calcium oxide (Fisher) under reduced pressure for 24 hours and then fractionally distilled. Tetramethylenesulfone (sulfolane, SF, Aldrich) was refluxed with sodium hydroxide pellets under reduced pressure for 10 hours and then fractionally distilled repeatedly until 1 ml of sulfolane did not develop a visible color within 7 minutes after the addition of an equal volume of 100% sulfuric acid. Acetone (AC, Mallinckrodt), acetonitrile (AN, Mallinckrodt) and tetrahydrofuran (THF, Baker) were refluxed over calcium hydride and then fractionally distilled. Methanol (Mallinckrodt) was refluxed over magnesium turnings and iodine for 12 to 24 hours and then fractionally distilled under nitrogen at atmospheric pressure.

All of these solvents after fractional distillation were transferred in a dry box under a nitrogen atmosphere and further dried for 4-20 hours over freshly activated $3\overset{\circ}{A}$ or $4\overset{\circ}{A}$ molecular sieves. These sieves were washed with distilled water, then dried at $110^{\circ}C$ for several days, and finally

N
S
u
c
f
s
(o
Af
tra
wit
wat

activated to $500^{\circ}C$ under a nitrogen atmoshpere for 24 hours. Solvents such as methanol, DMSO and even acetone decompose and turn yellow after a prolonged standing over molecular sieves (116). The water content of purified solvents was determined using a Varian Aerograph Model 920 gas chromatograph and was found to be always below 100 ppm. The purity of these solvents was also checked by ^{13}C NMR.

The deuterated solvents, chloroform-d (Aldrich Gold Label), acetonitrile-d_3, acetone-d_6, D_2O and methanol-d_4, all from Stohler Isotope Chemicals, were used as received.

3. Sample Preparation

In view of the hydroscopic nature of the nonaqueous solvents and of the reagents, all of the solutions were prepared in a dry box under a nitrogen atmosphere. Samples for mole ratio studies by ^{205}Tl NMR (or ^{13}C NMR) were usually prepared by weighing out the various amount of the complexing ligand (or salt) into a 2 ml volumetric flask followed by dilution with the metal ion solution (or ligand solution) which was previously prepared by dissolving the salt (or the ligand) in a desired solvent or mixed solvents. After dissolution of the ligand (or salt), the solutions were transferred to 10 mm or 8 mm NMR tubes, capped, and wrapped with teflon tape to prevent both contamination by atmospheric water and solvent evaporation.

In the case of the studies of competitive solvation of

Tl^+ ion in mixed solvents, the solutions were prepared by
mixing the desired solvent mixture with concentrated
thallium(I) salt solution which was previously prepared by
dissolving the thallium(I) salt in one of the two solvents.
The resultant mole fraction of each solvent in binary solvent
can be calculated from the known volume and specific gravity
of the solvent.

4.   Intrumental Measurements

   A.   Thallium-205 and Lithium-7 NMR

   All ^{205}Tl and ^7Li measurements were carried out on a
highly modified Varian DA-60 pulsed Fourier transform mode
spectrometer equipped with a wideband probe capable of multi-
nuclear operation (117).   The spectrometer was equipped with
an external proton lock to maintain the stability of the
magnetic field at 14 Kilogauss (1.4 Tesla).   The nicolet FT-
NMRD program (118) was operated by a Nicolet 1080 computer
system for the data acquisition and Fourier transform.
Lithium-7 and thallium-205 were measired at 23.32 MHz and
34.61 MHz respectively.   Non-spinning 10 mm OD NMR tubes
(Wilmad) were used in all studies.   The temperature was
controlled to ± $1^{\circ}C$ as monitored with a calibrated Doric
digital thermocouple.

   In the studies of temperature dependence of the ^{205}Tl
chemical shifts, each sample tube was left in the probe for
15 minutes to reach the equilibrium temperature before

measurement.

The difference of ^{205}Tl chemical shifts in some studied systems was enormous, therefore, most ^{205}Tl NMR data were measured with the highest spectral width (SW) range of DA-60,25000 Hz, which correspounds to 722 ppm for the ^{205}Tl nuclei. The errors of ^{205}Tl chemical shifts depend on the line width of the resonance line and the signal to noise (S/N) ratio. As the line becomes broader or the S/N ratio becomes smaller, the chemical shift measurement becomes less accurate. In some systems, the maximum chemical shift range of ^{205}Tl is smaller than 1000 Hz (29 ppm), in such cases, small spectral width, such as 1000 Hz, can be used for increasing the resolution of the measurement. If, in a studied system, the ^{205}Tl chemical shift range is over 25000 Hz (maximum spectral width on DA-60), the foldover effect (aliasing effect) has to be monitored for very carefully, otherwise a wrong ^{205}Tl chemical shift measurement can be obtained.

As shown in Figure 10, which shows the expected and its serial NMR signal of mirror images are symmetrical about the vertical lines which represent the carrier waves with radio-frequcies V_o, $V_o \pm SW$, $V_o \pm 2SW$, ----- $V_o \pm nSW$.
These images only appear if the Fourier Transform calculation is performed for the frequencies outside the range SW. However, any _real_ line lying outside the sweepwidth SW which derived by wrong selection of radio frequency gives an image at an incorrect chemical shift of the spectrum. This

Fi

Fi
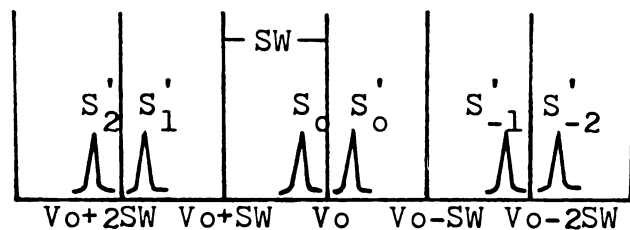
Figure 10. The mirror images obtained from a real line S_0 as a result of Fourier transformation.
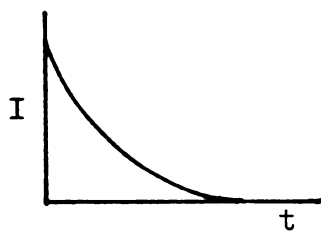
Figure 11. Free induction decay for a set of identical nuclei with Lamor frequency, Vs, excited by a pulse of frequency exactly equal to Vs.

phenomenon must be eliminated to avoid incorrect interpretations.

On the DA-60, the radiofrequency is controlled by mixing an adjustable frequency synthesizer and a 56.4563 MHz RF transmiter. The resonance frequency, Vs, of sample can be obtained by adjusting the frequency synthesizer, until the free induction decay (FID) observed by the oscilloscope, has the shape shown in Figure 11. The total, anticipated, real spectrum of the studied system can be included in the real region by applying a suitable excitation frequency V_O at the edge of the spectrum, and by selecting an appropriate SW which is greater than the expected chemical shift range.

If the FID signal is very weak, we cannot use the above method to find the resorance frequency.

In this case, the following method can be used. On the DA-60, in the same acquisition time, the NMR intensity appearing in the real region is stronger than the one occuring in the imaginary region, so, the radio frequency, V_O, can be selected untill the strongest NMR signal is obtained, then the resonance frequency can be calculated from V_O and the chemical shift of the resonance signal. Figure 12 shows that the relative intensity of ^{205}Tl in an aqueous solution of 1.5 M thallium(I) acetate (A) and 0.3 M thallium(I) nitrate (B) in which the resonance frequency of 34.6164 MHz for (A) and 34.6119 MHz for (B) are calculated. The resonance frequency V_S of the sample can be calculated by the expression
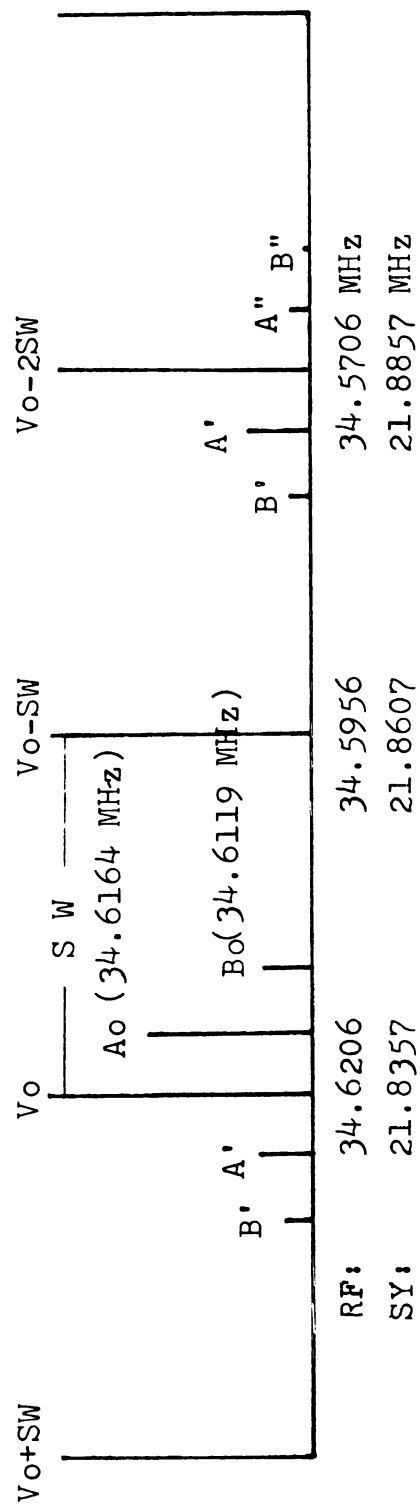
Figure 12. The real and imaginary NMR spectra of 1.5 M thallium(I) acetate (A) and 0.3 M thallium(I) nitrate (B) on DA-60 spectrometer (SY: synthesizer frequency, RF: resonance frequency, SW: 25000 Hz).

V_s

wh

qu

ch

fr

ir

8

wi

s

c

a

c

I

t

s

s

a

w

t

t

t

$$V_s \text{ (MHz)} = 56.4563 - SY - SW + CU \qquad (2.1)$$

where SY and CU are the synthesizer and the cursor fre-
quencies in MHz. Figure 12 shows that the magnitude of the
chemical shift increases with increasing SY or decreasing
frequency V_o in real region but the inverse effect is found
in imaginary region.

In ^{7}Li NMR measurements a sepctral width of 1000 Hz with
8K memory was used, and the chemical shifts were accurate to
within ± 0.1 ppm. In ^{205}Tl NMR measurements, generally a
spectral width of 25000 Hz with 8k memory was used. In this
case, the accuracy of the chemical shift is within ± 0.5 ppm.

B. Chemical Shift Reference and Correction

The chemial shift of thallium-205 was first referred to
a 1.5 M aqueous solution of thallium(I) acetate, and then
corrected to an infinitely dilute aqueous solution of the
Tl^+ ion. The correction value for 1.5 M aqueous solution of
thallium(I) acetate solution is +124 ppm. All ^{7}Li chemical
shift measurements are referenced to an external standard
solution of 4 M $LiClO_4$ in H_2O. Reference solutions for ^{205}Tl
and ^{7}Li measurements were sealed in 5 mm NMR tubes which
were coaxially sealed into 10 mm tubes. The space between
the two tubes was evacuated and vaccum-sealed. In this way,
the chemical shift of reference solution will not be affected
by ambient temperature change (119). In this thesis the

d

f

v

T

T

r

r

δ

δ
c

Wh

su

pe

ch

th

is

Equ

whe

of

we

sal

neg

wit

9.

downfield chemical shift (high resonance frequency shift) from the reference is indicated as positive. The sign convention for NMR spectrum will be discussed in APPENDIX 1. The same external reference method was used in our studies. The reported chemical shifts were corrected for the differences in bulk diamagnetic susceptibility between sample and reference according to the following equations (120).

$$\delta_{corr} = \delta_{obs} + \frac{2\pi}{3} (K_{sample} - K_{reference}) \qquad (2.2)$$

$$\delta_{corr} = \delta_{obs} + \frac{4\pi}{3} (K_{reference} - K_{sample}) \qquad (2.3)$$

Where $K_{reference}$ and K_{sample} are the unitless volumetric susceptibility (121) of the reference and sample solvent respectively, δ_{corr} and δ_{obs} are the corrected and observed chemical shifts respectively. Equation (2.2) is applied to the DA-60 spectrometer in which the applied magnetic field is transverse across the long axis of the sample tube, while Equation (2.3) applies to the Bruker WM-250 spectrometer where the polarizing magnetic field is along the long axis of the cylindrical sample tube. Dilute solutions (0.01 M) were used in our study, so the contribution of the added salt to the volumetric susceptibility of the solution was neglected (121). The correction values for various solvents with respect to water on DA-60 and WM-250 are given in Table 9. Line widths at half-height ($\Delta\nu$) of about 12-20 Hz was

observed without spinning. Two solvent properties, dielectric constant and Gutmann donor member (122,123) are also listed in Table 9.

C. Proton and Carbon-13 NMR

All ^{1}H and ^{13}C NMR measurements were obtained on a Bruker WM-250 spectrometer operating at a resonance frequency of 250.13 MHz and 62.89 MHz for ^{1}H and ^{13}C respectively. The spectrometer was locked by deuterium signal operating at a fixed frequency of 38.397 Mhz to maintain the stability of the megnetic field at 58.75 KG. The proton RF frequency is derived from a 10 MHz master quartz oscillator, mixed with a synthesizer frequency to 83.38 MHz, pulsed and then tripled to 250.13 MHz and amplified to 25 watts. The spectrometer was coupled to an Aspect 1000 minicomputer with 48K of memory. The probe heads are equipped for internal ^{2}D locking, ^{1}H decoupling and variable temperature.

The sample solution of ^{13}C was usually contained in an 8 mm o.d. NMR tube (Wilmad) which was coaxially centered by teflon spacers in a 10 mm o.d. NMR tube containing deuterated solvent as the lock. The sample solution of ^{1}H was contained in an 5 mm o.d. NMR tube which contains some deuterated solvent as the lock. The reported ^{13}C chemical shifts were corrected for the differences in bulk diamagnetic susceptibility between sample and reference according to equation (2.3).

Table 9. Key Solvent Properties and Correction for Diagnostic C

Table 9. Key Solvent Properties and Correction for Diamagnetic Susceptibility on the Varian DA-60 and on the Bruker WM-250.

Solvent	Dielectric Constant	Gutmann[b] Donor Number	BVDS[a] $\delta \times 10^6$	Correction[c] on DA-60 δ_{corr} (ppm)	Correction[c] on WM-250 δ_{corr} (ppm)
Nitro-methane	35.9	2.7	-0.319	+0.689	-1.378
Aceto-nitrile	38.0	14.1	-0.534	+0.390	-0.78
Sulfolane	42.0	14.8	-	-	-
Propylene carbonate	65.0	15.1	-0.634	+0.180	-0.360
Acetone	20.7	17.0	-0.460	+0.545	-1.09
Methanol	32.7	25.7	-0.515	+0.429	-0.858
N,N-dimethyl-formamide	36.7	26.6	-0.500	+0.308	-0.616
Dimethyl-sulfoxide	46.7	29.8	-0.605	+0.241	-0.482
Pyridine	12.4	33.1	-0.612	+0.226	-0.452
Water	78.5	33.0	-0.720	+0.000	+0.000
Hexamethyl-phosphoramide	30.0	38.2	-	-	-

[a]Bulk Volume Diamagnetic Susceptibility. [b]Reference (122,123). [c]$\delta = \delta_{obs} + \delta_{corr}$

D. <u>Data Handling</u>

The formation constant of complexes in various system and ion association constants of lithium salts were calculated on a CDC-6500 computer by fitting the NMR data with appropriate equations using a non-linear least squares program KINFIT (124).

CHAPTER III

COMPLEXATION OF THALLIUM(I) SALTS
BY 18-CROWN-6 AND ITS SUBSTITUTED
ANALOGS IN VARIOUS SOLVENTS

1. Introduction

The significant correlation of selectivity with cavity size for crown ethers is restricted essentially to 18-crown-6 and its substituted analogs. The main purpose of this thesis is to study the complexation of the Tl^+ ion with 18-crown-6 and its substituted analogs in various solvents, especially in nonaqueous solvents. Such studies provide useful information for separation chemistry and a valuable model to investigate the transportation of metal ion across synthetic or natural biological membranes.

It has been found that nuclear magnetic resonance of alkali nuclei, such as ^7Li, ^{23}Na and ^{133}Cs is one of the most powerful techniques for studying the complexation of metal ions with macrocycles in aqueous as well as in non-aqueous solutions (57,97,126,127). Thallium-205 NMR has also become an important probe for investigating the complex-ation and solvation characteristics of the Tl^+ ion (57,110-112) which has been proposed as an NMR probe for studies of the role of potassium ions in biological systems (18). The chemical shift of thallium-205 is very sensitive to the chem-ical environment change of thallium(I) ion (101), so that the NMR chemical shift and linewidth of the Tl^+ ion may give valuable information about the ion-ligand, ion-solvent, and ion-ion interactions.

The complexation reaction of 18C6 with thallium(I) ion has been studied quite extensively in aqueous solution, but less attention has been paid to studies of the complexing abilities between thallium(I) ion and a series of derivatives of 18C6. The work presented in this chapter investigates the complexation reaction of the Tl^+ ion with a series of crowns, such as 18C6, DC18C6, DB18C6, DA18C6 and DT18C6, in aqueous and several nonaqueous solvents by using thallium-205 and carbon-13 NMR techniques. These studies not only provide the stability constants of different complexes but also give useful information about the effects of the solvent, and the different donor atoms of the ligands. Typical solvents, such as nitromethane, acetonitrile, acetone, sulfolane, dimethyl-sulfoxide and hexamethylphosphoramide were chosen as the reaction media.

2. <u>Selection of External Reference Solution for Thallium-205 NMR.</u>

The external reference method was selected for thallium-205 NMR studies. This method is advantageous in eliminating the possibility of intermolecular interactions or chemical reactions between the reference compound and the sample solution. Two aqueous solutions, 1.5 M thallium(I) acetate and 0.3 M thallium(I) nitrate, were chosen as the external references. Occasionally, these two solutions have been used for detecting the foldover effect which is described in

detail in section II-4-A. The chemical shift of thallium-205 was first referred to an external reference, and then corrected to that of an infinitely dilute aqueous solution of Tl^+ ion. Downfield (paramagnetic) shifts are taken as positive.

The thallium-205 chemical shifts of thallium(I) perchlorate and thallium(I) nitrate in water solution are given in Table 10 and the variation of thallium-205 chemical shift as a function of thallium(I) salt concentration are plotted in Figure 13. In both solutions, the ^{205}Tl chemical shift varies linearly with the concentration of the thallium(I) salt and the two lines intersect at the point of zero salt concentration (infinitely-dilute solution).

An increase in the concentration of thallium(I) salt in an aqueous solution results in the replacement of solvent molecules in the thallium ion inner solvation sphere by anions. The effect of these replacements may either increase or decrease the electron density of the cation depending on the properties of the anion. Comparing this with the results obtained by Shih (45), we can conclude that the replacement of solvent molecules by symmetric polyatomic anions such as PF_6^-, ClO_4^-, BPh_4^-, and NO_3^-, will reduce the electron density of the cation resulting a upfield shift for paramagnetic nuclei, while for halide anions the replacement will increase the electron density of the cation inducing a downfield shift of the resonance. The possible reason may be that, in a

Table 10. Thallium-205 Chemical Shifts of Thallium(I) Salts in Water at 25°C.

Salt	Concentration (M)	δ (ppm)
TlNO$_3$	0.4000	- 2.0
	0.3000	0
	0.2000	1.7
	0.1000	3.5
	0.0500	4.6
	0.0010	5.9
	0.0005	5.1
TlClO$_4$	0.5000	-22.8
	0.4000	-17.8
	0.3000	-12.9
	0.2000	- 6.9
	0.1000	- 1.4
	0.0500	1.7
	0.0250	3.3
	0.0050	5.3
	0.0025	5.0
	0.0010	5.2
	0.0008	5.1
	0.0005	5.3
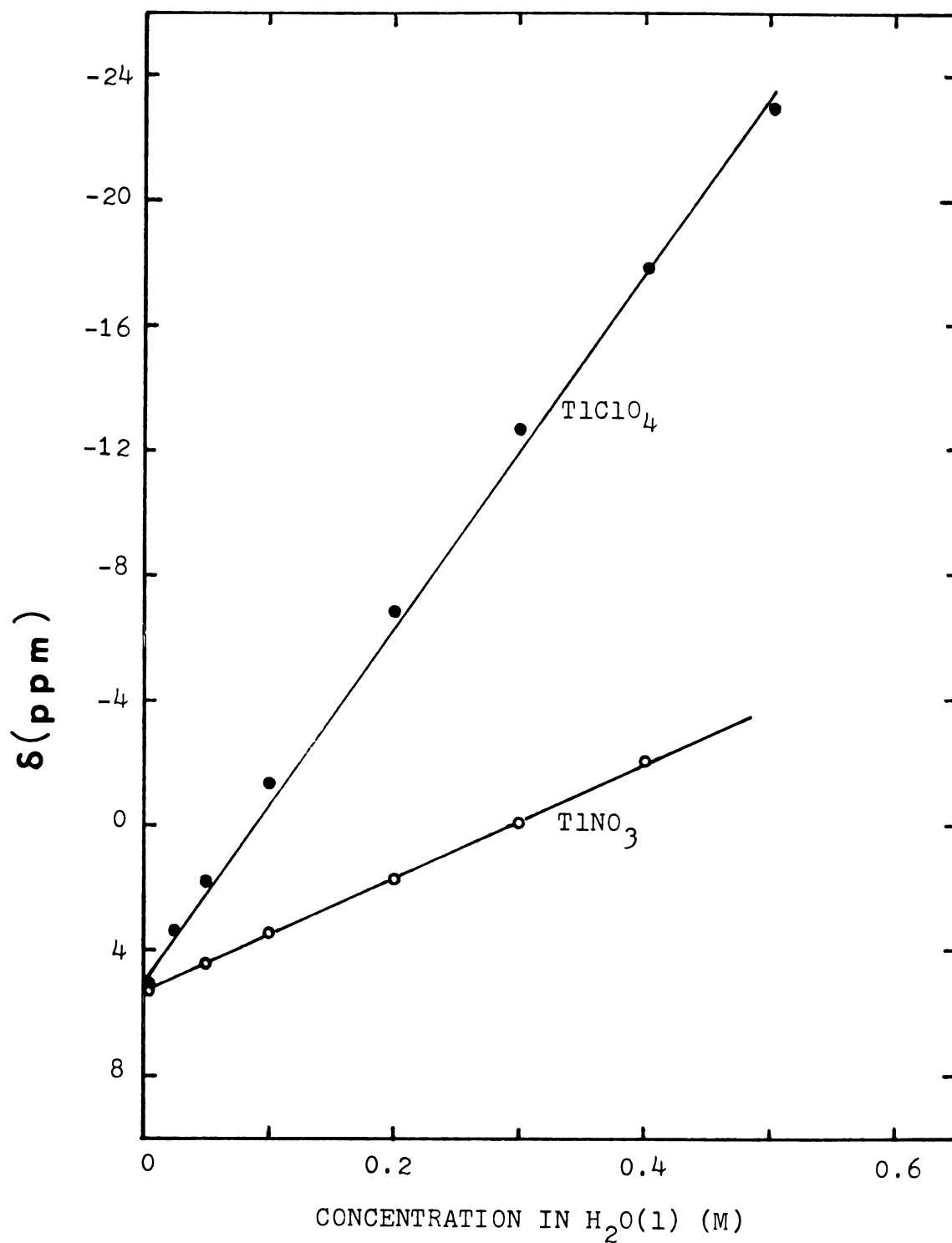
Figure 13. Thallium-205 chemical shifts vs. thallium(I) salt concentration in water at 25°C (0.3 M $TlNO_3$ in H_2O as reference).

symmetric polyatomic anion, the negative charge can be distributed on its large surface homogeneously, so it becomes a poor electron donating group relative to halide anions.

The measurement indicates that the ^{205}Tl chemical shift for 0.3 M of thallium(I) nitrate and 1.5 M of thallium(I) acetate are, a 5.5 ppm upfield shift and a 124 ppm downfield shift referenced to infinite-dilution aqueous Tl^+ ion solution as zero. According to these measurements, one can calculated the chemical shifts by the following relationships,

$$\delta_s = \delta_o - \delta_{r1} - 5.5 \qquad (3.1)$$

or

$$\delta_s = \delta_o - \delta_{r2} + 124 \qquad (3.2)$$

where δ_s is the corrected sample chemical shift, δ_{r1} and δ_{r2} are the observed chemical shifts of 0.3 M $TlNO_3$ and 1.5 M $TlOOCCH_3$ external standard solutions respectively, δ_o is the observed sample chemical shift.

3. Results and Discussion

A. Complexation of the Tl^+ Ion by DB18C6

The compound $TlClO_4$ is readily soluble in many organic solvents and should be only slightly associated when the dielectric constant of solvent is high. Therefore, this salt was chosen for our complexation studies. The dependence of the Tl-205 chemical shift on the mole fraction of DB18C6/$TlClO_4$

in various solvents is given in Table 11 and these data are plotted as shown in Figure 14. It is obvious that the solvent plays an important role in the complexation process.

Figure 14 shows that the thallium-205 resonance shifts downfield with increasing the DB18C6/Tl$^+$ molar ratio in the solvents with low Gutmann donor numbers such as nitromethane, sulfolane and acetonitrile, but it moves upfield in high solvating solvents, such as dimethylformamide, dimethylsulfoxide and hexamethylphosphoramide. The data show that, in most studied solvents, the ligand ring size is adequate to accomodate the Tl$^+$ ion resulting in the formation of 1:1 complexes. In Figure 14, two straight lines with intersection at 1 (ligand/metal ion) in the mole ratio plot in nitromethane solution, compared with the plots in other solvents, is an indication of the formation of a stronger complex between DB18C6 and Tl$^+$ ion in nitromethane than in all other studied solvents. However, in dimethylsulfoxide and hexamethylphosphoramide solutions, the ^{205}Tl chemical shift varies linearly with increasing DB18C6/Tl$^+$ mole ratio which indicates that the further addition of crown must provide a change in the environment of the Tl$^+$ ion or be used to form weak complexes and hence produces a chemical shift which varies linearly with ligand (crown) concentration.

It is obvious that, in the (Tl·DB18C6)$^+$ complex, the Tl$^+$ cation sits in the crown cavity and is only partially encapsulated, and may form an ion-pair with the anion. In the

Table 11. Dependance of the Tl-205 Chemical Shifts on DB18C6/TlClO$_4$(0.01 M) in Various Solvents.

NM			AN			SF		
L/Tl$^+$	δ(ppm)	Δν(Hz)	L/Tl$^+$	δ(ppm)	Δν(Hz)	L/Tl$^+$	δ(ppm)	Δν(Hz)
0	-373.4	39	0.00	-218.00	18	0.00	-267.9	23
0.33	-322.3	57	0.49	-174.53	18	0.35	-251.8	244
0.50	-292.3	58	1.00	-129.99	18	0.56	-242.7	66
0.72	-262.5	57	1.39	-130.00	18	0.82	-233.2	41
1.00	-220.1	57	1.71	-130.88	18	1.04	-227.0	41
1.31	-220.4	57	2.04	-131.23	18	1.39	-224.8	23
1.72	-222.2	38	3.40	-132.73	18	1.94	-224.3	23
2.00	-221.0	38	4.37	-132.82	18	3.00	-224.1	23
2.40	-222.3	38	5.34	-133.97	18	4.23	-223.9	17
3.14	-222.4	38						

Table 11. Continued.

DMF			DMSO[a]			HMPA[a]		
L/Tl$^+$	δ(ppm)	Δν(Hz)	L/Tl$^+$	δ(ppm)	Δν(Hz)	L/Tl$^+$	δ(ppm)	Δν(Hz)
0.00	122.9	29	0	394.6	120	0.00	519.9	686
0.38	73.8	50	0.22	394.5	120	0.43	520.1	910
0.61	46.6	66	0.55	392.9	150	0.72	517.4	1113
0.96	6.9	72	0.78	388.1	162	1.06	516.8	900
1.38	-18.7	72	1.17	384.6	168	1.36	515.3	985
1.93	-48.2	53	1.53	383.1	162	1.69	514.3	1000
2.76	-73.0	47	2.14	375.4	162	2.42	511.6	900
			2.53	374.0	186			
			3.36	363.3	210			
			4.03	356.9	210			
			4.56	351.6	210			
			5.28	341.2	210			

[a]Concentration of TlClO$_4$ is 0.005 M.
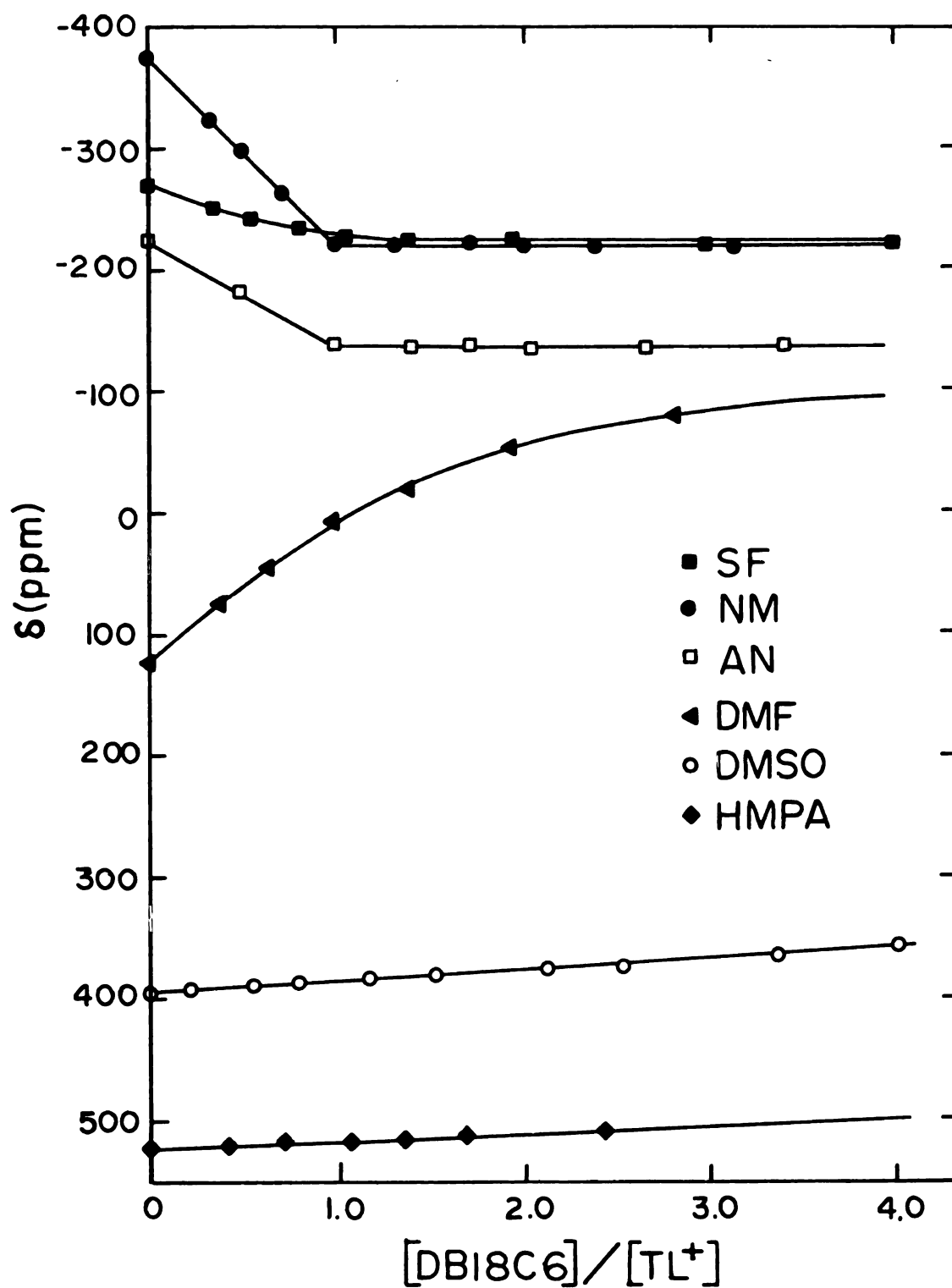
Figure 14. Thallium-205 chemical shifts vs. DB18C6/Tl$^+$ mole
ratio in various solvents.

studied system, the Tl^+ ion may exist in the following solute species: free Tl^+ ions, ion-paired Tl^+ ions, complexed Tl^+ ions, and ion-paired complexed Tl^+ ions. When the exchange between various Tl^+ ions is fast on the NMR time scale, only a population averaged chemical shift is observed. Those can be represented by:

$$\delta_{obs} = \sum_i X_i \delta_i \qquad\qquad (3.3)$$

$$\sum_i X_i = 1$$

where X_i and δ_i are the mole fractions and chemical shifts of the species containing the thallium(I) cation, and δ_{obs} is the observed chemical shift. The complexation reactions between the thallium(I) salt (TlX) and the crown ether (C) in solution may be represented by:

$$Tl^+ + solvent \rightleftharpoons Tl^+ \cdot solvent \qquad\qquad (3.4)$$

$$Tl^+ + X^- \underset{}{\overset{K_{ip}}{\rightleftharpoons}} Tl^+ \cdot X^- \qquad\qquad (3.5)$$

$$Tl^+ + C \underset{}{\overset{K_c}{\rightleftharpoons}} (Tl \cdot C)^+ \qquad\qquad (3.6)$$

$$TlC^+ + X^- \underset{}{\overset{K_{ic}}{\rightleftharpoons}} TlC^+ X^- \qquad\qquad (3.7)$$
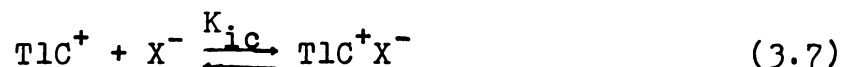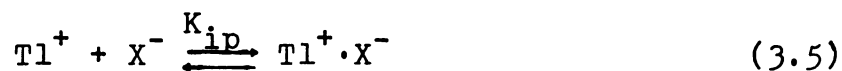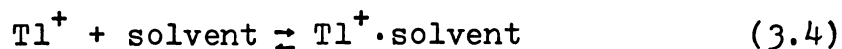
in which $Tl^+ \cdot solvent$, $Tl^+ X^-$, $Tl \cdot C^+$ and $TlC^+ X^-$ are the

solvated Tl^+ ions, ion-paired Tl^+ ions, complexed Tl^+ ions and ion-paired complexed Tl^+ ions respectively. It is important to note that both contact and solvent-separated ion-pairs exist in Tl^+X^- and TlC^+X^-. Since the minimum concentration of the Tl^+ ion measured on the DA-60 is about 10^{-4} M and the ^{205}Tl linewidth increases dramatically with decreasing Tl^+ ion concentration (112), the constants, K_{ip} and K_{ic}, are difficult to measure by NMR techniques. Unfortunately, there are no data available in the literature concerning the ion pair formation constants of thallium(I) perchlorate in various solvents. Therefore, the formation constants appeared in our work are <u>lower limits</u> which represent the <u>relative</u> complexing abilities of the ligands in various solvents. In our work, we assume that complexation is the major cause of the variation of the chemical shift. According to this assumption, the equation (3.3) can be represented as

$$\delta_{obs} = \delta_{f'}X_{f'} + \delta_c X_c \tag{3.8}$$

where
$$\delta_{f'}X_{f'} = \delta_f X_f + \delta_{ip}X_{ip} + \delta_{ic}X_{ic} \tag{3.9}$$

The relative formation constants of the 1:1 ($Tl^+ \cdot DB18C6$) complex were obtained by analyzing the ^{205}Tl chemical shift versus mole ratio data with a weighted nonlinear least-squares curvefitting program (124) with the equation:

$$\delta_{obs} = [(KC_M^T - KC_L^T - 1) + (K^2 C_L^{T2} + K^2 C_M^{T2} - 2K^2 C_L^T C_M^T + 2KC_L^T +$$

$$2KC_M^T + 1)^{\frac{1}{2}}](\frac{\delta_M - \delta_{ML}}{2KC_M^T}) + \delta_{ML} \qquad (3.10)$$

In equation (3.10), the total concentration of the cation (C_M^T) and the ligand (C_L^T) are known, δ_M is determined by measuring the cationic chemical shift in the absence of the ligand. Two unknown quantities, K and δ_{ML}, can be calculated by an iteration method using the program KINFIT, starting with reasonable estimates of K and δ_{ML} and adjusting K and δ_{ML} value until the calculated chemical shifts correspond to the experimental values within the error limits of the measurement. The calculated formation constants (K) and the limiting chemical shifts (δ_{ML}) of the $Tl^+ \cdot DB18C6$ complex in various solvents are shown in Table 12. For very stable $Tl^+ \cdot$ crown complex, only the lower limit of $K=10^5$ could be obtained by our technique.

The total thallium-205 chemical shift range for the complexation study of $(Tl \cdot DB18C6)^+$ complex in acetone was only 5 ppm. A 1000 Hz spectral width (28 ppm for ^{205}Tl) was, therefor, selected in this study. The thallium-205 chemical shift-mole ratio data for complexation of Tl^+ by DB18C6 in acetone are shown in Table 13. It is interesting to note that in acetone solution the ^{205}Tl resonance shifts downfield as the $DB18C6/Tl^+$ mole ratio increases from 0 to 1. Shifts upfield with further addition of the ligand are shown in Figure 15. These results show that in acetone solution DB18C6 froms

Table 12. Stability Constants and Limiting Chemical Shifts of $(DB18C6 \cdot Tl)^+$ and $(Cis-syn-cis-DC18C6 \cdot Tl)^+$ in Various Solvents.

Solvents	ε	DN	$(DB18C6 \cdot Tl)^+$		$(cis-syn-cis-DC18C6 \cdot Tl)^+$	
			Log K_f	δ_{lim}(ppm)	Log K_f	δ_{lim}(ppm)
NM	35.9	2.7	> 5	-222.4 ± 0.2	> 5	-105.0 ± 0.2
AN	38.0	14.1	> 5	-137.3 ± 0.2	> 5	- 92.0 ± 0.2
AC	20.7	17.0	3.39 ± 0.22 (1:1) 1.36 ± 0.22 (2:1)	-235.6 ± 0.4 (1:1) -294.8 ± 98.9 (2:1)	> 5	-137.5 ± 0.2
SF	42.0	14.8	4.04 ± 0.06	-223.8 ± 0.1	4.10 ± 0.07	-127.1 ± 0.2
DMF	36.1	26.6	2.13 ± 0.03	-143.8 ± 5.1	2.78 ± 0.06	- 51.3 ± 2.2
H_2O	78.5	33.0	1.50 ± 0.02[a]	-	2.44 ± 0.04[b]	-
DMSO	45.0	29.8	≈ 0	-	1.26 ± 0.04	-196.6 ± 34.9
HMPA	30.0	38.2	≈ 0	-	-	-

[a] Reference (59)
[b] Reference (10)

Table 13. The Variation of ^{205}Tl Chemical Shifts with DB18C6/TlClO$_4$(0.004 M) in Acetone (SW=1000 Hz).

L/Tl$^+$	δ(ppm)	$\Delta\nu$(Hz)
0	-240.4	15
0.21	-239.5	15
0.42	-238.9	18
0.50	-238.5	16
0.56	-238.1	16
0.69	-237.9	18
0.80	-237.9	16
0.97	-237.7	18
1.08	-237.8	18
1.18	-237.9	18
1.35	-238.2	16
1.50	-238.7	16
1.70	-239.5	16
1.87	-239.8	18
2.05	-240.5	18
2.29	-241.4	20
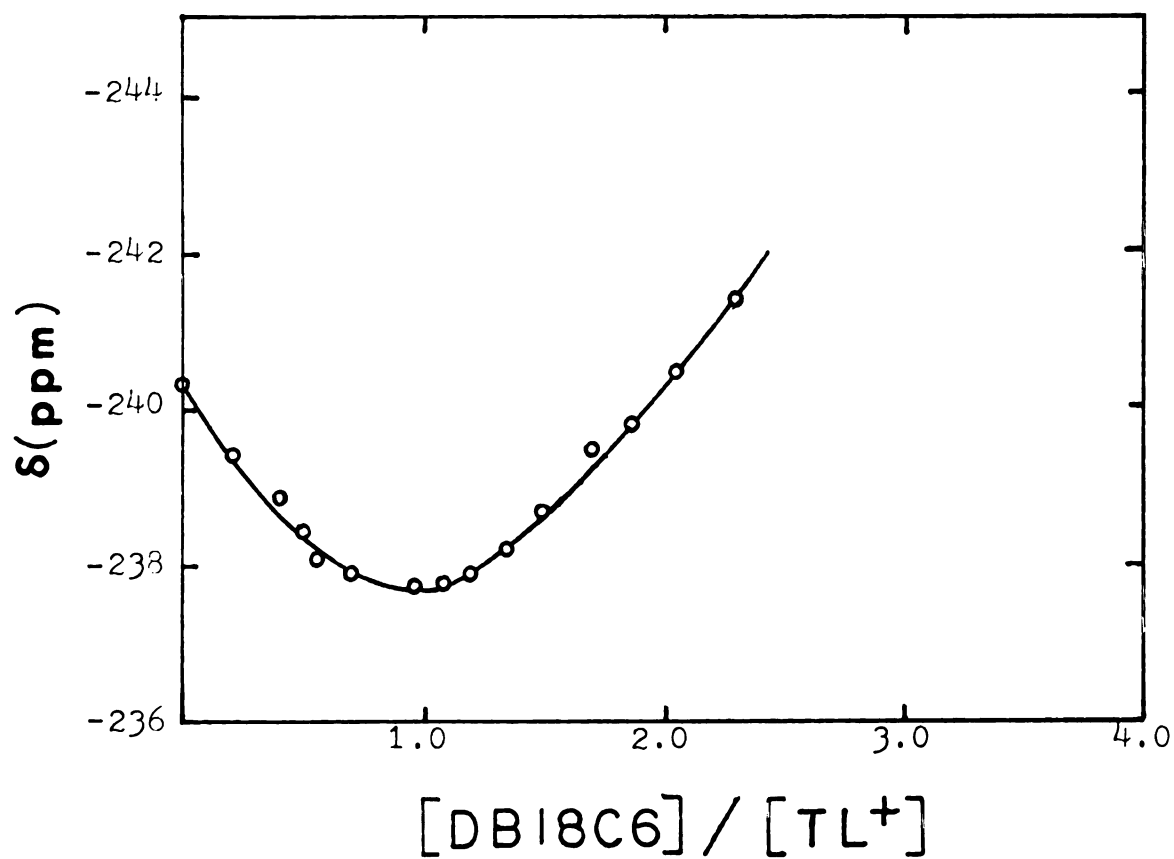
Figure 15. Chemical shifts of Tl-205 vs. DB18C6/Tl$^+$ (0.004 M) mole ratio in acetone.

both 1:1 and 2:1 complexes with the thallium(I) ion. In
this system, the observed chemical shift can be expressed as

$$\delta_{obs} = \delta_M X_M + \delta_{ML} X_{ML} + \delta_{ML_2} X_{ML_2} \qquad (3.11)$$

where M, ML and ML_2 are the solvated cations, 1:1 complexed
metal ions and 2:1 complexed metal ions respectively. The
complex formation constants K_1 and K_2 can be calculated by
the methods described in APPENDIX 2-B. The calculated for-
mation constants and limiting chemical shifts are also shown
in Table 12.

The data collected in Table 12 show that the stability
constants of the $(DB18C6 \cdot Tl)^+$ complex in various solvents
vary in the order nitromethane, acetonitrile > sulfolane >
dimethylformamide > water > dimethylsulfoxide, hexamethyl-
phosphoramide. In general, as shown in Table 12, the sta-
bility of the complex increases with decreasing solvent
Gutmann donor number. These results indicate that, in com-
plexation reactions, the donor ability of a solvent plays a
more important role than the dielectric constant. It is
obvious that in strongly solvating solvents the competition
between the solvent molecules and the ligands for the coor-
dination sites of the cation should decrease the formation
constant of the complex. The formation constant of the
$(DB18C6 \cdot Tl)^+$ complex in acetonitrile seems too large to be
determined accurately by NMR techniques which is coincident

with the previously reported value, log K=4.90 (48).

Table 12 shows that the limiting chemical shifts of the (DB18C6·Tl)$^+$ complex in sulfolane, nitromethane, acetonitrile and dimethylformamide vary by as much as 100 ppm. These results indicate that in this complex the Tl$^+$ ion is only partially encapsulated by the ligand, and the solvent molecules and/or counter ions can still interact with the vacant coordination sites of the complexed Tl$^+$ ion.

B. Complexation of the Tl$^+$ ion by cis-syn-cis-DC18C6

The measured thallium-205 chemical shifts at different ligand/Tl$^+$ mole ratios for complexation of the Tl$^+$ ion by cis-syn-cis-DC18C6 in various solvents are given in Table 14 and plotted in Figure 16. The results show that only 1:1 complexes are formed in these systems. In nitromethane and sulfolane solutions, the ^{205}Tl resonance cannot be observed when the ligand/Tl$^+$ mole ratio is between 0 and 1, due to a dramatic increase in the linewidth. A probable reason for this line broadning is the slow exchange of Tl$^+$ ions between solvated and complexed sites. When the ligand/Tl$^+$ mole ratio is greater than 1, all Tl$^+$ ions are complexed by the crown ligand, and the ^{205}Tl linewidth become small again.

The relative formation constants of the 1:1 complex have been obtained by analyzing the ^{205}Tl chemical shift versus mole ratio data as described in section III-3-A. The calculated formation constants and limiting chemical shifts for

Table 14. Dependance of ^{205}Tl Chemical Shifts on cis-syn-cis-DC18C6/TlClO$_4$ (0.01 M) in Various Solvents.

	NM		AN			AC		
L/Tl$^+$	δ(ppm)	Δν(Hz)	L/Tl	δ(ppm)	Δν(Hz)	L/Tl	δ(ppm)	Δν(Hz)
0.00	-372.8	37	0.00	-233.3	12	0.00	-238.4	14
0.30	-	-	0.30	-193.0	185	0.42	-196.3	220
0.43	-	-	0.50	-163.4	223	0.60	-175.3	211
0.92	-119.2	324	0.90	-110.8	192	0.87	-150.0	99
1.01	-107.6	155	1.01	- 96.9	33	0.95	-142.1	50
1.20	-107.4	152	1.20	- 96.0	33	1.26	-138.7	44
1.48	-107.2	148	1.52	- 95.2	33	1.68	-138.4	44
2.02	-106.8	155	2.03	- 95.0	28	2.12	-137.8	32
2.78	-106.0	150	2.30	- 94.6	28	2.71	-137.6	32
3.33	-105.2	159	3.42	- 94.5	25	3.38	-137.2	32
			4.42	- 92.6	25	4.01	-137.0	26
						4.62	-136.8	26

Table 14. Continued.

SF			DMF			DMSO		
L/Tl$^+$	δ(ppm)	Δν(Hz)	L/Tl$^+$	δ(ppm)	Δν(Hz)	L/Tl$^+$	δ(ppm)	Δν(Hz)
0.00	-265.6	12	0.00	130.0	27	0.00	364.6	146
0.22	-235.5	940	0.15	109.0	140	0.31	343.0	280
0.55	-190.4	1758	0.40	72.0	236	0.67	314.1	318
0.68	-	-	0.56	56.2	285	1.01	284.3	384
0.83	-155.6	973	0.87	19.3	261	1.30	267.5	377
1.00	-139.6	478	1.07	3.8	253	1.45	259.8	482
1.10	-134.5	363	1.25	-6.4	174	1.91	236.2	531
1.37	-129.8	363	1.58	-17.3	171	2.32	211.5	561
1.80	-128.3	355	1.80	-30.7	161	2.99	179.1	579
2.85	-128.2	350	2.50	-33.2	142	3.56	159.5	579
3.42	-127.8	177	3.53	-37.9	119	4.36	130.9	500
4.35	-127.0	168	4.19	-45.3	114	5.17	107.3	512

- resonance spectrum cannot be obtained.
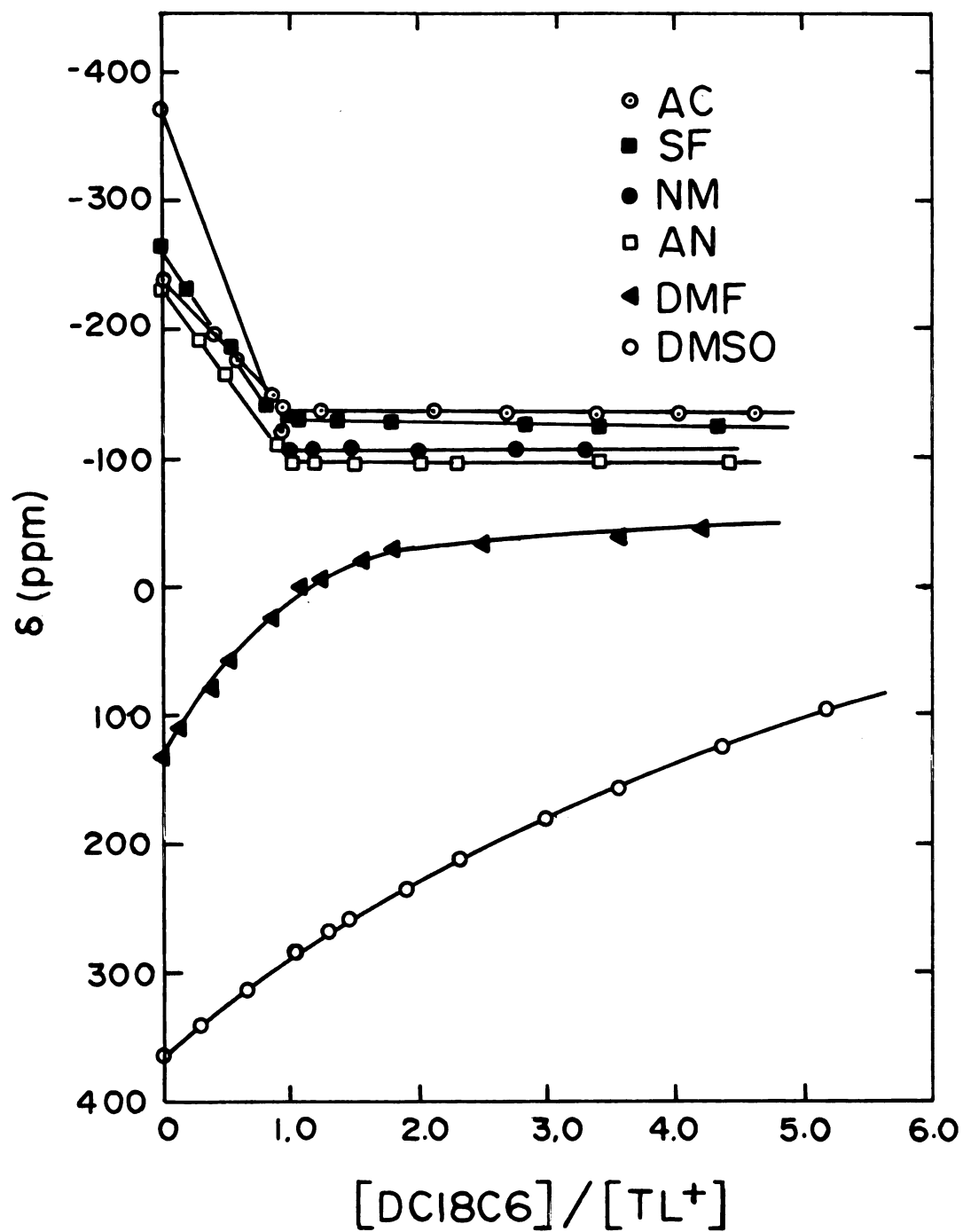
Figure 16. Chemical shifts of Tl-205 <u>vs.</u> the cis-syn-
cis-DC18C6/Tl$^+$ mole ratio in various
solvents.

the $(cis\text{-}syn\text{-}cis\text{-}DC18C6 \cdot Tl)^+$ complex in various solvents are presented in Table 12. The results show that the variation of the solvents can significantly affect the binding properties of the ligand. In solvents with weak solvating ability such as nitromethane, acetonitrile and acetone, the ^{205}Tl chemical shift is strongly affected by addition of the ligands, and the mole ratio plot consists of two straight lines intersecting at the 1:1 mole ratio. This behavior indicates that the Tl^+ ion is strongly complexed by the cis-syn-cis-DC18C6.

In such cases, the formation constants cannot be determined by NMR techniques and we can only conclude that the $\log K_f > 5$. It should be noted that, in an acetonitrile solution, polarographic measurements by Hofmanova et al. (48) gave a $\log K_f$ value of 7.40.

The stability constants of the $(cis\text{-}syn\text{-}cis\text{-}DC18C6 \cdot Tl)^+$ complex in various solvents decrease with increasing Gutmann donor number of the solvents (Table 12) in the order nitromethane, acetonitrile, acetone > sulfolane > demethylformamide > dimethylsulfoxide > hexamethylphosphoramide.

C. <u>Complexation of the Tl^+ Ion by 18C6</u>

The complexation between the thallium(I) ion and 18C6 in organic solvents such as nitromethane, acetonitrile, acetone, dimethylformamide and dimethylsulfoxide, has been studied previously (57). The studies of the same complex in two more

solvents, such as the sulfolane and hexamethylphosphoramide, were used as a supplement for a series of comparisons with other comparable complexes. Thallium-205 chemical shifts at different $18C6/Tl^+$ mole ratios are given in Table 15 and illustrated in Figure 17 which show that only 1:1 complex is formed in the two solutions.

The relative formation constants have been obtained as described in APPENDIX 2-A. For comparison purposes, the results of this work and Rounaghi's work (57) are collected in Table 16. The data show that the formation constant of the complex in hexamethylphosphoramide, log K_f=1.35, is much lower than those in dimethylsulfoxide, water, dimethyl-formamide, sulfolane, acetone, acetonitrile, and nitromethane solutions. These results reflect the much stronger Tl^+ ion solvation by hexamethylphosphoramide as compared with other solvents. Of these solvents, hexamethylphosphoramide has highest Gutmann donor number (DN=38.2) but an intermediate dielectric constant (θ=30.0). Once again, the results verify that, in the complexation reaction, the donor ability of a solvent plays a more important role than the dielectric constant.

The complexation reaction was also studied by carbon-13 NMR. The data are listed in Table 17. By fitting the variation of the ^{13}C chemical shift versus the $TlClO_4/18C6$ mole ratio (Figure 18), the stability constant of log K_f= 3.43 $\pm$ 0.08, was obtained, which is in good agreement with the value

Table 15. The Variation of ^{205}Tl Chemical Shifts with 18C6/TlClO$_4$ (0.01 M) Mole Ratio in SF and HMPA.

	SF			HMPA	
L/Tl$^+$	δ(ppm)	Δν(Hz)	L/Tl$^+$	δ(ppm)	Δν(Hz)
0	-267.4	31	0.00	471.9	300
0.30	-250.1	677	0.76	402.6	400
0.64	-229.5	610	1.23	364.0	400
0.79	-221.2	554	1.60	337.0	400
0.86	-217.8	475	1.90	317.2	602
0.97	-212.5	264	2.23	293.8	624
1.05	-210.2	123	2.93	242.9	663
1.17	-209.0	70	3.40	237.0	663
1.40	-208.0	65	4.26	203.8	663
1.97	-207.4	40	5.00	177.2	663
2.61	-207.3	35	5.50	165.0	663
			5.90	152.2	663
			7.02	130.2	663
			7.90	110.1	663
			8.80	96.7	663
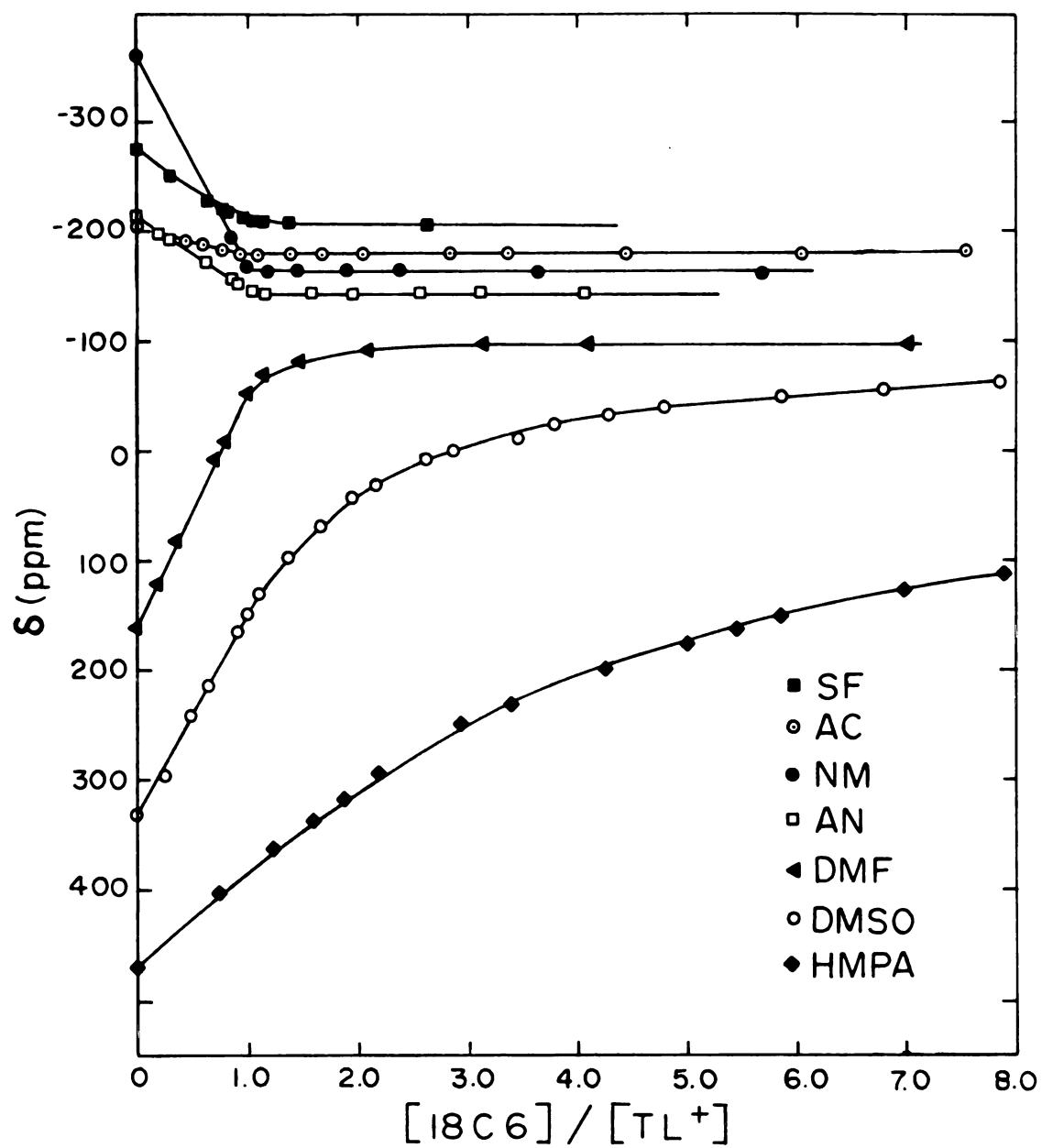
Figure 17. Chemical shifts of Tl-205 vs. 18C6/Tl$^+$ mole
ratio in various solvents.

Table 16. Stability Constants and Limiting Chemical Shifts of $(18C6 \cdot Tl)^+$, $(DA18C6 \cdot Tl)^+$ and $(DT18C6 \cdot Tl)^+$ in Various Solvents.

Solvents	$(18C6 \cdot Tl)^+$		$(DA18C6 \cdot Tl)^+$		$(DT18C6 \cdot Tl)^+$	
	Log K_f	δ_{lim}(ppm)	Log K_f	δ_{lim}(ppm)	Log K_f	δ_{lim}(ppm)
NM	> 5[a]	-165.0±0.2	> 5	651.3±0.2	> 5[a]	250.0±0.2
AN	> 5[a]	-147.5±0.2	> 5	700.3±0.2	4.16±0.06	388.7±0.3
AC	> 5[a]	-187.6±0.2	> 5	737.0±0.2	3.12±0.04	316.2±0.9
SF	4.23±0.04	-207.1±0.1	> 5	706.1±0.2	2.66±0.03	346.0±3.0
DMF	3.43±0.08[b]	-125.6±0.6	3.55±0.06	766.5±0.6	1.19±0.06	168.2±3.0
H_2O	2.27±0.04[c]	-	0.96±0.01	824.7±13.4	-	-
DMSO	1.92±0.01[a]	- 80.0±0.2	2.39±0.02	666.0±2.7	≈ 0	-
HMPA	1.35±0.02	-114.5±15.0	-	-	≈ 0	-

[a]Reference (57)
[b]Studied by ^{13}C NMR
[c]Reference (10)

Table 17.   The Variation of ^{13}C Chemical Shifts with
Tl^+/18C6(0.04 M) in DMF with AN-d_3 as Reference.

Tl^+/L	δ(ppm)
0.00	69.95
0.21	69.82
0.36	69.70
0.52	69.62
0.60	69.56
0.69	69.51
0.76	69.48
0.87	69.42
1.00	69.36
1.10	69.35
1.20	69.34
1.37	69.33
1.67	69.32
2.03	69.32
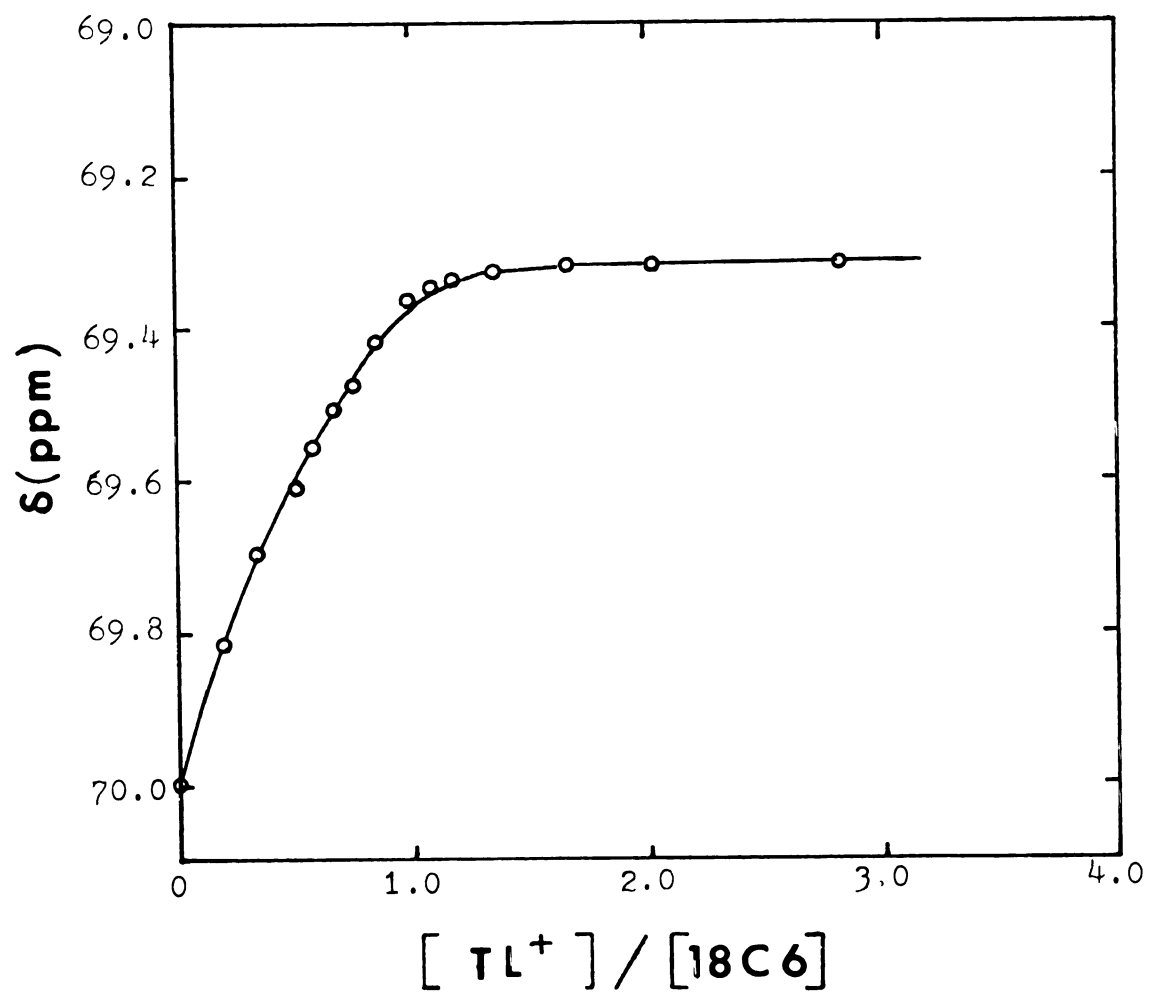
Figure 18. Chemical shifts of C-13 <u>vs</u>. $Tl^+/18C6(0.04$ M) mole ratio in dimethylformamide.

of log K_f=3.35±0.06, obtained by ^{205}Tl NMR (57). The results clearly show that both ^{205}Tl and ^{13}C NMR techniques can be used for complexation study. However, in general, ^{205}Tl nuclei are a better NMR probe than ^{13}C nuclei because the ^{205}Tl resonance is more sensitive to the change of the environment of the Tl$^+$ ion.

D. Complexation of the Tl$^+$ ion by DA18C6

The complexation between DA18C6 and the Tl$^+$ ion has been previously investigated in this laboratory by Shamsipur (70). At that time, he did not notice the foldover effect (section II-4-A) therefore, incorrect ^{205}Tl chemical shift measurements were obtained.

The variations of the ^{205}Tl chemical shift with the DA18C6/TlClO$_4$ mole ratio in various solvents are shown in Table 18 and 19. The plots of the ^{205}Tl chemical shift as a function of the DA18C6/TlClO$_4$ mole ratio are shown in Figure 19. It seems that only 1:1 complex is formed in all studied solvents. In the solvents of weak donor ability such as nitromethane, acetonitrile, acetone and sulfolane, the resonant frequency of ^{205}Tl is strongly affected by the addition of the ligand, and the plot (Figure 19) consists of two straight lines with an intersection at a 1:1 DA18C6/Tl$^+$ mole ratio. These results indicate the existance of a very stable complex;the lower limit for the formation constants determined by NMR techniques, Log K_f=5, is reported for these

Table 18. Thallium-205 Chemical Shift-Mole Ratio Data for 0.01 M TlClO$_4$ Complex with DA18C6 in Various Solvents at 24°C.

L/Tl$^+$	NM δ(ppm)	NM Δν(Hz)	L/Tl$^+$	AN δ(ppm)	AN Δν(Hz)	L/Tl$^+$	AC δ(ppm)	AC Δν(Hz)
0.00	-372.8	36	0.00	-233.3	14	0.00	-238.4	14
0.42	-	-	0.63	-	-	0.59	-	-
0.95	619.4	458	1.03	698.2	45	0.80	-	-
1.02	650.3	98	1.42	698.5	36	0.95	733.5	94
1.44	650.5	86	1.85	698.7	28	1.06	733.6	40
2.01	650.7	76	2.24	699.2	21	1.41	733.7	36
2.50	651.0	72	2.95	699.8	21	1.96	733.8	36
3.24	651.3	60	3.26	699.9	21	2.53	733.9	36
4.05	651.2	51	3.89	699.7	21	3.20	734.8	36
4.76	651.3	42	4.36	700.2	21	4.02	735.9	36
						4.82	736.8	36

Table 18. Continued.

L/T1$^+$	SF^a δ(ppm)	SF^a Δν(Hz)	DMF L/T1$^+$	DMF δ(ppm)	DMF Δν(Hz)	DMSO L/T1$^+$	DMSO δ(ppm)	DMSO Δν(Hz)
0.00	−266.7	21	0.00	131.3	40	0.00	364.4	228
0.13	−	−	0.25	286.3	1272	0.34	433.9	290
0.27	−	−	0.36	−	−	0.61	473.1	303
0.57	−	−	0.80	600.7	580	0.93	517.0	289
0.71	−	−	1.05	700.9	284	1.28	546.4	259
0.86	700.4	103.5	1.20	720.1	232	1.71	576.2	186
1.07	700.2	214	1.45	735.8	101	1.97	589.8	168
1.18	701.2	179	1.56	740.5	94	2.23	601.2	136
1.41	702.2	51	2.08	748.6	82	2.85	620.3	136
1.96	704.1	51	2.15	749.3	87	3.32	627.6	128
2.40	704.1	51	2.80	757.0	75	4.04	630.9	120
2.88	705.2	51	3.91	759.9	62	4.85	635.7	96
4.10	706.1	51	5.13	762.7	56			

Table 19. Thallium-205 Chemecal Shift-Mole Ratio Data for 0.01 M $TlClO_4$ Complex with DA18C6 in H_2O at $24°C$.

L/Tl^+	δ (ppm)	$\Delta\nu$ (Hz)
0.00	− 2.5	21
0.15	7.6	27
0.27	18.3	39
0.53	35.0	42
0.63	40.1	45
0.76	46.5	59
0.90	55.1	78
1.05	63.0	70
1.20	73.2	66
1.41	85.2	71
1.70	95.6	78
2.10	121.4	71
2.76	152.7	71
2.76	152.7	78
3.89	204.0	71
4.50	227.0	71
5.20	252.0	78
5.72	268.7	71
7.00	307.6	71
9.26	364.4	71
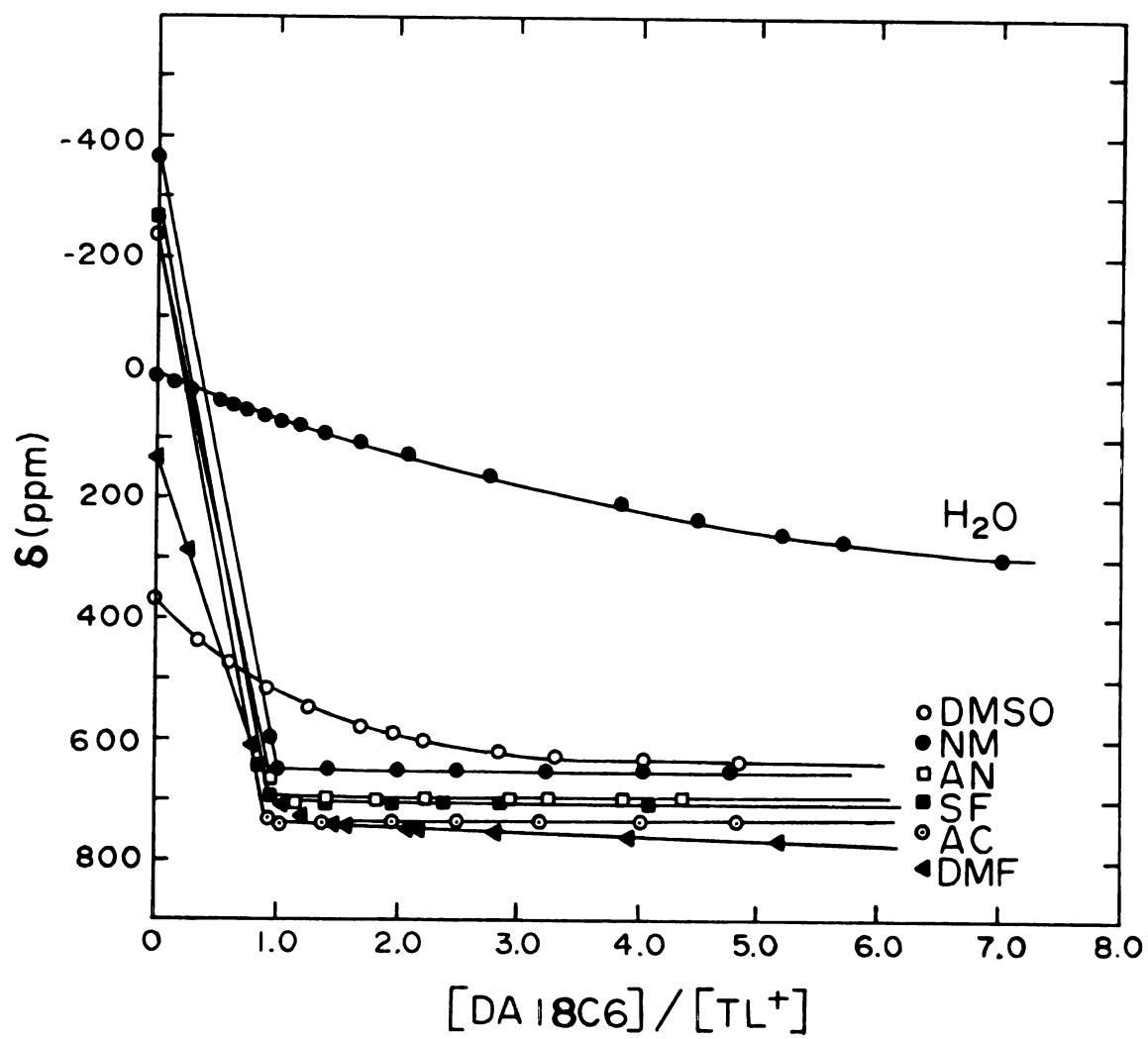
Figure 19. Chemical shifts of Tl-205 vs. DA18C6/Tl$^+$ mole ratio in various solvents.

solvents. It is interesting to note that in nitromethane, acetonitrile, acetone and sulfolane solutions all of the ^{205}Tl chemical shift differences between solvated Tl$^+$ ion and the thallium(I) complex are over 1000 ppm which is larger than the maximum spectral width, 722 ppm, on the DA-60 spectrometer. In these studied systems, we need to shift the detecting window frequently by the procedures described in section II-4-A to avoid the appearance of the foldover effect.

The calculated relative formation constants and limiting chemical shifts for the (DA18C6·Tl)$^+$ complex in various solvents are listed in Table 16. The data indicate that the stability constants of the (DA18C6·Tl)$^+$ complex in various solvents decrease in the order nitromethane, acetonitrile, acetone, sulfolane > dimethylformamide > dimethylsulfoxide > water. This is the same order as shown in the (18C6·Tl)$^+$, (DB18C6·Tl)$^+$, and (cis-syn-cis-DC18C6·Tl)$^+$ complexes. The results indicate that, even in the complex of the mixed donor crown ether and Tl$^+$ ion, the donor number scale of a solvent shows a more significant role than the dielectric constant.

In Figure 19, the data show that the thallium-205 resonance shifts downfield with an increasing DA18C6/Tl$^+$ mole ratio even in high donor ability solvents, such as dimethylformamide and dimethylsulfoxide, which is not the same trend as found with (18C6·Tl)$^+$ (DB18C6·Tl)$^+$, and (cis-syn-cis-DC18C6·Tl)$^+$ complexes. The results indicate that the interaction force between the Tl$^+$ ion and the ligand is stronger

in $(DA18C6 \cdot Tl)^+$ than in $(18C6 \cdot Tl)^+$, $(DB18C6 \cdot Tl)^+$ and (cis-syn-cis-DC18C6 \cdot Tl)^+$ complexes, so that even in the high solvating solvent the ^{205}Tl chemical shift still shifts downfield.

E. Complexation of the Tl^+ Ion by DT18C6

The complex of Tl^+ ion with DT18C6 in nitromethane, acetone, acetonitrile and dimethylformamide has been previously studied in this laboratory (57). These studies were extended to three more solvents: sulfolane, dimethylsulfoxide and hexamethylphosphoramide (Table 20). The formation constants of this complex were compared with those of its analogs, such as $(18C6 \cdot Tl)^+$, $(DB18C6 \cdot Tl)^+$, (cis-syn-cis-DC18C6 \cdot Tl)^+$ and $(DA18C6 \cdot Tl)^+$. In dimethylsulfoxide and hexamethylphosphoramide soultions, the ^{205}Tl chemical shift does not change with increasing $DT18C6/Tl^+$ mole ratio (Figure 20) which indicates that no complex is formed. The stability constant of log $K_f = 2.66 \pm 0.03$ for the $(DT18C6 \cdot Tl)^+$ complex in sulfolane was obtained.

The complexation between the Tl^+ ion and DT18C6 in acetonitrile was studied and the measured ^{205}Tl chemical shift at different ligand/Tl^+ mole ratios are given in Table 20 and plotted in Figure 20. Previously, Rounaghi (57) reported that both 1:1 and 2:1 complexes were formed in this system. After repeated study, we found that their conclusion was incorrect due to Rounaghi's disregard of foldover effect.

Table 20. Thallium-205 Chemical Shift-Mole Ratio Data for 0.01 M TlClO$_4$ complex with DT18C6 in Various Solvents at 24°C.

AN[a]		AC		SF[b]			DMSO	
L/Tl$^+$	δ(ppm)	L/Tl$^+$	δ(ppm)	L/Tl$^+$	δ(ppm)	Δν(Hz)	L/Tl$^+$	δ(ppm)
0.00	-231.8	0.00	-236.9	0.00	-267.6	23	0.00	360.3
0.60	137.0	0.51	15.3	0.17	-197.2	991	0.29	359.8
0.75	225.2	0.71	96.8	0.59	3.4	1881	0.73	358.7
0.80	250.3	0.90	151.2	0.78	68.1	1326	0.93	359.3
0.86	285.0	1.01	173.9	0.90	96.2	1032	1.23	361.4
0.93	322.2	1.28	223.9	1.10	141.2	892	2.13	360.5
0.95	333.0	1.82	267.6	1.42	199.6	1078	2.60	359.8
0.99	349.5	2.22	232.6	1.80	237.0	720	3.95	359.3
1.04	362.5	2.99	295.6	2.24	262.0	304	4.71	361.5
1.17	375.0	3.54	296.8	3.25	287.5	167		
1.25	377.2	5.30	305.5	4.55	312.5	66		
1.30	379.3							
1.40	383.2							
1.60	387.4							
2.35	387.4							
3.36	387.7							
4.75	387.6							

Table 20. Continued.

L/Tl$^+$	HMPA	
	δ(ppm)	Δν(Hz)
0.00	470.5	220
0.30	470.6	244
0.79	470.8	244
1.52	470.8	286
2.10	471.0	286
2.51	471.0	280
3.20	471.0	280

[a]Concentration of TlClO$_4$ is 0.02 M

[b]Studied at 31°C
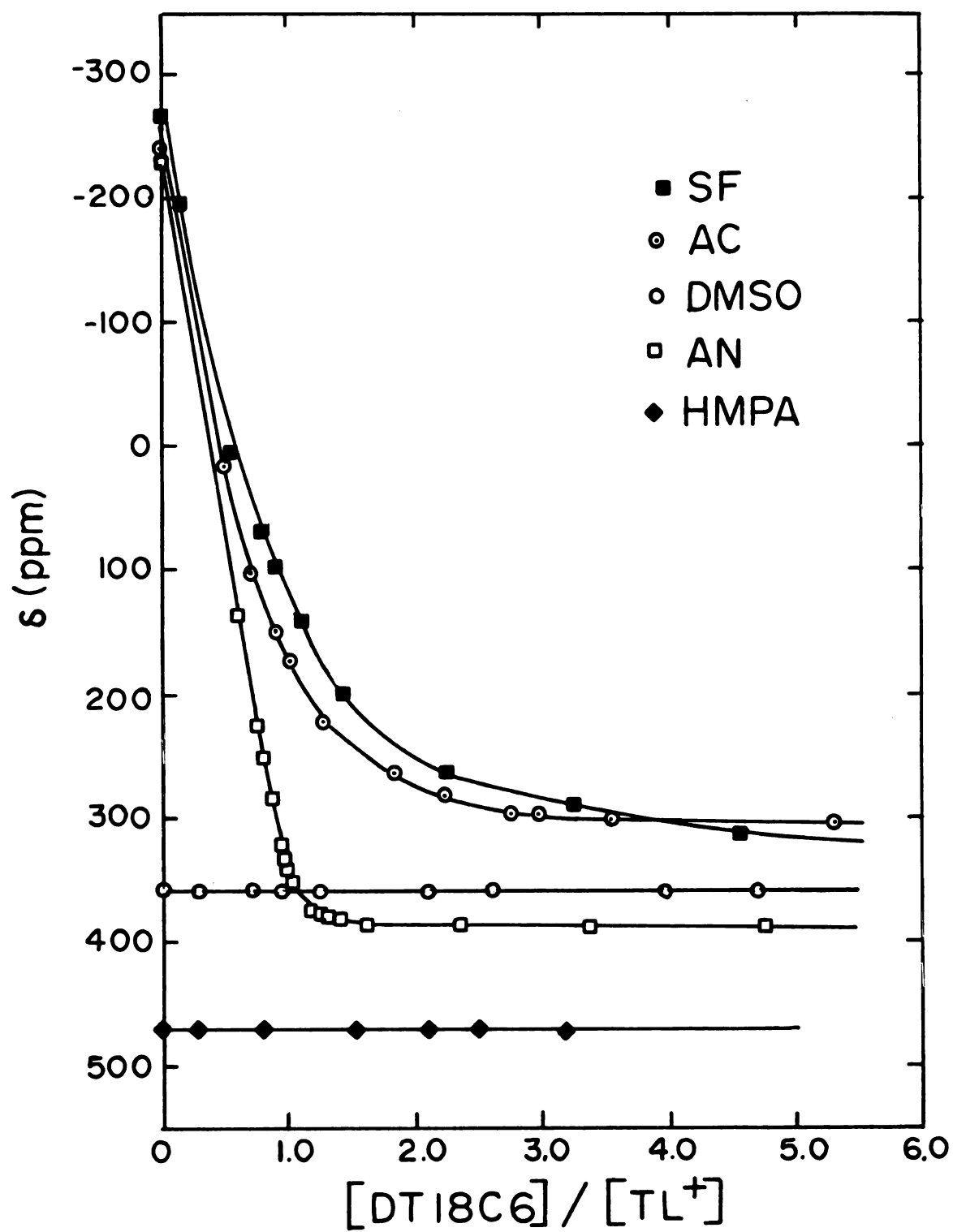
Figure 20. Thallium-205 chemical shifts vs. DT18C6/Tl$^+$ mole ratio in various solvents.

The stability constant and limiting chemical shift obtained from our data are $\log K_f = 4.16 \pm 0.06$ and $\delta_{lim} = 388.7 \pm 0.3$ ppm respectively.

F. Comparison of the Results

The stability constants of the Tl^+ ion complexes with 18C6 and its analogs in various solvents, which were obtained in this work and by previous investigators (10,57,59), are collected in Table 21. The results show that the complex stability decreases in the order $(DA18C6 \cdot Tl)^+ > (18C6 \cdot Tl)^+ > (cis\text{-}syn\text{-}cis\text{-}DC18C6 \cdot Tl)^+ > (DB18C6 \cdot Tl)^+ > (DT18C6 \cdot Tl)^+$. Previous reports (43,64-66) show that the complexation of macrocyclic polyethers with alkali or alkaline earth ions is weakened appreciably as -NH- is substituted for -O- in the crown ether ring. However, the inverse result is observed for $(DA18C6 \cdot Tl)^+$ complex as was also found in the $(DA18C6 \cdot Ag)^+$ complex (43). The possible reason may be due to the fact that the basicity of the nitrogen atom is softer than that of the oxygen atom which produces an increase in the bond strength between the soft Tl^+ ion and the nitrogen donor atom.

The presence of two aliphatic cyclohexo substitutents in cis-syn-cis-DC18C6 increases the rigidity of the crown ether ring causing a drop in the stability of $(cis\text{-}syn\text{-}cis\text{-}DC18C6 \cdot Tl)^+$ as compared with the $(18C6 \cdot Tl)^+$ complex. In the $(DB18C6 \cdot Tl)^+$ complex, two benzo rings lend rigidity to the

Table 21. Stability Constants of the Thallium(I) Complexes in Various Solvents.

Solvents	ε^a	DN^b	Log K_f				
			$18C6 \cdot Tl^+$	$DB18C6 \cdot Tl^+$	$DC18C6\text{-}A \cdot Tl^{+c}$	$DA18C6 \cdot Tl^+$	$DT18C6 \cdot Tl^+$
NM	35.9	2.7	$> 5^d$	> 5	> 5	> 5	$> 5^d$
AN	38.0	14.1	$> 5^d$	> 5	> 5	> 5	4.16 ± 0.06
AC	20.7	17.0	$> 5^d$	$3.39\pm0.02(1:1)$ $1.36\pm0.22(2:1)$	> 5	> 5	3.12 ± 0.04
SF	42.0	14.8	4.23 ± 0.04	4.04 ± 0.06	4.10 ± 0.07	> 5	2.66 ± 0.03
DMF	36.1	26.6	3.43 ± 0.08^e	2.13 ± 0.03	2.78 ± 0.06	3.55 ± 0.03	1.19 ± 0.06
H_2O	78.5	33.0	2.27 ± 0.04^f	1.50 ± 0.02^g	2.44 ± 0.04^f	0.96 ± 0.01	0.93 ± 0.14^d
DMSO	45.0	29.8	1.92 ± 0.01^d	≈ 0	1.26 ± 0.04	2.39 ± 0.02	≈ 0
HMPA	30.0	38.2	1.35 ± 0.02	≈ 0	-	-	≈ 0

a Solvent dielectric constant
b Gutmann donor number
c DC18C6-A is cis-syn-cis-DC18C6
d Reference (57)

e Studied by ^{13}C NMR
f Reference (10)
g Reference (59)

ligand and withdraw electrons from the basic oxygen donors, thus decreasing the bonding between the Tl^+ ion and the ligand. The aliphatic cyclohexo substituent contained in cis-syn-cis-DC18C6 is more flexible than the benzene substituent in DB18C6, so that the stability constant of the (cis-syn-cis-DC18C6·Tl)$^+$ complex is larger than that of the (DB18-C6·Tl)$^+$ complex.

In the same solvent, the stability constant of the (DT18C6·Tl)$^+$ complex is smaller than those of the other four complexes. Two factors seem to be important in causing this drop of the stability constant. The first factor is that the structure of the DT18C6 in solution may be the same as in the solid state which directs its two sulfur atoms away from the cavity to make the cavity too small to fit the Tl^+ ion exactly. The other factor may be that only the outwardly turned sulfur atoms of DT18C6 participate in coordiantion with the Tl^+ ion which is the case of $PdCl_2$·DT18C6 complex (Figure 8).

Pearson (128) has suggested that the interaction of metal ions and ligands can be explained in terms of their "hardness" or "softness". This principle states that "Hard acid prefer harder bases". From the above discussion, it is obvious that the interaction force between S-Tl (soft base-soft acid) is stronger than that between O-Tl (hard base-soft acid). Although the thallium(I) ion prefers binding

with the two sulfur atoms on DT18C6 rather than with the oxygen atoms on 18C6, a decrease in the stability constant is observed for the (DT18C6·Tl)$^+$ complex. The possible reason may be due to the fact that there are six O-Tl coordination bonds in the (18C6·Tl)$^+$ complex but only two S-Tl bonds in (DT18C6·Tl)$^+$. A total interaction force of six weak O-Tl bonds may be larger than the sum of two strong S-Tl bonds.

The data collected in Table 21 clearly indicate that the solvent plays an import role in the complexation process. It is interesting to note that in acetone DB18C6 forms both 1:1 and 2:1 (ligand:metal) complexes with the Tl$^+$ ion. In all of the other systems studied, only the 1:1 complex has been found. The results show that the stability constants of five studied complexes in various solvents generally decrease with increasing Gutmann donor number of the solvent. It can be concluded that, in a complexation reaction, the donor ability of a solvent plays a more important role than the dielectric constant. When the complexation reaction takes place in a strongly solvating solvent, such as dimethyl-sulfoxide or hexamethylphosphoramide, the solvent molecules exhibit a strong competition with the ligand for the coordination sites of the cation and produce a decrease in the complex formation constant. The stability constants of five complexes in various solvents decrease with increasing Gutmann donor number in the order nitromethane > acetonitrile > acetone >

sulfolane > dimethylformamide > water > dimethylsulfoxide >
hexamethylphosphoramide.

Ion pairing has been proposed as a possible factor to
affect chemical shift for ^{7}Li (129,130), ^{23}Na (103,104) and
^{133}Cs(105) NMR. Because Li$^+$ and Na$^+$ have quite small ionic
radii compared to Tl$^+$ or Cs$^+$, it might be expected that
solvation would be more important in determining the shift
for the Li$^+$ and Na$^+$ ions. The Cs$^+$ and Tl$^+$ ions have larger
ionic radii and are less strongly solvated. In this case,
ion pairing would be expected to be much more important,
especially in a nonaqueous solvent with low dielectric con-
stant. Figure 21 shows that the thallium-205 chemical shift
range of the solvated Tl$^+$ ion in different solvents is $\approx$900
ppm. In general, the ^{205}Tl resonance shifts upfield in low
solvating solvents such as nitromethane, sulfolane, acetone,
and acetonitrile, but shifts downfield in high solvating sol-
vents such as dimethylformamide, dimethylsulfoxide and hexa-
methylphosphoramide.

It is also interesting to note that in low solvating
solvents, such as nitromethane, sulfolane, acetone and aceto-
nitrile, the limiting ^{205}Tl chemical shifts of (Tl·18C6)$^+$,
(Tl·DB18C6)$^+$ and (DC18C6·Tl)$^+$ complexes are downfield compared
with the solvated Tl$^+$ ion but they shift upfield in highly
solvating solvents, such as hexamethylphosphoramide, dimethyl-
sulfoxide, dimethylformamide and water. When complexation
reactions take place in a low solvating solvent, the ligands
play an important role in determining the electron density
around Tl$^+$ ion. In the complexes (18C6·Tl)$^+$, (DB18C6·Tl)$^+$ and
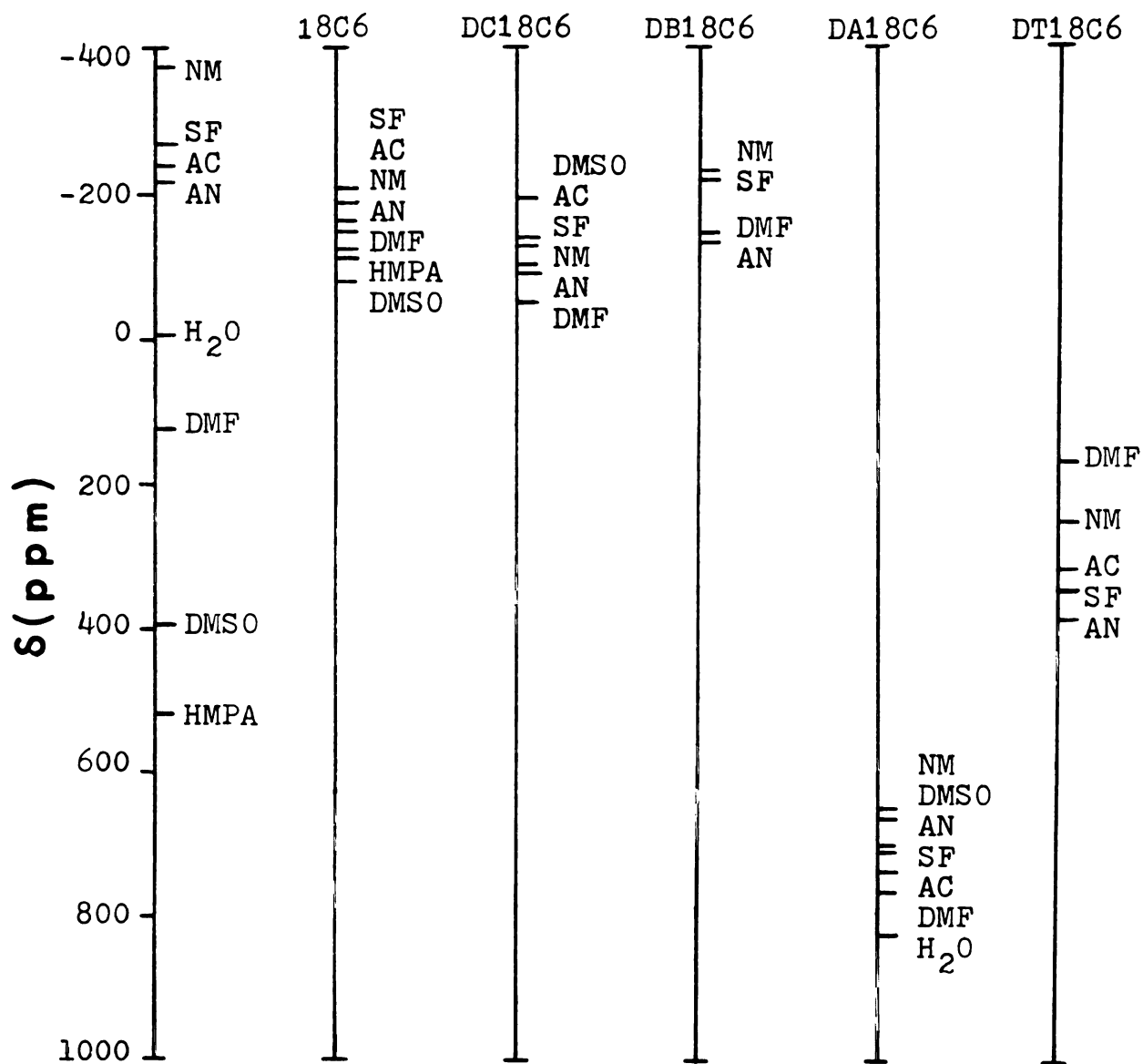
Figure 21. Thallium-205 chemical shifts of solvated Tl^+ ion and the limiting chemical shifts of $(Tl^+$-Crown) complexes.

(cis-syn-cis-DC18C6·Tl)$^+$, the electron density of the Tl$^+$ ion is enhanced by the encircling electronegative oxygen atoms, which results in a downfield shift.

In a highly solvating solvent, the Tl$^+$ ion is enclosed tightly by the solvent molecules. This arrangement causes extensive sp hybridization ($5d^{10}$ 6sp) and result in enhancing the electron density of the Tl$^+$ ion greatly. When a complexation reaction takes place, the ligand molecule will replace the solvent molecules occupying several coordination sites around the Tl$^+$ ion. In general, crown ether molecules are more rigid than solvent molecules, which will create several vacancies around the Tl$^+$ ion as the complex is formed. Some of these vacancies are too small to accommodate a single solvent molecule. Therefore, in the complex, the electron density around the Tl$^+$ ion will be less as compared with the solvated Tl$^+$ ion inducing an upfield shift.

However, in all of the solvents studied, the limiting chemical shifts of (Tl·DA18C6)$^+$ and (Tl·DT18C6)$^+$ move downfield compared with the solvated Tl$^+$ ion. A possible reason may be due to the fact that the thallium(I) ion is a soft acid which may prefer to coordinate with sulfur and nitrogen atoms (soft base) rather than with oxygen atoms (hard base). The electron density around the Tl$^+$ ion may be increased by the effect of these acid-base coordination bonds which will induce a downfield shift.

As shown in Figure 21, the limiting chemical shifts of

all five complexes studied in various solvents span a 200

ppm range, which clearly indicate that in all of the comp -

plexes, the thallium(I) ion is only partially encapsulated,

and the solvent molecules and counter ions can still in-

teract with the vacant coordination sites of the complexed

Tl^+ ion.

The data summarized in Tables 11, 14, 15 18 and 20

clearly show that in some solvents, the linewidth of the

^{205}Tl resonance broadens dramatically as the ligand/Tl^+ mole

ratio varies between 0 and 1. The examples of ^{205}Tl NMR

spectrum with different linewidths are shown in Figure 22.

The possible reason for this line broadening is intermediate

exchange of the Tl^+ ion between solvated and complexed sites.

In these cases, the temperature was decreased to make the

lifetime at each site (τ_A and τ_B) become large, with the

interaction time (τ) increased according to the following

equation(131).

$$\tau = \frac{\tau_A \ \tau_B}{\tau_A + \tau_B} \qquad (3.12)$$

where τ_A and τ_B are the lifetimes of solvated Tl^+ ion and

complexed Tl^+ ion respectively. If τ_A and τ_B become large

enough to make τ be larger than the NMR time scale, the broad

line will be resolved into two separated lines which repre-

sent the complexed and solvated Tl^+ ions. The condition

required to separate two resonance lines is

1881 Hz

1326 Hz

352 Hz

197 Hz

66 Hz

23 Hz
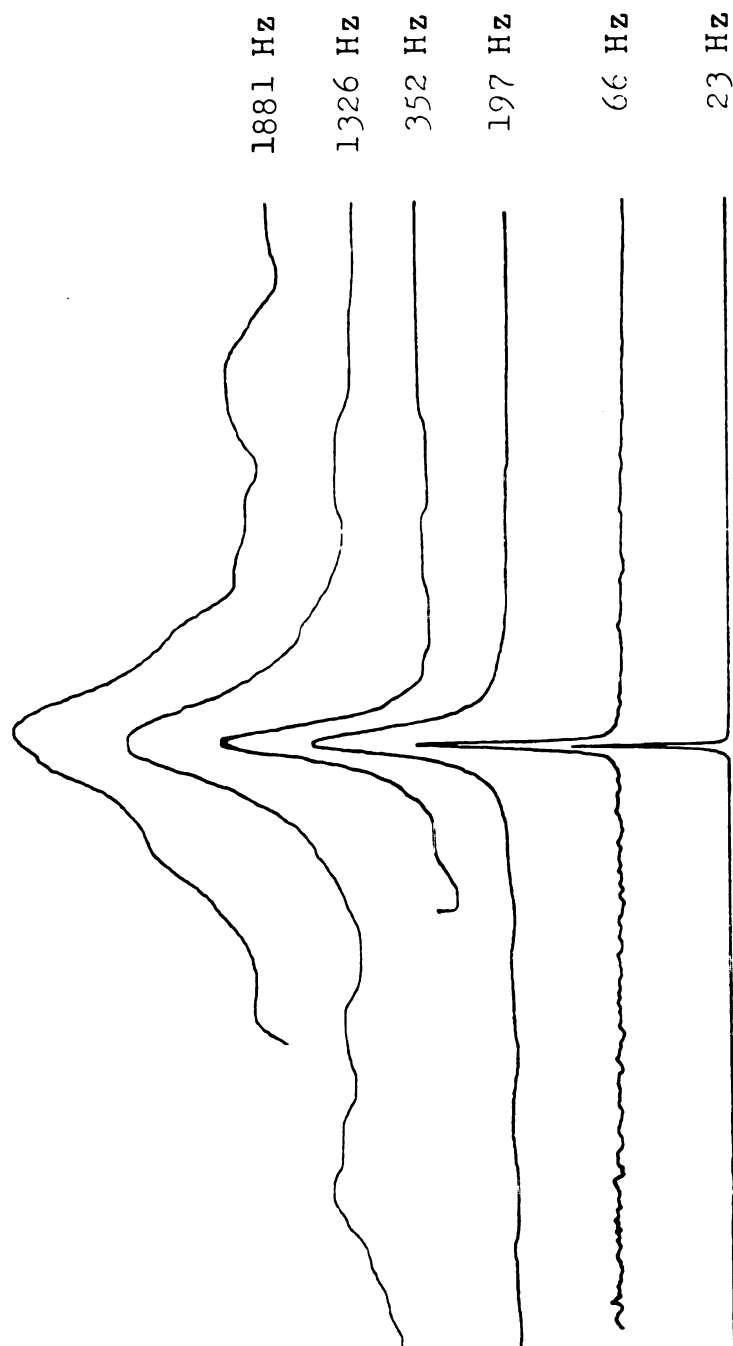
Figure 22. Thallium-205 NMR spectra of different linewidths.

$$\tau > \frac{\sqrt{2}}{\pi \, \Delta \nu} \qquad\qquad (3.13)$$

where $\Delta \nu$ is the frequency (Hz) difference between sites A and B. However, in our systems, the ^{205}Tl linewidth increased with decreasing temperature, but the resonance could not be resolved into two separate lines. In some case (Table 14 and 15), the resonance of ^{205}Tl became too broad to be measured when the ligand/Tl$^+$ mole ratio was around 0.5.

CHAPTER IV

THERMODYNAMIC STUDIES OF THALLIUM(I)

SALTS WITH 18-CROWN-6 AND ITS

SUBSTITUTED ANALOGS IN SEVERAL

SOLVENTS

1. Introduction

The thermodynamic properties of macrocyclic complexes have been under active investigation during the past decade. It seems, however, that most of the attention has been focused on alkali cation complexes. Few thermodynamic studies have been reported for the complexation of the Tl^+ ion with 18-crown-6 and its substituted analogs. Izatt and co-worker (10) have determined the thermodynamic parameters (ΔG_c^o, ΔS_c^o, and ΔH_c^o) for the complexation of the Tl^+ ion with the crown ethers 18C6, DC18C6 and DT18C6 (28), in aqueous solution by calorimetric techniques. They found that the complexation reactions of $(18C6 \cdot Tl)^+$, $(DC18C6 \cdot Tl)^+$ and $(DT18C6 \cdot Tl)^+$ are all enthalpy stabilized ($\Delta H_c^o < 0$) but entropy destabilized ($\Delta S_c^o < 0$).

The present work reports the use of ^{205}Tl NMR to study thallium(I) complexation with the crown ethers 18C6, DB18C6 and DT18C6, in several nonaqueous solvents at different temperatures, in order to show how the thermodynamic parameters for the complexation reaction are affected by the nature of the medium, the cavity size and the substitution of two oxygen atoms by two sulfur atoms.

2. Thermodynamic Study of The Complexation of the Tl^+ Ion by 18C6.

The complexation of the Tl^+ ion by 18C6 in various solvents has been studied and discussed in detail in section III-3-C. In order to have a better understanding of the thermodynamic behavior of this complexation reaction, we have studied the complexation of 18C6 with thallium(I) perchlorate (0.01 M) in sulfolane and dimethylformamide solutions at various temperatures. The data obtained from these studies are collected in Tables 22 and 23. In all cases studied here, only one thallium-205 resonance signal was found which indicate a fast exchange between the complexed and solvated Tl^+ ion. As shown in Table 22, for both solvents, the line-width of ^{205}Tl resonance become broad as the ligand/Tl^+ mole ratio is varied between 0 an and 1. It decreases gradually as temperature is increased. The possible reason is due to intermediate exchanges existing between two Tl^+ sites (i.e. the solvated ion and complexed ion) at low temperature. Figures 23 and 24 show the variation of ^{205}Tl chemical shifts as a function of 18C6/Tl^+ mole ratio in sulfolane and di-methylformamide at various temperatures. It is obvious that the curvature of the plot decreases with increasing tempera-ture which demonstrates the formation of a weaker complex at higher temperature. Therefore, in both solvents, the com-plexation of the Tl^+ ion by 18C6 is an exothermic reaction. In both solvents the plots show a clear break around the mole ratio of 1:1 (metal ion:ligand), which indicates that a 1:1 complex is formed. In sulfolane the NMR resonance of th Tl^+

Table 22. Thallium-205 Chemical Shift-Mole Ratio Data for 0.01 M TlClO$_4$ Complex with 18C6 in SF at Various Temperatures.

L/Tl$^+$	31°C		43°C		54°C	
	δ (ppm)	Δν (Hz)	δ (ppm)	Δν (Hz)	δ (ppm)	Δν (Hz)
0	-267.4	31	-259.4	26	-254.5	23
0.30	-250.1	677	-240.0	576	-231.5	239
0.64	-229.5	610	-218.8	556	-211.3	313
0.79	-221.2	554	-209.0	325	-203.1	283
0.86	-217.8	475	-204.5	287	-199.5	127
0.97	-212.5	264	-202.1	109	-195.7	124
1.05	-210.2	124	-200.5	93	-192.7	79
1.17	-209.0	70	-197.0	75	-189.4	72
1.40	-208.0	65	-196.4	47	-188.9	23
1.97	-207.4	40	-195.8	40	-188.7	23
2.61	-207.3	35	-195.5	35	-187.6	29

Table 22. Continued.

L/Tl$^+$	66°C		77°C		93°C	
	δ(ppm)	Δν(Hz)	δ(ppm)	Δν(Hz)	δ(ppm)	Δν(Hz)
0	-249.2	33	-245.5		-240.3	26
0.30	-226.6	92	-221.3	146	-214.8	113
0.64	-204.3	191	-198.9	127	-191.9	105
0.79	-195.5	116	-193.8	127	-182.8	66
0.86	-192.1	116	-186.5	93	-179.4	63
0.97	-188.6	93	-182.0	79	-175.6	53
1.05	-185.3	79	-178.2	72	-173.0	63
1.17	-181.9	78	-176.8	63	-169.7	66
1.40	-181.6	54	-175.6	40	-167.4	45
1.97	-131.0	54	-173.2	40	-165.2	38
2.61	-179.8	30	-172.6	25	-164.3	23

Table 23. Thallium-205 Chemical Shift-Mole Ratio Data for 0.01 M TlClO$_4$ Complex
with 18C6 in DMF at Various Temperatures.

L/Tl$^+$	24°C		38°C		52°C	
	δ(ppm)	Δν(Hz)	δ(ppm)	Δν(Hz)	δ(ppm)	Δν(Hz)
0	134.2	29.1	136.0	30.2	138.3	35.6
0.15	93.9	409.5	97.3	189.9	98.8	118.7
0.34	57.4	594.8	55.7	293.5	62.8	161.4
0.62	- 15.5	507.1	- 5.1	273.5	6.1	144.2
0.81	- 55.7	348.4	- 40.3	162.2	- 28.8	124.9
1.08	- 96.9	202.7	- 75.7	148.1	- 53.4	124.8
1.44	-110.5	88.1	- 95.4	101.6	- 80.2	112.6
1.80	-116.9	71.0	-100.5	59.1	- 88.3	82.1
2.42	-122.3	46.6	-108.7	52.6	- 96.6	86.8
3.31	-123.9	46.6	-111.7	41.6	-100.5	92.9
4.03	-122.5	52.6	-110.5	41.6	-100.1	86.8
4.77	-124.3	28.2	-113.2	35.5	-103.9	44.1

Table 23. Continued.

L/Tl$^+$	65°C		79°C		93°C	
	δ(ppm)	Δν(Hz)	δ(ppm)	Δν(Hz)	δ(ppm)	Δν(Hz)
0.00	140.9	51.6	143.3	76.0	150.3	82.1
0.15	103.6	80.7	112.7	79.9	117.5	39.3
0.34	81.6	130.9	90.7	82.1	100.2	63.8
0.62	22.7	161.4	38.6	124.6	55.6	124.8
0.81	- 17.1	124.8	4.3	130.9	30.7	124.8
1.08	- 36.0	82.1	- 9.6	94.3	8.0	94.3
1.44	- 59.7	88.2	- 33.2	88.1	- 8.7	82.1
1.80	- 68.0	63.8	- 45.6	155.3	- 19.6	130.9
2.42	- 84.8	76.5	- 65.8	106.5	- 44.4	63.7
3.31	- 85.5	94.3	- 71.9	155.3	- 53.5	57.6
4.03	- 87.4	88.1	- 74.2	94.3	- 58.3	70.5
4.77	- 93.7	51.5	- 81.4	45.4	- 68.5	45.4

Figure 23. Chemical shifts of Tl-205 vs. 18C6/TlClO$_4$ (0.01 M)
mole ratio in sulfolane at different temperatures.
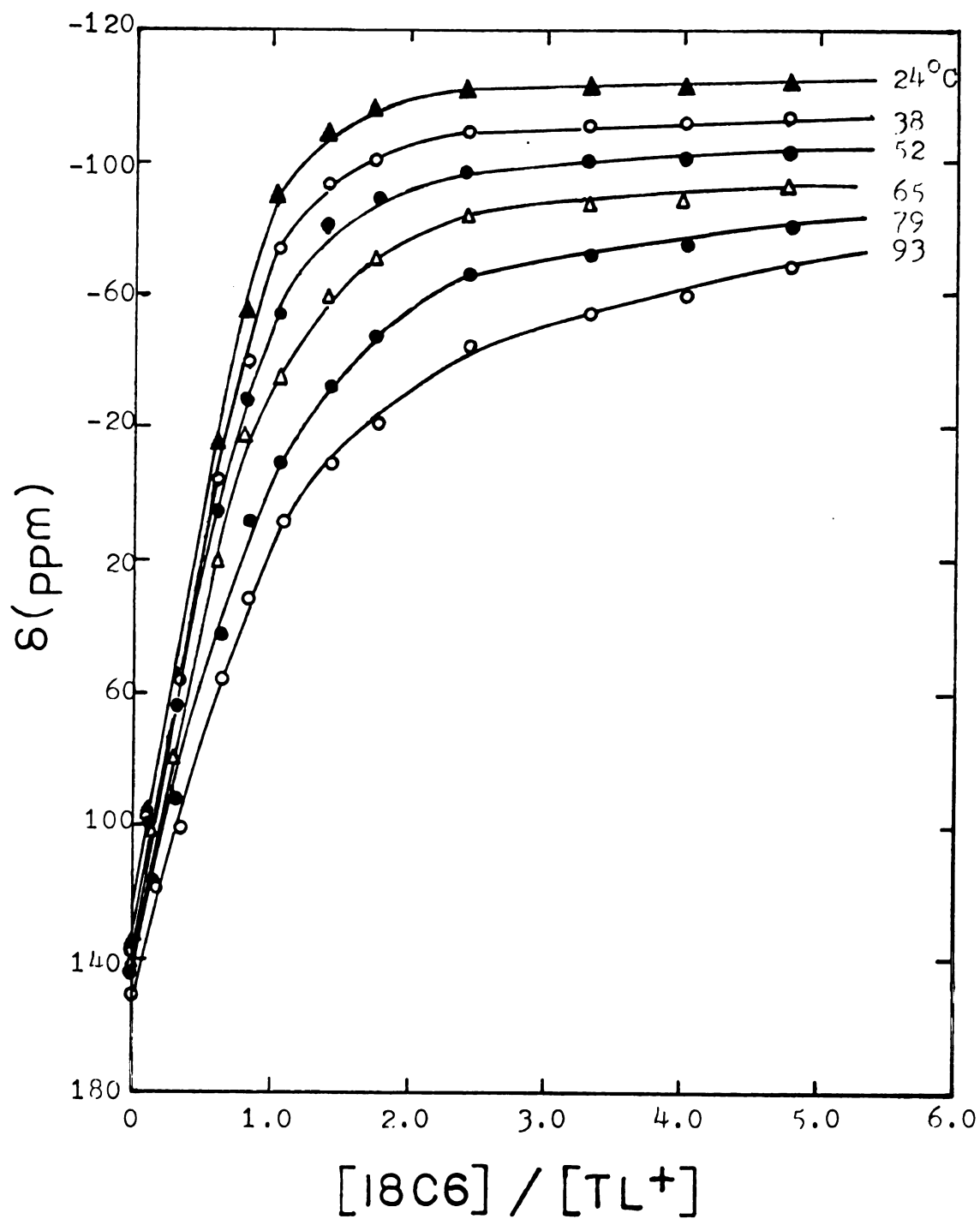
Figure 24.   Chemical shifts of ^{205}Tl $\underline{vs.}$ 18C6/TlClO$_4$(0.01 M) mole ratio in DMF at various temperatures.

ion shifts downfield with an increasing 18C6/Tl$^+$ mole ratio at various temperatures but it shifts upfield in dimethylformamide.

Formation constants and limiting chemical shifts of the (18C6·Tl)$^+$ complex in sulfolane and dimethylformamide at various temperatures were computed and the results are listed in Table 24. As expected, the stability constant varies inversely with the temperature.

The thermodynamic parameters ΔG_c^O, ΔH_c^O and ΔS_c^O were calculated from the temperature dependence of the equilibrium constant according to the following thermodynamic expression:

$$-RT \ln K_f = \Delta G_c^O - T\Delta S_c^O$$

$$\ln K_f = \frac{-\Delta H_c^O}{RT} + \frac{\Delta S_c^O}{R} \qquad (4.1)$$

Van't Hoff plots of $\ln K_f$ versus $\frac{1}{T}$ for the (18C6·Tl)$^+$ complex in sulfolane and dimethylformamide are shown in Figure 29. The thermodynamic parameters of the complexation reaction were obtained by fitting $\ln K_f$ _vs._ 1/T with a linear least squares program. The enthalpies (ΔH_c^O) and the entropies (ΔS_c^O) of the complexation were obtained from the slopes and interceps of the plot. These results with the ΔG_c^O values (at 30°C) were collected in Table 24. These data indicate that, in sulfolane, the (18C6·Tl)$^+$ complex is enthalpy and and slightly entropy stabilized, whereas, the same complex

Table 24. Temperature Dependance of the Formation Constants and Limiting Chemical Shifts of (18C6·Tl)$^+$ Complex in SF and DMF.

Solvent	Temperature(°C)	Log K_f	δ_{lim}(ppm)	Thermodynamic Parameters
SF	31	4.23 ± 0.04	-207.1 ± 0.1	$\Delta G_c^o(30^oC) = -5.92 \pm 0.65$ Kal/mole
	43	4.13 ± 0.07	-195.2 ± 0.1	
	54	4.04 ± 0.25	-187.6 ± 0.3	$\Delta H_c^o = -5.36 \pm 0.48$ Kcal/mole
	66	3.92 ± 0.13	-179.6 ± 0.3	
	77	3.71 ± 0.08	-172.5 ± 0.2	$\Delta S_c^o = 1.87 \pm 1.46$ cal/mole·°K
	93	3.60 ± 0.05	-162.2 ± 0.2	
DMF	24	3.62 ± 0.10	-125.6 ± 0.6	$\Delta G_c^c(30^oC) = 4.89 \pm 0.30$ Kal/mole
	38	3.37 ± 0.07	-115.7 ± 0.7	
	52	3.13 ± 0.05	-107.7 ± 0.9	$\Delta H_c^o = -8.66 \pm 0.22$ Kcal/mole
	65	2.90 ± 0.07	- 99.6 ± 2.0	
	79	2.64 ± 0.05	- 93.3 ± 2.2	$\Delta S_c^c = -12.44 \pm 0.68$ cal/mole·°K
	93	2.43 ± 0.05	- 86.7 ± 3.4	

in dimethylformamide is ethalpy stabilized but entropy destabilized.

The measured enthalpy change (ΔH^o_c) for a complexation reaction in solution reflects the energy change between reactants and products which include (a) the bond energy of the cation-donor atom bonds (b) the solvation energy of reactants and products (i.e., ion solvent interaction, ligand solvent interaction and complex solvent interaction). Several factors contribute to ΔS^o_c which include (1) ligand and cation desolvation, (2) solvation of the complex, (3) change of complex formation from cation and ligand, (4) internal entropy change of the ligand upon complexation caused by configurational entropy changes between reactants and products.

Among these four factors, the configurational entropy change of the ligand upon complexation may be more pronounced as compared with the other factors. The thermodynamic data collected in Table 24 show that quite different ΔS^o_c values are observed in sulfolane and dimethylformamide. In sulfolane, the overall entropy change is small which shows that the rigidity of solvated and complexed ligand is almost the same in this solvent. However, in dimethylformamide, a negative entropy change indicates that the complexed 18C6 is more inflexible than the solvated 18C6. The ΔH^o_c value is also solvent dependent because the solvation energies for the Tl^+ ion , the ligand and the complex vary with the solvent.

3. Thermodynamic Study for the Complexation of the Tl^+ Cation by DB18C6.

The thallium-205 chemical shift-mole ratio data for the $(DB18C6 \cdot Tl)^+$ complex in sulfolane and dimethylformamide at various temperatures are listed in Tables 25 and 26. The data are plotted in Figures 25 and 26. In sulfolane the Tl-205 resonance shifts downfield with an increasing $DB18C6/Tl^+$ mole ratio but an upfield shift of the ^{205}Tl resonance was observed in dimethylformamide.

The formation constants and limiting chemical shifts of the $(DB18C6 \cdot Tl)^+$ complex in sulfolane and dimethylformamide at various temperatures were calculated and the results are listed in Table 27. The limiting chemical shift difference between $31^{\circ}C$ and $95^{\circ}C$ in sulfolane is 10 ppm and 110 ppm in dimethylformamide. The possible reason may be that, at high temperature, the complex becomes more flexible and the high solvating solvent can approach closely to the Tl^+ ion and change the electron density around the complexed thallium(I) ion inducing a large chemical shift change.

The Van't Hoff plot of ln K_f versus $\frac{1}{T}$ is shown in Figure 29 and the calculated thermodynamic parameters are presented in Table 27. In both solvents, the complexation reaction is enthalpy stabilized ($\Delta H_c^o < 0$) but entropy desta-bilized ($\Delta S_c^o < 0$), and the variation of enthalpy and entropy

Table 25. Thallium-205 Chemical Shift-Mole Ratio Data for 0.01 M TlClO$_4$ Complex with DB18C6 in SF at Various Temperatures.

L/Tl$^+$	31°C		45°C		58°C	
	δ(ppm)	Δν(Hz)	δ(ppm)	Δν(Hz)	δ(ppm)	Δν(Hz)
0.00	-267.9	23	-260.8	23	-255.5	17
0.35	-251.8	244	-248.1	66	-244.2	35
0.56	-242.7	66	-240.5	41	-237.0	23
0.82	-233.2	41	-231.5	41	-230.5	29
1.04	-227.0	41	-226.1	23	-224.1	23
1.39	-224.8	23	-293.7	23	-222.7	17
1.94	-224.3	23	-223.1	35	-221.1	17
3.00	-224.1	23	-222.9	23	-220.3	17
4.23	-223.9	17	-222.7	17	-219.4	17

Table 25. Continued.

L/Tl$^+$	71°C		83°C		95°C	
	δ(ppm)	Δν(Hz)	δ(ppm)	Δν(Hz)	δ(ppm)	Δν(Hz)
0.00	-250.8	17	-244.8	17	-240.5	17
0.35	-240.2	67	-236.7	53	-233.8	67
0.56	-234.9	47	-227.3	47	-225.5	53
0.82	-228.7	41	-225.1	53	-224.5	47
1.04	-224.2	41	-223.9	47	-223.3	53
1.39	-221.0	41	-219.7	23	-220.2	23
1.94	-219.6	23	-219.0	23	-217.8	21
3.00	-219.0	23	-217.5	21	-216.3	21
4.23	-217.1	17	-216.5	17	-214.6	17

Table 26. Thallium-205 Chemical Shift-Mole Ratio Data for 0.01 M TlClO$_4$ Complex with DB18C6 in DMF at Various Temperatures.

L/Tl$^+$	24°C		40°C		52°C	
	δ(ppm)	Δν(Hz)	δ(ppm)	Δν(Hz)	δ(ppm)	Δν(Hz)
0.00	122.9	29	124.3	36	125.2	32
0.38	73.8	50	81.3	36	92.6	32
0.61	46.6	66	61.0	44	75.8	48
0.96	6.9	72	25.6	38	40.9	30
1.38	-18.7	72	5.7	50	27.0	44
1.93	-48.2	53	-22.8	56	3.2	48
2.76	-73.0	47	-47.5	56	-23.5	60

Table 26. Continued.

L/Tl$^+$	64°C		79°C		92°C	
	δ(ppm)	Δν(Hz)	δ(ppm)	Δν(Hz)	δ(ppm)	Δν(Hz)
0.00	126.4	23	125.4	23	126.3	23
0.38	102.0	42	108.5	48	113.1	42
0.61	85.6	44	100.4	42	106.9	29
0.96	55.6	24	76.2	24	89.9	42
1.38	46.3	42	64.4	36	76.6	29
1.93	26.0	48	51.2	42	67.4	42
2.76	- 0.3	48	30.7	44	49.7	48
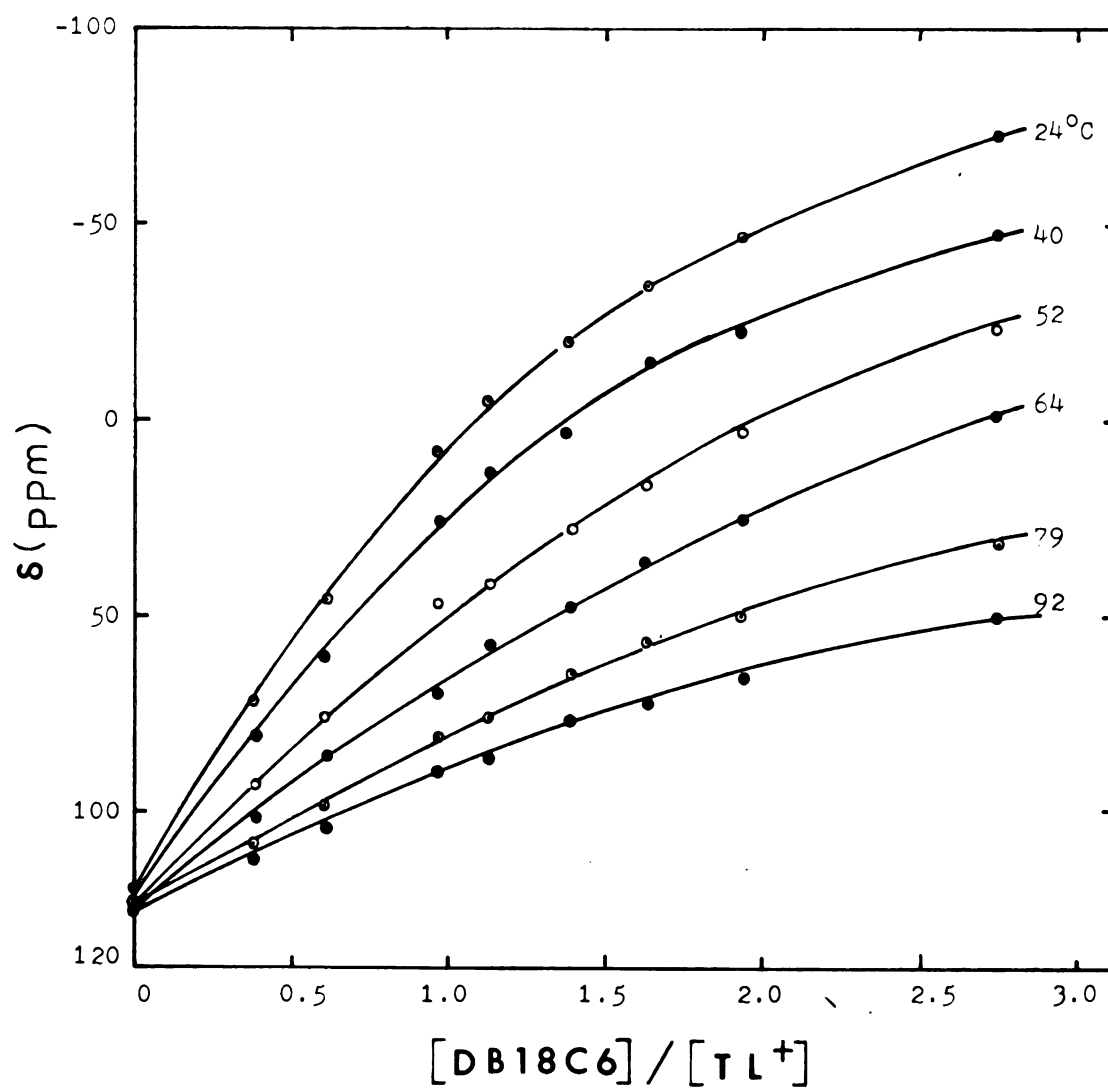
Figure 25. Chemical shifts of Tl-205 vs. DB18C6/Tl$^+$(0.01 M)
mole ratio in DMF at various temperatures.
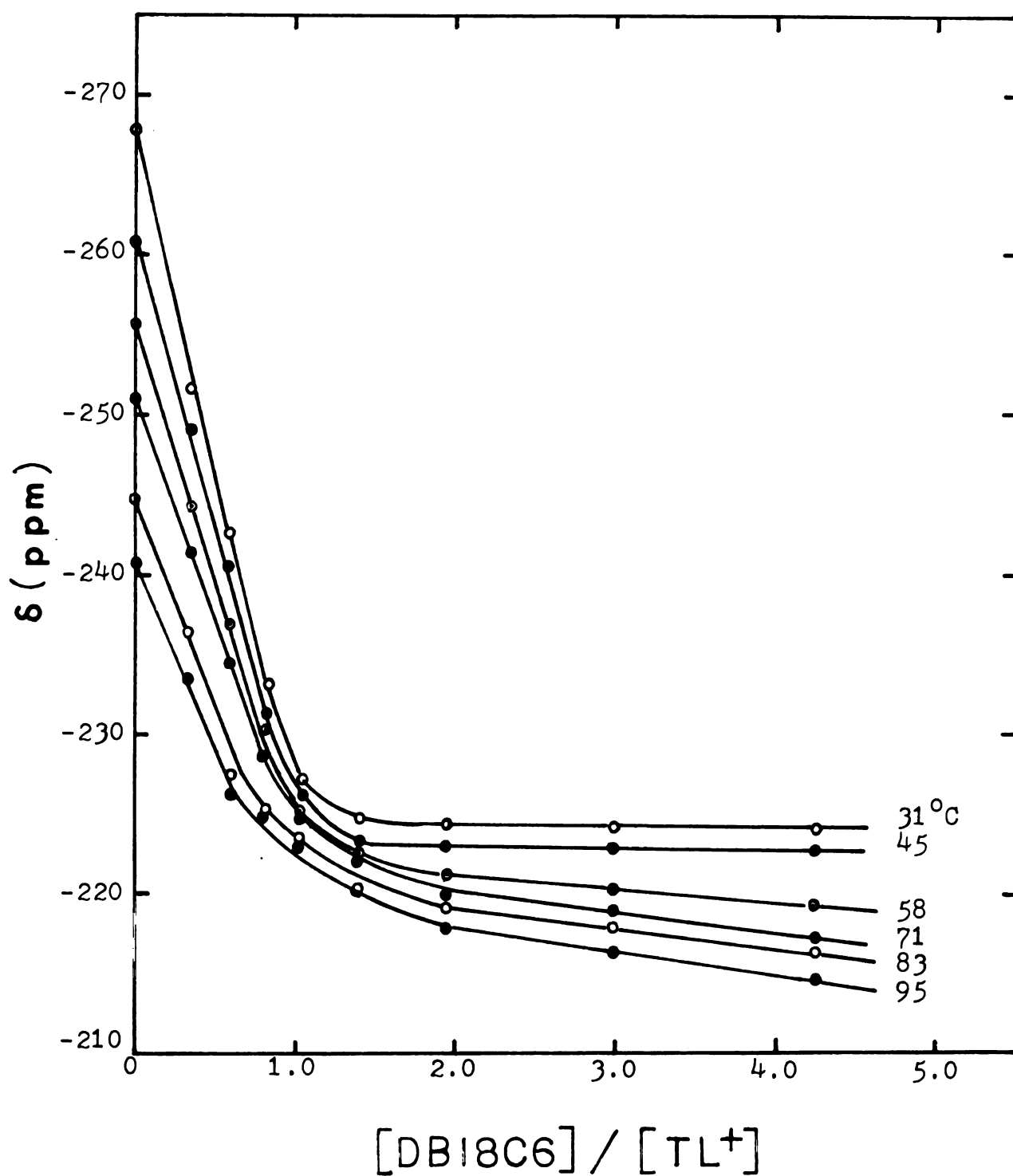
Figure 26. Chemical shifts of Tl-205 vs. DB18C6/Tl⁺(0.01 M) mole ratio in SF at various temperatures.

Table 27. Temperature Dependance of the Formation Constants and Limiting Chemical Shifts of (DB18C6·Tl)⁺ Complex in SF and DMF.

Solvent	Temperature (°C)	Log K_f	δ_{lim}(ppm)	Thermodynamic Parameters
SF	31	4.04 ± 0.06	-223.8 ± 0.1	ΔG°_c = -5.68 ± 1.66 Kal/mole at 30°C
	45	3.88 ± 0.04	-222.6 ± 0.1	
	58	3.26 ± 0.07	-210.1 ± 0.2	ΔH°_c = -11.50 ± 1.23 Kcal/mole
	71	3.03 ± 0.11	-216.7 ± 0.5	
	83	2.87 ± 0.04	-215.5 ± 0.2	ΔS°_c = -19.20 ± 3.67 cal/mole·°K
	95	2.69 ± 0.12	-213.4 ± 0.8	
DMF	24	2.13 ± 0.03	-143.8 ± 5.1	ΔG°_c = -2.89 ± 0.27 Kal/mole at 30°C
	40	2.01 ± 0.05	-128.8 ± 8.7	
	52	1.83 ± 0.08	-123.1 ± 18.1	ΔH°_c = -4.98 ± 0.20 Kcal/mole
	64	1.71 ± 0.12	-110.8 ± 29.2	
	79	1.58 ± 0.12	- 75.6 ± 29.9	ΔS°_c = -6.92 ± 0.62 cal/mole·°K
	92	1.60 ± 0.17	- 34.5 ± 32.4	

values is much dependent on solvent. The entropy destabili-
zation of the complex may be due to a change in the ligand
configuration entropy. Dibenzo-18-crown-6 in the free state
may be more flexible than in a complexed state because it
becomes more ordered as it forms a complex with the Tl^+ ion.

4. **Thermodynamic Study for the Complexation of the Tl^+**
   Cation by DT18C6.

The effect of the temperature on the Tl-205 resonance for
the $(DT18C6\cdot Tl)^+$ complex was determined at different DT18C6/
Tl^+ mole ratios in acetone and sulfolane. Thallium-205 chem-
ical shifts measured at different temperature are listed in
Table 28 and 29. The plots of the ^{205}Tl chemical shift
versus DT18C6/Tl^+ mole ratio at various temperatures are
shown in Figure 27 and 28. In both solvents, at all studied
temperatures, the thallium-205 resonance shifts downfield
with an increasing DT18C6/Tl^+ mole ratio, while the curvature
of the plot increases with decreasing temperature indicating
the formation of more stable complex at lower temperature.

In the case of the $(DT18C6\cdot Tl)^+$ complex in acetone, as
the studied temperature is as low as $-31^{\circ}C$, the mole ratio
plot consists of two straight lines intersecting at a 1:1
ratio (Figure 27) which clearly demonstrates that only the
1:1 complex is formed. At $-31^{\circ}C$, $-9^{\circ}C$ and $1^{\circ}C$, when the
ligand/Tl^+ mole ratio varies between 0 and 1, the ^{205}Tl

Table 28. Mole Ratio-Chemical Shift Data for $TlClO_4$ (0.01 M) in the Presence of DT18C6 in AC at Different Temperatures.

L/Tl+	Temperature $^\circ C$						
	-9.1	0.8	10.5	20.2	27.8	30	39.6
0.00	-244.19	-242.61	-239.61	-236.79	-236.86	-234.15	-231.15
0.51	-	-	17.50	10.27	15.33	3.04	-5.07
0.71	-	-	114.14	100.91	96.83	90.33	75.52
0.90	-	-	177.32	166.21	151.24	148.62	120.23
1.01	233.70	221.70	207.25	189.43	173.86	172.50	151.00
1.28	274.61	265.09	253.63	238.46	223.95	221.00	200.89
1.82	293.31	290.49	285.37	276.73	267.59	265.44	249.39
2.22	296.12	297.18	294.54	289.25	282.49	281.13	269.50
2.99	300.89	302.11	301.41	299.64	295.64	295.06	287.48
3.54	301.42	301.42	301.46	299.48	296.77	295.24	288.01
5.30	300.01	304.59	305.82	306.35	305.50	305.30	302.65

Table 29. Thallium-205 Chemical Shift-Mole Ratio Data for 0.01 M $TlClO_4$ Complex with DT18C6 in SF at Various Temperatures.

L/Tl^+	31°C		45°C		74°C	
	δ(ppm)	$\Delta\nu$(Hz)	δ(ppm)	$\Delta\nu$(Hz)	δ(ppm)	$\Delta\nu$(Hz)
0.00	-267.6	23	-256.8	18	-246.0	20
0.17	-197.2	991	-196.8	357	-200.7	77
0.59	3.4	1881	-62.5	892	-73.7	169
0.78	68.1	1326	24.2	867	-35.3	197
0.90	96.2	1032	60.1	815	-16.1	188
1.10	141.2	892	102.2	832	16.0	205
1.42	199.6	1078	162.2	748	69.4	169
1.80	237.0	720	197.1	352	107.2	123
2.24	262.0	304	233.6	197	152.0	123
3.25	287.5	167	272.5	169	210.6	118
4.55	312.5	66	296.1	100	245.6	91

Table 29. Continued.

L/Tl+	85°C		92°C		109°C	
	δ(ppm)	Δν(Hz)	δ(ppm)	Δν(Hz)	δ(ppm)	Δν(Hz)
0.00	-243.3	17	-240.2	17	-235.0	21
0.17	-195.4	66	-204.0	44	-195.7	36
0.59	- 92.2	117	-101.2	107	-125.5	70
0.78	- 57.2	123	- 80.3	123	-104.8	88
0.90	- 35.2	164	- 55.4	123	- 83.2	102
1.10	- 8.1	167	- 23.4	123	- 56.4	155
1.42	45.4	196	20.6	107	- 26.8	76
1.80	79.2	155	65.2	123	11.7	101
2.24	123.1	228	100.5	178	44.8	123
3.25	182.5	117	152.5	128	97.6	101
4.55	222.4	68	205.1	91	152.0	85
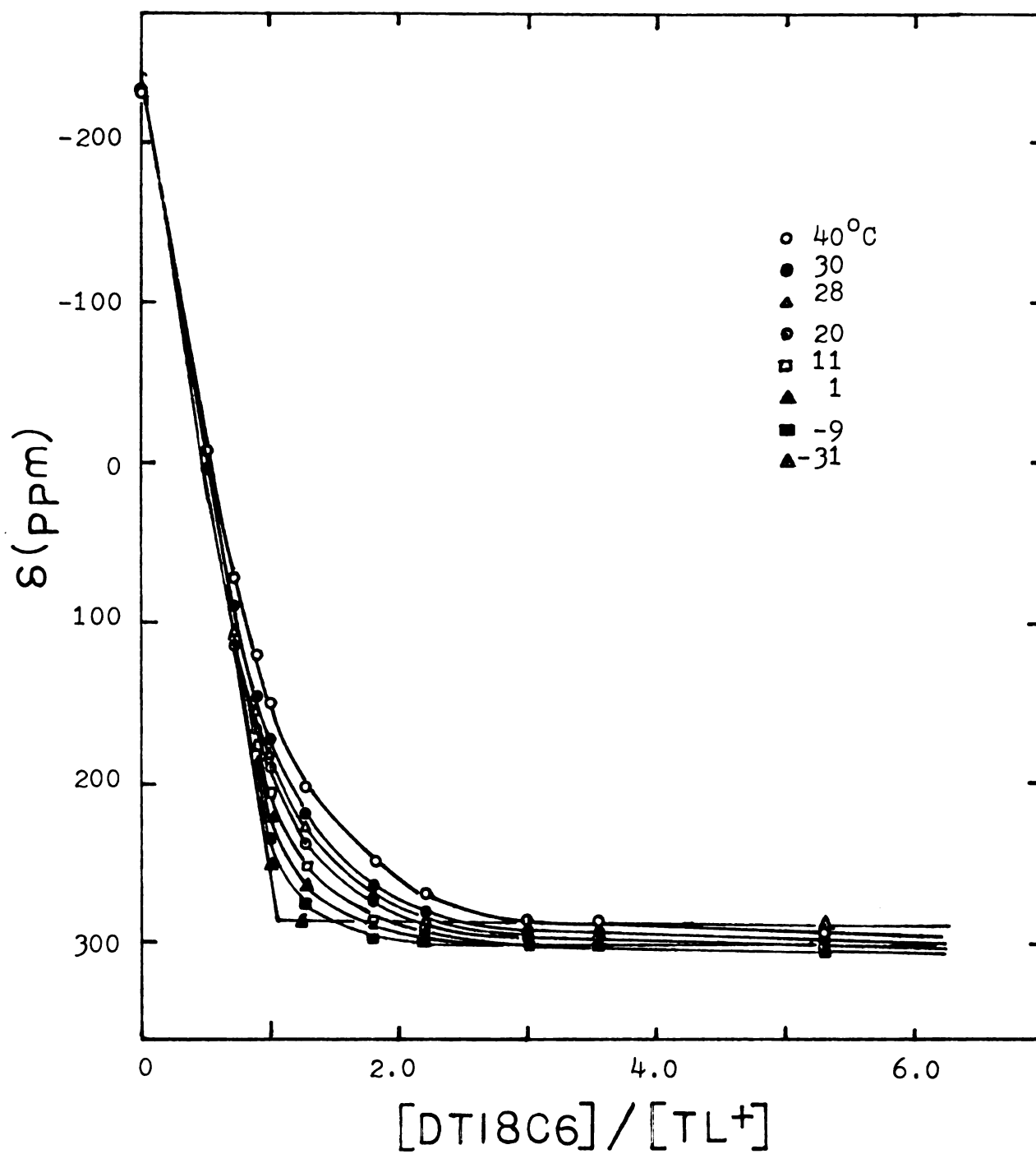
Figure 27. Chemical shifts of ^{205}Tl $\underline{vs.}$ DT18C6/Tl$^+$(0.01 M) mole ratio in AC at different temperatures.
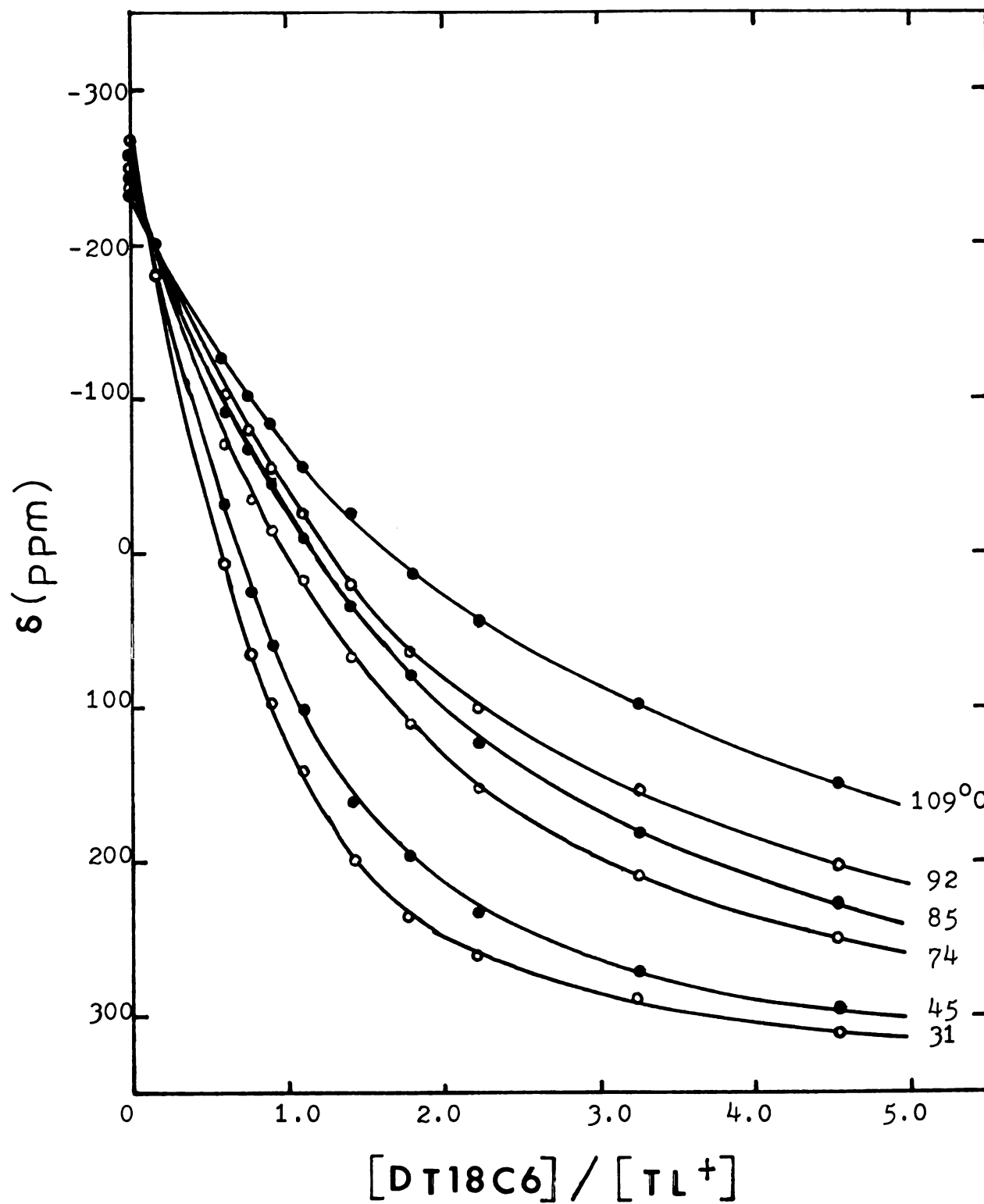
Figure 28.   Chemical shifts of ^{205}Tl vs. DT18C6/Tl$^+$(0.01 M) mole ratio in SF at different temperatures.

resonance becomes too broad to be measured on our DA-60 NMR (Table 28).

The formation constants and the limiting chemical shift of the $(DT18C6 \cdot Tl)^+$ complex at various temperatures in acetone and sulfolane were calculated as explained previously (APPENDIX 2-A) and are tabulated in Table 30. Plots of $\ln K_f$ versus $\frac{1}{T}$ for these data are shown in Figure 29 and the corresponding ΔH_c^o and ΔS_c^o are shown in Table 30. Thermodynamic parameters indicate that, in acetone and sulfolane solutions, the complex is enthalpy stabilized but entropy destabilized and ΔH_c^o and ΔS_c^o values vary with the nature of the solvent. The entropy destabilization of the complex $(\Delta S_c^o < 0)$ may be due to the fact that 18C6 is more flexible uncomplexed than when complexed to Tl^+ ion (configurational entropy).

5. Comparison of the Thermodynamic Parameters

Thermodynamic parameters obtained for complexing of the Tl^+ ion by 18C6, DB18C6 and DT18C6 in several nonaqueous solvents are listed in Table 24, 27 and 30. It is interesting to note that the thermodynamic data in all systems except for the $(18C6 \cdot Tl)^+$ complex in sulfolane show that the complexation reaction is enthalpy stabilized $(\Delta H_c^o < 0)$ but entropy destabilized $(\Delta S_c^o < 0)$. These may due to a change in both the Tl^+ ion and ligand from a loose structure in the free state to a "rigid" structure in the complexed state

Table 30. Temperature Dependence of the Formation Constants and Limiting Chemical Shifts of $(DT18C6 \cdot Tl)^+$ Complex in AC and SF.

Solvent	Temperature(°C)	Log K_f	δ_{lim}(ppm)	*Thermodynamic Parameters
AC	-9	3.85 ± 0.12	303.8 ± 1.1	$\Delta G^o_c(30^oC)= -4.20 \pm 0.11$
	1	3.60 ± 0.06	307.7 ± 0.8	
	11	3.41 ± 0.04	310.5 ± 0.7	$\Delta H^o_c= -7.61 \pm 0.08$
	20	3.22 ± 0.04	313.7 ± 1.1	
	28	3.07 ± 0.03	316.2 ± 0.9	$\Delta S^o_c= -11.23 \pm 0.25$
	30	3.04 ± 0.04	316.2 ± 1.4	
	40	2.86 ± 0.04	319.3 ± 1.9	
SF	31	2.66 ± 0.03	346.0 ± 3.0	$\Delta G^o_c(30^oC)= -3.67 \pm 0.17$
	45	2.44 ± 0.03	352.6 ± 6.5	
	74	2.10 ± 0.02	354.5 ± 6.0	$\Delta H^o_c= -5.91 \pm 0.13$
	85	2.00 ± 0.01	348.7 ± 4.7	
	92	1.90 ± 0.02	351.6 ± 10.5	$\Delta S^o_c= -7.39 \pm 0.38$
	109	1.78 ± 0.02	315.2 ± 10.7	

* The unit for thermodynamic parameters is;

$\Delta G^o_c=$ Kal/mole , $\Delta H^o_c=$ Kal/mole , $\Delta S^o_c=$ cal/mole·°K
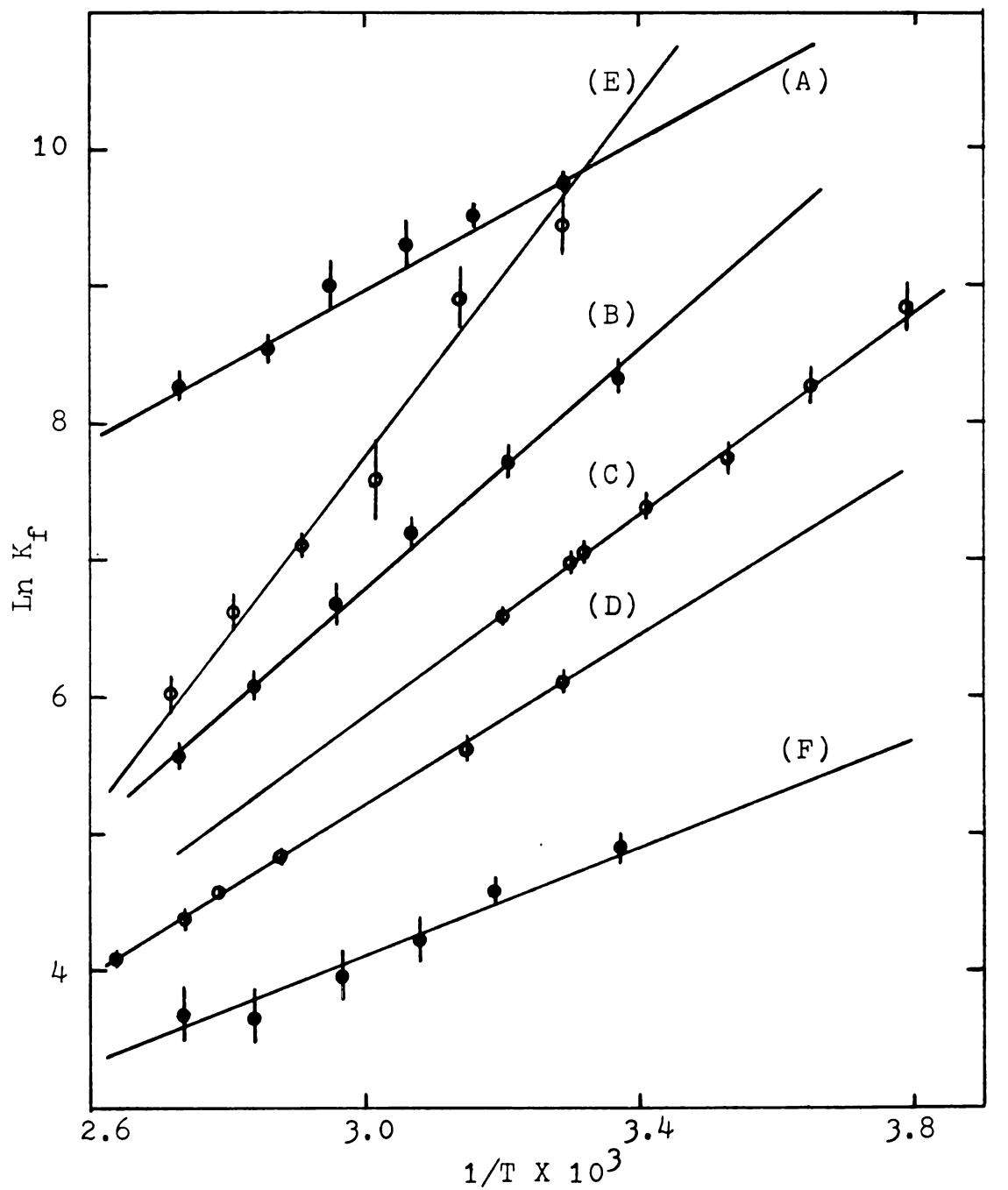
(A) 18C6·Tl$^+$ in SF   (D) DT18C6·Tl$^+$ in SF

(B) 18C6·Tl$^+$ in DMF   (E) DB18C6·Tl$^+$ in SF

(C) DT18C6·Tl$^+$ in AC   (F) DB18C6·Tl$^+$ in DMF

Figure 29. A plot of ln K_f vs. 1/T for the complexation of the Tl$^+$ ion with 18C6 and its analogs.

inducing a negative entropy change.

Generally, in the same temperature range, the limiting chemical shift difference in a high solvating solvent is larger than that in a low solvating solvent. This may be due to the fact that, at high temperature, the complex becomes more flexible to allow high solvating solvent molecules to approach the Tl^+ ion and affect the electron density of Tl^+ ion inducing a larger limiting chemical shift ragne.

At the present time, the literature information on the interaction of solvent molecules with ligands is quite sparse, additional studies on ligand-solvent interactions are required before the thermodynamic data can be fully understood.

CHAPTER V

THALLIUM-205 NMR STUDY OF THE IONIC

SOLVATION AND COMPLEXATION OF THALLIUM(I)

ION IN MIXED NONAQUEOUS SOLVENTS

1. Introduction

The behaviour of electrolytes in solutions depends predominantly on ion-ion and ion-solvent interactions. The former interaction is, in general, stronger than the latter. Only in a solvent with a high dielectric constant at low solute concentrations, where the salt is completely dissociated, can the ion-ion interactions be neglected. In this case, ion-solvent interactions become more important. Ion-solvation has been treated much more frequently in pure aqueous or non-aqueous solvents than in mixed solvents. It is interesting to see how far the solvation of ions in mixed solvents can be explained in terms of the ionic behaviour in the pure medium. Although solvent-solvent interactions are much weaker than ion-solvent interactions, they must be taken into consideration. Therefore, ion solvation has been studied in binary solvent mixtures.

While the solvation of thallium(I) ion in various highly solvating mixed solvents has been studied extensively (101, 107-110), the solvation of the Tl^+ ion in the mixed solvents of low solvating and high solvating power has not been previously reported. Investigations of the complexation of some macrocyclic ligands with the alkali and alkaline earth cations in mixed solvents have been restricted to water/methanol systems by the use of the calorimetric technique (12).

Complexation of the Cs^+ ion by several crown ethers and cryp-
tand-222 in nonaqueous mixed solvents have also been studied
by ^{133}Cs NMR by Rounaghi (129).

We were interested in studying both thallium(I) salts and
thallium(I) complexes in mixed solvents in order to see how
the nature of the medium affects the ion solvation and the
stability of crown complexes. In this chapter, we describe
preferential solvation studies of the Tl^+ ion in several
mixed solvents such as NM/DMSO, AN/DMSO, PC/DMSO, THF/DMSO,
HMPA/DMSO, DMF/DMSO, AN/DMF and H_2O/DMF. A study of the Tl^+
ion complexed by macrocyclic ligands, such as DA18C6 and
DT18C6, in DMF/H_2O and DMF/AN mixed solvents respectively,
is also reported.

2. Preferential Solvation of the Thallium(I) Ion in Mixed Solvents

The preferential solvation of the Tl^+ ion was studied
in several binary solvent systems by the NMR technique.
Thallium-205 chemical shifts were measured as a function of
solvent composition in a binary solvent system at $24^{\circ}C$. The
data are shown in Table 31 and are plotted in Figures 30-33.
In mixed solvents, it is possible to see bound and bulk ion
signals from both solvents (132). However, only one Tl^+ ion
resonance was observed in our systems which suggests that the
exchange between the bound Tl^+ ion and bulk Tl^+ ion is fast

Table 31. Thallium-205 Chemical Shifts of TlClO$_4$ in Mixed Solvents.

NM/DMSO (0.005 M TlClO$_4$)		PC/DMSO (0.005 M TlClO$_4$)		AN/DMSO (0.01 M TlClO$_4$)		THF/DMSO (0.005 M TlClO$_4$)	
mole % of NM	δ(ppm)	mole % of PC	δ(ppm)	mole % of AN	δ(ppm)	mole % of THF	δ(ppm)
0.00	390.0	0.00	389.2	0.00	365.4	0.00	389.0
12.74	391.5	17.18	392.9	13.07	365.0	8.90	390.2
24.75	400.0	35.62	394.1	25.27	367.3	17.99	391.1
36.04	400.3	55.43	396.8	36.70	367.7	36.94	392.3
46.71	400.8	76.82	383.0	47.43	367.1	56.84	393.4
66.35	409.3	88.18	335.4	57.49	367.5	77.83	377.0
75.42	410.5	93.46	266.5	66.98	369.4	88.77	338.9
84.02	411.2	97.01	144.1	75.90	367.1	94.36	244.6
92.21	391.0	98.50	28.4	84.40	362.2	97.17	169.1
95.32	356.0	100	-273.5	92.41	328.0	99.43	30.0
98.09	279.7			94.34	299.1	100	- 81.5
99.05	166.7			96.24	268.6		
100	-337.2			98.15	181.5		
				99.26	-109.9		
				100	-228.7		

Table 31. Continued.

DMF/DMSO (0.01 M TlClO₄)		HMPA/DMSO (0.01 M TlClO₄)		DMF/AN (0.01 M TlClO₄)		DMF/H₂O (0.01 M TlClO₄)	
mole % of DMF	δ(ppm)	mole % of HMPA	δ(ppm)	mole % of DMF	δ(ppm)	mole % of DMF	δ(ppm)
0.00	365.4	0.00	365.4	100.0	133.7	100.0	133.7
9.26	360.1	4.35	376.5	92.8	133.2	90.1	130.2
18.71	352.2	14.89	394.8	79.5	132.5	84.8	128.5
28.27	346.9	28.97	416.0	73.2	132.1	67.7	127.7
38.01	337.7	37.96	426.0	61.4	131.6	48.3	126.7
47.89	326.8	48.08	433.6	50.6	130.1	41.1	118.2
52.97	310.4	62.04	441.2	40.6	120.5	33.1	110.6
68.20	291.8	78.62	446.2	31.3	118.2	25.9	91.8
78.62	264.3	88.61	446.3	22.6	107.5	22.9	82.7
89.21	213.7	100	443.5	14.6	82.5	13.5	46.6
100	125.4			10.7	64.5	9.1	35.5
				7.1	41.2	2.5	7.8
				3.5	0.3	0.0	- 2.5
				1.7	- 94.1		
				0.0	- 233.3		

Figure 30. Chemical shifts of ^{205}Tl vs. mole % of NM or PC in NM/DMSO or PC/DMSO mixed solvents (0.005 M TlClO$_4$).
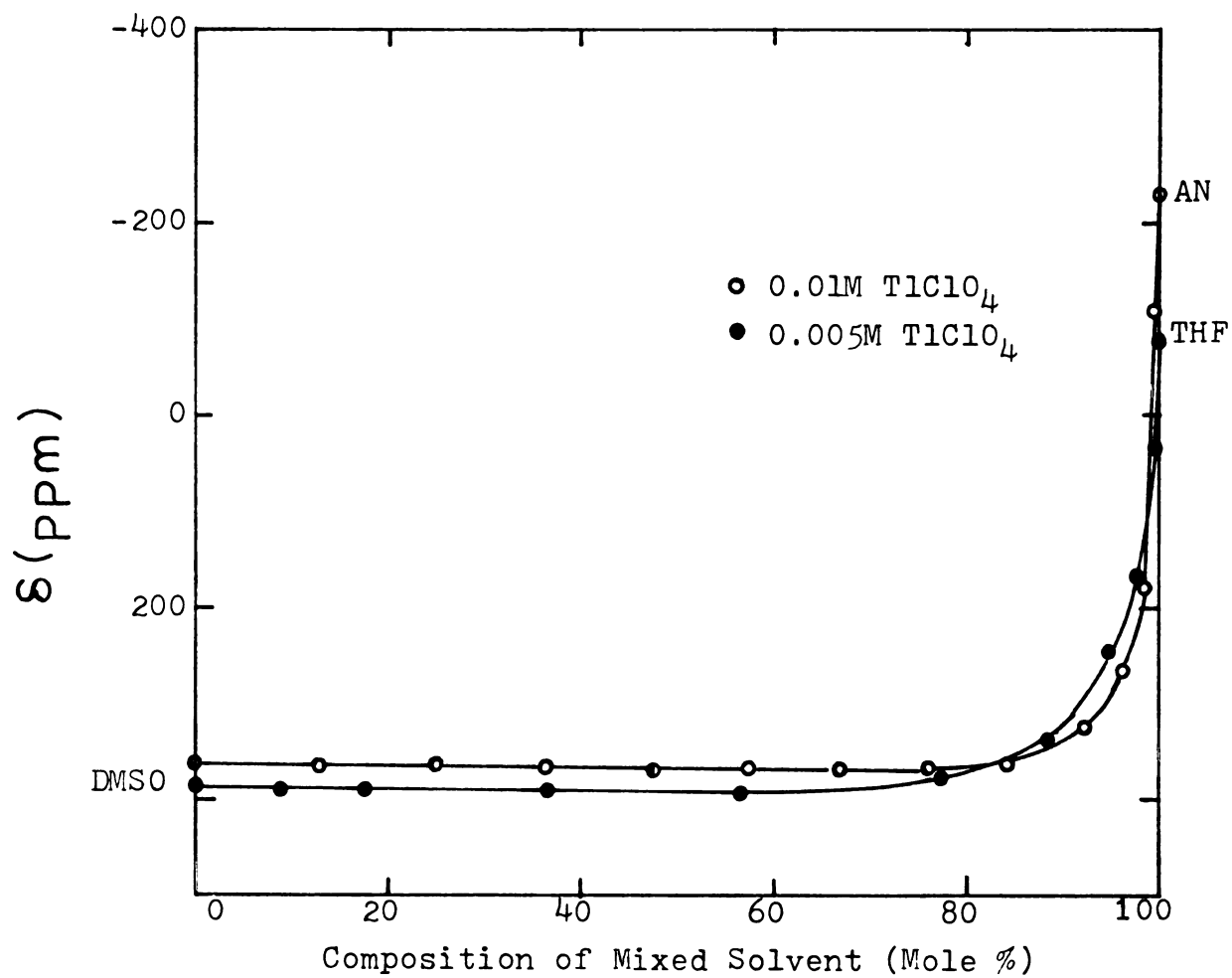
Figure 31. Thallium-205 chemical shifts vs. mole % of AN or THF in AN/DMSO or THF/DMSO mixed solvents.
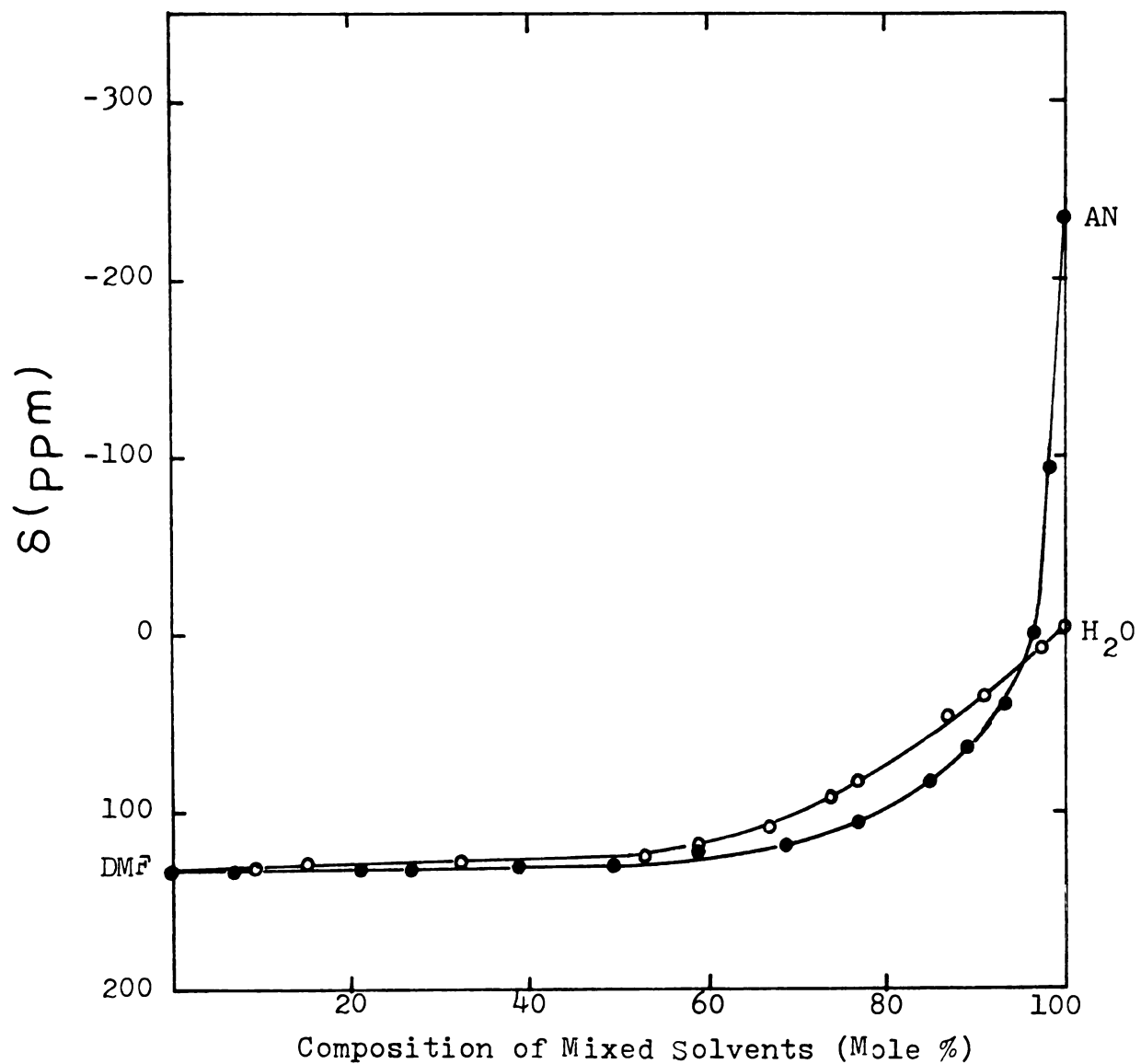
Figure 32. Thallium-205 chemical shifts <u>vs.</u> mole % of AN
or H_2O in AN/DMF or H_2O/DMF mixed solvents
$(0.01$ M $TlClO_4)$.
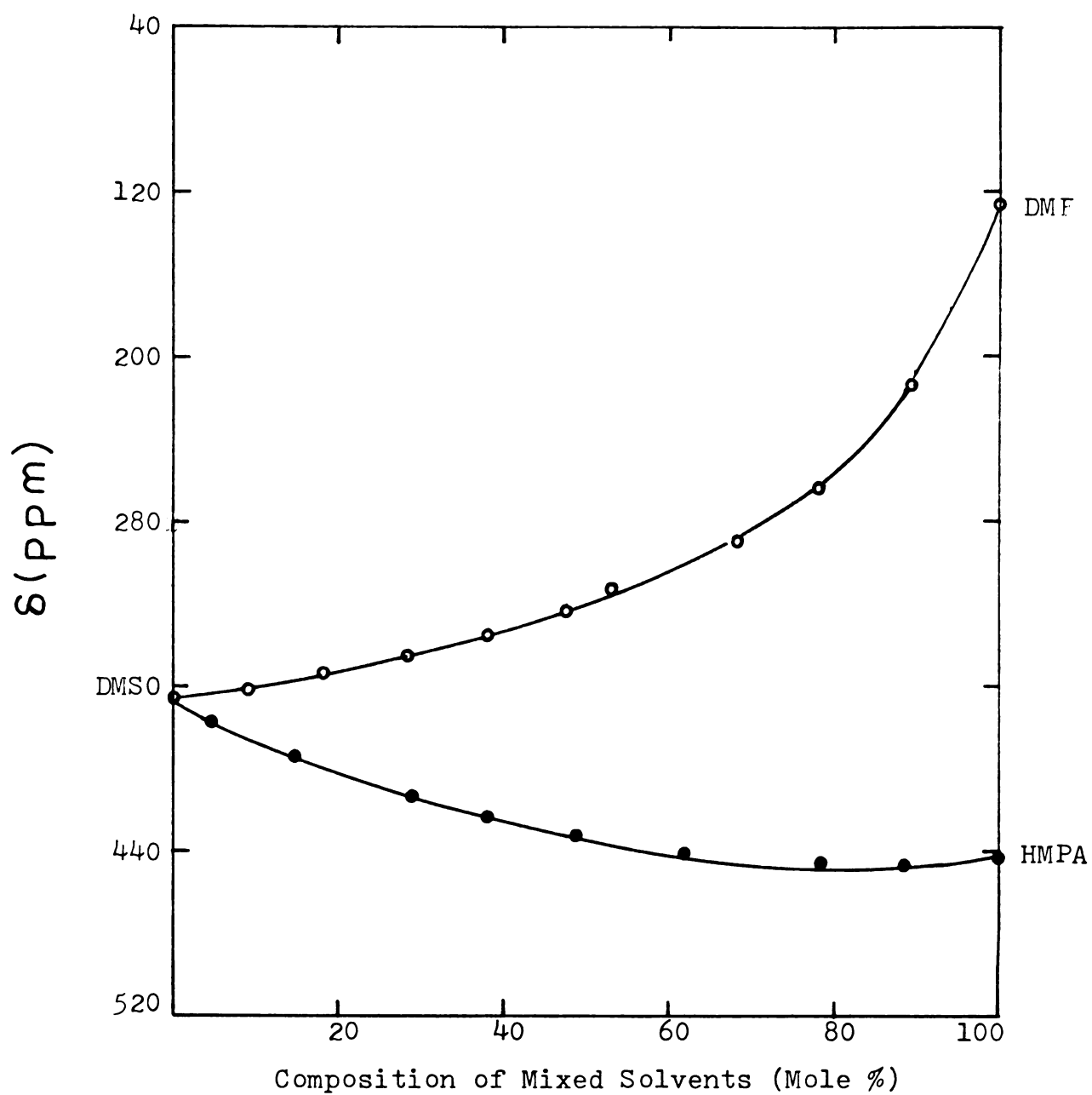
Figure 33. Chemical shifts of ^{205}Tl vs. mole % of DMF or HMPA in DMF/DMSO or HMPA/DMSO mixed solvents (0.01 M TlClO$_4$).

when compared to the NMR time scale. Figures 30-33 show plots of the thallium-205 chemical shifts versus the mole fraction of PC, NM, THF, AN, DMF, HMPA, AN, H_2O in PC/DMSO, NM/DMSO, THF/DMSO, AN/DMSO, DMF/DMSO, HMPA/DMSO, AN/DMF, H_2O/DMF mixed solvents respectively. The concentration of $TlClO_4$ in these solutions were 0.01 M or 0.005 M, depending on the solubility of the salt in each mixture. In all of the systems studied, the ^{205}Tl shift range varies from 100 ppm to 700 ppm. If there was equal solvation of the Tl^+ ion by the two solvents, a linear relationship between the two shift extremes would be expected. This linear behavior would indicate that the solvation sphere composition is the same as the bulk solvent mixture composition. Previous studies of preferential solvation (103,104,133-138) have shown that, when the observed chemical shift in a mixed solvent lies off the interpolated straight line, it lies closer to the shift of one pure solvent depending on which component preferentially solvates the ion.

All of the measurements (Figures 30-33) show a nonlinear dependence for our systems, which indicates that the solvation sphere of the Tl^+ ion contains a higher concetration of one solvent than the bulk solvent mixture (a preferential solvation). In the case of preferential solvation, the solvation sphere composition can be estimated by comparing the experimental curve with the ideal curve. For example, in the PC/DMSO system (Figure 30), for an observed Tl^{205} shift at a

composition in the bulk mixture of X_{pc}= 0.90, the solvation

sphere composition can be found by moving horizontally to

the ideal curve giving a solvating sphere composition of

X_{pc}= 0.12. This extrapolation indicates that PC competes

less strongly in the solvation sphere than does DMSO.

The results shown in Figures 30-33 clearly indicate that the

nature of the medium plays an important role in the solvation

process.

Two conclusions regarding preferential solvation may be

drawn from the data in Figures 30-33. First, when the donor

number difference of two mixed solvents is larger than 10

(NM/DMSO, PC/DMSO, AN/DMF and THF/DMSO), the thallium-205

resonance signal shifts slightly downfield until the mole

fraction of the solvent with the lower donor number in the

mixed solvent is around 0.8, then it abruptly shifts upfield.

However, when the donor number difference between two mixed

solvents is smaller than 10 (DMF/DMSO, HMPA/DMSO and DMF/H_2O),

the shift of ^{205}Tl changes gradually with the solvent

composition. It is of interest to note this initial down-

field shift disappears as the salt concentration is decreased

(Figure 34). Second, if a greater downfield shift is observed

in one solvent versus another, preferential solvation of the

Tl^+ ion by the former solvent in mixed solvents is seen. This

second observation was also made by Zink and co-workers (133).

The solvent dependence of the shift arises primarily from

the paramagnetic term in Ramsey's equation (APPENDIX 1).
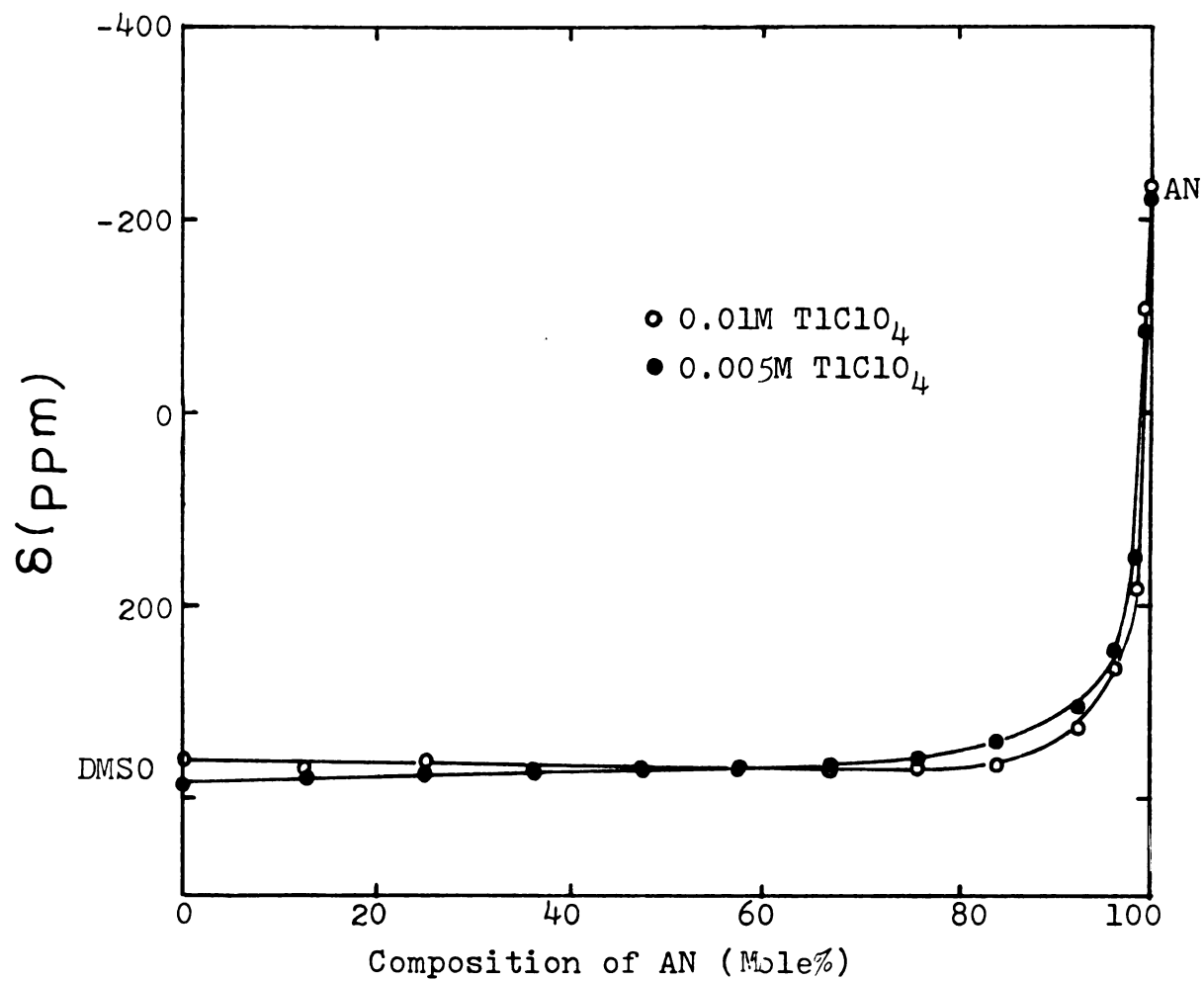
Figure 34. Thallium-205 chemical shifts vs. mole % of AN in AN/DMSO mixed solvents.

This term, β_p, is due to the mixing of the excited-state angular momentum into the ground state. Two conditions are necessary for β_p to be nonzero: (1) there must be metal p character in the ground state and (2) an excited state must exsit possessing an angular momentum of the proper symmetry to mix with the ground state. The magnitude of the β_p term is therefore, determined by the amount of the metal p character in the ground state and by the energy separation between the ground state and excited states that are being mixed.

In the ground state, a Tl^+ ion with a $4d^{10} 5s^2$ configuration is in a spherically symmetric electrostatic field. When the symmetry of the environment is decreased, the Tl^+ ion will suffer an extensive mixing of the $4d^{10} 5s 5p$ and $4d^{10} 5p^2$ configurations into the ground state. In mixed solvent systems, a Tl^+ ion, surrounded by two different types of solvent molecules in the solvation sphere, will experience a variable amount of interaction with the two solvent species. The Tl^+-solvent interaction will cause some metal p character to appear in the ground state inducing an sp hybridization. This hybridization will affect the field symmetry of the Tl^+ ion and cause a downfield shift. The magnitude of the shift will depend on the degree to which the symmetry is lowered.

The hybridization of the Tl^+ ion caused by a non-spherically symmetric solvation sphere is related to the properties of the solvent which exist in the solvation sphere.

The main solvent-cation interaction should be an ion-dipole type, which varies with the dielectric constant or the donor ability of the solvent. The main effect of the solvent on cation-anion interactions is the ability of the solvent to shield the cation from the charge of the anion. This may be related to the bulk properties of the solvent.

In order to compare the bulk properties contributing to the shift, the Tl^+ ion chemical shift was measured in a series of binary mixed solvents (Figures 30-33). The mid-point on the curve between the shift extremes has been termed the "iso-solvation" point, which is the point where the mole percent of both solvents in the solvation sphere is 50. Iso-solvation values can be used to represent the relative solvating ability of the solvent. The iso-solvation points for several binary solvent systems are collected in Table 32. The iso-solvation value for the DMF/DMSO system is in good agreement with the value found by Zink (133). It is seen that the order of preferential solvation toward the Tl^+ ion is : HMPA > DMSO > H_2O > PY > DMF > THF > PC > AN > NM.

By comparing these results with dielectric constants or donor numbers of solvent (Table 33), a good correlation was observed between the iso-solvation point and the donor number of the solvent in various binary solvent systems as shown in Figure 35. The above results clearly indicate that the mole % of DMSO at the iso-solvation point increases with increasing donor number of the second solvent. The data show that the donicity of a solvent is more important than its

Table 32. Preferential Solvation Data of Several Binery
Solvent Systems.

Binary Solvent Systems	Isosolvation Point
NM/DMSO	0.005 MF[b] DMSO
AN/DMSO	0.014 MF DMSO
PC/DMSO	0.020 MF DMSO
THF/DMSO	0.028 MF DMSO
DMF/DMSO	0.168 MF DMSO
PY/DMSO[a]	0.25 MF DMSO
H_2O/DMSO	0.27 MF DMSO
HMPA/DMSO	0.790 MF DMSO
AN/DMSO	0.17 MF DMSO
H_2O/DMF	0.02 MF DMF

[a]Reference (109).   [b]MF: mole fraction

Table 33. The Gutmann Donor Number and Dielectric Constant
of Several Solvents.

Solvent Parameter	NM	AN	PC	THF	DMF	DMSO	H_2O	PY	HMPA
Gutmann Donor Number	2.7	14.1	15.1	20.0	26.6	29.8	33.0	33.1	38.2
Dielectric Constant	35.9	38.0	70	7.6	36.1	45.0	78.5	12.3	30.0
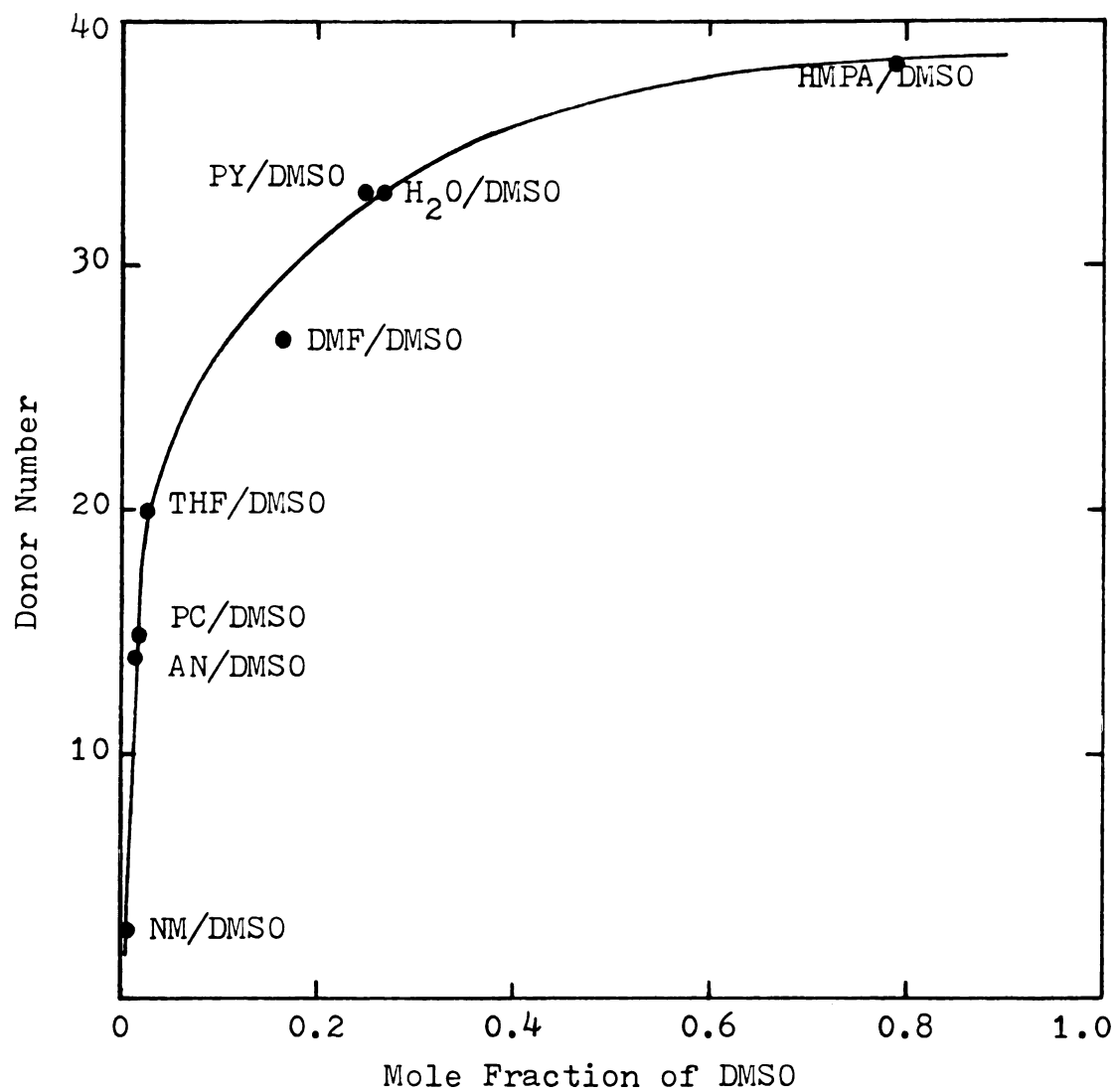
Figure 35. The plot of Gutmann donor number vs. iso-solvation point in several DMSO binary mixtures with other solvents.

dielectric constant scale in determining its relative sol-
vating ability.

Convington et al. (134-136) have recently developed a
quantitative model for competitive solvation. In their
papers, they present an equation of preferential solvation
which allows the calculation of geometric equilibrium con-
stants and the changes in free energy as the solvation shell
of an ion is progressively changed from one solvent to an
other. In Figures 30-33, most of the thallium-205 chemical
shift curves go through a minimum at about $X_p = 0.8$, which
indicates that there is not only simple ion-solvent inter-
actions occuring in our systems, but also other factors such
as ion pair formation. These figures can not be fitted to
the Convington equation.

3. Complexation of the Tl^+ Ion by DA18C6 or DT18C6 in Mixed
   Solvents

The complexation of the Tl^+ ion by DA18C6 and DT18C6 in
various organic solvents has been studied, and the results
are shown in Table 20. In these solvents, only a few values
of the formation constants between 0 and 10^5 can be calcu-
lated precisely as discussed in Chapter III. It is interest-
ing to see how well the solvation of the Tl^+ ion complexes
in mixed solvents can be explained in terms of the complexed
Tl^+ ion behaviour in the pure solvent. Complexation of the
Tl^+ ion by DA18C6 or DT18C6 were studied in DMF/H_2O orDMF/AN

binary mixed solvents, respectively. Thallium-205 chemical shifts were determined as a function of the DA18C6/Tl$^+$ or DT18C6/Tl$^+$ mole ratio. The results are listed in Tables 34 and 35. In all cases, only one resonance of the metal ion was observed, suggesting that the exchange between two sites (free and complexed Tl$^+$ ion) is fast compared with the NMR time scale. Graphical representations of the results are shown in Figures 36 and 37. The results clearly indicated that the nature of the medium plays an important role in the complexation process. For example, as the mole fraction of DMF in DMF/H$_2$O (Figure 36) is increased, the plot shows pronounced curvature, which is good evidence for the formation of a stronger (DA18C6·Tl)$^+$ complex. When the DA18C6/Tl$^+$ mole ratio is varied between 0 and 1, the thallium-205 linewidth broadens as the mole % of DMF in DMF/H$_2$O is increased probably because the exchange between two sites (free and complexed Tl$^+$ ion) is slower in DMF than in H$_2$O.

The values of the formation constants and the limiting chemical shifts for (DA18C6·Tl)$^+$ and (DT18C6·Tl)$^+$ complexes in various compositions of mixed solvents are calculated by fitting the variation of the thallium-205 chemical shift with the ligand/Tl$^+$ mole ratio. The results are summurized in Table 36. The data once again show that the values of the stability constants (K_f) of (DA18C6·Tl)$^+$ and (DT18C6·Tl)$^+$ increase as the mole fractions of DMF and AN are increased. The results obtained for these systems appear reasonable

Table 34. Mole Ratio-Chemical Shift Data for DA18C6/TlClO$_4$(0.01 M) in DMF/H$_2$O Mixed Solvents at 24°C.

L/Tl$^+$	pure DMF		85% DMF/15% H$_2$O			48% DMF/52% H$_2$O		
	δ(ppm)	Δν(Hz)	L/Tl$^+$	δ(ppm)	Δν(Hz)	L/Tl$^+$	δ(ppm)	Δν(Hz)
0.00	131.3	40	0	128.5	21	0.00	130.7	17
0.25	-	-	0.15	-	-	0.21	273.0	1751
0.36	-	-	0.36	-	-	0.46	356.0	1732
0.80	600.7	580	0.91	645.6	836	0.65	474.8	1192
1.05	695.8	284	1.12	704.8	119	0.84	563.3	874
1.45	735.8	101	1.64	743.4	76	1.30	708.5	204
1.56	740.5	94	2.02	749.9	70	1.72	728.5	167
2.08	749.3	82	2.25	752.4	58	2.46	759.1	68
2.15	748.6	80	2.94	756.4	50	3.11	768.7	57
2.80	757.0	75	3.47	757.7	50	4.10	775.8	57
3.91	759.9	62	4.06	759.0	48	4.61	778.3	50
5.13	763.7	56	5.47	761.7	41	5.83	781.6	52

Table 34. Continued.

33% DMF/67% H₂O			23% DMF/77% H₂O			13% DMF/87% H₂O		
$L/T1^+$	δ(ppm)	Δν(Hz)	$L/T1^+$	δ(ppm)	Δν(Hz)	$L/T1^+$	δ(ppm)	Δν(Hz)
0.00	110.6	24	0.00	82.7	44	0.00	46.6	21
0.23	220.2	623	0.32	237.0	539	0.38	126.8	167
0.44	321.0	958	0.91	397.5	538	0.69	195.9	234
0.74	436.5	909	1.24	458.8	508	0.95	231.6	275
0.99	531.0	585	1.54	517.3	441	1.54	318.4	278
1.28	599.3	286	2.30	593.3	252	1.83	357.4	256
1.66	649.6	280	2.65	619.6	362	2.06	372.7	246
2.29	697.2	231	3.18	644.0	227	2.42	407.4	223
2.69	719.9	156	3.66	665.3	337	2.67	433.7	210
3.41	732.2	126	4.31	681.2	123	3.39	474.5	222
4.14	745.5	97	4.97	694.2	239	4.20	514.0	202
5.34	756.2	78	5.79	706.2	142	5.01	550.0	202

Table 35. Mole Ratio-Chemical Shift Data for TlClO$_4$(0.01 M) in the Presence of DT18C6 in AN/DMF Mixed Solvents at 24°C.

L/Tl$^+$	pure DMF[a]		79% DMF/21% AN[b]			61% DMF/39% AN		
	δ(ppm)	Δν(Hz)	L/Tl$^+$	δ(ppm)	Δν(Hz)	L/Tl$^+$	δ(ppm)	Δν(Hz)
0.00	133.7	33	0.00	132.5	26	0.00	131.6	31
0.35	135.2	33	0.22	135.2	26	0.30	137.6	31
0.69	137.1	31	0.39	136.2	26	0.51	140.0	31
0.98	138.0	32	0.64	138.6	26	0.74	143.4	31
1.20	138.0	31	0.91	140.6	31	1.05	145.6	31
1.60	140.0	27	1.11	142.2	31	1.21	147.1	31
2.04	141.5	35	1.53	144.4	31	1.50	150.1	31
2.82	143.1	32	1.80	146.6	26	1.77	153.7	31
3.32	144.7	39	2.16	148.7	31	2.29	157.0	31
4.06	146.2	37	3.37	154.8	31	2.87	159.7	31
5.25	148.6	35	4.34	159.2	31	4.10	168.8	31
6.04	149.9	37	7.04	169.3	31	5.13	175.3	31

[a]SW= 5000 Hz

[b]SW= 10000 Hz

Table 35. Continued.

41 % DMF/59% AN			23% DMF/77% AN			11% DMF/89% AN		
L/T1$^+$	δ(ppm)	Δν(Hz)	L/T1$^+$	δ(ppm)	Δν(Hz)	L/T1$^+$	δ(ppm)	Δν(Hz)
0.00	120.5	21	0.00	107.5	21	0.00	64.5	23
0.22	129.4	21	0.15	122.1	21	0.27	130.6	48
0.45	136.0	21	0.39	137.5	21	0.37	142.9	54
0.73	142.9	21	0.51	153.7	35	0.57	181.7	54
0.86	146.9	26	0.88	178.4	33	0.81	215.9	42
1.21	154.4	21	1.05	188.1	33	1.03	242.9	42
1.50	160.1	21	1.40	204.8	33	1.35	271.5	30
2.09	171.4	21	1.75	216.6	35	1.65	287.2	30
2.92	183.7	21	2.18	230.7	33	2.07	302.0	30
3.98	195.7	21	2.88	244.8	33	2.50	310.8	27
5.52	208.2	26	3.26	252.1	33	3.88	324.5	27
7.86	221.9	26	5.06	270.6	33	5.60	329.6	27
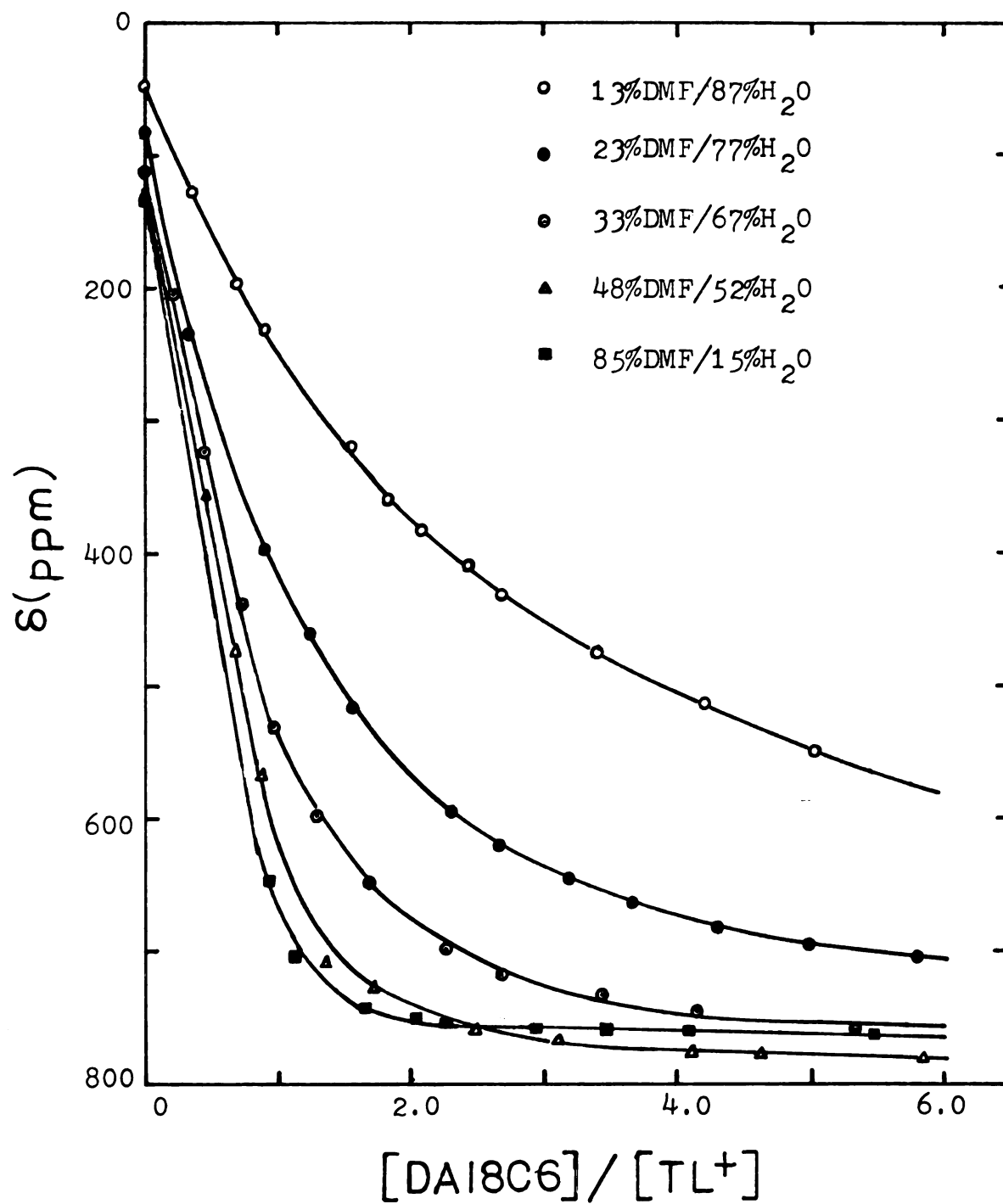
Figure 36. Thallium-205 chemical shifts <u>vs.</u> DA18C6/TlClO$_4$(0.01M) mole ratio in DMF/H$_2$O systems.
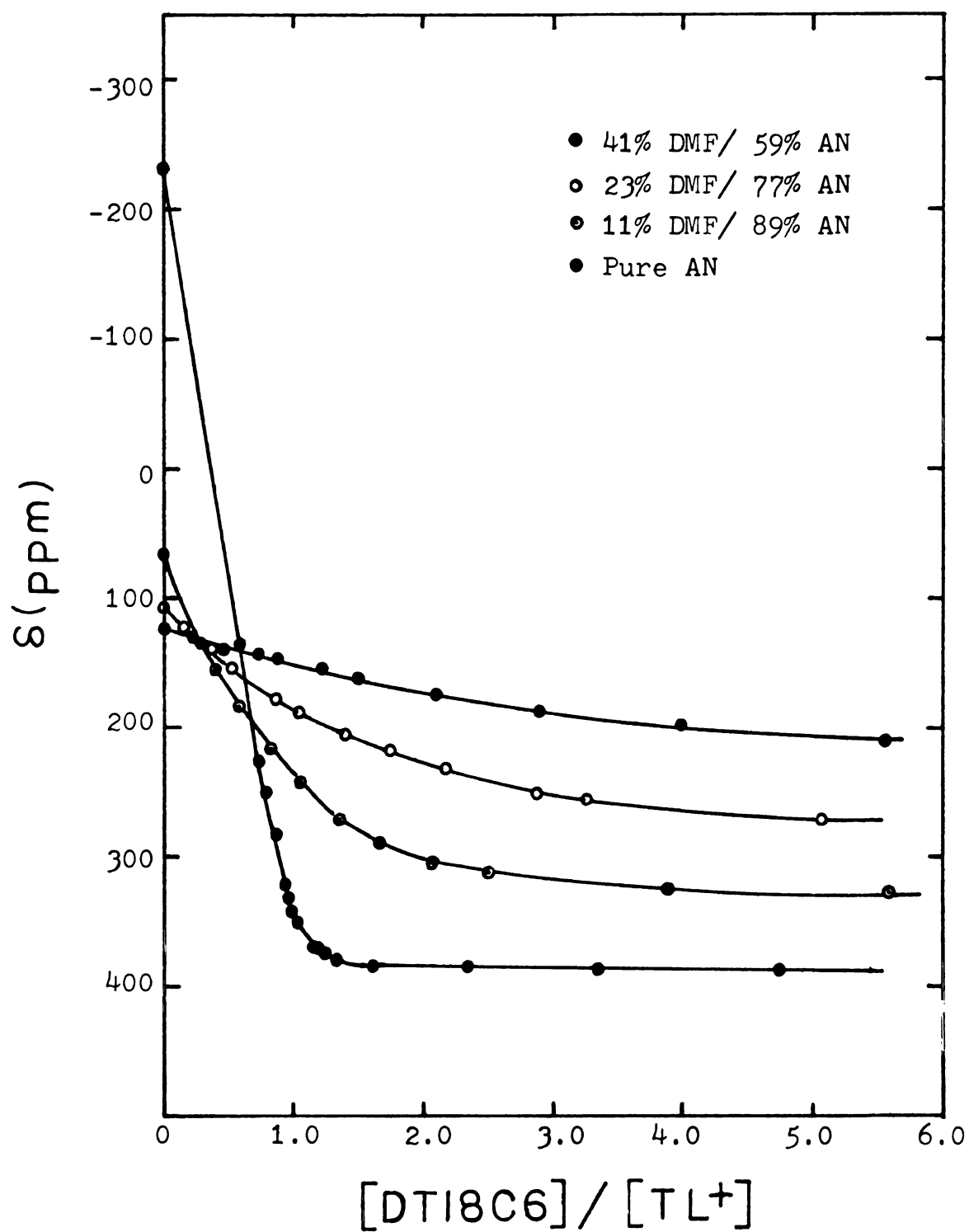
Figure 37. Chemical shifts of Tl-205 vs. mole ratio of (DT18C6)/(Tl+) in DMF/AN mixed solvents.
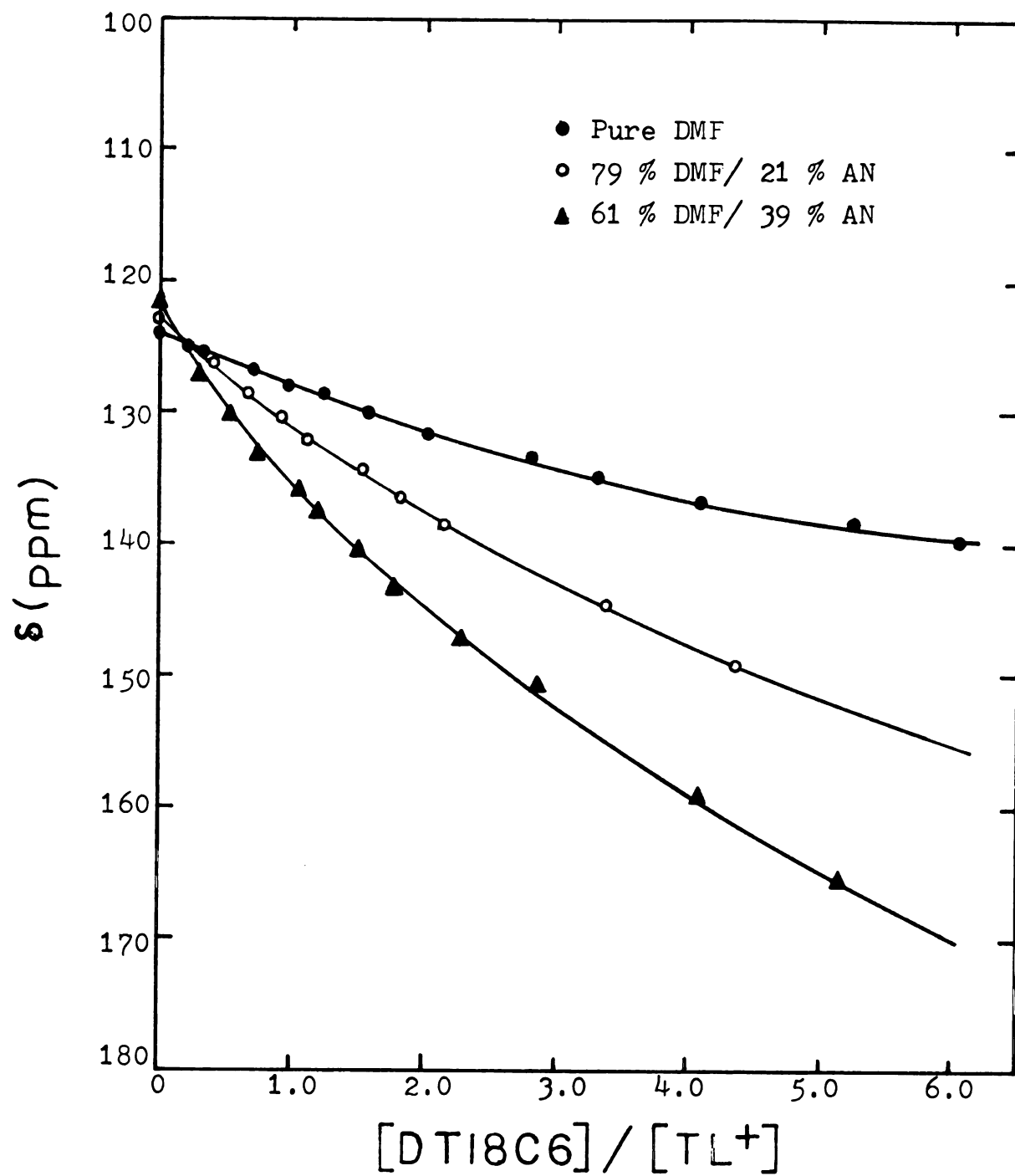
Figure 37. Continued.

T

S

p
8
4
3
2
1
p

p
8
7

2
N

Table 36. Log of Formation Constants and Limiting Chemical Shifts for $(DA18C6 \cdot Tl)^+$ and $(DT18C6 \cdot Tl)^+$ Complexes in Mixed Solvents.

Solvent	Log K_f	Limiting Chemical Shift (ppm)
$(DA18C6 \cdot Tl)^+$		
pure DMF	3.55 ± 0.03	766.5 ± 0.1
85% DMF/15% H_2O	3.59 ± 0.03	764.8 ± 0.4
48% DMF/52% H_2O	3.09 ± 0.03	792.6 ± 1.1
33% DMF/67% H_2O	2.65 ± 0.02	790.0 ± 2.3
23% DMF/77% H_2O	2.26 ± 0.02	776.8 ± 3.7
13% DMF/87% H_2O	1.70 ± 0.02	783.6 ± 13.5
pure H_2O	0.96 ± 0.01	824.7 ± 13.4
$(DT18C6 \cdot Tl)^+$		
pure AN	4.16 ± 0.06	388.7 ± 0.3
89% AN/11% DMF	2.70 ± 0.01	341.4 ± 0.5
77% AN/23% DMF	2.00 ± 0.02	309.2 ± 3.2
59% AN/41% DMF	1.50 ± 0.02	265.5 ± 2.7
39% AN/61% DMF	1.46 ± 0.07	205.3 ± 7.0
21% AN/79% DMF	1.20 ± 0.04	203.6 ± 4.2
pure DMF	1.19 ± 0.06	168.2 ± 3.0

because solvents with large donor number, such as DMF (D.N.= 26.6) in DMF/AN and H_2O (D.N.= 33) in H_2O/DMF, have relatively larger solvating ability for the Tl^+ ion, hence a smaller complex formation constant is obtained. The variation of the stability constants of $(DT18C6 \cdot Tl)^+$ or $(DA18C6 \cdot Tl)^+$ with composition of mixed solvents is plotted in Figure 38.

It is interesting to note that, in all cases, the limiting chemical shifts for the complexed Tl^+ ion are dependent on the solvent composition suggesting that the complexed Tl^+ ion is only partially insulated from the solvent molecules.
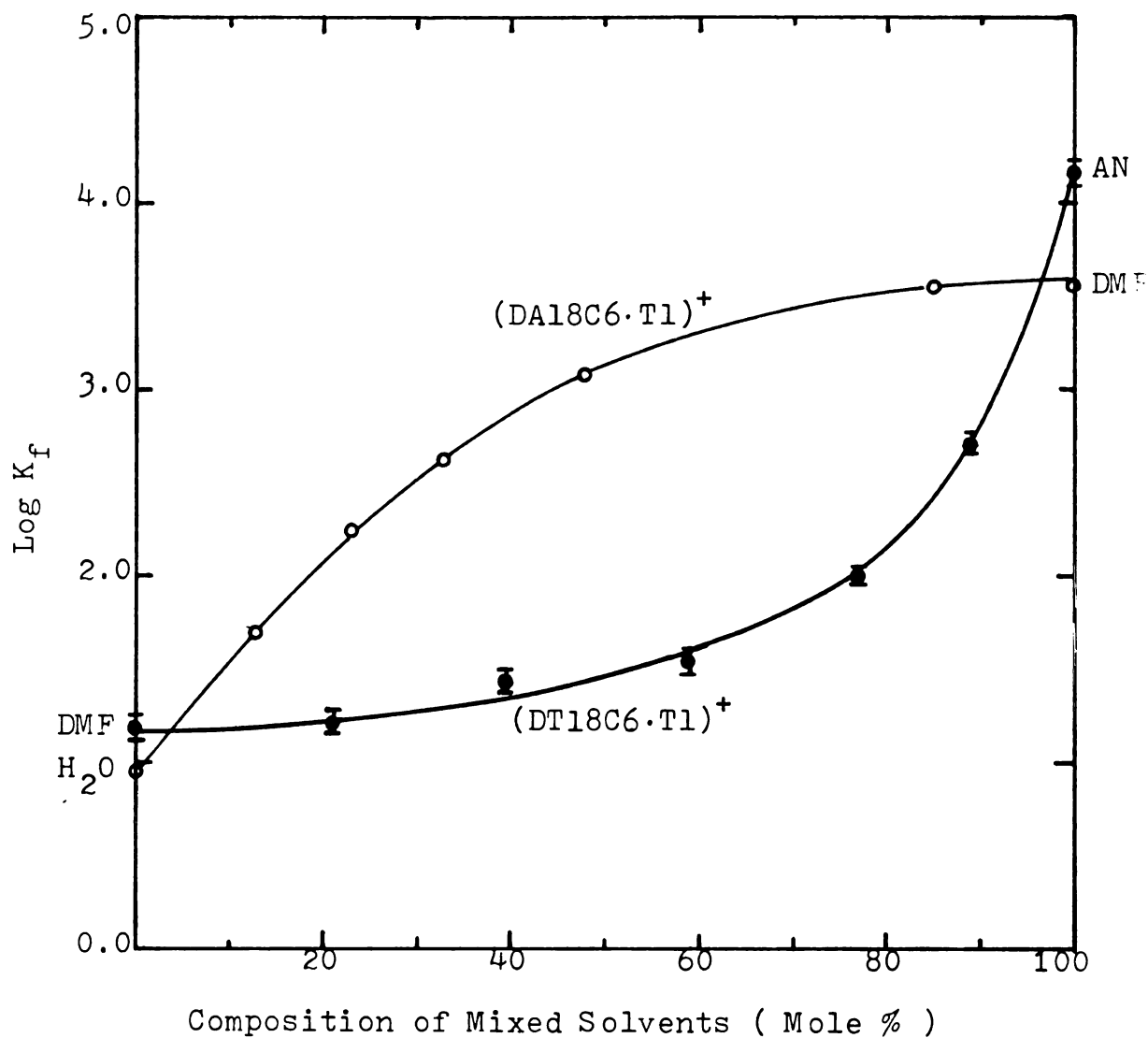
Figure 38. Log of stability constants of $(DT18C6 \cdot Tl)^+$ and $(DT18C6 \cdot Tl)^+$ complexes vs. solvent composition in DMF/AN and H_2O/DMF mixed solvents.

CHAPTER VI

MISCELLANEOUS

1. Complexes of 18-crown-6 and Its Analogs Studied by
    Proton and Carbon-13 NMR

Although x-ray studies give conformations of the metal
complexes of 18-crown-6 and its analogs (35,59,67,77) in the
solid state, it is apparent that the structures may be dis-
torted by such factors as intermolecular hydrogen bonding
and crystal packing relative to the "free" molecule (139,140).
Furthermore, since most chemical reactions are carried out
in solution, it is important to establish conformations in
this state. Nuclear magnetic resonance studies have been
used to elucidate the effects of the factors such as ring
substituents, donor atoms and central metal size on crown
ring conformation. We have chosen the NMR method because of
its unique ability to give the desired information provided
that the complexes are suitably designed.

Complexation of the thallium(I) ion by 18C6 and its
analogs in various solvents has been presented in Chapter
III of this thesis. The results show that the conformation
of DT18C6 changes during complexation. Proton and carbon-13
NMR were used to identify this conformational change. In
this thesis, all chemical shifts of the ^{13}C resonance are
referenced to the methyl group of MeOD.

As shown in Figure 17, the complex, $(18C6 \cdot Tl)^+$ formed in
DMF results in a upfield shift for the carbon-13 resonance.
Figure 39 shows ^{13}C NMR spectra of 18C6 (0.02 M) in AN-d_3
with MeOD as an external reference. Since all carbon nuclei
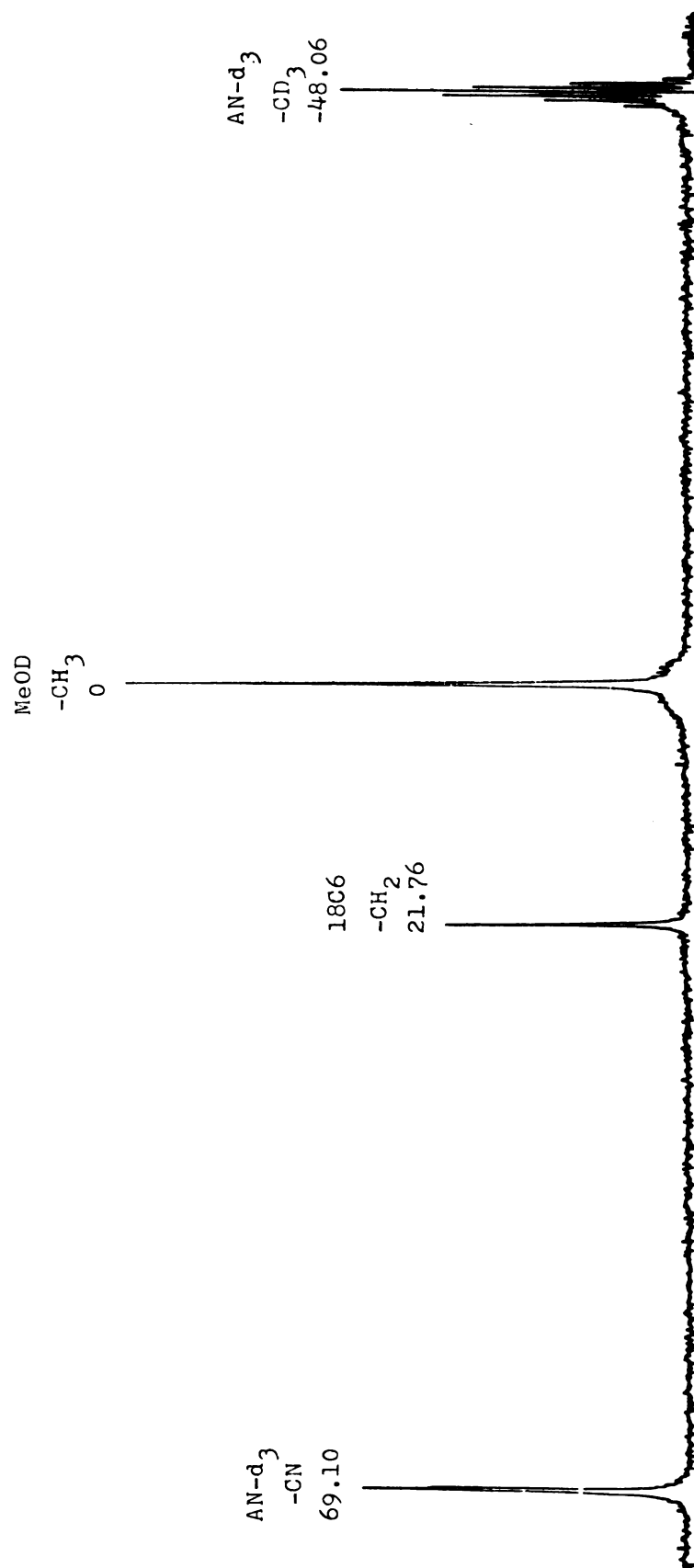
Figure 39. Carbon-13 NMR spectra of 18C6 (0.02 M) in AN-d_3 with MeOD as reference.

in 18C6 are magnetically equivalent, only one ^{13}C resonance at 21.76 ppm appears in this spectrum and it shifts upfield (Table 37) as the metal ion/18C6 mole ratio is increased (i.e. the complex is formed). The ligand DB18C6 has three sets of equivalent carbon nuclei (C(1), C(2) and C(3) in Figure 40). The two benzo rings on DB18C6 withdraw electrons from the crown ring, therefore the electron density on the carbon atoms decrease in the order C(1) > C(2) > C(3). Consequently, the chemical shifts of C(1), C(2) and C(3) on DB18C6 in DMF are 19.66 ppm, 20.96 ppm and 100.01 ppm respectively. Similarly in DMSO the chemical shifts of C(1), C(2) and C(3) are 19.43 ppm, 20.75 ppm and 99.78 ppm respectively. Table 38 shows that in both solvents, all three ^{13}C resonance frequencies shift upfield as Tl$^+$/DB18C6 mole ratio is increased, and the chemical shift change is in the order C(3) > C(1) > C(2).

Three sets of carbon nuclei (C(1), C(2) and C(3) in Figure 41) are found in DA18C6. In DA18C6, the electron withdrawing ability of the oxygen atom is higher than that of the nitrogen atom, therefore, the electron density on carbon decreases in the order C(1) > C(2) > C(3). The result is that the chemical shifts of C(1), C(2) and C(3) on DA18C6 in AN are 0.54 ppm, 21.38 ppm and 21.66 ppm respectively. Table 39 shows that all of these three ^{13}C resonance frequencies shift upfield as the cation/DA18C6 mole ratio is increased, and the chemical shift change is in the order C(2) > C(3) > C(1).

Table 37. Carbon-13 Chemical Shift-Mole Ratio Data for 18C6 Complex with Cation in AN-d$_3$ Solution.

Salt	M$^+$/18C6	δ(ppm)
18C6		
0.02 M	0	21.76
KPF$_6$	1.68	21.52
AgNO$_3$	1.65	21.74
TlClO$_4$	1.61	21.21
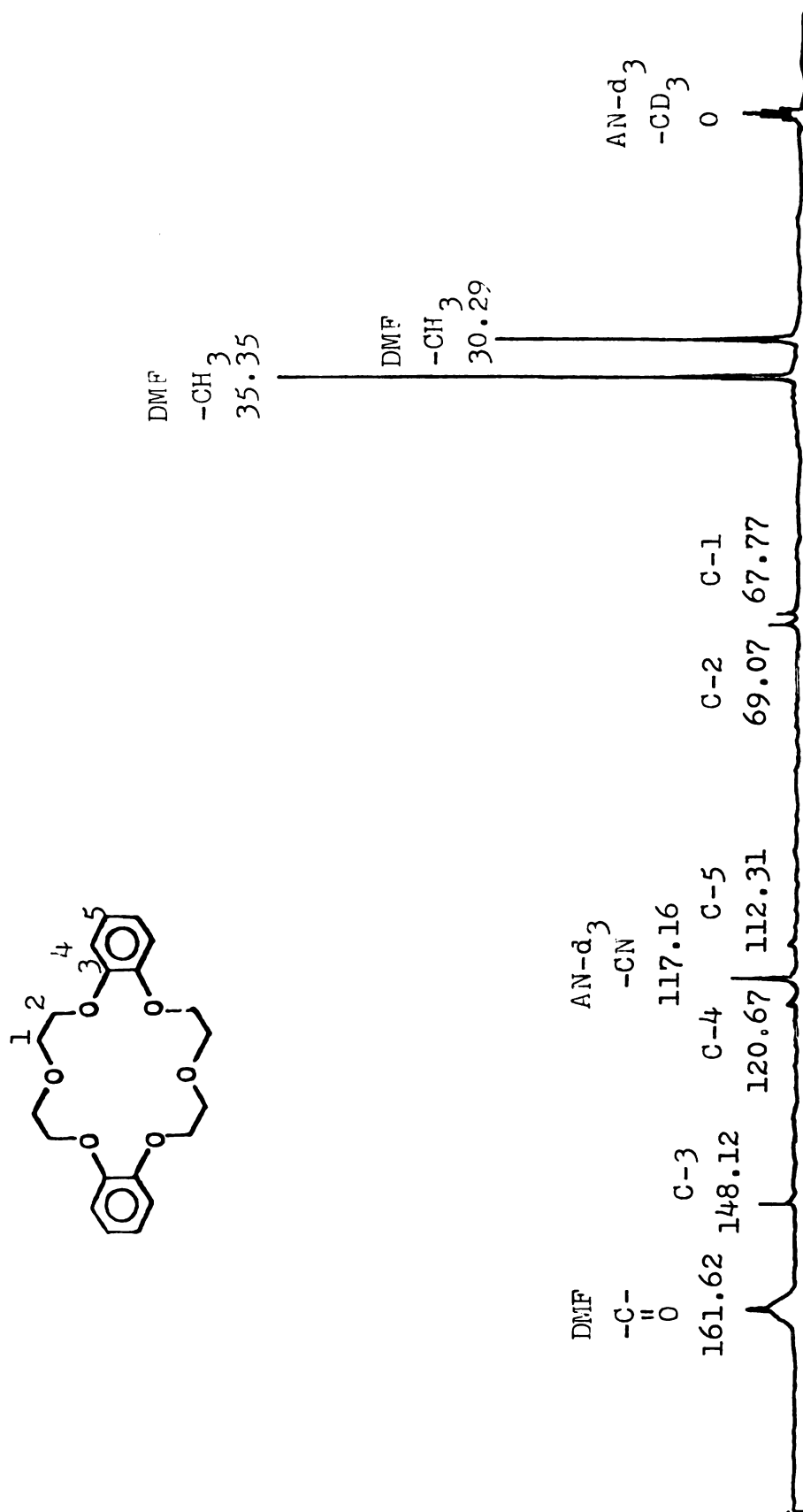
Figure 40. Carbon-13 NMR spectra of DB18C6 (0.04 M) in DMF with AN-d_3 as reference.

Table 38. Carbon-13 Chemical-Mole Ratio Data for DB18C6 Complex with $TlClO_4$ in DMF and DMSO.

0.05 M DB18C6 $\frac{Tl^+}{DB18C6}$	Solvent	$\delta\, C(1)$ (ppm)	$\delta\, C(2)$ (ppm)	$\delta\, C(3)$ (ppm)	$\frac{Tl^+}{DB18C6}$	Solvent	$\delta\, C(1)$ (ppm)	$\delta\, C(2)$ (ppm)	$\delta\, C(3)$ (ppm)
0	DMF	19.66	20.96	100.01	0	DMSO	19.43	20.75	99.78
0.43		19.48	20.89	99.81	0.38		19.25	20.71	99.60
0.82		19.33	20.83	99.63	0.79		19.15	20.62	99.50
0.98		19.24	20.80	99.54	1.65		19.03	20.59	99.33
1.17		19.20	20.78	99.48					

Figure 41. Carbon-13 NMR spectra of DA18C6 (0.04 M) in AN with AC-d$_6$ as reference.

Table 39. Carbon-13 Chemical Shift-Mole Ratio Data for DA18C6 Complex with Cation

Table 39. Carbon-13 Chemical Shift-Mole Ratio Data for DA18C6 Complex with Cation in AN with MeOD as Reference.

Salt	DA18C6	M^+/DA18C6	C(1) δ(ppm)	C(2) δ(ppm)	C(3) δ(ppm)
	0.02 M	0	0.59	21.46	21.65
	0.04 M	0	0.54	21.38	21.66
TlClO$_4$	0.02 M	0.56	0.52	20.13	20.75
		1.38	0.32	19.34	20.01
KPF$_6$	0.04 M	1.38	0.52	20.97	21.66

F...
w...
o...
c...
t...
i...
r...
u...
t...
s...

k...
r...
d...
c...
u...
s...

t...
r...
a...
l,...
ca...
as...
th...

Three sets of carbon nuclei (C(1), C(2) and C(3) in
Figure 42) are also found in DT18C6. In DT18C6, the electron
withdrawing ability of the oxygen atom is higher than that
of the sulfur atom, therefore the electron density of the
carbon atom decreases in the order C(1) > C(2) > C(3), and
the chemical shifts of C(1), C(2) and C(3) on DT18C6 (0.04 M)
in acetonitrile are -17.12 ppm, 21.72 ppm and 23.26 ppm
respectively. Table 40 indicates that ^{13}C resonance shifts
upfield for C(2) and C(3) but shifts downfield for C(1) as
the cation/DT18C6 mole ratio is increased, and the chemical
shift change is in the order C(3) > C(1) > C(2).

In the identification of the ^{13}C resonance for three
kinds of carbon as described above, we assume that carbon
nuclei are diamagnetic nuclei. Since the ^{13}C chemical shift
differences between C(1) and C(2) on DB18C6, C(2) and C(3)
on DT18C6 or DA18C6 are very small, the peak assignment is
unsure. Isotopic labeling studies are required for exact
site assignment.

Comparing the results described above, it is interesting
to note that the C-13 resonance of all carbons on the crown
ring of (18C6·M^{+}), (DB18C6·Tl^{+}) and (DA18C6·M^{+}) complexes
are upfield (shielding) compared with the respective free
ligands. On the other hand, in the (DT18C6·M^{+}) complex,
carbons 2 and 3 shift upfield but carbon 1 shifts downfield
as compared with the free DT18C6. The crystal structure of
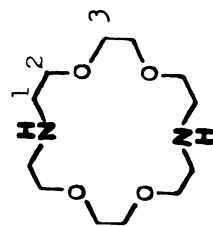the DT18C6·PdCl$_2$ complex (77) shows that only outwardly
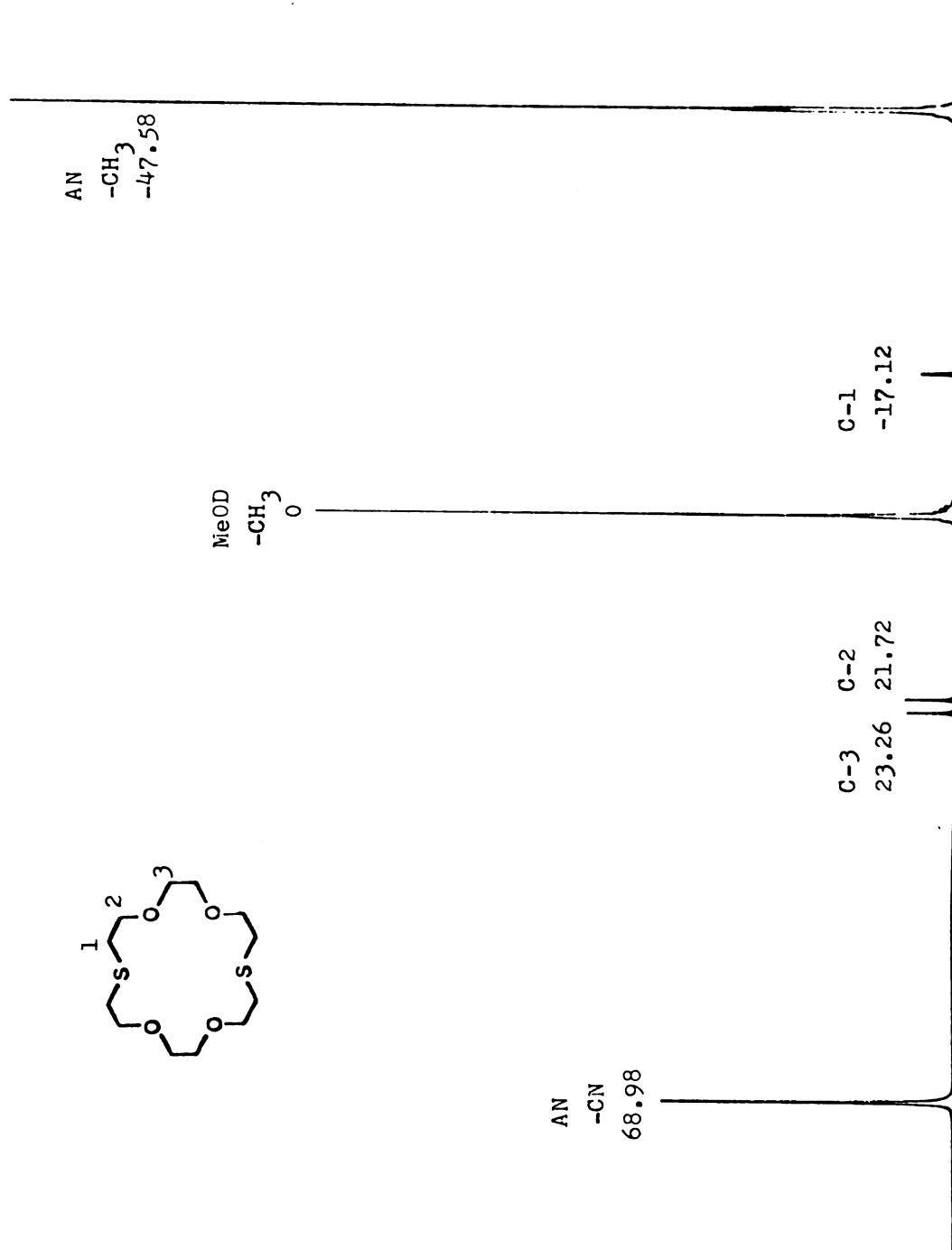
Figure 42. Carbon-13 NMR spectra of DT18C6 (0.04 M) in AN with MeOD as reference.

Table 40. Carbon-13 Chemical Shift-Mole Ratio Data for DT18C6 Complex with
Various Cations in AN or AC with MeOD as Reference.

Salt	DT18C6	Solvent	M^+/DT18C6	C(1)	C(2)	C(3)
	0.04 M	AN	0	-17.12	21.72	23.26
AgNO$_3$			0.43	-15.89	21.41	21.09
			1.03	-14.42	21.03	18.34
	0.02 M		0	-17.08	21.75	23.29
TlClO$_4$			0.50	-16.45	21.19	21.59
			1.08	-15.92	20.62	19.94
KPF$_6$			0.50	-16.96	21.68	22.59
			1.01	-16.87	21.59	22.09
KBPh$_4$			1.03	-16.86	21.56	21.91
	0.04 M	AC	0	-17.34	21.85	23.55
KPF$_6$			0.49	-17.26	21.78	23.26
			0.99	-17.20	21.73	23.06

turned sulfur atoms participate in coordination with the Pd^{2+} ion. The complexing strength of 18C6 and its analogs with the Tl^+ ion, shown in Table 21, generally decrease in the order DA18C6 > 18C6 > cis-syn-cis-DC18C6 > DB18C6. These results suggest that only two sulfur atoms take part in the coordination with the Tl^+ ion. The ^{13}C resonance data discussed above seem to suggest that, in solution, $(DT18C6 \cdot Tl)^+$ has the following structure (C). While, $(DT18C6 \cdot Ag^+)$ has the other structure (D), since stability constants of 18C6 and its analog with the Ag^+ ion are in the order DA18C6 > DT18C6 > 18C6 > DB18C6 (10, 59, 63, 76).

(C) (D)
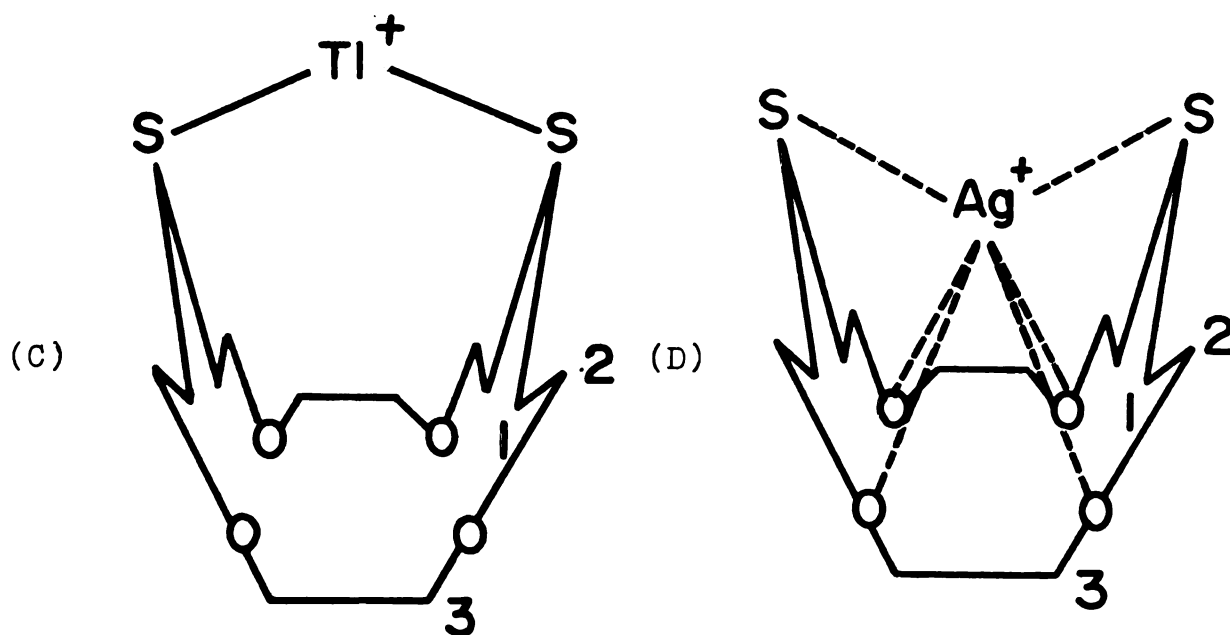
It is obvious that there is a quite strong angle strain on carbon 1 site which may induce a downfield chemical shift. Conformational changes on complexation, were also studied by proton resonance spectra. Acetonitrile-d_3 was selectes as the solvent in all studied systems and all chemical shifts resonances are referenced to the hydrogen nuclei in acetonitrile.

In 18C6 and its complexes, all protons are magnetically equivalent, therefore, only a single resonance is obtained. It is intesting to note that this resonance shifts downfield (Table 41) as the metal ion/18C6 mole ratio is increased.

Three sets of ^1H nuclei are found in DT18C6 as shown in Figure 43. Figures 43 and 44 show the proton NMR spectra of DT18C6 and its complex with the K^+ ion which show that the protons on the carbons (C(1) and C(2)) form two triplets with a 1:2:1 intensity ratio since this system is made up of two sets of magnetically equivalent nuclei (an A_2X_2 system) (141). While the protons on the carbons C(3) between two oxygen atoms are made up of one set of magnetically equivalent nuclei (an X_n system), therefore their resonance appears as a singlet with chemical shift 1.611 ppm (δ_5, δ_6). The calculated NMR parameters are shown in Table 42.

Proton NMR spectra (Figure 51) of the two complexes, $(DT18C6 \cdot Tl)^+$ and $(DT18C6 \cdot Ag)^+$, show some multiplets existing in two triplets. On the Bruker WM-250, the DISNMR program is more powerful than the general proton program, on which gaussian multiplication (GM) and zero filling techniques can be used to improve the resolution of the spectra. The technique uses 8K or 16K memory for acquisition and gaussian mutiplication, then with the 64K memory for fourier transforms (FT). After treating the NMR spectra (Figure 45) with this technique, a better resolution spectrum as shown in Figure 46 was obtained.

Table 41. Proton Chemical Shift-Mole Ratio Data for 18C6 Complex with Various Cations in AN-d$_3$.

Salt	18C6	$M^+/18C6$	δ(ppm)
	0.02 M	0	1.568
KPF$_6$		1.68	1.626
AgNO$_3$		1.65	1.574
TlClO$_4$		1.61	1.666
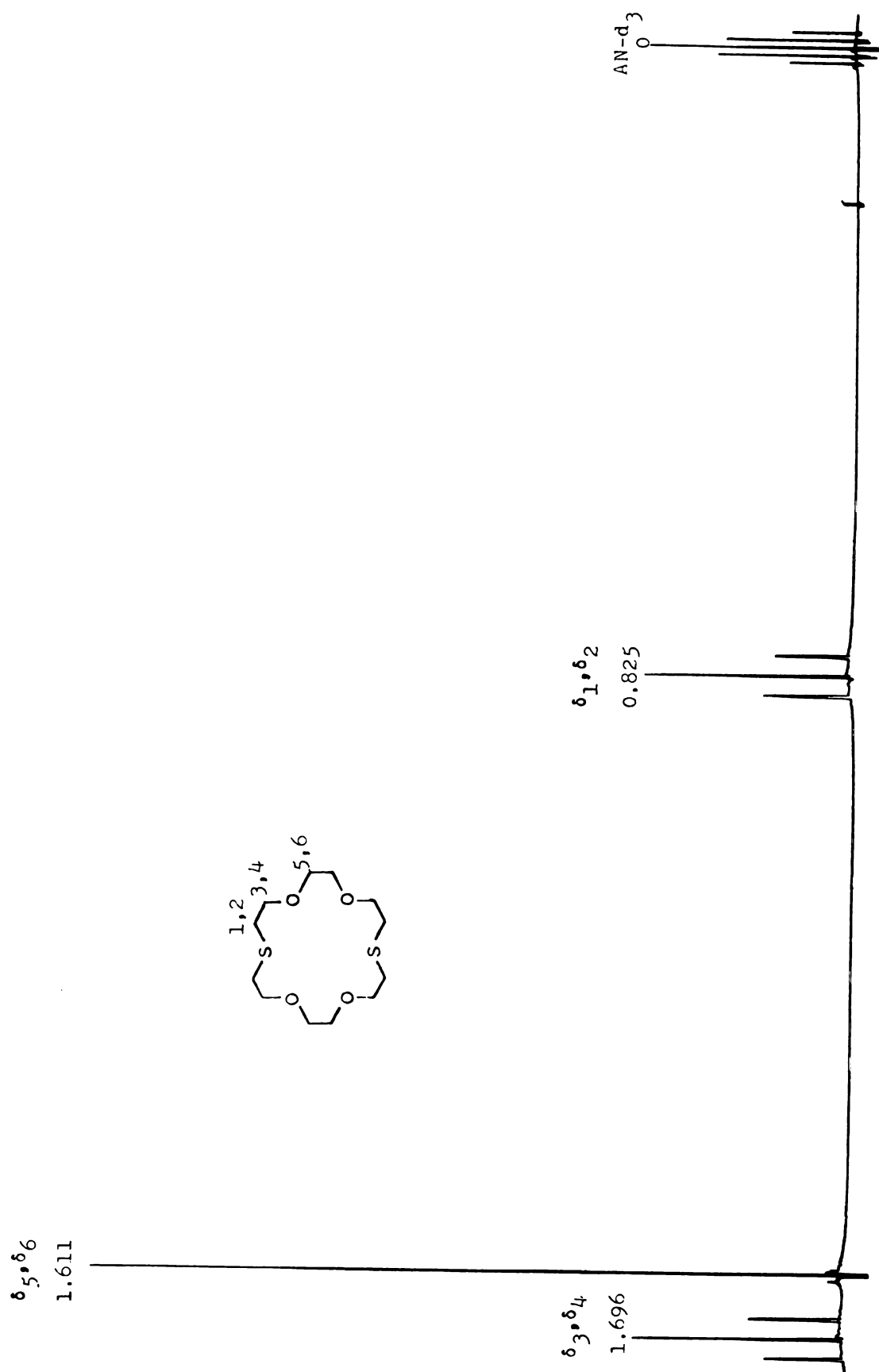
Figure 43. Proton NMR spectra of DT18C6 (0.02 M) in AN-d_3.

Figure 44. Proton NMR spectra of $\dfrac{KPF_6}{DT18C6}$ = 1.01 in AN-d_3.

Table 42. Proton NMR Parameters of DT18C6 and Its Complexes.

Salt	DT18C6 M^+/DT18C6	δ_1,δ_2 [a]	δ_3,δ_4	δ_5,δ_6	J_{12},J_{34} [b]	J_{13},J_{24}	J_{14},J_{23}	RMS [c]
DT18C6 0.02 M	0	0.825	1.696	1.611		6.6 [d]		
KPF$_6$	1.01	0.838	1.694	1.629		6.2 [d]		
TlClO$_4$	1.00	0.961	1.779	1.694	1.9	6.3	4.2	0.076
0.04 M	0	0.825	1.695	1.610		6.6 [d]		
AgNO$_3$	1.21	1.078	1.741	1.672	1.8	6.3	4.1	0.105

[a,b] Chemical shifts are downfield from acetonitrile in ppm, coupling constants are in Hz.

[c] RMS is root mean square error.

[d] J_{AX} in A_2X_2 system.
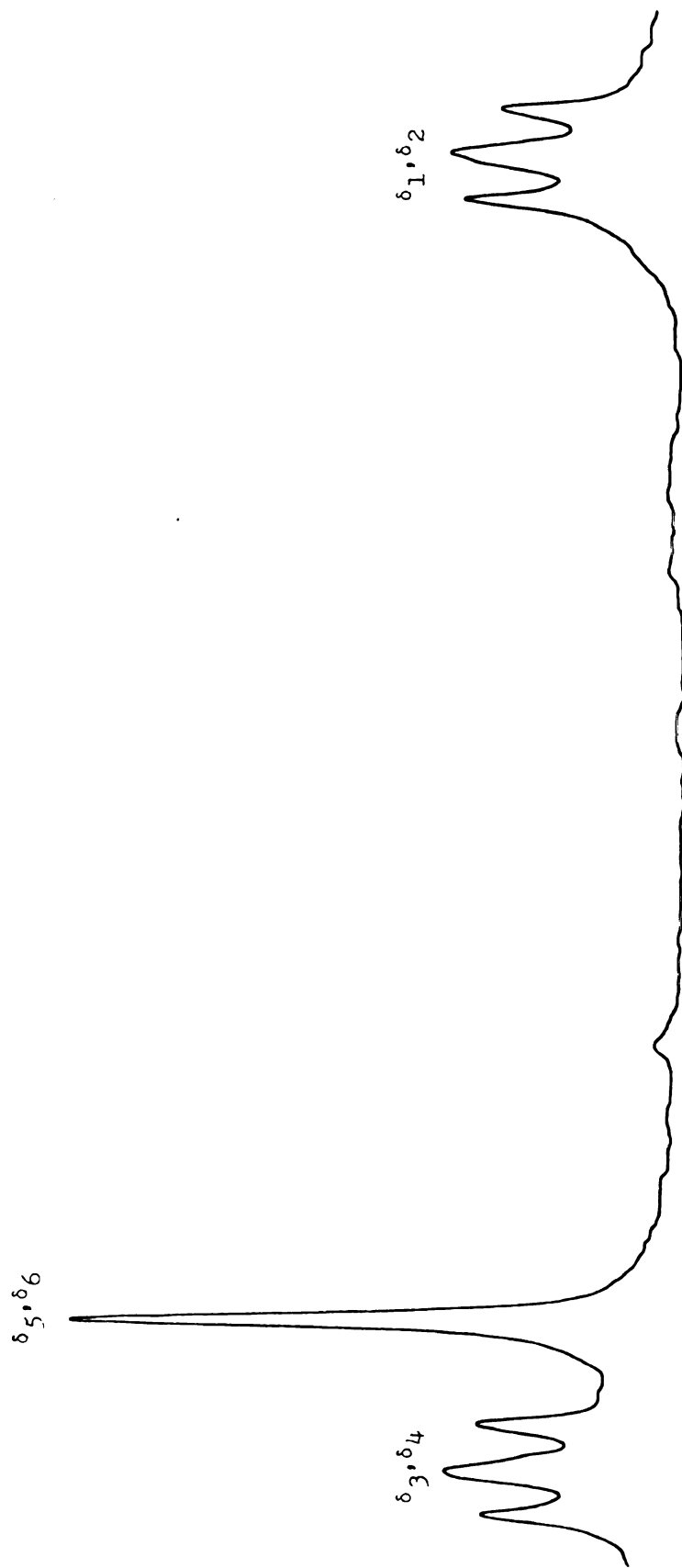
Figure 45. Proton NMR spectra of $(DT18C6 \cdot Ag)^+$ complex in AN-d_3.
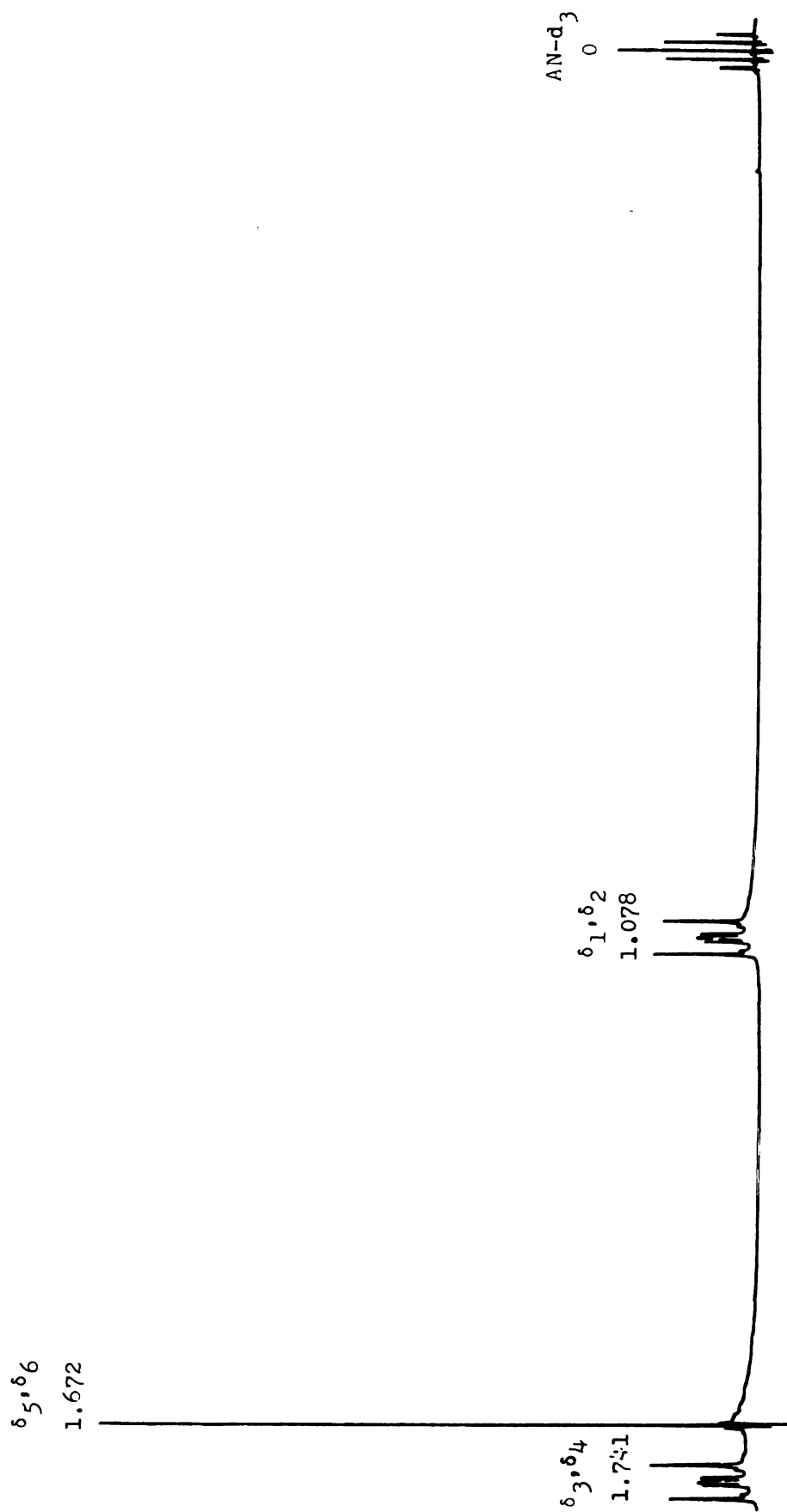
Figure 46. Proton NMR spectra of $(DT18C6 \cdot Ag)^+$ complex after treating with gaussian multiplication.

Figure 46 shows that the resonance spectra of the two sets protons on the carbons between oxygen and sulfur which are very symmetrical about its midpoint (Figure 47) and yield solutions indicative of an AA'XX' system (142). The proton signal (Figure 47) was simulated by using the PANIC program (LAOCOON type program) provided by the Bruker company. These calculations require estimated coupling constants, the number of non-equivalent nuclei and the estimated chemical shifts as input to obtain the best fit between experimental and simulated spectra. After the iteration calculation by the PANIC program, a root mean square (RMS) error estimated for the adjusted parameters is given. The simulation spectrum is shown in Figure 48. The calculated NMR parameters of proton resonance spectra of the $(DT18C6 \cdot Tl)^+$ and $(DT-18C6 \cdot Ag^+)$ complexes are given in Table 42. The simulation method indicates again that the two sets protons on the carbon between oxygen and sulfur are an AA'XX' system. This type of spin system is implied that $J_{13}=J_{24} \neq J_{14}=J_{23}$ as indicated in Table 42. These two sets of protons (1,2 and 3,4) are said to be chemical-shift-equivalent nulei but magnetically nonequivalent. The results clearly indicate that, in good agreement with the results studied by ^{13}C NMR, there is a conformation change as the complex is formed.

In the $(DT18C6 \cdot K^+)$ complex, two sets of protons on the carbons between the oxygen and sulfur atoms are magnetically equivalent nuclei belonging to an A_2X_2 system. This result
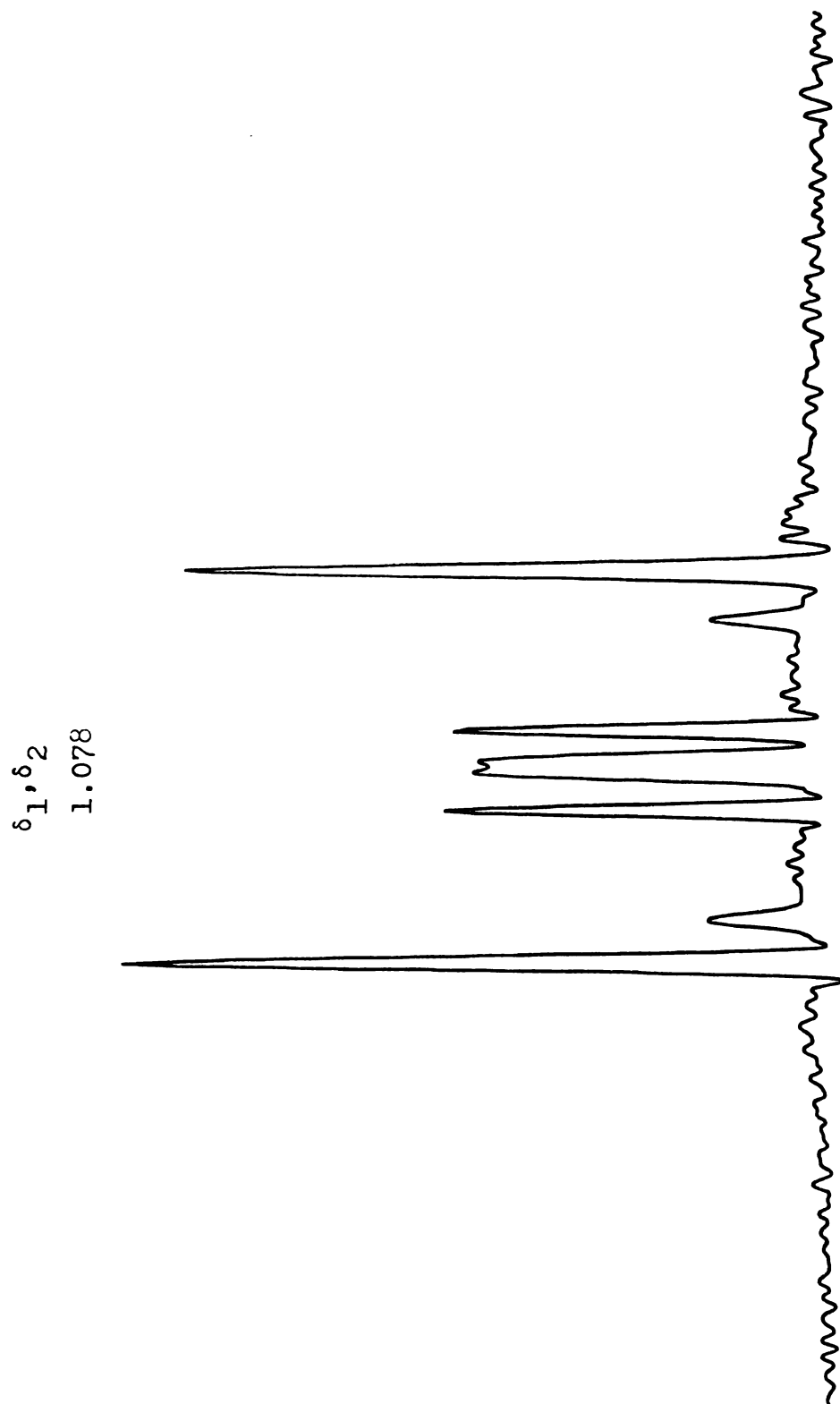
Figure 47. Proton NMR spectra of proton 1 and 2 in $(DT18C6 \cdot Ag)^+$ complex after treating with gaussian multiplication.
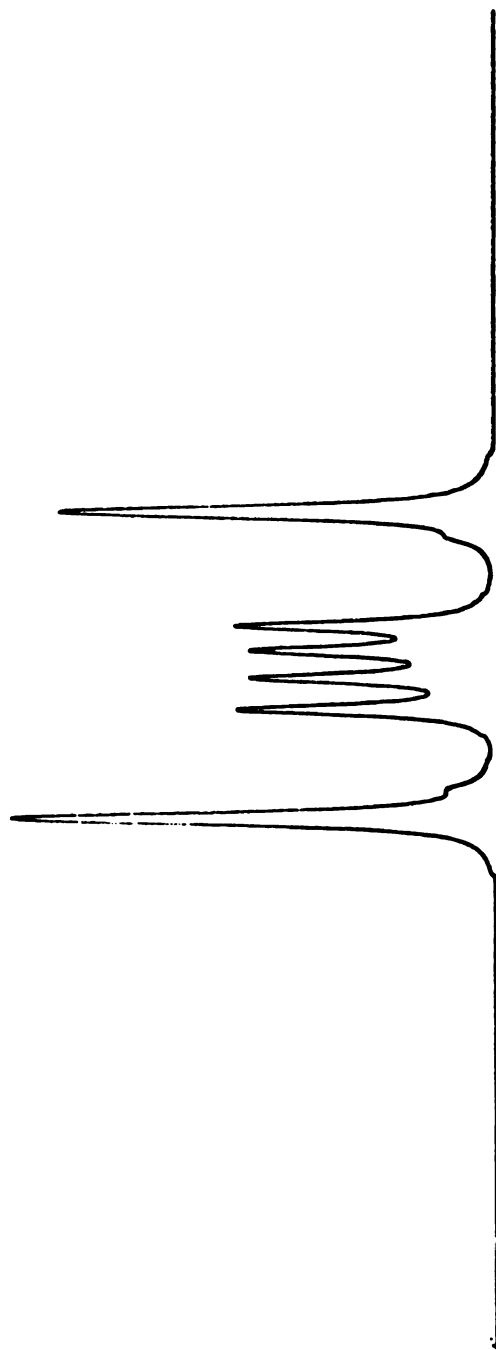
Figure 48. The simulative proton NMR spectra (AA'XX' system) of (DT18C6·Ag)$^+$ complex.

may indicate that a very weak complex is formed between the K^+ ion and DT18C6, therefore, the conformation of DT18C6 in the complex is still flexible, and the two hydrogen atoms on the same carbon (carbon 1 or 2) remain magnetically equivalent nuclei. The small ^1H and ^{13}C chemical shift changes for the $(DT18C6 \cdot K^+)$ complex as compared with the free ligand (Tables 39 and 42) also seems to incidate that a very weak complex is formed between K^+ and DT18C6.

Table 42 indicates that all ^1H resonances shift down-field as the complex is formed and the chemical shift change is in the order: ^1H on C(1) > ^1H on C(3) > ^1H on C(2). The results indicate that $J_{13}=J_{24}$ and $J_{14}=J_{23}$ in both the $(DT-18C6 \cdot Tl)^+$ and $(DT18C6 \cdot Ag)^+$ complexes which demonstrate that the time-averaged dihedral angle θ between protons on C(1) and C(2) are $\theta_{13}=\theta_{24}$ and $\theta_{14}=\theta_{23}$. The result, $J_{12}=J_{34}$, shows that the H-C-H angles of geminal protons on C(1) and C(2) are also the same $(\theta_{12}=\theta_{34})$. All of these results clearly indicate that the conformation A is preferred over the conformation B $(\theta_{14} \neq \theta_{23})$.

(A)

(B)
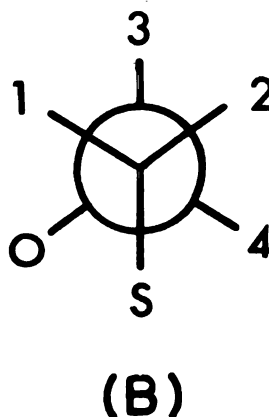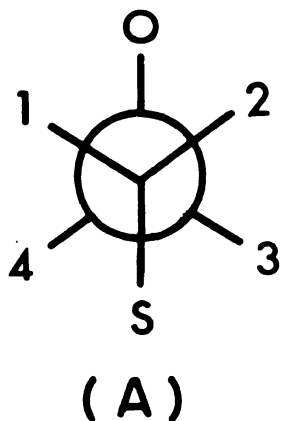
These coupling constants were also used to obtain the dihedral and H-C-H angles of geminal protons by the well known relationship first described by Karplus (143-145). Since the coupling constants, $J = A\cos^2\theta - B\cos\theta + C$, are constants affected by the nature of the substituent attached to the vicinal carbon atoms, the direct reading of the angle θ from the magnitude of the J value is not real. In the case of the $(DT18C6 \cdot Ag)^+$ and $(DT18C6 \cdot Tl)^+$ complexes, the predicted angles are $\theta_{14} = \theta_{23} = 34°$, $\theta_{12} = \theta_{34} = 116°$, and $\theta_{13} = \theta_{24} = 150°$ which results in $\theta_{13} = \theta_{12} + \theta_{23} = 150°$. However, the total $(\theta_{12} + \theta_{23} + \theta_{34} + \theta_{44})$ is equal to $300°$ instead of $360°$.

The proton NMR spectra of DA18C6 are shown in Figure 49 in which the AA'XX' system is indicated for the two sets of protons on the carbon atom between the oxygen and the nitrogen. The same type of proton NMR spectra was also obtained for the $(DA18C6 \cdot Tl^+)$ and $(DA18C6 \cdot K^+)$ complexes. These proton signals were simulated by the PANIC program and the calculated NMR parameters are shown in Table 43. It is interesting to note that all ^{1}H resonances shift downfield as the complex is formed. The chemical shift change is in the order: [1]H on C(1) > [1]H on C(3) > [1]H on C(2). Table 43 shows that the coupling constants of DA18C6 and its complex at the same site are nearly the same value. These results demonstrate that there is no conformational change as the complex is formed. The results show the angles are
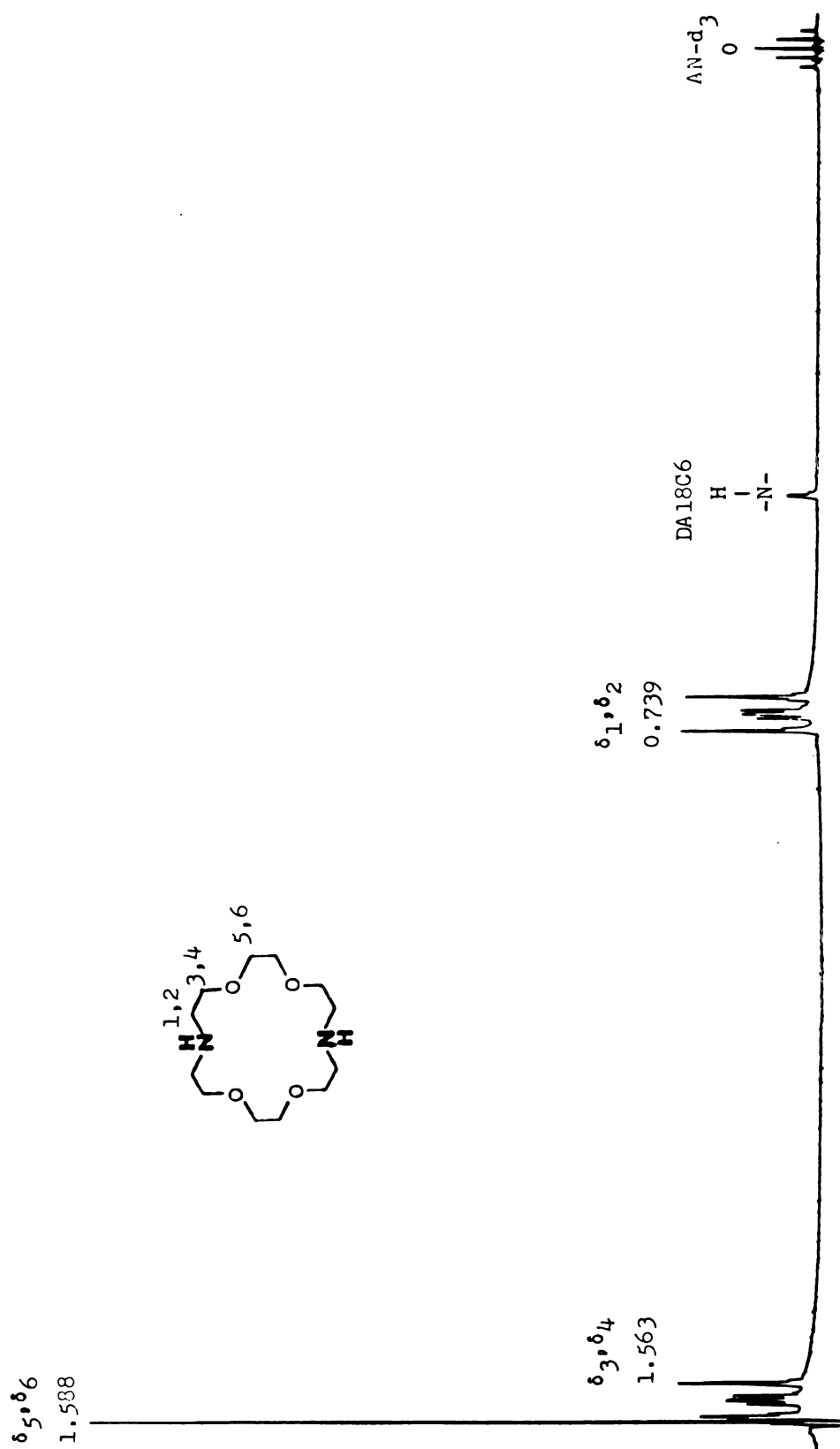
Figure 49.   Proton NMR spectra of DA18C6 (0.02 M) after treating with gaussian
multiplication.

Table 43. Proton NMR Parameters of DA18C6 and Its Complexes.

Salt	M^+/DA18C6	δ_1,δ_2 [a]	δ_3,δ_4	δ_5,δ_6	J_{12},J_{34} [b]	J_{13},J_{24}	J_{14},J_{23}	RMS [c]
DA18C6 0.02 M	0	0.739	1.563	1.588	1.9	5.9	3.6	0.079
TlClO$_4$	1.46	0.858	1.620	1.676	1.7	6.0	3.4	0.117
KPF$_6$	1.38	0.761	1.514	1.592	1.8	5.9	3.3	0.107

[a,b] Chemical shifts are downfield from acetonitrile in ppm, coupling constants are in Hz.

[c] RMS is root mean square error.

$\theta_{13}=\theta_{24}$, $\theta_{12}=\theta_{34}$ and $\theta_{14}=\theta_{23}$ which indicate that conformation A is more favored than conformation B in the DA18C6 and its complex as in the case of $(DT18C6 \cdot Ag)^+$ or $(DT18C6 \cdot Tl)^+$ complexes.

2. Ion Pair Formation Studies of Lithium Perchlorate and Lithium Chloride in Sulfolane.

Using conductance measurements, Prue and co-workers (146) showed that the ion pair association constants of $LiClO_4$ and LiCl in sulfolane are 6.5 and 13860 respectively. Lithium-7 NMR studies of ion pair association constants for both salts in sulfolane have been used to compare with the data obtained by the conductance technique. The results obtained are shown in Table 44 and are plotted in Figure 50. Figure 50 shows that the ^7Li chemical shifts are constant for all concentrations of $LiClO_4$ in sulfolane which indicates that there is no ion pair existing in the detectable concentration range of $LiClO_4$ in sulfolane. From the plot of the ^7Li chemical shift versus concentration of $LiClO_4$ (Figure 50), the chemical shift of the free Li^+ ion was found to be at -1.3 ppm. Table 44 and Figure 50 also show that the chemical shift changes from -0.48 ppm to -0.95 ppm as the concentration of LiCl changes from 9.32×10^{-2} M to 2.69×10^{-4} M. Selecting -1.3 ppm as the chemical shift value for the free lithium ion, the ion pair formation constant for LiCl was calculated by fitting with the KINFIT program (APPEDIX 3). The calculated ion pair
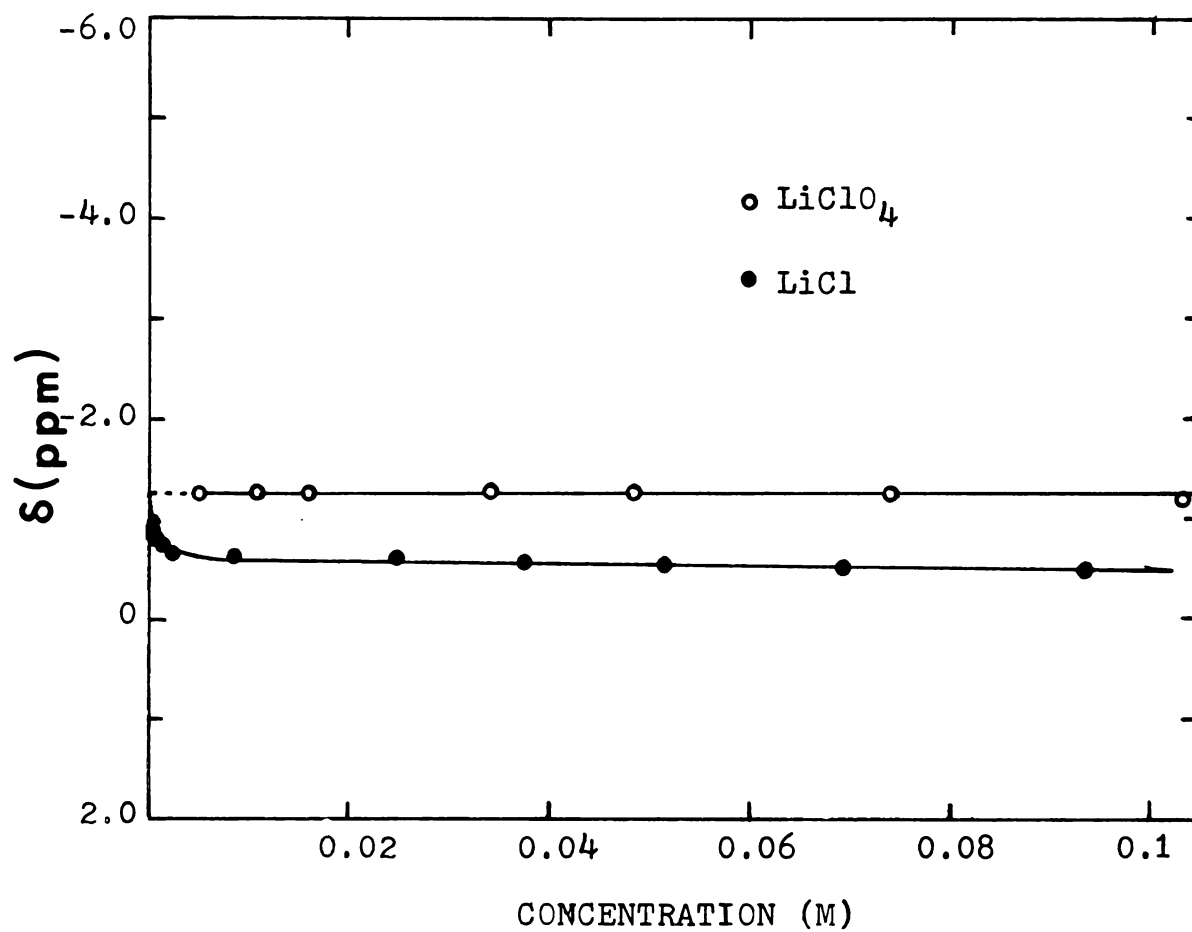
Figure 50. Lithium-7 chemical shifts vs. concentration of LiCl and LiClO$_4$.

Table 44. Lithium-7 Chemical Shift-Concentration Data for $LiClO_4$ and LiCl in Sufolane at $31^{\circ}C$.

Concentration of $LiClO_4$ (M)	δ(ppm)	Concentration of LiCl (M)	δ(ppm)
5.04×10^{-1}	-1.14	9.32×10^{-2}	-0.48
3.59×10^{-1}	-1.33	6.96×10^{-2}	-0.51
1.57×10^{-1}	-1.24	5.19×10^{-2}	-0.55
1.03×10^{-1}	-1.19	3.77×10^{-2}	-0.58
7.42×10^{-2}	-1.27	2.48×10^{-2}	-0.61
4.84×10^{-2}	-1.28	8.96×10^{-3}	-0.63
3.43×10^{-2}	-1.27	2.24×10^{-3}	-0.69
1.60×10^{-2}	-1.23	8.96×10^{-4}	-0.65
1.07×10^{-2}	-1.24	4.48×10^{-4}	-0.76
5.03×10^{-3}	-1.27	2.69×10^{-4}	-0.95

formation constant for LiCl in sulfolane is log K_{ip}= 4.35$\pm$ 0.22 which is in good agreement with the value, log K_{ip}= 4.14, found by conductance techniques (146).

PART II

Mass Spectrometry Studies of Cyclic
and Linear Polyethers

1. Introduction

Since the pioneering work of Pederson on the preparation and properties of crown ethers in 1967 (1), these macrocyclic ligands are becoming increasingly important in many fields of chemistry. Crown ethers have attracted much interest since they form complexes with various cations (2-8) and also with many organic molecules (178)in the liquid phase.

In the gas phase, however, the study of these complex formations by ion-molecule reactions has not been investigated. Before ion-molecule reactions involving macrocyclic polyethers can be performed, the mass spectra of crowns such as 12-crown-4, 15-crown-5, 18-crown-6 and 21-crown-7 must be determined and explained. These spectra can be used as a reference for comparison with the spectra obtained by ion-crown reaction studies from which the species formed by ion-molecule reactions can be identified. Also, their fragmentation patterns are of interest since these represent a class of highly functionalized molecules.

To date, a number of mass spectral studies of substituted crown ethers have been reported (147-153). In this thesis, the 70eV electron impact (EI) spectra of a series of crowns such as
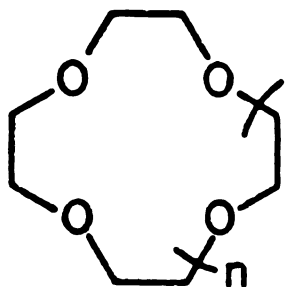
n = 1, 12-crown-4   (I)

n = 2, 15-crown-5   (II)

n = 3, 18-crown-6   (III)

n = 4, 21-crown-7   (IV)

are reported.

After comparing the similarities and trends of the mass spectra, the fragmentation mechanisms of these macrocycles were developed and a linear polyether intermediate was proposed. In order to verify the proposed fragmentation pathways, the mass spectra of two linear polyethers were taken at 70eV and ion abundances as a function of electron energy for 18-crown-6 were also studied. The pressure dependence of mass spectra of these crowns will also be discussed.

2. Historical Review

A. Electron Impact Mass Spectra

Electron impact (EI) can be described as the collision of energetic electrons with gas phase molecules. In

the typical mass spectrometer source the pressure is so low that an ion once formed is either detected or lost by collision with a wall without interaction with any other molecule or ion. In this case, the dissociation of an ion is clearly a unimolecular process and each ionized molecule is an isolated system with energy conserved independently. When a beam of energetic electrons is directed through a gas, some electrons in the beam may interact with the molecules present and then be scattered. At low electron velocities, this scattering is elastic, but at high velocities, energy may be transfered from incident electrons to the gas molecules. The energy transfer from an energetic electron to a gas molecule in a collision often transforms the gaseous molecule to an activated complex (superexcited state) and then is ionized.

Diatomic molecules such as H_2, N_2, NO, and HF, have relatively few and widely separated electronic states. In electron impact, the energy transfer from an energetic electron to a gas molecule in a collision often converts the molecules to some activated complexes. The energy transfer step proceeds quite rapidly (10^{-16} sec), so it yields only electronic adjustment without change in bond length (Franck-Condon Process). The lifetime of an activated complex for a diatomic molecule is very short ($< 10^{-11}$ sec), so it will decompose before "quasi-equilibrium" is reached (154).

The concept that fragmentation of diatomic ions could be

described by the Franck-Condon principle was first proposed in 1928 by Condon and Smyth (155,156). The idea was that direct ionization produced vertical transitions from the molecular ground state to the various ionic electronic states. Depending on the electron energy, the shape and the location of each of the ion potential energy curves which lie directly above that of the ground state of the neutral molecule, one would observe the characteristic yield of fragmentation with characteristic kinetic energy distributions. The various possible excitation mechanisms are shown in Figure 51. This process has recently been reviewed in detail by Rosenstock (157).

In the case of large molecules, the rate of dissociation of the activated complex is slower (lifetime $> 10^{-11}$sec) than the rate of redistribution of energy in the internal degrees of freedom, both electronic and vibrational, so that a "quasi-equilibrium" among these energy states is established before ion decomposition takes place (158).

Quantitative description of the fragmentation of large molecules is based on quasi-equilibrium theory (159,160). According to this theory, the fragmentation processes of the molecular ion can be considered separately from the act producing the ionization and internal excitation energy dis-tribution. Further, the fragmentation processes can be described as a series of competing, consecutive unimolecular reactions. The dissociation mechanism in a polyatomic species can be described as a motion along a multidimensional

(a) AB + e → AB‡ + 2e   (b) AB + e → AB‡ * + 2e

(c) AB + e → AB‡ * + A⁺ + B + 2e (d) AB + e → A⁺ + B + 2e
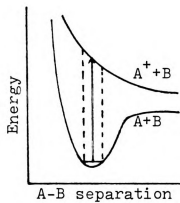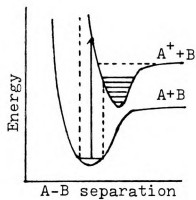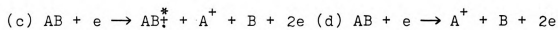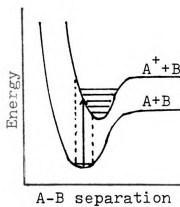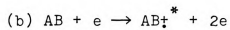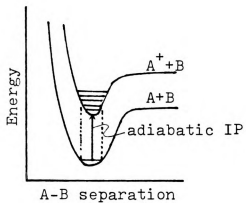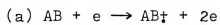
Figure 51.   Electron impact ionization of the molecule AB
(an excited state is indicated by *).

reaction coordinate separable from all other internal coordinates through an activated complex configuration. It often consists of a sequence of steps and is therefore controlled by several bottlenecks. The complicated and multistep nature of the dissociation reaction results in a natural tendency toward energy randomization (161). The probability function, P(E), and the rate constant, K(E), of various possible decompositions of an ion depend on its structure and internal energy, but not on the method used in initial ionization and the structure of precursor. The rate constant for a decomposition reaction is described by the Rice-Ramsperger-Kassel-Marcus (RRKM) theory (162):

$$K(E) = \frac{\alpha}{h} \frac{G^*(E-E_o)}{N(E)}$$

Where h is Planck's constant, α is a symmetry factor, $G^*(E-E_o)$ is the total number of quantum states of the transition state between zero and $(E-E_o)$, and N(E) is the density of states of the reacting ion. The relationship of P(E) and K(E) with ion internal energy for unimolecular ion decomposition has been discussed in detail by Bente and co-workers (163,164).

In the case of larger molecules impacted by electrons, significant numbers of them are initially in higher vibrational level of their ground electronic state; they become an activated complexes after collision with energetic

electrons. The dissociation products are formed after energy
randomization of the activated complex. Depending on the
energy of the incident electron, various dissociation pro-
ducts can be produced in the ways shown in Figure 52.
Positive-ion mass spectrometry can be used for studying
ionic products from pathways c,d,e,f,g,h and l.

B. The Mass Spectra of Crown Ethers

Mass spectrometry has been widely used for the elucida-
tion of the structures of crown ethers with one or more
aromatic or heteroaromatic substituents. However, in most
cases, only the molecule compositions are described. To date
only a few detailed fragmentation patterns have been reported.

The fragmentation patterns of several cyclic ethers such
as p-dioxane and tetrahydrofuran, under various electron
impact energy were examined early by Collin et al.(147,165).
The ionization and appearance potentials of numerous ions
have been determined and then used to interpret the dissocia-
tion mechanism. Linear intermediates were used to explain
the mass spectra of such small cyclic ethers, i.e.

$$\left[\text{dioxane}\right]^{+} \longrightarrow \begin{array}{l} [C-C-O-C-C-O]^{\ddagger} \\ [C-O-C-C-O-C]^{\ddagger} \end{array} \longrightarrow \text{FRAGMENTS}$$

$$e + M$$
$$\downarrow$$
$$e + M^*(\text{activated complex})$$

$F_1^- + F_2$	(a)	electron capture/fragmentation
M^-	(b)	resonance capture
$M^+ + 2e$	(c)	ionization
$M^+ + 2e + h\nu_f$	(d)	ionization/excitation
$F_1^+ + F_2 + h\nu_f$	(e)	ionization/fragmentation/excitation
$(M^+)^* + 2e \longrightarrow M^{2+} + 3e$	(f)	double ionization
$F_1^+ + F_2 + 2e$	(g)	ionization/fragmentation
$F_3^+ + F_4 + 2e$	(h)	rearrangement/ionization/fragmentation
$M + e + h\nu_f$	(i)	excitation
$F_1 + F_2^+ + e + h\nu_f$	(j)	fragmentation/excitation
$F_1 + F_2 + e$	(k)	fragmentation
$F_1^+ + F_2^- + e$	(l)	ion pair formation

Figure 52. The pathways of electron impact decomposition for gas phase molecules.

Initial C-O cleavage was preferred over C-C cleavage in such small cyclic ethers. In the case of tetrahydrofuran m/z 44 was the base peak and the configuration of $\vee\!\!\!\downarrow\!\!\!\diagup$ was suggested for this ion.

In 1970, the mass spectra of catechol polymethylene diether homologs of the type
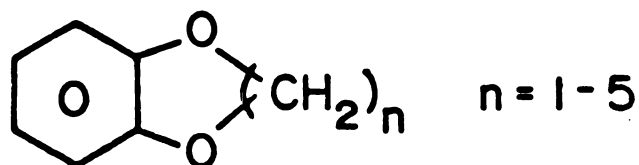
were reported by Biemann et al. (148). Deuterium labeling experiments have been used to identify the fragmentation mechanism. The results show these compounds are structurally similar to crown ethers, but behave much differently on fragmentation.

In 1974, Liotta et al. (149,166)reported the synthetic pathways for 12C4, 15C5 and 18C6. They also reported 6 ions mass spectra but did not discussed the spectra in detail.

In 1975, the mass spectra of a series of benzo-crown ethers were correlated and compared with those of open-chain analogs. Mass spectra of some deuterated analogs were used to formulate the fragmentation pathways. The loss of C_2H_4O units in these series of crown ethers was discussed (150).
In 1977, Oliveira et al.(151) reported the mass spectra of dibenzo-18-crown-6 (DB18C6) and three of its nitro derivatives.

Metastable ions were used to identify the fragmentation
mechanism. The fragmentation patterns of DB18C6 suggested
that ring contraction through loss of C_2H_4O occurs. Three
derivatives dissociate by ring contraction as well as through
losses of O, NO and NO_2 species. In the same year, the de-
tailed mass spectra of several serial compounds of the type

n = 0-6
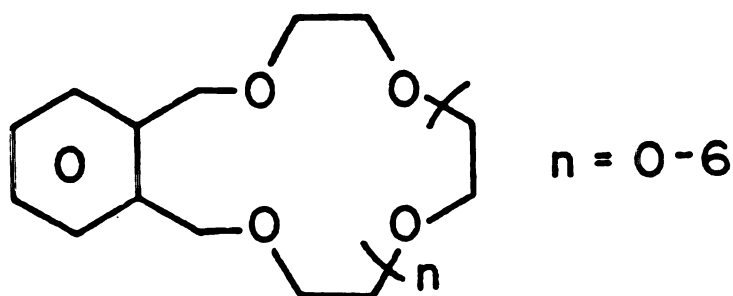
were reported by Gray and co-workers (152). High resolution
measurements and metastable ion analysis were used to iden-
tify the product ion structures and to postulate the fragmen-
tation mechanisms. In all cases, m/e 45 with the proposed
structure
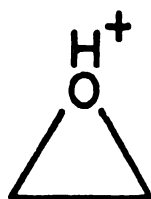
was the base peak. The m/e 177,133,89,45 series was always

observed. The initial site of ionization on the aromatic group is presumed.

In 1980, Whitney and Jaeger (153) reported the mass spectra of pyridyl crown ethers. The spectra of some deuterium labeled analogs of pyridyl crown ethers coupled with high resolution measurements were used to formulate the fragmentation mechanisms. Fragmentation by loss of C_2H_4O units was observed. These were complex spectra in which the total ion current was not carried by a small number of ions.

3. Experimental

A. Reagent Purification

Linear polyethers, triethylene glycol dimethyl ether (Aldrich, 3-EGDME) and tetraethylene glycol dimethyl ether (Aldrich, 4-EGDME) were distilled under vaccum and middle fraction was taken. Macrocyclic polyethers 12-crown-4 (Aldrich, 12C4) and 15-crown-5 (Aldrich, 15C5) were also purified by the procedure described above. The ligand 18-crown-6 (18C6) was purified by the method described in Section II-1 of Part I. The ligand, 21-crown-7 (Parish, 21C7) was used as received.

B. Sample Preparation

The samples were prepared by dissolving 0.1 ml of 3-EGDME, 4-EGDME, 12C4, 15C5. 21C7 or 0.05 g of 18C6 in 1 ml of methanol respectively.

C. Instrumentation

The mass spectra of crown ethers and linear polyethers
were obtained by using a Hewlett Packard 5985 gc/ms/ds spec-
trometer. The HP 5985 GC/MS is a complete system including an
HP-5840A GC, digitally temperature controlled dual chemical
ionization/electron impact ion source, quadrupole mass filter,
electron multiplier detector, differentially pumped vaccum
system, ion gauge controller, ionization region pressure
gauge, gas inlet probe, programmable direct insertion probe,
inlet vaccum system, GC/MS jet separator interface direct
transfer line, and a direct capillary interface also provided.

The data system includes an HP 21MXE series micropro-
grammable 16-bit computer with 32K of memory; HP 7900 A dual
disc drive. The usable mass range is from 10 to 1000 atomic
mass unit. The ionization energy (EI) range is from 10 to
250 eV.

The samples of crown ethers were introduced both via the
GC (0.1 ul injections using a 25 meters OV-1 capillary
column) and the direct insertion probe. Samples of 3-EGDME
and 4-EGDME were introduced via the GC with 0.1 ul injection
using a 2 mm(ID) x 6 ft column packed with 5% SE-30 on 80/100
mesh Gas Chrom. Q. 70eV electron impact (EI) spectra of linear
polyethers and crown ethers were taken. Mass spectra (70 eV
EI) at different crown pressure have been determined. Elec-
tron impact spectra of 18C6 at a series of electron energies
were also taken.

4. Results and Discussion

A. Mass Spectra of Unsubstituted Crown Ethers

The mass spectra of 12C4, 15C5, 18C6 and 21C7 are shown in Figure 53. The ion abundances and preferred molecular composition of principle fragment ions are listed in Table 45. It is interesting to note that the spectra are essentially identical. In all cases, m/z 45 is the base peak. The spectra are dominated by protonated small crown ethers such as m/z 177 (protonated 12C4), m/z 133 (protonated 9C3), m/z 89 (protonated p-dioxane) and m/z 45 (protonated ethylene oxide). This series of 177, 133, 89, 45, corresponds to the successive loss of the C_2H_4O unit (44 u). After comparing our results and the mass spectra of similar crown compounds presented in previous works as described in our historical review, an interesting framework is developed. According to this framework, the fragment pathways are proposed and the mass spectra of ligands I-IV can be interpreted.

Comparison of the results shown in Table 45 and Figure 53 lead to the following observations:

1. The mass spectra of compounds I-IV are essentially identical with m/z 45 as base beak.

2. In all cases, the molecule ion was not found.

3. The highest mass ion of significance in compound III and IV is m/z 177, while in compound I and II
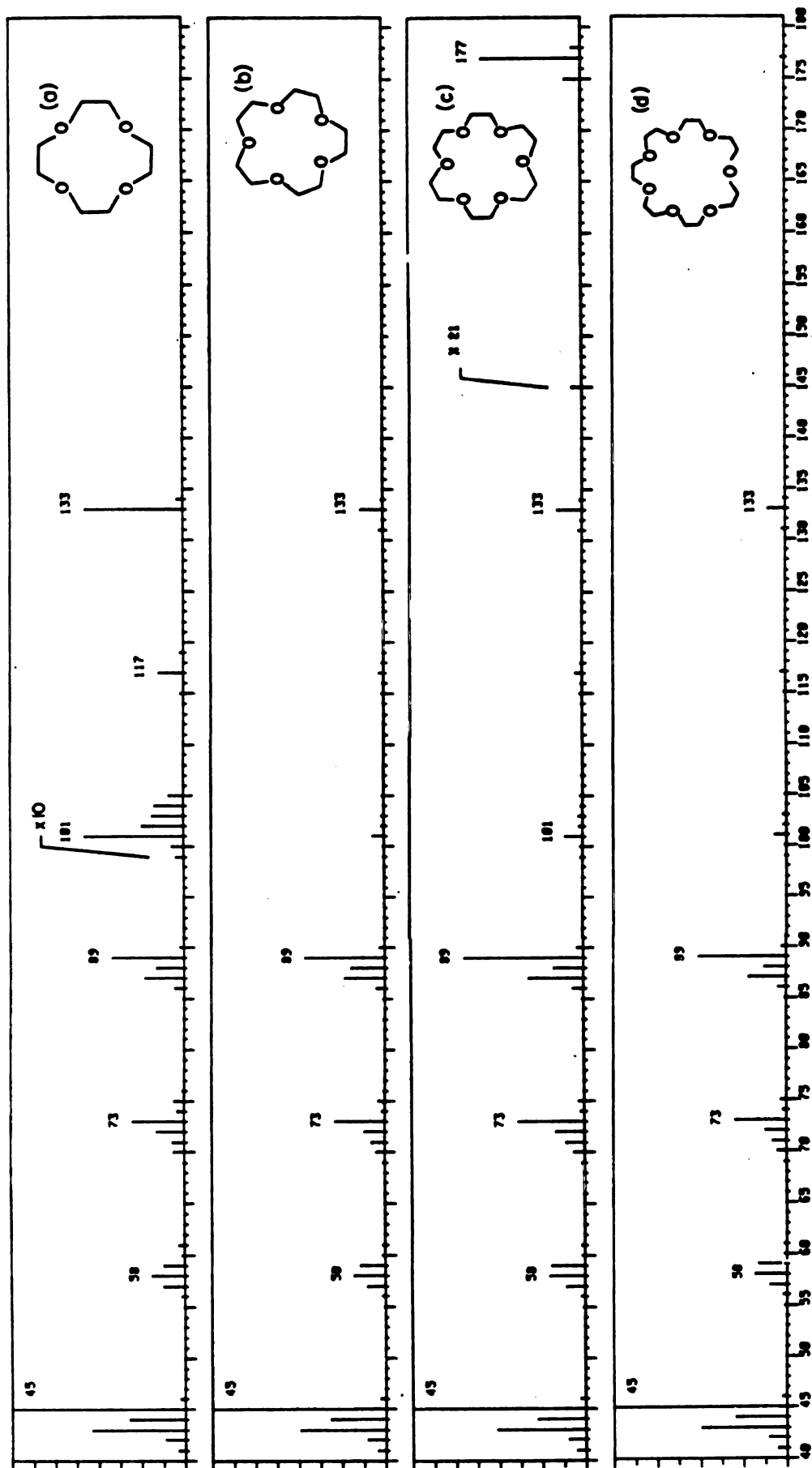
Figure 53. The 70 eV mass spectra of (a) 12C4 (b) 15C5 (c) 18C6 (d) 21C7.

Table 45. Principal Fragment Ions in the 70 eV Mass Spectra of Crown Ethers.

Fragment Ion (m/z value)	12C4[a]	15C5[b]	18C6[c]	21C7[d]	Elemental Composition
41	4	5	5	5	C_2HO
42	11	10	10	10	C_2H_2O
43	53	50	52	49	C_2H_3O
44	32	31	28	30	C_2H_4O
45	100	100	100	100	C_2H_5O
55		1	1	1	C_3H_3O
56	2	2	2	2	C_3H_4O
57	12	11	11	10	C_3H_5O
58	18	17	21	19	$C_2H_2O_2, C_3H_6O$
59	12	15	20	18	$C_2H_3O_2, C_3H_7O$
60	1	1	2	1	$C_2H_4O_2$
61	3	1	1	1	$C_2H_5O_2$
69	1	1	1	1	C_4H_5O
70	6	6	6	6	C_4H_6O
71	7	8	11	10	C_4H_7O
72	16	13	17	15	$C_3H_4O_2, C_4H_8O$
73	29	32	41	35	$C_3H_5O_2, C_4H_9O$
74	4	2	2	2	$C_3H_6O_2$
75	6	4	4	4	$C_3H_7O_2$
85		1	1	1	$C_4H_5O_2$
86	5	5	7	6	$C_4H_6O_2$

Table 45. Continued.

Fragment Ion (m/z value)	12C4[a]	15C5[b]	18C6[c]	21C7[d]	Elemental Composition
87	22	26	33	29	$C_4H_7O_2$
88	16	20	18	16	$C_4H_8O_2$
89	41	50	73	70	$C_4H_9O_2$
90	2	2	3	3	$C_4H_{10}O_2$
99		1	1	1	$C_5H_7O_2$
100	1	1	1		$C_5H_8O_2, C_4H_4O_3$
101	6	7	10	10	$C_4H_5O_3, C_5H_9O_2$
102	2	2	2	2	$C_4H_6O_3, C_5H_{10}O_2$
103	2	2	3	3	$C_4H_7O_3, C_5H_{11}O_2$
104	2		1		$C_4H_8O_3$
105	1	1	1	1	$C_4H_9O_3$
115		1	2	2	$C_6H_{11}O_2$
117	1	3	4	4	$C_6H_{13}O_2$
131		2	2	2	$C_6H_{11}O_3$
133	6	14	15	15	$C_6H_{13}O_3$
134		1	1	1	$C_6H_{14}O_3$
177		1	3	3	$C_8H_{17}O_4$

[a] 12C4, 12-crown-4, M.W = 176
[b] 15C5, 15-crown-5, M.W.= 220
[c] 18C6, 18-crown-6, M.W.= 264
[d] 21C7, 21-crown-7, M.W.= 308

is m/z 133.

4. The predominant fragments of I-IV are small proto-
   nated ethers at m/z 177,133,89,45 which are separated
   in mass by the basic crown ether unit, C_2H_4O.

From the similarities of the spectra, a preferred sec-
ondary structures of several intermediates can be assumed in
the fragmentation pathway for crown ethers. In general, it
makes little sense to assume specific secondary structure for
molecules fragmentation in gas phase. Crown ethers may pro-
vide us with an exception, since they are highly function-
alized molecules.

As the size of molecules, which are studied in mass
spectrometry, increases generally the "exactness" of frag-
mentation pathways described are frequently decreased.
Fragmentation mechanisms are often presented which accurately
describe the results, but involve interaction of parts of the
molecule which are not obvious (e.g. interaction of groups
on opposite sides of a large ring). This is, of course, due
to the fact that molecules drawn in two dimensions are actual-
ly three dimensional.

Analysis of the fragmentation patterns of compounds I-IV
was facilitated by considering preferred secondary structures
of several intermediates. Thus, both two and three dimen-
sional species will be shown. The fragmentation scheme as
shown in Figure 54 is proposed. The points at which each com-
pound enters the scheme are indicated. The protonated 12C4
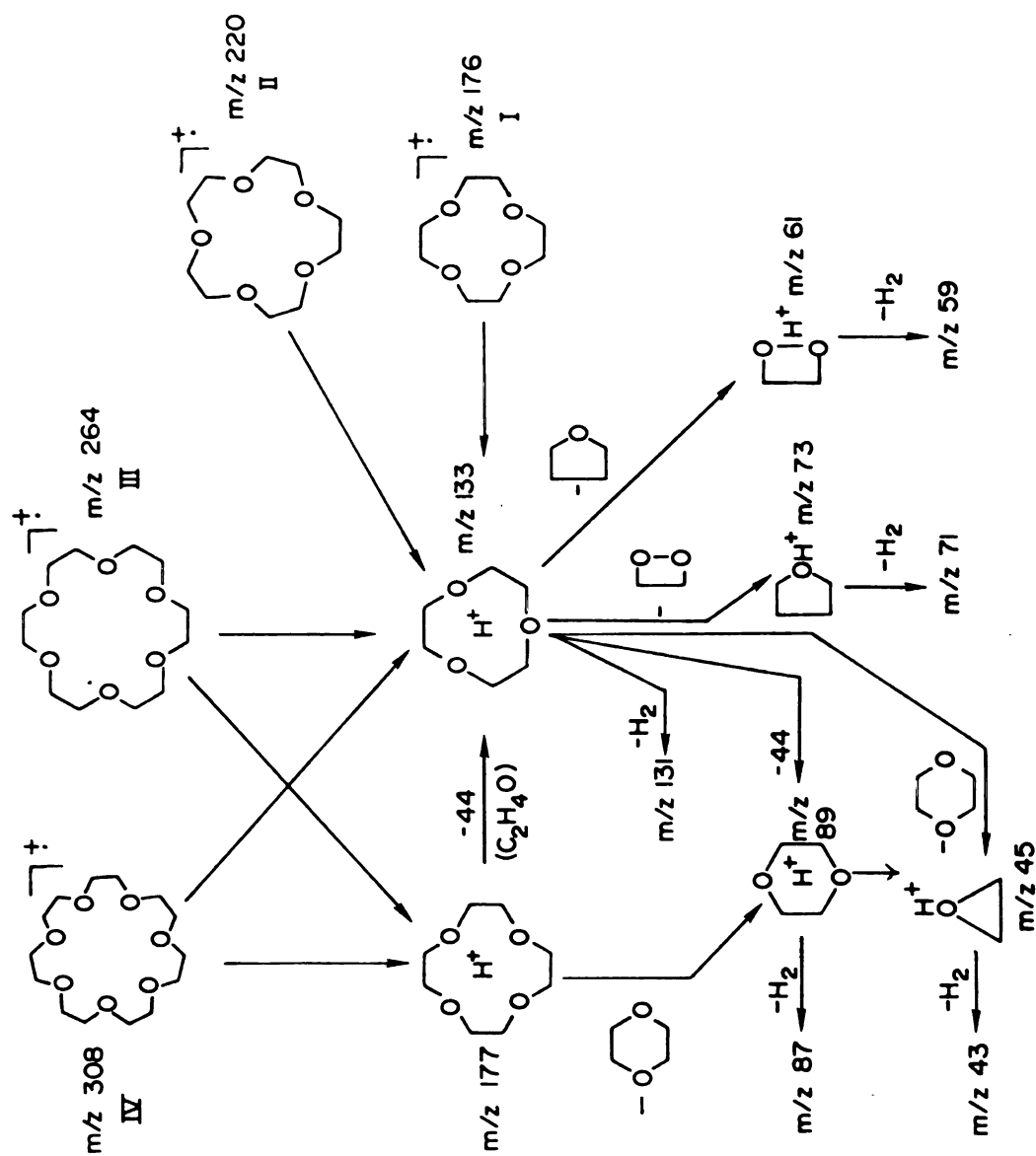
Figure 54. Fragmentation scheme for crown ethers.

and 9C3 ions at m/z 177 and 133 are proposed as intermediates for the low mass ions. The formation of m/z 177 and 133 ions will be discussed, followed by a discussion of mechanisms leading to important low mass series.

Figure 55 indicates the fragmentation mechanism of 18-crown-6 through which m/z 177 and 133 ions are formed. Ultraviolet photoelectron spectroscopy shows that the ionization of crown ether occurs at a nonbonding electron on the oxygen rather than a bonding electron of the oxygen or carbon (167). The preferred structure for the neutral molecule (168, 169) which contains two intramolecular hydrogen bonding between $O(1)$ and $CH_2(5)$ is shown in Figure 55. Presumably, hydrogen bonds have an important influence on the establishment of the secondary structure. Also, hydrogen bonds should enhance the probability of intramolecular hydrogen transfer which is shown as the first step. Following this step, the ring opens to form a linear intermediate, V. Figure 55 also shows intermediate structures through which protonated 12C4 and 9C3 are formed. This mechanism parallels solution behavior. The acid catalyzed polymerization of ethylene oxide gives a distribution of crown ethers in which 12-crown-4 is predominant. This is explained in terms of the secondary structure of the polymer of the type $(C_2H_4O)_n$ which is helical, with one "revolution" of the chain occuring every 12 skeletal atoms. In solution, the polymerization reaction of ethylene oxide stops in a cyclization step after four
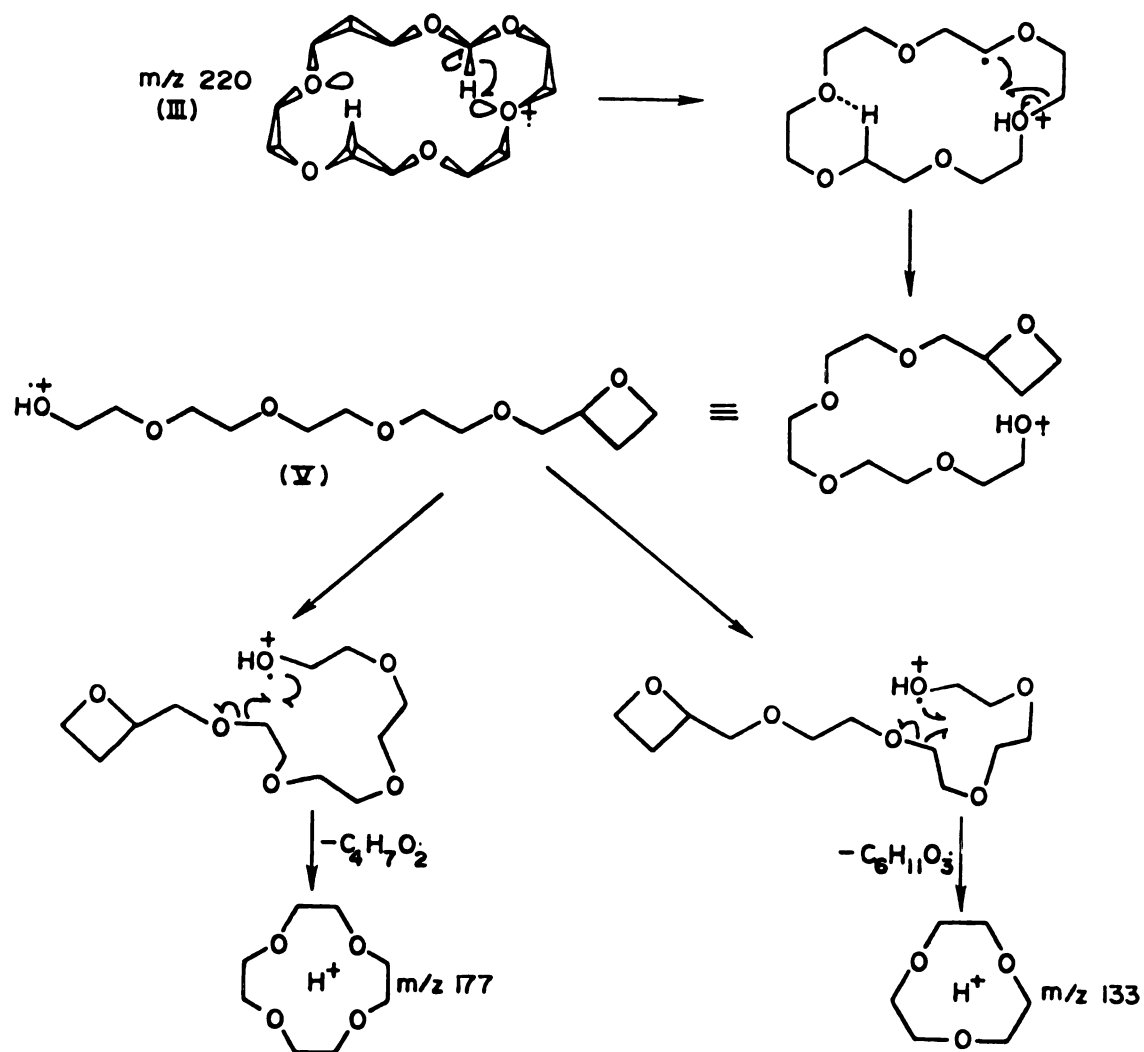
Figure 55. The formation of protonated 12-crown-4 and
protonated 9-crown-3 from 18-crown-6 via a
linear intermediate.

C_2H_4O units are catenated (168,169). Thus, the preferred secondary structure of a $(C_2H_4O)_n$ chain in solution can be used to predict the product of recyclization of the linear intermediate in the gas phase. Through the same linear intermediate, protonated 9-crown-3 can be formed as shown in Figure 55.

This mechanism is consistent with the spectra of the four compounds. The mechanism enables compounds III and IV to form m/z 177 (and 133) but not compound I and II. Thus, it is consistent with the fact that the highest mass ion of significance for compound I and II is m/z 133.

It should be noted that the specific recyclization of a linear intermediate such as V is a low energy process, since one C-O bond is formed as another C-O bond is broken.

The formation of m/z 133 from compound I can be explained either by the recyclization of an intermediate similar to V, or by direct elimination of C_2H_3O from the molecular ion. Figure 56 shows this process.

Again, a specific secondary structure brings a specific carbon and oxygen into close proximity, favoring the process. The three dimensional structure shown in Figure 56 represents the structure of crystalline 12C4, as determined by x-ray crystallography (170). This secondary structure appears to predominate also in dilute solution (168,169) and may be the preferred conformer in the gas phase. Electron diffraction
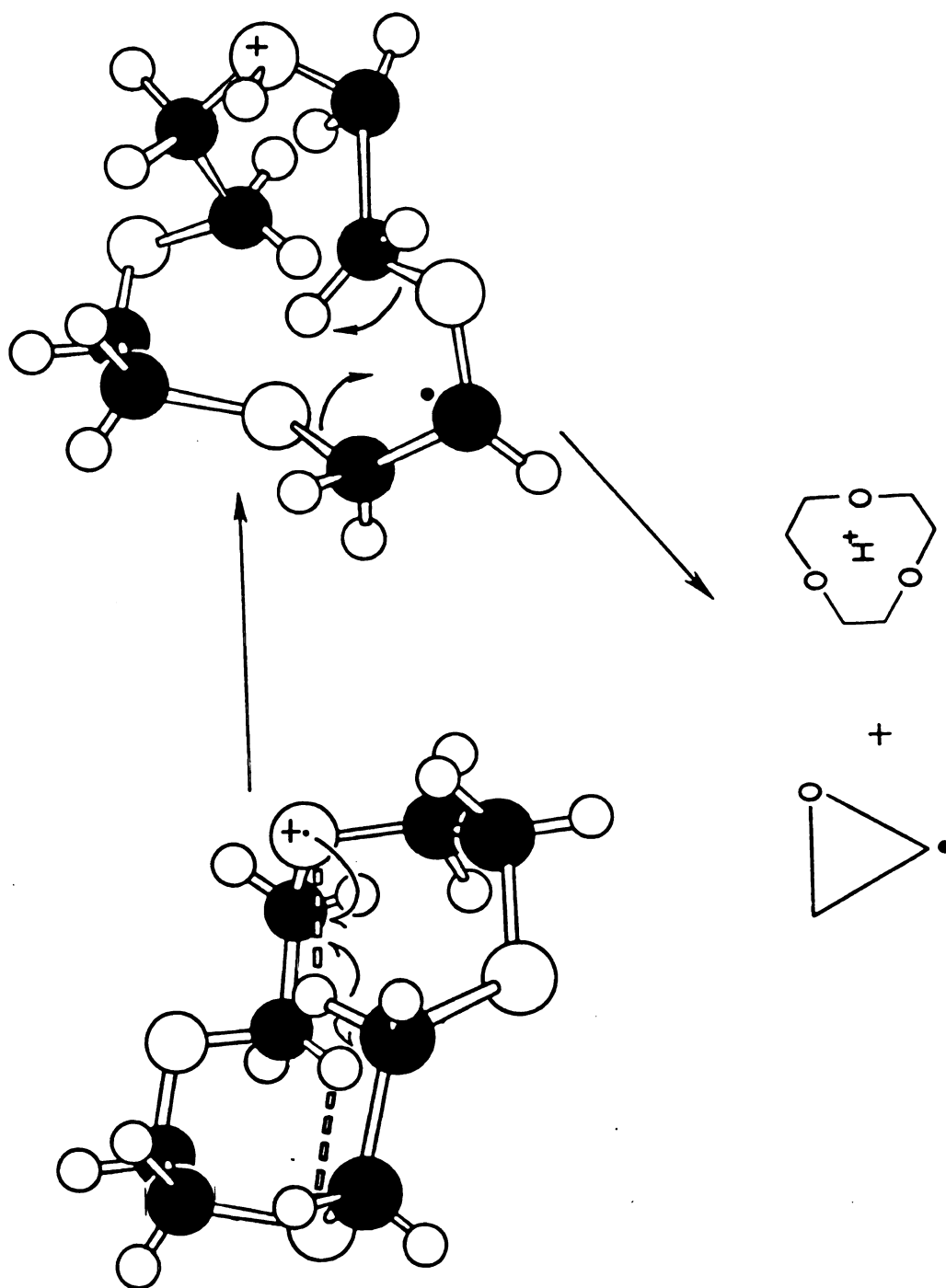
Figure 56. Fragmentation of 12-crown-4 to form protonated 9-crown-3.

studies of gas phase cyclic polyethers do show the presence
of one predominant secondary structure (171). Again, spe-
cific structures may be preferred since cyclic polyethers
with repeating C_2H_4O units do appear to have an $O(1)-CH_2(5)$
interaction (H-bond via a six membered ring) (168), except
in p-dioxane.

Thus, we propose that these compounds fragment via a
linear intermediate similar to V, and form smaller protonated
crowns via preferred intermediates. This would predict very
similar spectra for larger crowns.

As shown in Figure 54 fragmentation of species m/z 177
and especially m/z 133 leads to the formation of smaller mass
ions. There may well be other recyclizations possible from
intermediate V to give the major low mass ions 89 and 45 (p-
dioxane is a minor product in the polymerization of ethylene
oxide), however we feel that their formation, as shown in
Figure 54, is more likely. In compounds such as the benzo-
crowns reported by Gray (152), the observed 177,133,89,45
series are in ratios similar to those reported here. Meta-
stables confirming the fragmentation of 177→89, 133→89 and
89→45 were reported (152), supporting m/z 133 as an important
precursor for the lower masses.

The fragmentation of m/z 133 is shown in Figure 57. It
may be expected that crown ethers are good bases - i.e., the
crown "cavity" may have a high proton affinity. However,
the cavity is too large to cause overlap of many oxygen lone
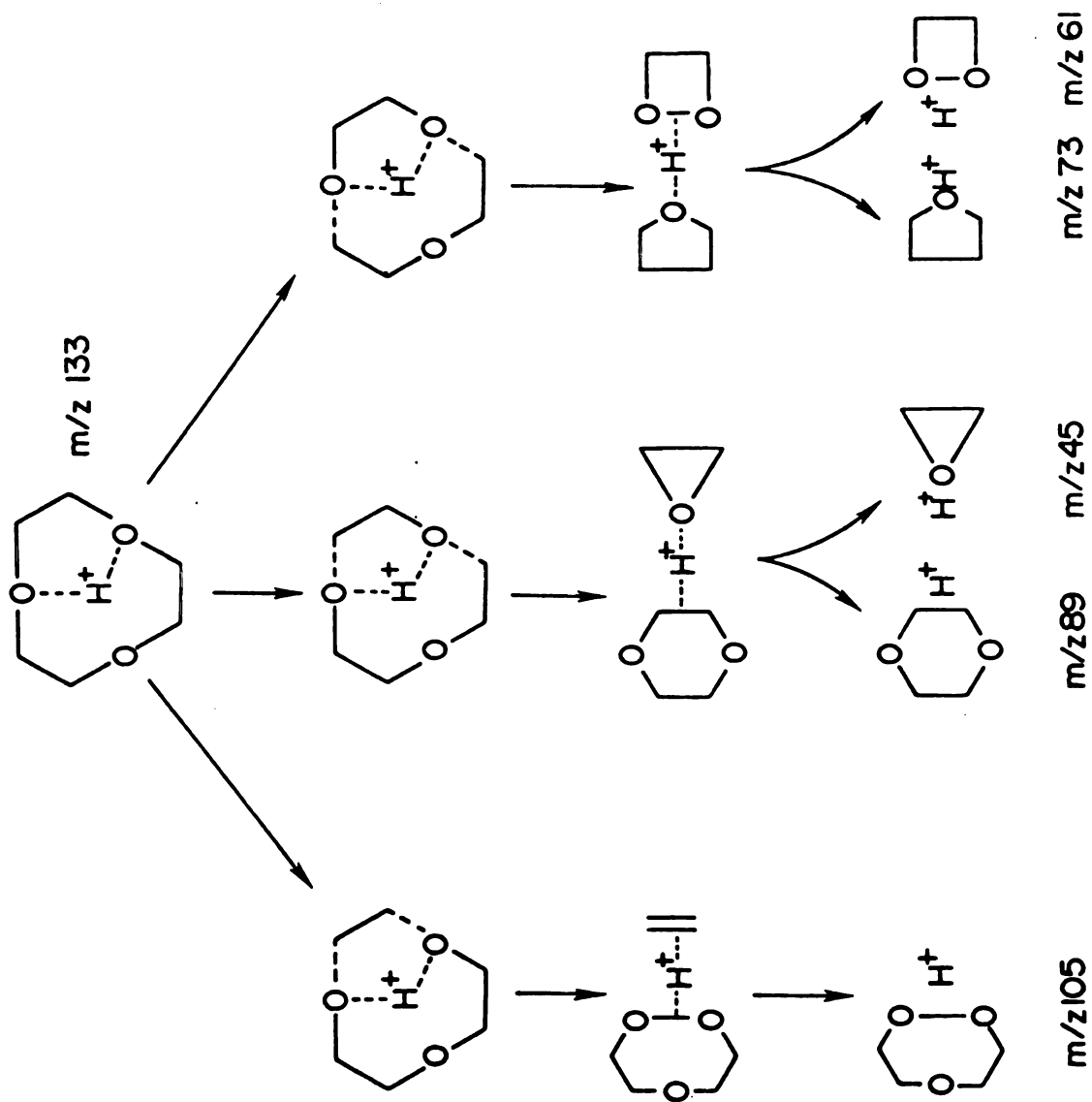
Figure 57. The dissociation of protonated 9-crown-3.

pairs with one proton. Studies with other small atomic ions (172) such as Cr^+ suggest that two crown oxygens can interact with one ion. The interaction can bring parts of the molecule closer together for the formation of new bonds (smaller rings). Figure 55 shows that a number of products can be accurately predicted . It is shown that protonated 9-crown-3 can result in proton bound complexes (of smaller ethers) which dissociate. This scheme not only predicts ions at m/z 89 and 45, but accurately predicts ions at m/z 73 and 61 as well.

Thus, our results, and the results of Gray (152) for similar aromatic crown ethers, suggests the following:

1. Following ionization, an intramolecular hydrogen shift initiates ring opening.

2. Reclosure of the linear intermediate follows secondary structures which are preferred in solution.

3. Most of the low mass ions are formed via m/z 133.

It is expected that 9-crown-3 will give a similar mass spectrum, however this compound is not commercially available. Also, ions such as m/z 45 would not be expected from p-dioxane because no intramolecular hydrogen transfer via a six-membered ring would be expected.

B. **Mass Spectra of Unsubstituted Crown Ethers at High Sample Pressure**

The mass spectra of these crown ethers are extremely pressure dependent. Tables 45 and 46 show the intensity of ion species of these compounds at two different sample pressure respectively. At high sample pressure the following observations can be found.

1. The base peak of III and IV is shifted from m/z 45 to m/z 89.

2. The parent ion and protonated parent ion (M+1) is formed.

3. The protonated ethers at m/z 177,133,89 are specially intensified.

All of these observations are due to the fact that the base peak, m/z 45, with a protonated ethylene oxide structure as shown previously. As the sample pressure is increased, the parent ion increases in intensity due to charge transfer, forming more parent ions. The intensity of the protonated parent ion is increased because the proton transfer occurs between a protonated crown ether and the neutral crown ether molecules. The evidence for a protonated ether is intensified due to the dissociation of the protonated parent ion and proton transfer between protonated ether and neutral fragments. As m/z 177 and 133 signals increase in intensity, all of the fragment ions would be increased by the mechanisms shown in Figures 54 and 57 (m/z 105,89,73,61). These observations may explain previously reported six ions mass spectra of 15C5 (149), in which m/z 89 is given as base peak,

Table 46. Principal Fragment Ions in the 70 eV Mass Spectra at High Sample Pressure of Crown Ethers.

Fragment Ion (m/z value)	12C4[a]	15C5[b]	18C6[c]	21C7[d]	Elemental Composition
41	5	5	5	6	C_2HO
42	12	11	9	8	C_2H_2O
43	63	62	48	47	C_2H_3O
44	34	32	24	24	C_2H_4O
45	100	100	92	95	C_2H_5O
55	1	1	1	1	C_3H_3O
56	2	2	2	2	C_3H_4O
57	15	13	11	11	C_3H_5O
58	23	21	19	20	$C_2H_2O_2, C_3H_6O$
59	14	18	18	21	$C_2H_3O_2, C_3H_7O$
60	2	2	1	2	$C_2H_4O_2$
61	4	1	1	4	$C_2H_5O_2$
69	1	2	2	3	C_4H_5O
70	8	7	7	7	C_4H_6O
71	10	13	11	12	C_4H_7O
72	24	18	18	20	$C_3H_4O_2, C_4H_8O$
73	46	59	43	48	$C_3H_5O_2, C_4H_9O$
74	5	3	2	3	$C_3H_6O_2$
75	8	6	4	6	$C_3H_7O_2$
85	1	1	1	2	$C_4H_5O_2$
86	12	11	9	10	$C_4H_6O_2$

Table 46. Continued.

Fragment Ion (m/z calue)	$12C4^a$	$15C5^b$	$18C6^c$	$21C7^d$	Elemental Composition
87	45	53	45	51	$C_4H_7O_2$
88	33	40	25	26	$C_4H_8O_2$
89	88	99	100	100	$C_4H_9O_2$
90	4	5	5	5	$C_4H_{10}O_2$
99	1	2	2	3	$C_5H_7O_2$
100	2	2	2	9	$C_5H_8O_2, C_4H_4O_3$
101	16	20	16	16	$C_4H_5O_3, C_5H_9O_2$
102	6	5	4	4	$C_4H_6O_3, C_5H_{10}O_2$
103	5	5	4	5	$C_4H_7O_3, C_5H_{11}O_2$
104	5	1	1	1	$C_4H_8O_3$
105	2	3	2	2	$C_4H_9O_3$
115	1	4	3	4	$C_6H_{11}O_2$
117	5	2	8	9	$C_6H_{13}O_2$
131	1	10	5	6	$C_6H_{11}O_3$
133	20	56	30	34	$C_6H_{13}O_3$
134	1	4	2	2	$C_6H_{14}O_3$
177	0.5	3	6	7	$C_8H_{17}O_4$
221		0.3	0.5	2	$C_{10}H_{21}O_5$
264			0.1	0.1	$C_{12}H_{24}O_6$
265			3	0.1	$C_{12}H_{25}O_6$
309				0.3	$C_{14}H_{29}O_7$

[a]12C4, 12-crown-4, M.W.= 176 [b]15C5, 15-crown-5,M.W.=220
[c]18C6, 18-crown-6, M.W.= 264 [d]21C7, 21-crown-7,M.W.=308

and the parent ion (M^+) and protonated parent ion $(M+1)^+$ appear in 18C6 (166,173).

Ion cyclotron resonance (ICR) experiments were performed on the ions discussed above to confirm the fact that they are formed in part from reaction of m/z 45 at high pressure. ICR studies also reveal that m/z 43 protonates crowns and leads to many of the same products (173).

C. Mass Spectra of 18-crown-6 at Different Electron Energies

A fragmentation path can be identified by the observation of metastable ions, but these are limited to reactions with lifetimes > 10^{-6}sec. Isotope labeling is another useful tool for determing the fragmentation mechanism. In the previous report (148,150-153), both methods have been used to identify the fragmentation mechanism for substituted crown ethers. We attempt, here, to determine the appearance potentials of the fragment ions. With these, the decomposition pathways may be determined (174).

The mass spectra of 18-crown-6 at various electron energies between 10-100 eV are shown in Figures 58-60. The ion abundances (% of total ionization) of fragment ions at different electron energies are listed in Table 47, and plotted in Figures 61 and 62. Comparing these results, the following observations can be made:

1. In all cases, the base peak is m/z 45.
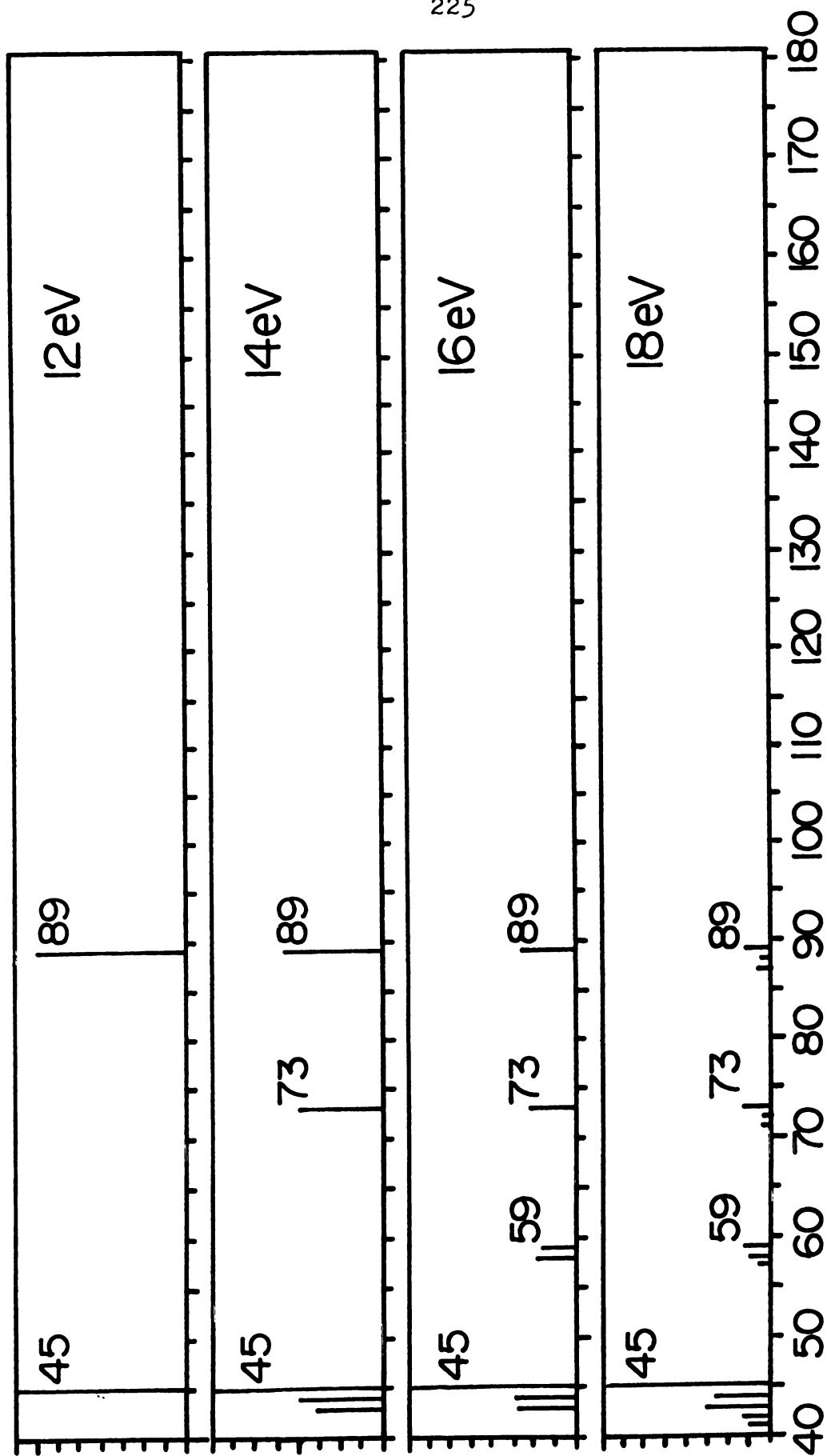
Figure 58. The mass spectra of 18C6 at various electron energies (12-18 eV).
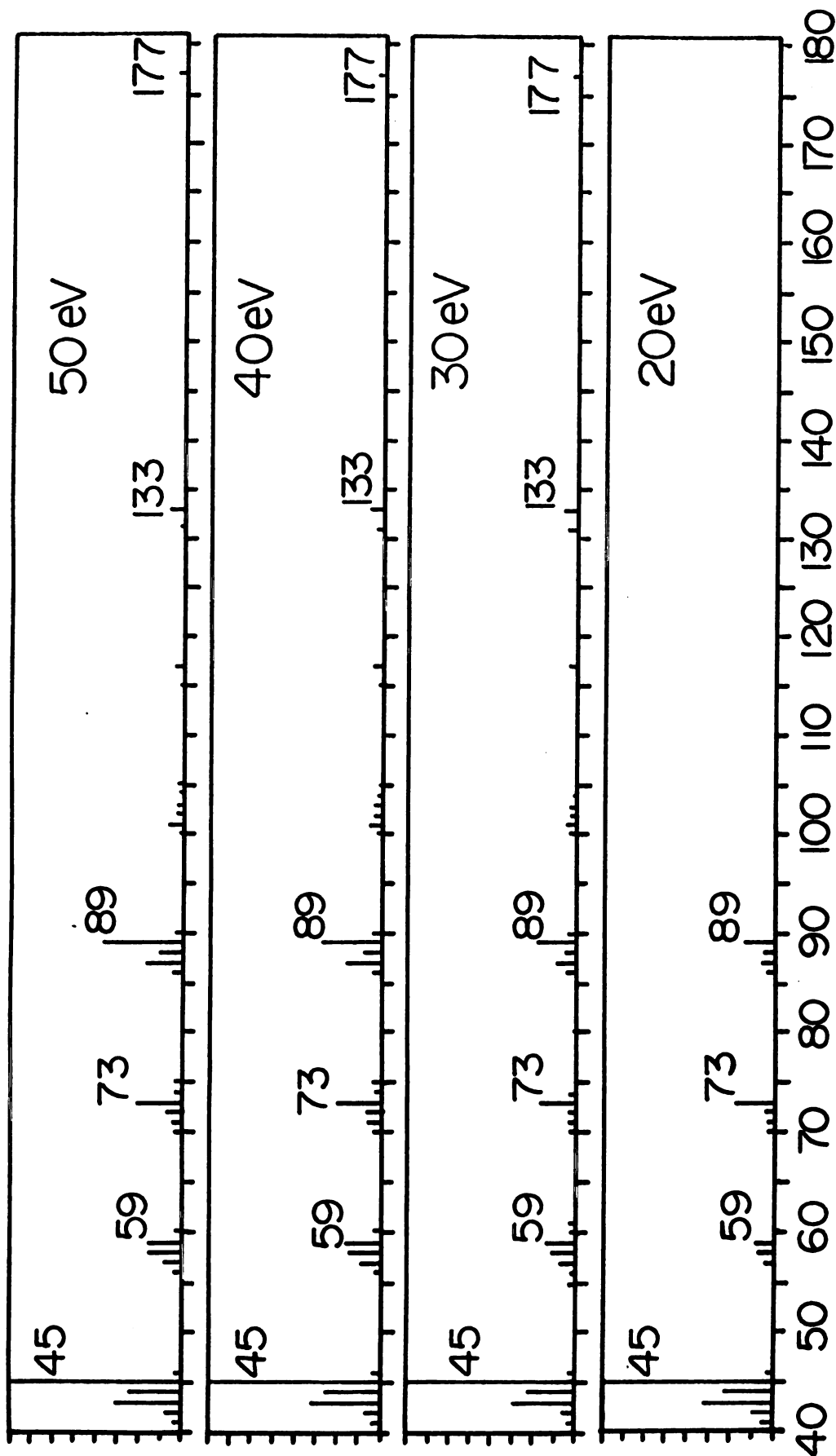
Figure 59. The mass spectra of 18C6 at various electron energies (20-50 eV).
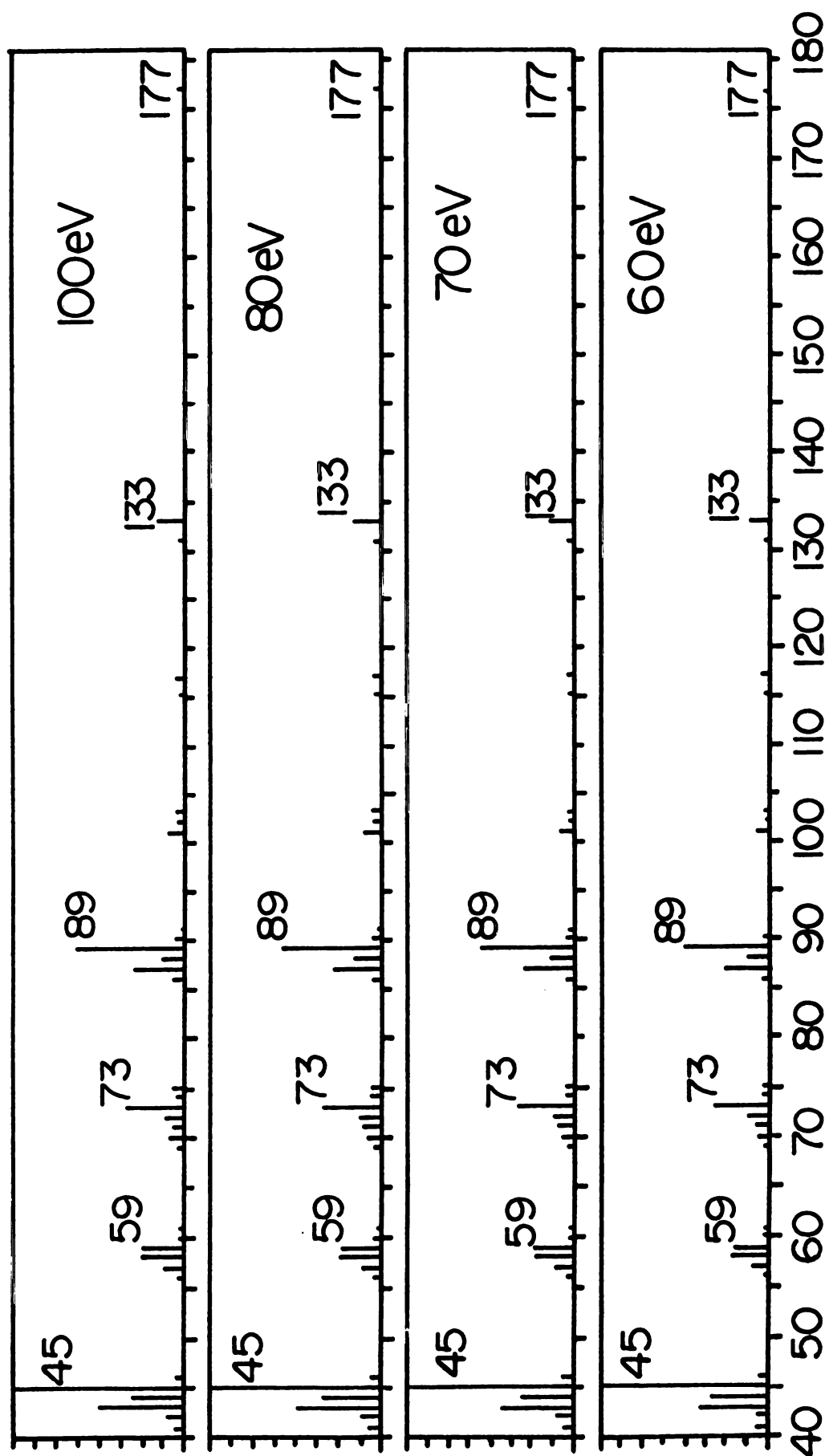
Figure 60. The mass spectra of 18C6 at various electron energies (60-100 eV).

Table 47. Principal Fragment Ions in the 10-100 eV Mass Spectra of 18-crown-6.

m/z[a]	10	12	14	16	18	20	30	40	50	60	70	80	100	E.C.	A.P.[c]
41					2.1	2.3	1.5	1.2	1.1	1.0	1.0	1.0	1.0	C_2HO	16-18
42					3.4	3.9	3.2	2.6	2.3	2.0	2.0	2.0	1.0	C_2H_2O	16-18
43			13.2	13.0	12.6	15.3	11.9	10.2	9.9	9.2	9.0	9.0	8.8	C_2H_3O	12-14
44			15.8	13.1	10.9	12.2	9.1	7.8	7.7	7.8	6.7	6.4	6.2	C_2H_4O	12-14
45		54.5	36.8	38.1	34.4	32.2	30.4	25.4	24.0	22.0	20.9	21.3	19.7	C_2H_5O	10-12
55							0.3	0.2	0.2	0.3	0.2	0.2	0.2	C_3H_3O	20-30
56							0.5	0.4	0.5	0.4	0.4	0.4	0.4	C_3H_4O	20-30
57					2.1	2.1	2.3	2.3	2.2	2.3	2.1	2.1	2.1	C_3H_5O	16-18
58				5.9	4.6	3.3	4.0	4.2	4.2	4.2	4.1	4.0	3.8	$C_2H_2O_2$ C_3H_6O	14-16
59				5.9	5.5	4.7	4.4	4.3	4.2	4.1	4.1	4.1	4.0	$C_2H_3O_2$ C_3H_7O	14-16
60							0.3	0.3	0.3	0.3	0.3	0.3	0.3	$C_2H_4O_2$	20-30
61							0.2	0.3	0.3	0.3	0.3	0.3	0.3	$C_2H_5O_2$	20-30
69							0.2	0.2	0.2	0.3	0.3	0.2	0.2	C_4H_5O	20-30

Table 47. Continued-1.

m/z^a	10	12	14	16	18	20	30	40	50	60	70	80	100	$E.c.^b$	$A.P.^c$
70							1.0	1.1	1.1	1.2	1.3	1.2	1.2	C_4H_6O	20-30
71					2.5	1.0	1.4	1.6	1.7	1.7	1.8	1.7	1.7	C_4H_7O	16-18
72					2.1	1.4	1.9	2.3	2.3	2.4	2.5	2.6	2.6	$C_3H_4O_2$ C_4H_8O	16-18
73			15.8	9.5	7.1	5.8	5.9	6.2	6.4	6.4	6.7	6.7	6.6	$C_3H_5O_2$ C_4H_9	12-14
74							0.3	0.4	0.4	0.4	0.4	0.4	0.4	$C_3H_6O_2$	20-30
75							0.7	0.6	0.7	0.7	0.7	0.7	0.7	$C_3H_7O_2$	20-30
85							0.1	0.1	0.2	0.2	0.1	0.1	0.1	$C_4H_5O_2$	20-30
86						1.0	0.9	1.0	1.1	1.0	1.1	1.1	1.1	$C_4H_6O_2$	18-20
87					3.8	2.5	3.5	4.8	5.0	5.3	5.9	5.8	6.2	$C_4H_7O_2$	16-18
88					2.5	1.8	1.7	2.2	2.4	2.4	2.7	2.6	2.8	$C_4H_8O_2$	16-18
89		45.5	18.4	11.9	6.3	4.7	7.1	9.9	10.9	11.6	12.8	13.0	13.7	$C_4H_9O_2$	10-12
90							0.3	0.5	0.5	0.6	0.6	0.6	0.6	$C_4H_{10}O_2$	20-30
99							0.1	0.1	0.2	0.1	0.1	0.2	0.2	$C_5H_7O_2$	20-30

Table 47. Continued-2.

m/z[a]	10	12	14	16	18	20	30	40	50	60	70	80	100	E.C.[b]	A.P.[c]
100							0.1	0.1	0.1	0.1	0.1	0.1	0.1	$C_5H_8O_2$ / $C_4H_4O_3$	20-30
101							1.0	1.4	1.4	1.6	1.9	1.7	1.9	$C_4H_5O_3$ / $C_5H_9O_2$	"
102							0.3	0.4	0.6	0.4	0.4	0.4	0.4	$C_4H_6O_3$ / $C_5H_{10}O_2$	"
103							0.3	0.5	0.5	0.4	0.5	0.5	0.6	$C_4H_7O_3$ / $C_5H_{11}O_2$	"
104							0.2	0.2	0.2	0.3	0.2	0.2	0.3	$C_4H_8O_3$	"
105							0.2	0.2	0.3	0.4	0.3	0.3	0.4	$C_4H_9O_3$	"
115							0.2	0.2	0.2	0.3	0.3	0.3	0.3	$C_6H_{11}O_2$	"
117							0.4	0.6	0.7	0.7	0.8	0.9	0.9	$C_6H_{13}O_2$	"
131							0.2	0.3	0.4	0.4	0.5	0.5	0.5	$C_6H_{11}O_3$	"
133							1.1	1.9	2.1	2.3	2.6	2.6	2.8	$C_6H_{13}O_3$	"

Table 47. Continued-3.

m/z^a	10	12	14	16	18	20	30	40	50	60	70	80	100	E.C.[b]	A.P.[c]
134								0.1	0.1	0.2	0.2	0.2	0.2	$C_6H_{14}O_3$	30-40
177							0.1	0.2	0.3	0.3	0.4	0.4	0.5	$C_8H_{17}O_4$	20-30

[a] Fragment ion (m/z) value.
[b] Elemental composition.
[c] Apperance potential (in eV).

2. The molecular ion was not found.

3. The small protonated ethers at m/z 177, 133, 89,
    45 are predominant fragments when the electron energy
    is higher than 20 eV.

The approximate appearance potentials for various ions
are listed on Table 47. Figure 61 shows that the molecular
ion dissociates to m/z 45 and 89 directly at low electron
energy (< 20 eV). The ion intensity of m/z 45 and 89 de-
creases as the fragment ions such as m/z 43, 44, 57, 58, 59,
73, 87, are formed. These seems indicate that m/z 43 and
44 ions are produced from m/z 45 and m/z 57, 58, 59, 73, 87,
come from m/z 89. As the electron energy is increased, the
high mass ions (i.e. m/z 177, 133, 89, 87) increase in in-
tensity.

Table 47 shows that the decreasing and increasing ion
intensities are not equal. Due to the inaccuracy of ion
intensity measurement, the appearance potential measurement
can not be used for exact identification of fragmentation
mechanisms.

The calculation of heats of formation of fragment ions
are difficult due to the following reasons:

1. The appearance potential measured in HP-5985 GC/MS
    is not reproduced well.

2. The structures of neutral fragments are still unknown
    so the heats of formation are difficult to estimate.
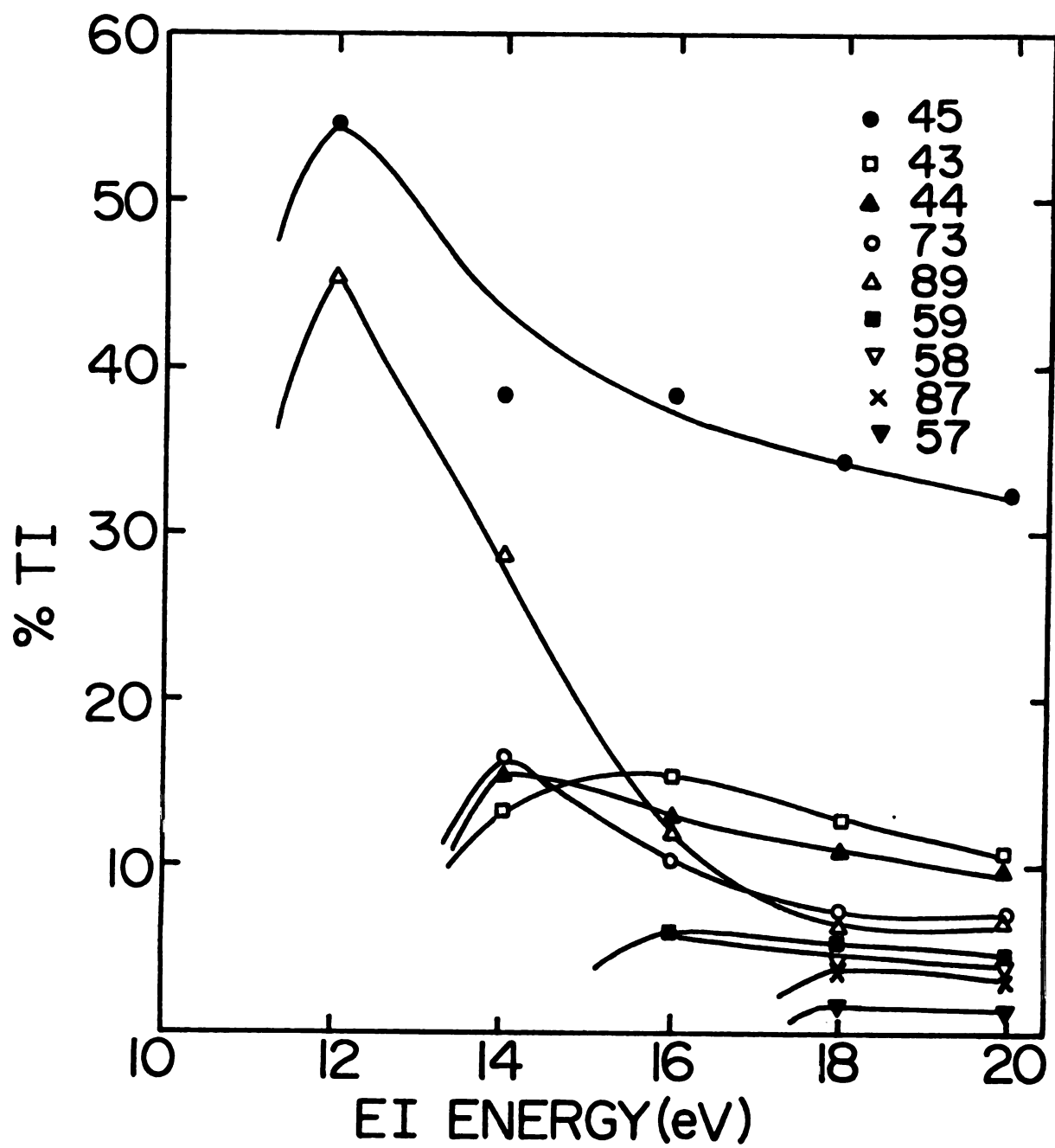
Figure 61. Ion abundance (% of total ionization) as a function of electron energy (in eV).
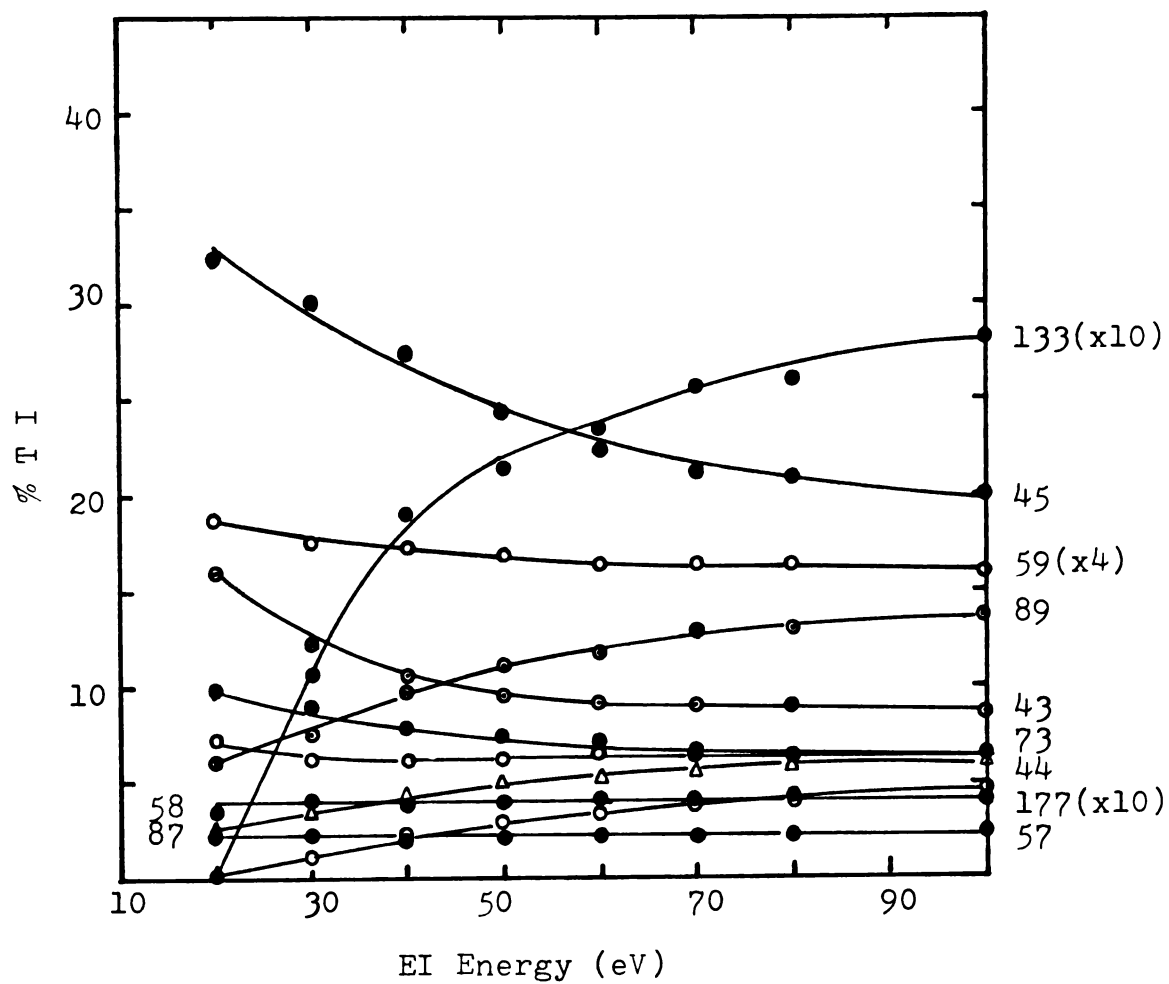
Figure 62. Ion abundances (% of total ionization) as a function of electron energy (in eV) for 18C6.

D. <u>Mass Spectra of Some Linear Polyethers</u>

In the fragmentation mechanism of crown ethers, a linear polyether intermediate are proposed. If this is true, there should be some similarities in the mass spectra of crown ethers and linear polyethers. With this goal, the electron impact mass spectra of 4-EGDME and 3-EGDME were taken at 70 eV. The spectra are shown in Figure 63. The ion abundances and preferred composition of principle fragment ions are listed in Table 48. The results show the following interesting observations.

1. The spectra of 4-EGDME and 3-EGDME are essentially identical.

2. The molecular ion is not observed.

3. The highest mass ion of significance in 4-EGDME and 3-EGDME are m/z 177 and m/z 133 respectively.

4. The small protonated ethers at m/z 177,133,89,45, separated in mass by ether unit, C_2H_4O, are predominant ions.

5. The base peak of both compounds are m/z 59.

The ionization of a nonbonding electron on oxygen seems to start from second or third oxygen atom in both compounds. The fragmentation mechanisms shown in Figures 64 and 65 proposed. Due to the inductive effect, the oxygen attracts an electron pair to form m/z 59, 103, 147 or attracts one electron to form m/z 119 (Figure 64). Comparing the mass spectra of crown ether and linear polyether. It shows that
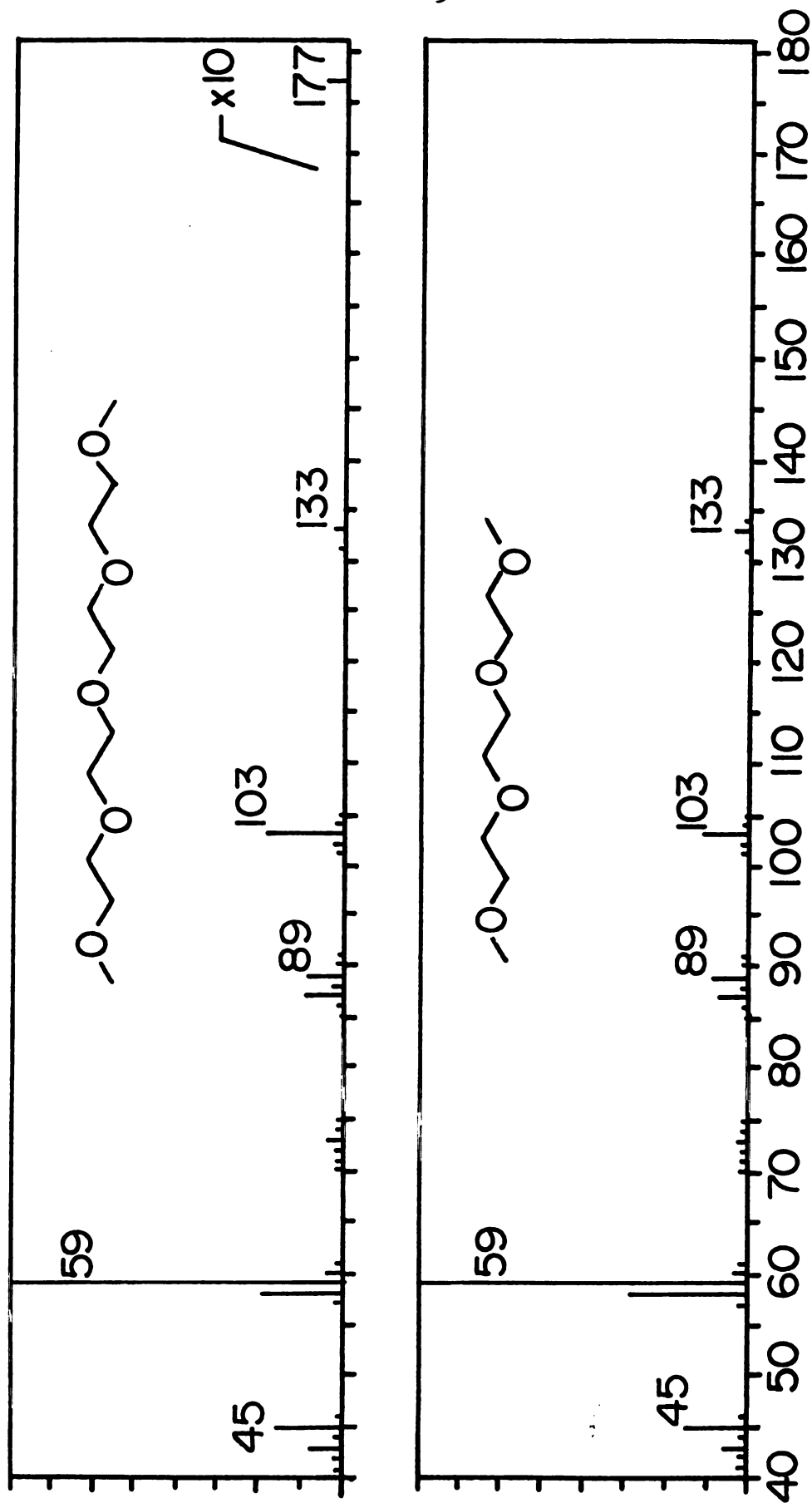
Figure 63. The 70eV mass spectra of tetraethylene glycol dimethylether and triethylene glycol dimethylether.

Table 48. Principal Fragment Ions in 70 eV Mass Spectra
of Linear Polyether.

Fragment Ion (m/z value)	3-EGDME[a]	4-EGDME[b]	Elemental Composition
41	1	1	C_2HO
42	1	1	C_2H_2O
43	7	8	C_2H_3O
44	2	2	C_2H_4O
45	18	18	C_2H_5O
57	1	1	C_3H_5O
58	33	29	C_3H_6O
59	100	100	C_3H_7O
60	4	4	$C_2H_4O_2$
70	1	1	C_4H_6O
71	1	1	C_4H_7O
72	1	2	C_4H_8O
73	2	4	C_4H_9O
75	1	1	$C_3H_7O_2$
87	9	10	$C_4H_7O_2$
88	1	2	$C_4H_8O_2$
89	12	9	$C_4H_9O_2$
90	1	1	$C_4H_{10}O_2$
101	1	2	$C_5H_9O_2$
102	3	4	$C_5H_{10}O_2$
103	13	25	$C_5H_{11}O_2$

Table 48. Continued.

Fragment Ion (m/z value)	3-EGDME[a]	4-EGDME[b]	Elemental Composition
104	1	2	$C_4H_8O_3$
117	0	0.55	$C_5H_9O_3$
119	0.55	0.35	$C_5H_{11}O_3$
131	0	1	$C_6H_{11}O_3$
133	4	3	$C_6H_{13}O_3$
147	0	0.44	$C_7H_{15}O_3$
177	0	0.39	$C_8H_{17}O_4$

[a] 3-EGDME, triethylene glycol dimethylether M.W.= 178
[b] 4-EGDME, tetraethylene glycol dimethylether M.W.= 222

239
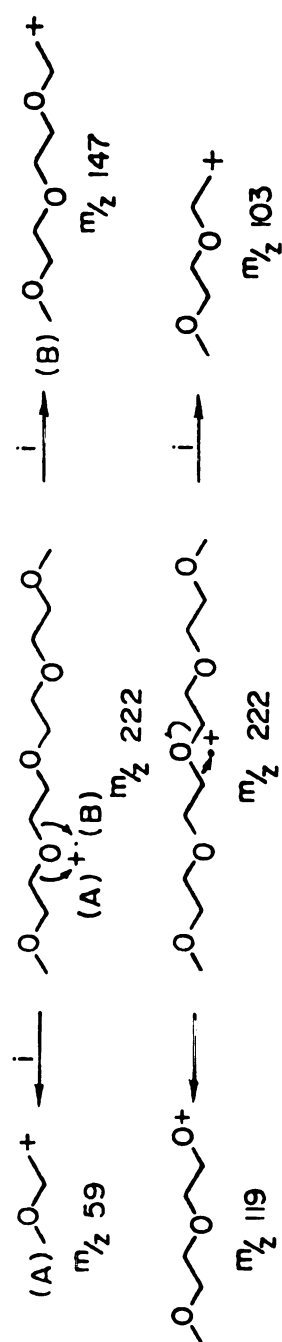
Figure 64. Fragmentation of 4-EGDME.
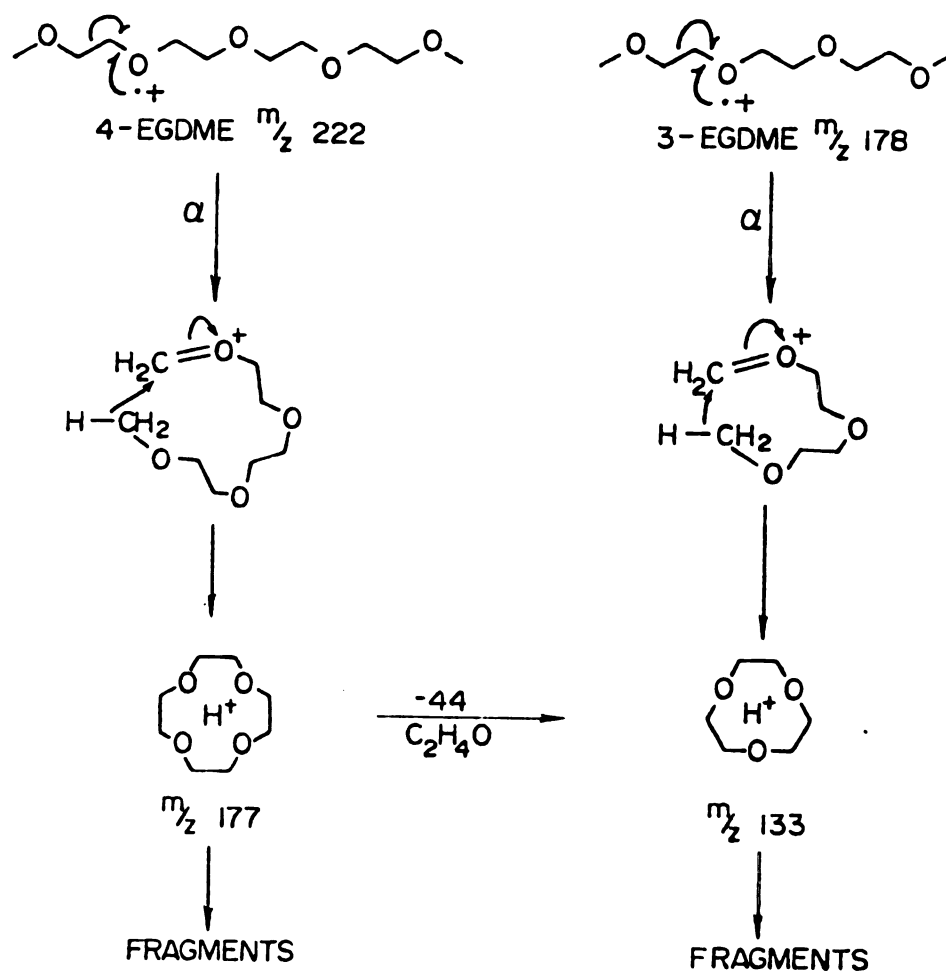
Figure 65. Fragmentation of 4-EGDME and 3-EGDME to form protonated crown ether.

3-EGDME has the same predominant ions (m/z 45, 89, 133) as shown in 12-crown-4 and 15-crown-5, while, 4-EGDME has the same characeric ions (m/z 45, 89, 133, 177) as shown in 18-crown-6 and 21-crown-7. These similarities can be used to support our proposed fragmentation mechanism for crown ethers in which a linear polyether intermediate was proposed.

Figure 65 indicates the mechanism through which m/z 177 and 133 are formed from 4-EGDME and 3-EGDME respectively. The protonated crown ethers are formed by α cleavage and ring closure procedures following the formation of the mole-cular ion. The fragmentation of protonated crown ethers is shown in Figure 17. According to the procedure, some ions such as m/z 45, 61, 73, 89, 105, are formed.

From the correlation of the mass spectra of linear poly-ethers and crown ethers, the fragmentation pathways which we proposed are reasonable and possibly can be used to predict the fragments of other highly functionalized crown ethers.

5. Suggestions for Further Studies

The following projects would be a logical continuation of this thesis work:

(1) Study of the influence of ion pair formation on the chemical shift of thallium(I) salt in binary solution mixtures.

(2) Investigation of the influence of ring size on the Tl^+ ion complexation, i.e. with 12C4, 15C5, 21C7, 24C8 crowns

and with cryptands C211, C221 and C222.

(3) Study of the kinetics of complexation in various solvents by dynamic NMR.

(4) Study macrocyclic complexes of the Tl^+ ion in molten salt.

(5) From the correlation of the mass spectra of linear polyethers and crown ethers, the fragmentation pathways which we proposed have proved to be reasonable. The mass spectra of DA18C6, DT18C6 and DC18C6 can be used to compare with the fragments which are predicated by our fragmentation pathways. Also, other techniques, such as isotopic labeling, metastable ion analysis and appearance potential measurements may be useful for exact identification of fragmentation mechanisms.

APPENDICES

APPENDIX 1

THE SIGN CONVENTION FOR NMR SPECTRA

The position of an NMR signal (represented by a chemical shift) is determined by the real magnetic field applied on the nucleus under study. A nucleus does not experiences the magnetic field which is applied to the sample (H_o) but a field, H, which has been altered by the screening of the electrons surrounding the nucleus. Thus at the nucleus the magnetic field is

$$H = H_o \, (1-\beta) \qquad\qquad (A.1)$$

The screen factor, β, which depends on the electronic environment of the nucleus is the sum of the various paramagnetic (β_p) and diamagnetic terms (β_d) (175)

$$\beta = \beta_{inter} + \beta_{intra}$$
$$= \beta_{inter} + \beta_d + \beta_p$$
$$= \beta_d + \beta_p \qquad\qquad (A.2)$$

Where β_{intra} is the intraatomic screening, while β_{inter} is the interatomic screening. The β_{inter} is generally very

small (< 2 ppm) and is usually neglected. The diamagnetic term ($\beta_d > 0$) is related to the diamagnetic currents due to the circulation of the electrons around the nucleus which leads to shielding of the nucleus. The second term, β_p is negative and is derived from the fact that electrons in a molecule are not always spherically symmetric about the nucleus. The presence of upaired electrons or p electrons near the nucleus is an important factor in determining β_p. A more representative equation for interpretation of a cation screeing factor in solution has been derived by Deverell and Richards (176).

Chemical shift data are usually measured in a dimensionless scale in ppm (parts per million) from the chosen reference. With the inclusion of the shielding factor at constant H_o, the Larmor equation relating to the resonance of a sample and a reference are

$$V_s = \frac{\gamma}{2\pi} H_o (1-\beta_s) \qquad\qquad (A.3)$$

$$V_r = \frac{\gamma}{2\pi} H_o (1-\beta_r) \qquad\qquad (A.4)$$

Where γ is nuclear magnetogyric ratio, V_s and V_r are the Larmor resonance frequencies of the sample and reference respectively, β_s and β_r are the screening factors of the sample and reference respectively. The chemical shift is written as:

$$\delta(\text{ppm}) = \frac{V_s - V_r}{V_r} \times 10^6 \qquad (A.5)$$

$$\cong (\beta_r - \beta_s) \times 10^6 \qquad (A.6)$$

According to Equation (A.6), $(V_s - V_r)$ is proportional to $(\beta_r - \beta_s)$ at constant H_0, so an increase in the resonance frequency implies a decrease in shielding for diamagnetic nuclei ($\beta > 0$). In the older literature both possible sign conventions have been used. According to IUPAC recommendation (177), the sign convention in relation to the FT NMR data contained herein are plotted as shown in Figure 66. In the case of diamagnetic nuclei studies, the screening factor is positive, so the graphical presentation for the NMR signal at the right hand side appears to be small ppm, low resonance frequency, upfield and shielding. While, for paramagnetic nuclei studies, since the screening factor is negarive, the NMR signal at the right hand side appears to be small ppm, low reasonance frequency, upfield and deshielding.

(A) Diamagnetic nucleus (^{1}H & ^{13}C)
    β > 0

S W

REAL
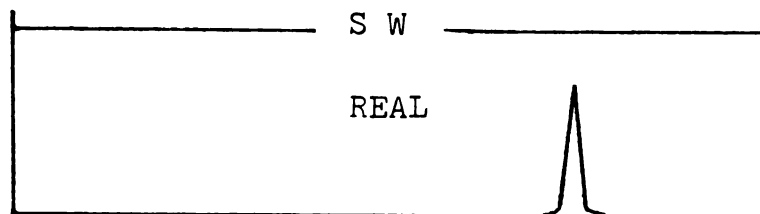
small δ(ppm)

upfield shift

shielding

low resonance frequency

high channel number

high e density

(B) Paramagnetic nucleus (^{23}Na, ^{39}K, ^{133}Cs & ^{205}Tl)
    β < 0

S W

REAL
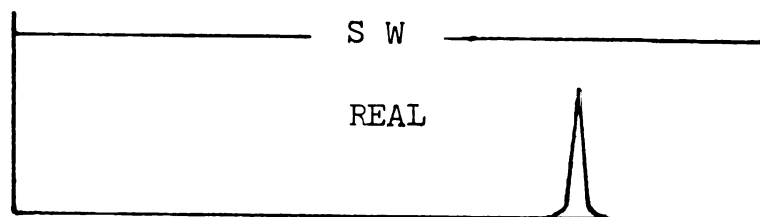
small δ(ppm)

upfield shift

deshielding

low resonance frequency

high channel number

low e density

Figure 66. The sign convention for NMR spectrum.

APPENDIX 2

DETERMINATION OF COMPLEX FORMATION CONSTANTS BY
THE NMR TECHNIQUE; DESCRIPTION OF THE COMPUTER
PROGRAM KINFIT AND SUBROUTINE EQUATIONS

A. Determination of Formation Constants for a 1:1 Complex

In the complexation reaction between crown (L) and
thallium(I) ions (M^+) in solution, the equilibrium for a 1:1
(metal ion:ligand) complexation reaction can be expressed as:

$$M^+ + L \rightleftarrows M^+L$$
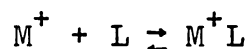
The KINFIT computer program was used to fit thallium-205 and
carbon-13 NMR chemical shift vs. mole ratio data to equation
(3.10) which was inserted into the SUBROUTINE EQUATION:

$$\delta_{obs} = [(Kc_M^T - Kc_L^T - 1) + (K^2 c_L^{T^2} + K^2 c_M^{T^2} - 2K^2 c_L^T c_M^T + 2Kc_L^T +$$

$$2Kc_M^T + 1)^{\frac{1}{2}}](\frac{\delta_M - \delta_{ML}}{2Kc_M^T}) + \delta_{ML} \qquad (3.10)$$

In order to fit this equation, two constants and two unknowns
are used in the FORTRAN code:

$$U(1) = \delta_{ML} \qquad\qquad U(2) = K$$

$$CONST\ (1) = C_M^T \qquad\qquad CONST\ (2) = \delta_M$$

The two input variables are the analytical concentration of the ligand (C_L^T, M) and the observed chemical shift (δ_{obs}, ppm) which are designed as XX(1) and XX(2) respectively in the FORTRAN code. Starting with an estimated values of K and δ_{ML}, the program fits the calculated chemical shift to the observed values by an iterative method. The data input includes the control cards and the NMR data. The cards include:

(1) The first control card contains the number of data points [columns 1-5 (F I5)], the maximum number of iterations allowed [column 11-15 (F I5)], the number of constants [column 36-40 (F I5)] and the convergence to the tolerance (0.0001 works well) in columns 41-50 (F 10.6).

(2) The second control card is a title card.

(3) The third control card contains the value of CONST(I) (C_M^T, M) in columns 1-10 (F 10.6) and CONST(2) (δ_M, ppm) in column 11-20 (F 10.6).

(4) The fourth control card contains the initial estimates of the unknowns U(1) and U(2) in columns 1-10 and 11-20 (F. 10.6) respectively.

(5) The fifth through Nth cards are the data cards which contain XX(1)= C_L^T in columns 1-10 (F. 10.6), the variance

on XX(1) in column 11-20, XX(2) [the chemical shift at XX(1)] in columns 21-30 (F 10.6) and the variance on XX(2) in columns 31-40 (F 10.6) followed by the same parameters for the next data point. Each card may contain two data points. The SUBROUTINE EQN and sample data are listed on the next page.

```
PNC CARD
JOB CARD
PASS WORD CARD
HAL , BANNER, LEE
RETURN,KINFT,LGO.
HAL, L*DYE, KINFT4=KINFT4.
FTN, B=LGO.
LOAD, KINFT4.
LGO.
7
  8
   9 CARD
      SUBROUTINE EQN
      COMMON KCUNT,ITAPE,JTAPE,IWT,LAF,XINCR,NCPT,NOVAR,NOUNK,X,U,ITMAX,  EQN4
     1WTX,TEST,I,AV,RESID,IAR,EPS,ITYP,XX,RXTYF,DX1I,FOP,FC,FU,P,ZL,TC,E   EQN4
     2IGVAL,XST,T,DT,L,M,JJJ,Y,CY,VECT,NCST,CCNST,NCAT,JCAT,MCPT,LOFT,      EQN4
     3YYY,CCNSTS
      COMMCN/FFECT/IMETH
      COMMCN/FOINT/KOPT,JOPT,XXX
      DIMENSION X(4,300),U(20),WTX(4,300),XX(4),FOP(300),FC(300),FU(300)  EQ
     1,P(20,21),VECT(20,21),ZL(300),TC(20),EIGVAL(20),XST(300),Y(10),
     2CY(10),CCNSTS(50,16),NCST(50),ISMIN(50),RXTYF(50),DX1I(50),IRX(50)
     3,MOPT(50),LCPT(50),YYY(50),CONST(16),XXX(15)
      GO TO (2,3,4,5,1,7,8,9,10,11,12)  ITYF
    1 CONTINUE
      ITAPE=60
      JTAPE=61
      WRITE (JTAPE,6)
    6 FORMAT(////////,* COMPLEXATION FORMATION CONSTANT *)
      NOUNK=2
      NOVAR=2
      RETURN
    7 CONTINUE
      RETURN
    8 CONTINUE
      RETURN
    2 CONTINUE
CCCCCCCCCCCCCCCCCCCCCCCCCCCCCCCCCCCCCCCCCCCCCCCCCCCCCCCCCCCCCCCCCCCCCCCCCCCCC
C     U(1)=S ML    U(2)=K    CONST(1)=CONC.M    CCNST(2)=S FREE M
C     XX(1)=CONC.LIGAND  ,XX(2)=S OBSERVED
CCCCCCCCCCCCCCCCCCCCCCCCCCCCCCCCCCCCCCCCCCCCCCCCCCCCCCCCCCCCCCCCCCCCCCCCCCCCC

      A=(U(2)**2)*(XX(1)**2)
      B=(U(2)**2)*(CONST(1)**2)
      C=-2.0*(U(2)**2)*(XX(1))*CONST(1)
      D=2.0*(U(2))*(XX(1))
      E=2.0*(U(2))*(CCNST(1))
      AA=(U(2))*(CCNST(1))
      BB=-(U(2))*XX(1)
      CC=(CONST(2)-U(1))/(2.*(CONST(1))*(U(2)))
      S=(((AA+BB-1.)+SQRT(ABS(A+B+C+D+E+1.)))*CC)+U(1)
      IF(IMETH.NE.-1) GO TO 35
      RETURN
   35 CONTINUE
      RESID=S-XX(2)
      RETURN
    3 CONTINUE
      RETURN
    4 CONTINUE
      RETURN
    5 CONTINUE
      IF(IMETH.NE.-1) GO TO 20
      RETURN
   20 CONTINUE
      RETURN
    9 CONTINUE
      RETURN
   10 CONTINUE
      RETURN
   11 CONTINUE
      RETURN
   12 CONTINUE
      RETURN
      END
7
 8
  9 CARD
****************************************************************
CONTROL CARD
TITLE CARD
CONSTANTS CARD
INITIAL ESTIMATE CARD
DATA CARD
****************************************************************
BLANK CARD
6
 7
  8
   9 CARD
```

(B) Determination of Formation Constants for 1:1 and 2:1
     Complex

The equilibria for this reaction can be expressed as

$$M^+ + L \rightleftharpoons ML^+ \qquad\qquad K_1 = C_{ML^+}/C_M \cdot C_L \qquad\qquad (A.7)$$

$$ML^+ + L \rightleftharpoons ML_2^+ \qquad\qquad K_2 = C_{ML_2^+}/C_{ML^+} \cdot C_L \qquad\qquad (A.8)$$
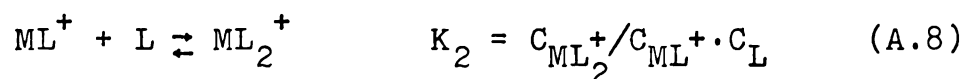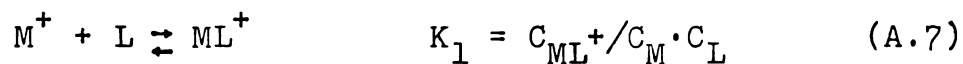
Where C represents the molarity of the species, C_M^T and C_L^T
denote the total concentrations of the metal ion and ligand
respectively. Then

$$C_M^T = C_M + C_{M^+} + C_{ML_2^+} = C_M(1 + K_1C_L + K_1K_2C_L^2) \qquad\qquad (A.9)$$

$$C_L^T = C_L + C_{ML^+} + 2C_{ML_2} = C_L + K_1C_MC_L + 2K_1K_2C_MC_L^2 \qquad\qquad (A.10)$$

(A.9) can be rearranged as

$$C_M = C_M^T / (1 + K_1C_L + K_1K_2C_L^2) \qquad\qquad (A.11)$$

Equation (A.10) can   also be written as

$$2K_1K_2C_MC_L^2 + C_L(1 + K_1C_M) - C_L^T = 0$$

Therefore

$$C_L = \frac{-(1 + K_1C_M) + [(1 + K_1C_M)^2 + 8K_1K_2C_MC_L^T]^{\frac{1}{2}}}{4K_1K_2C_M} \qquad\qquad (A.12)$$

The observed chemical shift is:

$$\delta_{obs} = X_M \delta_M + X_{ML} \delta_{ML} + X_{ML_2} \delta_{ML_2} \qquad \text{(A.13)}$$

In order to fit the calculated result with the experimental data, an expression for the relative mole fractions of all three species in terms of C_M^T and C_L^T is required. Two constants and four unknowns are used in the FORTRAN code:

$$U(1) = K_1 \qquad U(2) = K_2 \qquad U(3) = \delta_{ML} \qquad U(4) = \delta_{ML_2}$$

$$\text{CONST}(1) = C_M^T \qquad\qquad \text{CONST}(2) = \delta_M$$

The two input variables are the total concentration of ligand (C_M^T, M) and the observed chemical shift (δ_{obs}, ppm) which are designated as XX(1) and XX(2) respectively. In order to avoid determination of the solution to a cubic equation in order to obtain values of C_M and C_L and thus δ_{obs}, an iteration method was used. This method is achieved by applying a "do loop" in the EQN subroutine of the KINFIT program. The computer starts the calculation from given initial estimates for four unknows, and first calculates C_L, then used this newly computed C_L value to calculate C_M. Then, again these values are used to calculate C_L and so on until the ratio of the previous C_L to the current C_L is almost equal to one. The iteration stops by "jumping out" of the do loop when the difference between unity and ratio of the

new to the old C_L values is less than 10^{-5}. Then the current C_L and C_M values are used to compute the mole fractions of each component and thus δ_{obs}.

    The SUBROUTINE EQN and a sample data are listed on the following page.

```
PWC CARD
JOB CARD
PASS WORD CARD
HAL , BANNER, LEE
RETURN.KINPT.LGO.
HAL. L*DYE. KINPT4=KINPT4.
FTN, B=LGO.
LOAD, KINPT4.
LGO.
7
 8
  9 CARD
     SUBFOUTI:E ECH
     COMMON KFUNT.ITAPE.JTAPE.IVT.LAP.XINCR.NOPT.NOVAR.NOUNK.A.U.ITMAX.   EQN4
   1BTX.TEST.I.AV.RESID.IAR.EPS.ITYP.XX.RXTYP.OX11.FOP.FG.FU.P.ZL.TG.Z   EQN4
   21GVAL.XST.T.GT.L.M.JJJ.Y.DY.VECT.NCST.CONST.HDAT.JDAT.KOPT.LOPT.      EQN4
   3YYY.CONSTS                                                            EQN4
     COMMON/FHEDT/IMETH
     COMMON/PCINT/KOPT.JOPT.XXX
     DIMENSION X(4.300).U(20).WTX(4.300).XX(4).FOP(300).FO(300).FU(300)   EQN4
   1.F(20.21).VECT(20.21).ZL(300).TO(20).EIGVAL(29).XST(300).Y(10).       EQN4
   2DY(10).CCNSTS(50.16).NCST(50).ISMIN(50).RXTYP(50).OX11(50).IRX(50)    EQN4
   3.MOPT(50).LOPT(50).YYY(50).CONST(16).XXX(15)                          EQN4
     DIMENSION C(300).DIFF(300)
     GO TO (2.3.4.5.1.7.8.9.10.11.12)   ITYP
   1 CONTINUE
     ITAPE=60
     JTAPE=61
     WRITE (JTAPE.6)
   6 FORMAT(///////.* COMPLEXATION FORMATION CONSTANT *)
     NOUNK=4
     NOVAR=2
     RETURN
   7 CONTINUE
     RETURN
   8 CONTINUE
     RETURN
   2 CONTINUE
CCCCCCCCCCCCCCCCCCCCCCCCCCCCCCCCCCCCCCCCCCCCCCCCCCCCCCCCCCCCCCCCCCCCCCCCC
C    CONST(1)=TOTAL CONC. OF TL ION.  CONST(2)=S OF FREE ION
C    U(1)=K1   U(2)=K2  U(3)=S1   U(4)=S2
C    CONM=CONC. OF FREE TL ION.
CCCCCCCCCCCCCCCCCCCCCCCCCCCCCCCCCCCCCCCCCCCCCCCCCCCCCCCCCCCCCCCCCCCCCCCCC
     IF(XX(1).LT.CONST(1)) CONM=CONST(1)-XX(1)
     IF(XX(1).EQ.0.0) CONM=(-1.+SQRT(1.+4.*U(1)*CONST(1)))/(2*U(1))
     IF(XX(1).EQ.CONST(1).AND.U(1).GE.1.E9) GO TO 220
     IF(XX(1).GT.CONST(1)) CONM=1.E-7
     DIFF(1)=0.0
     C(1)=0.0
     DO 200 N=2.300
     IF (N.EQ.300) PRINT 100.N.XX(1)
  100 FORMAT(10X.*N=*.I3.5X.*XX(1)=*.F10.6)
     B=U(1)*CONM
     S=SQRT((1.+B)**2+8.*8*U(2)*XX(1))
     C(N)=(-(1.+B)+S)/(4.*8*U(2))
     D=1.+C(N)*U(1)*U(1)*U(2)*C(N)**2
     CONM=CONST(1)/D
     IF(XX(1).EQ.0.0) GO TO 250
     IF(C(N).EQ.0.0) C(N)=1.E-20
     RATIO=C(N-1)/C(N)
     DIFF(N)=ABS(1.-RATIO)
     IF(DIFF(N).GT.1.) PRINT 1000
 1000 FORMAT(10X.* ITERATION IS DIVERGED *)
     IF(DIFF(N).LT..00001) GO TO 250
  200 CONTINUE
  220 C(N)=CONM
     D=1.+U(1)*C(N)+U(1)*U(2)*C(N)**2
     CONM=CONST(1)/D
  250 F=CONM/CONST(1)
     COMP1=U(1)*CONM*C(N)/CONST(1)
     COMP2=U(1)*U(2)*CONM*C(N)**2/CONST(1)
     SOBS=CONST(2)*F+U(3)*COMP1+U(4)*COMP2                                EQN4
     IF(IMETH.NE.-1) GO TO 35
     XX(2)=SOBS
     RETURN
   35 CONTINUE
     RESID=SOBS-XX(2)                                                     EQN4
     RETURN                                                               EQN4
   3 CONTINUE                                                             EQN4
     RETURN
   4 CONTINUE
     RETURN
   5 CONTINUE
     IF(IMETH.NE.-1) GO TO 20
     RETURN
   20 CONTINUE                                                            EQN4
     RETURN                                                               EQN4
   9 CONTINUE
     RETURN
  10 CONTINUE
     RETURN
  11 CONTINUE
     RETURN
  12 CONTINUE                                                             EQN4
     RETURN                                                               EQN4
     END
7
 8
  9 CARD
**********************************************************
CONTROL CARD
TITLE CARD
CONSTANTS CARD
INITIAL ESTIMATE CARD
DATA CARD
**********************************************************
BLANK CARD
6
 7
  8
   9 CARD
```

APPENDIX 3

DETERMINATION OF ION-PAIR FORMATION CONSTANTS BY
THE NMR TECHNIQUE; DESCRIPTION OF THE COMPUTER
PROGRAM KINFIT AND SUBROUTINE EQUATION

The equilibrium for ion-pair formation can be expressed as

$$M^+ + X^- \overset{K_{ip}}{\rightleftharpoons} M^+ \cdot X^-$$
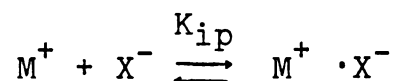
and

$$K_{ip} = \frac{A_{(M^+ \cdot X^-)}}{A_{M^+} \cdot A_{X^-}} = \frac{(M^+ \cdot X^-)}{(M^+)(X^-)\gamma_\pm^2} = K_c / \gamma_\pm^2$$

in which K_{ip}, K_c and $\gamma_\pm$ are the thermodynamic ion-pair formation constant, the concentration equilibrium constant and the mean activity coefficient respectively. By using the well known Debye-Huckel equation, $\gamma_\pm$ can be thus calculated as follows:

$$\gamma_\pm = \exp \left\{ \frac{-4.196 \times 10^6 \, |z_+ z_-| \, \sqrt{I}}{[(DT)^{\frac{1}{2}}]^3 [1 + \frac{50.29}{(DT)^{\frac{1}{2}}} \overset{o}{a}\sqrt{I}]} \right\} \tag{A.14}$$

In this equation z_+, z_- are the charges of the ions, I is the

molar ionic strength which is $\frac{1}{2} \sum_i C_i z_i^2$ (C = concentration summed over all species in the solution). D is the dielectric constant of the solvent and T and $\overset{o}{a}$ are the temperature ($^\circ$K) and the closest distance of approach of the ions in $\overset{o}{A}$.

The observed chemical shift is a population average of those of the free ion and the ion pair; i.e.

$$\delta_{obs} = \delta_F X_F + \delta_{ip} X_{ip}$$

$$= (\delta_F - \delta_{ip}) X_F + \delta_{ip} \qquad (A.15)$$

Where $X_F = [Li^+]/C_T^M$; and C_T^M is the total concentration of Li^+ in the system. Meterial balance gives

$$C_T^M = [Li^+] + [Li^+ \cdot X^-]$$

$$= [Li^+] + K_c [Li^+]^2$$

Therefore

$$[Li^+] = \frac{-1 \pm (1 + 4K_c C_M^T}{2K_c}$$

$$X_F = \frac{[Li^+]}{C_M^T} = \frac{-1 + (1 + 4K_c C_M^T)^{\frac{1}{2}}}{2K_c C^T} \quad \text{and} \quad K_C = K_{ip} \gamma_\pm^2$$

So that, finally

$$\delta_{obs} = \frac{-1 + (1 + 4K_{ip}C_M^T \cdot \gamma_\pm^2)^{\frac{1}{2}}}{2K_{ip}C_M^T \cdot \gamma_\pm^2} (\delta_F - \delta_{ip}) + \delta_{ip} \qquad (A.16)$$

Three constants and two unknowns are used in the FORTRAN code:

$U(1) = \delta_{ip}$ $\qquad\qquad$ $U(2) = K_{ip}$ $\qquad\qquad$ $CONST(1) = \delta_F$

$CONST(2) = (DT)^{\frac{1}{2}}$ $\qquad\qquad\qquad$ $CONST(3) = \overset{o}{a}$

In these studies, $\overset{o}{a} = 2.56\overset{o}{A}$, $\delta_F = -1.5$ ppm, $(DT)^{\frac{1}{2}} = 114.6$ were chosen. The two input variables are the concentration of the salt (C_M^T, M) and the observed chemical shift (δ_{obs}, ppm) which are designed as XX(1) and XX(2) respectively in FORTRAN code. Staring with an estimated value of δ_{ip} and K_{ip}, the program fits the calculated chemical shift observed values by an iteration method. The SUBROUTINE EQUATION and a sample data are listed on the next page.

```
PNC CARD
JOB CARD
PASS WORD CARD
HAL , BANNER, LEE
RETURN,KINFT,LGO.
HAL, L*DYE, KINFT4=KINFT4.
FTN, B=LGO.
LOAD, KINFT4.
LGO.
7
 8
  9 CARD
      SUEROUTINE EQN
      COMMON KOUNT,ITAPE,JTAPE,IWT,LAM,XINCR,MCPT,NOVAR,NOUNK,X,U,ITMAX,KINFISC1
     1WTX,TEST,I,AV,RESID,IAP,EPS,ITYF,XX,RXTYF,DX1I,FOP,FO,FU,P,ZL,TC,FKINFISC2
     2IGVAL,XST,T,DT,L,M,JJJ,Y,DY,VECT,NCST,CONST,NDAT,JDAT,MOPT,LOPT,
     3YYY,CONSTS
      COMMON/FEDT/IMETH
      COMMON/PUINT/KOPT,JOPT,XXX
      DIMENSION X(4,300),U(20),WTX(4,300),XX(4),FOP(300),FO(300),FU(300)
     1,P(20,21),VECT(20,21),ZL(300),T(20),EIGVAL(20),XST(300),Y(10),
     2DY(10),CONSTS(50,16),NCST(50),ISMIN(50),RXTYP(50),DX1I(50),IRX(50)
     3,MOPT(50),LCPT(50),YYY(50),CONST(16),XXX(15)
      GO TO (2,3,4,5,1,7,8,9,10,11,12),ITYP
    1 CONTINUE
      ITAPE=60
      JTAPE=61
      WRITE (JTAPE,6)
    6 FORMAT(///////////,* KINFIT - ION PAIR FORMATION CONSTANT *)
      NOUNK=2
      NOVAR=2
      RETURN
    7 CONTINUE
      RETURN
    8 CONTINUE
      RETURN
    2 CONTINUE
C     XX(1)=CONCENTRATION OF SALT
C     XX(2)=S=OBSERVED CHEMICAL SHIFT
C     U(1)=ION PAIRING LIMITING CHEMICAL SHIFT
C     U(2)=KIP,THERMODYNAMIC ION PAIRING FORMATION CONSTANT
C     CONK=KC, CONCENTRATION ION PAIRING FORMATION CONSTANT
C     CONST(1)=S OF FREE, CHEMICAL SHIFT CF FREE SOLVATED METAL ION
C     CONST(2)=SGRT OF(SOLVENT DIELECTRIC CONSTANT*TEMPERATURE IN KELVIN)
C     CONST(3)=A , ION-ION DISTANCE PARAMETER IN ANGSTRUM
      GEMA=EXP(-419800C.0*SQRT(XX(1))/(CONST(2)**3*(1.0+50.29*CONST(3)*
     1     SQRT(XX(1))/CONST(2))))
      CONK=U(2)*(GEMA**2.0)
      F=4.0*CONK*XX(1)
      S=((-1.0+SQRT(1.+F))/(2.*CONK*XX(1)))*(CONST(1)-U(1))+U(1)
      RESID=S-XX(2)
      RETURN
   35 CONTINUE
      RETURN
    3 CONTINUE
      RETURN
    4 CONTINUE
      RETURN
    5 CONTINUE
      RETURN
   20 CONTINUE
      RETURN
    9 CONTINUE
      RETURN
   10 CONTINUE
      RETURN
   11 CONTINUE
      RETURN
   12 CONTINUE
      RETURN
      END
7
 8
  9 CARD
**********************************************************
CONTROL CARD
TITLE CARD
CONSTANTS CARD
INITIAL ESTIMATE CARD
DATA CARD
**********************************************************
BLANK CARD
6
 7
  8
   9 CARD
```

REFERENCES

1. C. J. Pedersen, J. Am. Chem. Soc., 89, 7017 (1967).

2. N. S. Poonia and A. V. Bajaj, Chem. Rev., 79, 389 (1979).

3. J. J. Christensen, J. O. Hill, and R. M. Izatt, Science, 174, 459 (1971).

4. C. J. Pedersen and H. K. Frensdorff, Angew. Chem., Int. Ed. Engl., 11, 16 (1972).

5. A. I. Popov, Pure Appl. Chem., 41, 275 (1975).

6. J. M. Lehn, Pure Appl. Chem., 49, 857 (1977).

7. J. J. Christensen, D. J. Eatough, and R. M. Izatt, Chem. Rev., 74, 351 (1974).

8. D. Midgley, Chem. Soc. Rev., 4, 549 (1975).

9. I. M. Kolthoff, Anal. Chem., 51, 1R (1979).

10. R. M. Izatt, R. E. Terry, B. L. Haymore, L. D. Hansen, N. K. Dalley, A. G. Avondet, and J. J. Christensen, J. Am. Chem. Soc., 98, 7620 (1976).

11. E. Mei, A. I. Popov and J. L. Dye, J. Phys. Chem., 81, 1677 (1977).

12. R. M. Izatt, R. E. Terry, D. P. Nelson, Y. Chan, D. J. Eatough, J. S. Bradshaw, L. D. Hansen, and J. J. Christensen, J. Am. Chem. Soc., 98, 7626 (1976).

13. B. Spiess, F. Arnaud-Neu, and M. J. Shwing-weill, Helvetica Chemica Acta, 62, 1531 (1979).

14. M. Shamsipur, G. Rounaghi, and A. I. Popov., J. Solution Chem., 9, 701 (1980).

15. R. W. Briggs, and J. F. Hinton, J. Magn. Reson., 32, 155 (1978).

16. C. Moore and B. C. Pressman, Biochem. Biophs. Res. Commun., 15, 562 (1964).

17. J. M. Lehn, Struct. Bonding (Berlin), 16, 1 (1973).

18. M. R. Truter, Struct. Bonding (Berlin), 16, 71 (1973).

19. W. Simon, W. E. Morf, and P. Ch. Meier, Struct. Bonding (Berlin), 16, 161 (1973).

20. R. M. Izatt, D. J. Eatough, and J. J. Christensen, Struct. Bonding (Berlin), 16, 161 (1973).

21. A. Kotyk and K. Janacek, "Cell Membrane Transport", Plenum, London 1970.

22. E. E. Bittar, "Membrane and Ion Transport", Vol. 1. Wiley-Interscience, New York, 1970.

23. N. S. Poonia, J. Am. Chem. Soc., 96, 1012 (1974).

24. W. E. Morf, D. Ammann, E. Pretsch, and W. Simon, Pure Appl. Chem., 36, 421 (1973).

25. R. S. Cockrell, E. J. Harris and B. C. Pressman, Biochemistry, 5, 2325 (1966).

26. C. F. Reusch and E. L. Cussler, Am. Inst. Chem. Eng. j., 19, 736 (1973).

27. S. C. A. McLanghlin, G. Szabo, S. Ciani and G. Eisenman, J. Membrane Biol., 9, 3 (1972).

28. H. Lardy, Fed. Proc., 27, 1278 (1968).

29. H. K. Wipf, L. A. R. Pioda, Z. Stefanac, and W. Simon, Helv. Chim. Acta, 51, 377 (1968).

30. V. T. Ivanov, I. A. Laine, N. D. Abdullaev, L. B. Senyavina, E. M. Popov, Yu. A. Ovchinnikov, and M. M. Shemyakin, Biochem. Biophys. Res. Commun., 34, 803 (1969).

31. L. A. R. Pioda, H. A. Wachter, R. E. Dohner, and W. Simon, Helv. Chem. Acta., 50, 1373 (1967).

32. P. B. Chock, Proc. Natl. Acad. Sci. USA, 69, 1939 (1972).

33. J. H. Prestegard and S. I. Chan, J. Am. Chem. Soc., 92, 4440 (1970).

34. C. J. Pedersen, Fed. Proc., Fed. Amer. Soc. Exp. Biol., 27, 1305 (1968).

35. P. Seiler, M. Dobler, J. D. Dunitz, Acta Crystallogr. B 30, 2744 (1974).

36. M. A. Bush and M. R. Truter, J. Chem. Soc., Perkin II, 345 (1972).

37. N. S. Poonia, J. Inorg, Nucl. Chem. 37, 1855 (1975).

38. D. E. Fenton, M. Mercer, N. S. Poonia, and M. R. Truters, Chem. Commun., 66 (1972).

39. D. L. Hugher, J. Chem. Soc., Dalton Trans., 2374 (1975).

40. C. J. Pedersen, J. Am. Chem. Soc., 92, 386 (1970).

41. N. S. Poonia and M. R. Truter, J. Chem. Soc., Dalton Trans., 2062 (1972).

42. M. Shampsipur and A. I. Popov, J. Am. Chem Soc., 101, 4051 (1979).

43. H. K. Frensdorff, J. Am. Chem. Soc., 93, 600 (1971).

44. K. H. Wong, M. Bourgoin, and J. Smid, Chem. Commun., 715 (1974).

45. J. S. Shin, Michigan State University, Ph.D. Thesis (1978).

46. H. Dobler, J. D. Dunitz and B. T. Kilbourn, Helv. Chim. Acta., 52, 2573 (1969).

47. M. Dobler, J. D. Dunitz and J. Krajewski, J. Mol. Biol Biol., 42, 603 (1969).

48. A. Hofmanova, J. Koryta, M. Brezina, and M. L. Mittal, Inorg. Chim. Acta., 28, 73 (1978).

49. R. M. Izatt, D. P. Nelson, J. H. Rytting, B. L. Hayntore, J. J. Christensen, J. Amer. Chem. Soc., 93, 1619 (1971).

50. F. A. L. Anet, J. Krane, J. Dale, K. Daasvatn, and P. O. Kristiansen, Acta Chem. Scand., 27, 3395 (1973).

51. N. Matsuura, K. Umemoto, Y. Takeda, and A. Sasaki, Bull. Chem. Soc. Jpn., 49, 1246 (1976).

52. S. Lindenbaum, J. H. Rytting, and L. A. Sternson, in "Progress in Macrocyclic Chemistry", Vol. 1, R. M. Izatt and J. J. Christensen, Eds., Wiley-inter-Science New York, 1979 Chapter 2 and 5.

53. R. N. Greene, Tetrahedron Lett. 1793 (1972).

54. J. Dale and P. O. Kristiansen, Acta Chem. Scamd., 26, 1471 (1972).

55. G. W. Gokel, D. J. Cram, C. L. Liotta, H. P. Harris, and F. L. Cook, J. Org. Chem., 39, 2445 (1974).

56. G. W. Gokel, D. J. Cram, C. L. Liotta, H. P. Harris, and F. L. Cook, Org. Synth., 57, 30 (1977).

57. G. Rounaghi and A. I. Popov, J. Inorg. Nucl. Chem., 43, 911 (1981).

58. C. J. Pedersen, Org. Synth. 52, 66 (1972).

59. E. Schori, N. Nae, and J. Jagur-Grodzinski, J. Chem. Soc. Dalton Trans., 2381 (1975).

60. J. F. Stoddart and C. M. Wheatley, Chem. Commun., 390 (1974).

61. I. J. Burden, A. C. Coxon, J. F. Stoddart, and C. M. Wheatley, J. Chem. Soc., Perkin Trans., 1, 220 (1977).

62. G. W. Gokel, S. H. Korzeniowski, "Macrocyclic Polyether Syntheses", Berlin Heidelberg New York 1982, Chapter 4 and 6.

63. G. Anderegg, Helv, Chim. Acta 58, 1218 (1975).

64. D. L. Jhonston and W. D. Horrocks, Inorg. Chem., 10, 687 (1971).

65. R. W. Kluiber and G. Sasso, Inorg. Chim. Acta 4, 226 (1970).

66. M. Herceg and R. Weiss, Inorg. Nucl. Chem. Lett., 6, 435 (1970).

67. D. Moras, B. Metz, M. Herceg, and R. Weiss, Bull. Soc. Chim. Fr., 551 (1972).

68. B. Metz and R. Weiss, Acta Crystallogr. B29, 1088 (1973).

69. M. Herceg and R. Weiss, Acta Crystallogr, B29, 542 (1973).

70. M. Shamsipur, Michigan State University, Ph.D. Thesis (1979).

71. J. R. Dann, P. P. Chiesa, and J. W. Gates, Jr., J. Org. Chem., 26, 1991 (1961).

72. C. J. Pedersen, U. S. Patent 3,856,813, Dec. 24 (1974).

73. C. J. Pedersen, U. S. Patent 3,873,569, March 25 (1975).

74. C. J. Pedersen, J. Org. Chem., <u>36</u>, 254 (1971).

75. N. K. Dalley, J. S. Smith, S. B. Larson, K. L. Matheson, J. J. Christensen, and R. M. Izatt, J. Chem. Soc. Chem. Commun., 84 (1975).

76. R. M. Izatt, R. E. Terry, L. D. Hansen, A. G. Avondet, J. S. Bradshaw, N. K. Dalley, T. E. Jensen, B. L. Haymore, and J. J. Christensen, Inorg. Chim. Acta, <u>30</u>, 1 (1978).

77. B. Metz, D. Moras and R. Weiss, J. Inorg. Nucl. Chem., <u>36</u>, 785 (1975).

78. N. K. Dally and S. B. Larson, 33rd Nothwest Regional metting, American Chemical Society, Seattle, Washington, June, 1978, paper no. 138.

79. F. Vogtle and Weber, Angew. Chem., <u>89</u>, 126 (1974).

80. T. E. Jones, D. B. Rorabacher, and L. A. Ochrymowycz, J. Am. Chem. Soc., <u>97</u>, 7485 (1975).

81. J. D. Lamb, R. W. Izatt, C. S. Swain and J. J. Christensen, J. Am. Chem. Soc. <u>102</u>, 475 (1980).

82. R. H. Erlich, A. I. Popov, J. Am. Chem. Soc., <u>92</u>, 4989 (1970).

83. M. K. Wong, A. I. Popov, J. Phys. Chem., <u>75</u>, 56 (1971).

84. Y. M. Cahen, J. L. Dye, and A. I. Popov, J. Phys. Chem., <u>79</u>, 1289 (1975).

85. A. J. Smetana and A. I. Popov, J. Solution Chem., <u>9</u>, 183 (1980).

86. M. Shamsipur and A. I. Popov, J. Am. Chem. Soc., <u>101</u>, 4051 (1979).

87. J. M. Lehn and J. P. Sauvage, J. Am. Chem. Soc., <u>97</u>, 6700 (1975).

88. J. Cheney, J. P. Kintzinger, and J. M. Lehn, Nouv. J. Chim., <u>2</u>, 411 (1978).

89. E. Mei, A. I. Popov, and J. L. Dye, J. Am. Chem. Soc., <u>99</u>, 6532 (1977).

90. J. M. Lehn, and J. Simon, Helv. Chim. Scta, 60, 141 (1977).

91. N. N. L. Kirsch, R. J. J. Funck, E. Pretsch, and W. Simon, Helv. Chim. Acta, 60, 2326 (1977).

92. M. Bourgoin, K. H. Wong, J. Y. Hui, and J. Smid, J. Am. Chem. Soc., 97, 3462 (1975).

93. B. Tummler, G. Maass, E. Weber, W. Wehner, and F. Vogtle, J. Am. Chem. Soc., 99, 4683 (1977).

94. R. M. Izatt, J. D. Lamb, R. E. Asay, G. E. Maas, J. S. Bradshaw, J. J. Christensen and S. S. Moore, J. Am. Chem. Soc., 99, 6134 (1977).

95. R. M. Izatt, J. D. Lamb, G. E. Maas, R. E. Asay, J. S. Bradshaw, and J. J. Christensen, J. Am. Chem. Soc., 99, 2365 (1977).

96. A. Hourdakis and A. I. Popov, J. Solution Chem., 6, 299 (1977).

97. E. Mei. L. Liu, J. L. Dye and A. I. Popov, J. Solution Chem., 6, 771 (1977).

98. W. Sahmand A. Schwenk, Z. Naturforsch 29A, 1754 (1974).

99. R. W. Briggs and J. F. Hinton, J. Magn. Reson, 33, 363 (1979).

100. V. F. Bystrov, Yu. D. Gavilov, V. T. Ivanov, and Yu. A. Ovchinnikov, Eur. J. Biochem. 78, 63 (1977).

101. J. J. Dechter and J. I. Zink, J. Am. Chem. Soc., 97, 2937 (1975).

102. G. E. Maciel, J. K. Hancock, L. F. Lafferty, P. A. Mueller, and W. K. Musker, Inog. Chem. 5, 554 (1966).

103. R. H. Erlich and A. I. Popov, J. Am. Chem. Soc., 93, 5620 (1971).

104. M. Herlem and A. I. Popov, J. Am. Chem. Soc., 94, 1431 (1972).

105. J. D. Halliday, R. E. Richards, amd R. R. Sharp, Proc. R. Soc. London. Ser. A, 313, 45 (1959).

106. R. Freeman, R. P. H. Gasser, R. E. Richards, and D. H. Wheeler, 2, 75 (1959).

107. J. J. Dechter and J. I. Zink, J. Am. Chem. Soc., 98, 845 (1976).

108. C. Schramm and J. I. Zink, J. Magn. Reson. 26, 513 (1977).

109. R. W. Briggs and J. F. Hinton, J. Solution Chem., 7, 1 (1978).

110. R. W. Briggs and J. F. Hinton, J. Solution Chem., 6, 827 (1977).

111. R. W. Briggs and J. F. Hinton, J. Solution Chem., 8, 519 (1979).

112. R. W. Briggs, K. R. Metz, and J. F. Hinton, J. Solution Chem., 8, 479 (1979).

113. J. F. Hinton and K. R. Metz, J. Solution Chem., 9, 197 (1980).

114. G. W. Gokel and D. J. Cram, J. Org. Chem., 39, 6 (1974).

115. R. M. Izatt, B. L. Haymore, J. S. Bradshaw and J. J. Christensen, Inorg. Chem., 14, 3132 (1975).

116. G. E. Hiegel and K. C. Selk, Appl. Spectrosc., 33, 528 (1979).

117. D. D. Traficante, J. A. Simms, and M. Mulcay, J. Mag. Res., 15, 484 (1974).

118. J. W. Cooper, "An Introduction to Fourier Transform NMR and Nicolet 1080 Data System", Nicolet Instrument Corp., Madison, WI, 1972.

119. E. Mei, Ph. D. Thesis, Michigan State University, E. Lansing, Michigan (1977).

120. D. H. Live and S. I. Chan, Anal. Chem., 42, 791 (1970).

121. G. J. Templeman and A. L. Van Geet, J. Am. Chem. Soc., 94, 5578 (1970).

122. V. G. Gutmann and E. Wychera, Inorg. Nucl. Chem. Lett., 2, 257 (1966).

123. V. Gutmann, "Coordination Chemistry in Non-aqueous Solutions", Springer-Verlag, Wien-New York (1969).

124. V. A. Nicely and J. L. Dye, J. Chem. Ed., 48, 443 (1971).

267

125. M. E. Farago, Inorg. Chim. Acta, 23, 211 (1977).

126. R. L. Bonder, M. S. Greenberg, and A. I. Popov, Spectrosc. Leter., 9, 359 (1973).

127. E. T. Rouch, P. R. Handy, and A. I. Popov, Inorg. Nucl. Chem. Lett., 9, 359 (1973).

128. R. G. Pearson, J. Am. Chem. Soc., 85, 3535 (1963).

129. G. Rounaghi, Michigan State University, Ph. D. Thesis (1980).

130. R. H. Cox, H. W. Terry, Jr., J. May. Reson., 14, 317 (1974).

131. M. L. Martin, G. J. Martin and J. J. Delpuech, "Practical NMR Spectroscopy", Heydon, London, 1980.

132. J. H. Swinehart and H. Taube, J. Chem. Phys., 37, 1579 (1962).

133. J. J. Dechter and J. I. Zink, Inorg. Chem., 15, 1690 (1976).

134. A. K. Covington, T. H. Lilley, K. E. Newman, and G. A. Prothouse, J. Chem. Soc. Faraday Trans., 1, 963 (1973).

135. A. K. Covington, K. E. Newman, and T. H. Lilley, J. Chem. Soc. Faraday Trans., 1, 973 (1973).

136. A. K. Convigton, I. R. Lantzke, and J. M. Thain, J. Chem. Soc. Faraday Trans. 1, 1869 (1974).

137. A. K. Convington, and J. M. Thain, J. Chem. Soc. Faraday Trans., 1, 1879 (1974).

138. M. S. Greenberg and A. I. Popov, Spectrochim. Acta A, 31, 697 (1975).

139. C. J. Hawkins, "Absolute Configuration of Metal Complexes", Wiley-Interscience, New York, 1971.

140. W. R. Cullen, L. D. Hall, and J. E. H. Ward, J. Amer. Chem. Soc., 94, 5702 (1972), and references there in.

141. A. Ault, J. Chem. Educ., 47, 812 (1970).

142. J. W. Emsley, J. Feeney and L. H. Sutcliffe, "High Resolution Nuclear Magnetic Resonance Spectroscopy", Oxford, New York, 1966.

143. M. Karplus, J. Chem. Phys., 30, 11 (1959).

144. M. Karplus, J. Am. Chem. Soc., 85, 2870 (1963).

145. H. S. Gutowsky, M. Karplus and D. M. Grant, J. Chem. Phys., 31, 1278 (1959).

146. J. E. Prue and R. Fernandez-Prini, Farady Society, London. Transactions, 62, 1257 (1966).

147. J. E. Collin and G. Conde, Bull. Classe Sci., Acad. Roy. Belg., 52, 978 (1966).

148. P. Vouros and K. Biemann, Org. Mass Spectrom., 3 1317 (1970).

149. F. L. Cook, T. C. Caruso, M. P. Byrne , C. W. Bowers, D. H. Speck and C. L. Liotta, Tetrahedron Lett., 46, 4029 (1974).

150. D. A. Jaeger and R. R. Whitney, J. Org. Chem., 40, 92 (1977).

151. A. S. Goems and C. M. F. Oliveira, Org. Mass Spectrom., 12, 407 (1977).

152. R. T. Gray, D. N. Reinhoudt, K. Spaargaren, and J. F. de Bruijn, J. Chem. Soc., Perkins II, 206 (1977).

153. R. R. Whitney and D. A. Jaeger, Org. Mass Spectrom., 15, 343 (1980).

154. A. Maccoll, "Mass Spectrometry" International Review of Science, Physical Chemistry Series 2, Vol. 5, Butterworths, London and Boston (1975).

155. E. U. Condon and H. D. Smyth, Proc. Nat. Acad. Sci., 14, 871 (1928).

156. E. U. Condon, Phys. Rev., 35, 658 (1930).

157. H. M. Rosenstock, Int. J. Mass Spectrom. Ion Phys., 20, 139 (1976).

158. R. A. Marcus, J. Chem. Phys., 20, 359 (1952).

159. H. M. Rosenstock, M. B. Wallenstein, A. L. Wahrhaffig and H. Eyring, Proc. Nat. Acad, Sci., 38, 667 (1952).

160. H. M. Rosenstock, Advan. Mass Spectrom., 4, 523 (1968).

161. J. C. Lorquet, Org. Mass Spectrom., 16, 469 (1981).

162. W. Forst,"Theory of Unimolecular Reaction", Academic Press, New York (1973)

163. D. J. McAdoo, P. F. Bente III, M. L. Gross, and F. W. McLafferty, Org. Mass Spectrom., 9, 525 (1974).

164. P. F. Bente III, W. McLafferty, D. J. McAdoo, and C. Lifshitz, J. Phys. Chem., 79, 713 (1975).

165. J. E. Collin and G. Conde, Int. J. Mass Spectrom. Ion Phys., 1, 213 (1968).

166. C. L. Liotta, H. P. Harris and F. L. Cook, J. Org. Chem., 39, 2445 (1974).

167. M. Kajitani, A. Sugimori, N. Sato, K. Seki, H. Inokuchi and Y. Harado, Bull. Chem. Soc. Japan, 52, 2199 (1979).

168. J. Dale, Tetrahedron, 30, 1683 (1974).

169. J. Dale, Israel J. Chem., 20, 3 (1980)

170. P. Groth, Acta Chem., Scand., A32, 279 (1978).

171. E. E. Astrup, Acta Chem. Scand., A34 85 (1980).

172. S. Okada and S. Taniguchi, Annual Report of the Fadiation Center of Osaka Prefecture, 19, 85 (1978).

173. S. K. Huang, J. Allison, unpulbished results.

174. G. A. Junk and H. J. Svec, Z. Naturforsch, 23, 1 (1968).

175. N. F. Ramsey, Phys. Rev., 78, 699 (1950).

176. C. Deverell, and R. E. Richard, Mol. Phys., 10, 551 (1966).

177. "Recommendations for the Presentation of NMR Data for Publication in Chemical Journals", Pure Appl. Chem. 29, 627 (1972); 45, 217 (1976).

178. J. A. A. deBoer, D. N. Reinhoudt, S. Harkema, G. J. Van Hummel and F. de Jong, J. Am. Chem. Soc., 104, 4073 (1982).